

Final Project Report on RCCS Testing with the Air-based Natural convection Shutdown heat removal Test Facility (NSTF)

Nuclear Engineering Division

About Argonne National Laboratory

Argonne is a U.S. Department of Energy laboratory managed by UChicago Argonne, LLC under contract DE-AC02-06CH11357. The Laboratory's main facility is outside Chicago, at 9700 South Cass Avenue, Argonne, Illinois 60439. For information about Argonne and its pioneering science and technology programs, see www.anl.gov.

DOCUMENT AVAILABILITY

Online Access: U.S. Department of Energy (DOE) reports produced after 1991 and a growing number of pre-1991 documents are available free via DOE's SciTech Connect (<http://www.osti.gov/scitech/>)

Reports not in digital format may be purchased by the public from the National Technical Information Service (NTIS):

U.S. Department of Commerce National
Technical Information Service 5301
Shawnee Rd
Alexandria, VA 22312

www.ntis.gov

Phone: (800) 553-NTIS (6847) or (703) 605-6000

Fax: (703) 605-6900

Email: orders@ntis.gov

Reports not in digital format are available to DOE and DOE contractors from the Office of Scientific and Technical Information (OSTI):

U.S. Department of Energy
Office of Scientific and Technical Information
P.O. Box 62
Oak Ridge, TN 37831-0062

www.osti.gov

Phone: (865) 576-8401

Fax: (865) 576-5728

Email: reports@osti.gov

Disclaimer

This report was prepared as an account of work sponsored by an agency of the United States Government. Neither the United States Government nor any agency thereof, nor UChicago Argonne, LLC, nor any of their employees or officers, makes any warranty, express or implied, or assumes any legal liability or responsibility for the accuracy, completeness, or usefulness of any information, apparatus, product, or process disclosed, or represents that its use would not infringe privately owned rights. Reference herein to any specific commercial product, process, or service by trade name, trademark, manufacturer, or otherwise, does not necessarily constitute or imply its endorsement, recommendation, or favoring by the United States Government or any agency thereof. The views and opinions of document authors expressed herein do not necessarily state or reflect those of the United States Government or any agency thereof, Argonne National Laboratory, or UChicago Argonne, LLC.

Final Project Report on RCCS Testing with the Air-based NSTF

prepared by:

Darius D. Lisowski, Craig D. Gerardi, Dennis J. Kilsdonk, Nathan C. Bremer, Stephen W. Lomperski, Rui Hu, Adam R. Kraus, Matthew D. Bucknor, Qiuping Lv, Taeseung Lee, and Mitchell. T. Farmer

Nuclear Engineering Division, Argonne National Laboratory

August 2016

This page was intentionally left blank.

Executive Summary

The following report serves as a comprehensive summary of the air-based portion of the Natural convection Shutdown heat removal Test Facility (NSTF) program at Argonne National Laboratory (Argonne). Initiated in 2005 to generate validation data for the Next Generation Nuclear Plant (NGNP), the project was centered on an experimental testing program to study the behavior and bound the performance of Reactor Cavity Cooling System (RCCS) concepts. Parallel modeling and simulation efforts also have been performed to guide the design, fabrication, and operation of NSTF, as well as to assess the suitability of analysis methods for natural convection systems. The program operates under support from the Department of Energy (DOE) Office of Advanced Reactor Technologies (ART), and maintained compliance with NQA-1 2008 with 2009a in both administrative and technical portions of program activities.

The test facility constructed at Argonne stands nearly 26-m in total height and has been designed to represent a $1/2$ scale model of the primary features of the General Atomic (GA) RCCS design for their Modular High Temperature Gas cooled Reactor (MHTGR). The heated surface of the NSTF was constructed from prototypic, reactor-grade material and driven by a heat source originating from a forty-zone array of electric heaters. Supplying up to 220 kW of electric power, the array was able to accurately mimic the walls of a Reactor Pressure Vessel (RPV) through profile shaping to achieve axial or azimuthal skews. An integrated suite of data acquisition and high-resolution sensors have guided experimental practices and allowed the direct measurement of both system thermal hydraulic behavior and local phenomena. Measurement such as flow rates, gas and wall temperatures, and differential pressure by calibrated instrumentation ensured confidence in determining heat removal capacity and accurately observing system behavior. A weather station has characterized the ambient and meteorological boundary conditions that have shown to be

dominant factors in influencing the sensitive natural circulation phenomena. Additionally, high fidelity sensors including hot-wire probes and distributed temperature sensing fibers have introduced an unparalleled data density and insight into local flow and heat transfer modes.

The testing program, spanning a 33-month period from September 2013 until July 2016, completed over 2,250 hours of active test operations and 16 successful test runs. Studies of scaling, power shaping, flow path configuration, design basis accident conditions, weather influences, and off-normal scenarios were performed and compared against routinely repeated baseline test cases. Special considerations were made to include full-scale features and operating conditions, such as adjacent chimney roles, cosine power shaping, and the full time history of one Safety Related Design Condition (SRDC-II). The effects of weather and repeatability were assessed through regular testing of a baseline test case, scheduling select operations to occur during inclement weather, and isothermal testing for facility characterization purposes.

Final observations from the project have indicated that a high level of performance can be obtained from the air-RCCS concept design if the as-intended path of the natural circulation flow can be maintained. Disruptions of blocked riser channels (50% flow area tested), chimney short-circuit scenarios, strong asymmetries from the heated source, and moderate shifts in weather conditions were found to have negligible impacts on the overall heat removal performance. Measured temperature excursions by the RPV surface, an indicator of peak fuel temperatures, did not rise above 5% of normal values across the conditions tested.

However, cases were observed that progressed into severe degradation of heat removal performance and significant rise in heated plate temperatures. The most common condition observed was the downdraft of cold ambient air through one of the chimney stacks, an unintended behavior that disrupted test operations and required operator intervention to mitigate. The impact of this condition on the RCCS resulted in reduced flow rates by an average of 40%, increased gas temperatures by 15%, and a rise in heated surface temperatures

of over 10%. Strategies were implemented in the later portions of the testing program to mitigate these disruptions, which initially entailed operator intervention through the use of damper valves, and later the design and installation of program-specific chimney caps. These solutions proved effective during the majority of testing scenarios, however the project team was unable to guarantee complete effectiveness during early start-up periods. The coupling of low flow velocities, cold ductwork, large flow areas, and multiple parallel paths create a system that is readily destabilized with even minor flow disruptions.

Given the proximity of proposed HTR installations near chemical processing facilities, the project team examined one hypothetical scenario where heavy-gas (high purity argon) is drawn into the inlet of an RCCS. Under these conditions, the NSTF exhibited complete stagnation of system flow and subsequent failure of heat removal function. The introduction of 1,200 cu-feet of a heavy gas, twice the internal volume of the NSTF flow path, induced flow stagnation over a period spanning 19-minutes. Furthermore, re-circulation patterns occurred within the twelve riser channels, a first-of-a-kind observation for the testing program. While the mechanism of recovery is not fully understood and would require further studies, the observed response by the NSTF expanded the list of deficiencies for an air-based RCCS concept.

The data generated for the air-based portion of the NSTF project at Argonne was produced within a controlled, traceable, and NQA-1 compliant program. The project has directly supported the DOE mission for developing reliable and safe reactor technologies, and the produced data set is suitable for aiding design choices of future reactor concepts. Ultimately, the result of the accomplished work is well poised to guide the decision on the viability of RCCS concepts for passive decay heat removal in advanced reactors.

This page was intentionally left blank.

Contents

Executive Summary	i
Foreword	1
1 Introduction	3
1.1 Management of NQA-1 Requirements	5
1.2 Legacy NSTF	6
1.3 Design Basis	9
1.4 Scaling	12
1.4.1 Top-down Scaling	13
1.4.2 Scaling Summary	14
1.5 Testing Program	15
2 Experiment Method	19
2.1 Primary Testing Objectives	20
2.2 General Test Procedure	22
3 Test Assembly Description	25
3.1 Base Support and Cavity Framework	25
3.2 Flow Path Ducting	27
3.2.1 Inlet Downcomer	27
3.2.2 Inlet Plenum	29
3.2.3 Riser Ducts	31
3.2.4 Outlet Plenum	34
3.2.5 Chimney Stacks	37
3.2.6 Forced Blower Fans	40
3.3 Heated cavity	41
3.3.1 Unheated Paneling	42
3.3.2 Heated Wall	42
3.3.3 Primary Heated Plate	43
3.3.4 Heater Subpanels	46
3.3.5 Ceramic Heaters	48
3.3.6 Heated Wall Insulation Panels	48
3.4 Insulation	50
3.5 Operating Flexibility	52
3.6 As-built Summary	54

4	Test Assembly Sensors & Control	55
4.1	Data Acquisition	56
4.2	Sensors	57
4.2.1	Wall Thermocouples	59
4.2.2	Heat Flux Sensors	73
4.2.3	Meteorological	77
4.2.4	Differential Pressure	80
4.2.5	Inlet Flow and Humidity	83
4.2.6	Hot-wire Probes	86
4.2.7	Pitot Tubes	88
4.2.8	Gas Temperature	89
4.2.9	Luna Fiber Optic Temperature	93
4.3	Heater Power Control	101
5	Test Assembly Characterization	105
5.1	Isothermal Velocity Profile & Frictional Losses	106
5.2	Temperature Profiles	115
5.3	Heat Losses	121
5.4	Physical Properties	123
6	Computational Models & Analysis	129
6.1	Computational Codes	129
6.1.1	Experiment Support	130
6.1.2	System Level Modeling	132
6.1.3	Computational Fluid Dynamics Modeling	135
6.2	System Trends	140
6.3	Ambient Correlations	147
6.4	Prototypic Testing Conditions	152
6.4.1	GA-MHTGR Accident Scenario	152
6.4.2	Cosine Power Profile	156
6.4.3	Azimuthal Power Skew	159
7	Testing Results	163
7.1	Baseline Test Cases	166
7.1.1	General System Behavior at Baseline Conditions	167
7.1.2	Baseline Repeatability	172
7.2	Heated Source Variations	177
7.2.1	Cosine Shaping - Run013 & Run022	177
7.2.2	Azimuthal Shaping - Run026	180

7.3	Prototypic Studies	183
7.3.1	Accident Scenario Testing - Run014	183
7.3.2	Accident Weather Influences - Run018	185
7.3.3	Adjacent Chimney Roles - Run017	187
7.3.4	INERI Test Case - Run023	192
7.4	Off-normal Scenarios	196
7.4.1	Blocked Riser Channels - Run015	196
7.4.2	Heavy-gas Ingress - Run027	201
7.5	Meteorological Influences	215
7.5.1	Start-up Sensitivity - Run016	217
7.5.2	Wind Gusts	219
8	Discussion	223
8.0.1	Analytical and Computational Support	223
8.1	Lessons Learned	224
8.1.1	Sealed Fan Loft Damper Valve	227
8.1.2	Weather Mitigation Efforts	229
8.2	Collaborative Efforts	236
8.3	Design Viability	239
8.3.1	System Longevity	239
8.3.2	Full Scale Application	240
9	Conclusion	245
9.1	Program Impact	246
9.2	Relevance and Contributions to DOE Vision	247
9.3	Path Forward	248
	Acknowledgments	251
	References	253
	Appendix A: Project Organization	257
	Appendix B: QAPP Control Records	259
	Appendix C: Project Publications	261
	Appendix D: Data Review Meeting Minutes	263
	Appendix E: Testing Procedure	281
	Appendix F: DAQ Channel Listing	305

This page was intentionally left blank.

List of Figures

1	Original NSTF dimensions and design [9]	7
2	Original NSTF test section cross-section [9]	8
3	GA-MHTGR concept, single module shown [10]	10
4	Sketch of GA-MHTGR reactor building. RCCS highlighted in red [10]	11
5	Base support	26
6	Lower skeleton framework	26
7	Inlet downcomer (front view) and equivalent segment lengths	27
8	Flow conditioner	28
9	Geometric dimensions (plan view)	28
10	Inlet plenum. Duct stub shown connects to inlet downcomer, rectangular slotted holes connect to riser ducts. Interior volume measures 44" tall, 51.75 width (parallel to riser slots), and 59.75" deep, of which only 31.75" is available for the working gas due to the present of the false back wall.	30
11	Cross section of riser ducts (dimensional drawing above, picture below)	32
12	Top plate which bears the weight of the twelve riser ducts	33
13	View into the outlet plenum from opened east wall. False west wall visible behind riser tubes	34
14	Exploded view of north/south panels on outlet plenum	35
15	Cross section (east/west) of outlet plenum and surrounding insulation panels	36
16	Variable component locations on chimney ducting. Five butterfly valves and dual forced blowers	37
17	Valve position and resulting chimney duct flow area	38
18	Flow vs frequency for dual fan loft blowers	40
19	Plan view of NSTF heated cavity and test section. Heater surface is shown in red, riser ducts in blue. Hatched perimeter denotes insulated areas	41
20	Lower heated plate prior to installation. Eye hooks were temporarily installed for lifting, thermocouples visible	44
21	Dimensions and mounting hole specifications of primary heated plate (top shown)	45
22	Heated wall, heater subpanel assembly	46
23	AutoCAD drawing of heater subpanel with ceramic heaters outlined	47
24	Electrical detail of Main and Guard heating zones	49
25	Cross section of heated cavity outlining areas of insulation. Viewed from a north facing perspective	51

26	Facility configurations of chimney ductwork, arrow denotes air inlet. Blue (left): baseline, dual vertical, Red (left,center): reduced chimney discharge, Orange (right-center): single chimney vertical, Purple (right): adjacent inlet/outlet	53
27	Primary areas of flexibility, dimensions shown for ‘as-built’ configuration	54
28	Plan view of Building 308 and NSTF test operations	55
29	Communications overview	56
30	Heated plate thermocouple mounting method	59
31	iTi model BHT, 300 °C Polyimide HFT	73
32	Position of weather station of Bldg. 308 roof top	78
33	Picture of weather station of Bldg. 308 roof top	78
34	Diagram of miniature hot-wire probe, units in mm	86
35	Dwyer 160F pitot tubes installed along chimney ductwork. Right figure shows air ports that translate air velocity into fluid pressure	88
36	Placement of inlet and outlet instruments for riser	89
37	Typical rake junction locations, placed along upper plenum top panel and extending downward	92
38	Luna fiber setup, near base mount and fed from inlet plenum	94
39	Method of Luna fiber optic cables securement to capillary support tubes	95
40	Calibration curve for polyimide LUNA fibers, reference to thermocouple standard . .	97
41	Voltage (yellow) and current (green) phases from 480VAC heater circuit	102
42	Eurotherm power and Mini electrical wiring	103
43	Comparison of velocities as measured by flow meter (x-axis) and hot-wire (y-axis) .	108
44	Velocity profile of inlet downcomer via hot-wire probe. Tails near radial extremes are due to leakage past honey-comb grating of flow straightener	109
45	Frictional losses across a single chimney flow path, shown in raw units of Pascals . .	110
46	Frictional losses across inlet downcomer, in terms of K-factor	111
47	Isothermal losses across riser ducts in terms of fanning friction factor, f	112
48	Turbulence intensity at inlet conditions measured via hot-wire probes. Scatter at low Re-numbers occurs due to the very large duct diameter and relatively low velocities, which creates large fluctuations in the flow	113
49	Turbulence intensity at riser outlet conditions measured via hot-wire probes	114
50	New LUNA fiber sensors installed across 10-inch width of one riser duct (outlet) . .	115
51	Continuous temperature profile as measured at the exit plane of the riser ducts. Heat source originates from the left side of the figure, and the cold wall on the right side .	116
52	LUNA temperature profile across riser outlet face for varying conditions	117
53	Mounting of LUNA fibers within outlet plenum gas space	119
54	Riser #9, SuperDuct 2.0, gas fiber mounting method	120

55	Thermal efficiency of the NSTF, determined by separate effects testing at varying electric powers and flow rates	122
56	Regimes for free, forced, and mixed convection through for flow through vertical tubes, [29]. Red triangles indicate NSTF measured points for Run017, Run020, Run022, and Run023	128
57	Nodalization diagram of NSTF model in RELAP5-3D	134
58	Solid model of NSTF in STAR-CCM+	139
59	RELAP5 response of system parameters for variations in actual thermal power . . .	142
60	RELAP5 response of system parameters for variations in outdoor air temperature .	143
61	RELAP5 response of system parameters for variations in inlet air temperature . . .	144
62	RELAP5 response of system parameters for variations in wind speed	145
63	RELAP5 response of system parameters for variations in form loss coefficient	146
64	Fitting correlation, comparing existing data SPEF005	150
65	Fitting correlation, comparing new data SPEF007	150
66	Response surface of fitting correlation	151
67	GA documented decay heat load during DCC with small primary leak [10]	153
68	Heat rate for RPV generation and RCCS removal, GA-MHTGR DCC [10]	153
69	Decay heat curve scaled for NSTF operation	155
70	Overlay of GA-MHTGR and NSTF decay heat	155
71	Axial distribution for an typical HTR [42]	156
72	Cosine power skews with linear reference, GA mid-plane and bottom peaked	158
73	Group I	160
74	Group II	160
75	Schematic for air risers behind cross ducts [21]	161
76	Electric and thermal powers from baseline test case, Run011. Long dashed lines indicate steady-state period, and dotted line indicates target power	169
77	Axial temperatures for surfaces within the heated cavity, averaged over steady-state period at baseline conditions	170
78	Heat flux contributions to four faces of Riser 7, steady-state baseline conditions . . .	171
79	Thermal power, baseline repeats	174
80	Riser ΔT , baseline repeats	174
81	Riser wall temperature, baseline repeats	174
82	System flow rate, baseline repeats	174
83	Relation between ΔT and ambient temperature across baseline test cases. Wind speeds were significantly higher during Run003, Run011, and SPEF003 resulting in fluctuations of the trend line	175

84	Temperature profile across 10-inch exit face of riser ducts during linear and bottom peaked cosine power profiles, Run022	178
85	Run013 riser wall temperature, linear	179
86	Run013 riser wall temperature, mid cosine	179
87	Run022 riser wall temperature, linear	179
88	Run022 riser wall temperature, bottom cosine	179
89	Riser outlet gas temperatures for varying levels of azimuthal skews, Run026	180
90	1-D steady-state thermal analysis of azimuthal power skew at source and sink	182
91	Short-circuit region and flow paths. Blue arrows indicate fresh inlet air supply, dark red indicates originating heated exhaust from test section. Mixing occurs across the dashed boxed region by opening the damper and actuator LF-CX	189
92	Impact of 33% break initiated at t=57.6min. Average riser ΔT saw a 7.4°C rise	191
93	Impact of 33% break initiated at t=57.6min. Average riser heat flux saw a -9.33% reduction	191
94	Temperature profile across outlet face of riser ducts, LUNA fibers	195
95	Four stages of riser blockages during Run015, red arrows indicate heated surface	196
96	Closure flaps used to remotely actuate a riser blockage	197
97	Time history of system flow rate with various blockage stages indicated	199
98	Step change in flow rate as a function of riser blockage	200
99	Diagram of argon-enclosure, positioned on Bldg. 308 floor above inlet	204
100	Operation of heavy-gas enclosure: normal air draw, argon by-pass	207
101	Argon enclosure constructed above downcomer inlet	208
102	Extension from argon enclosure to inlet	209
103	Top view of argon enclosure	209
104	Gas sensor oxygen value and system flow rate, DataQuality027	210
105	Riser inlet (top) and outlet (bottom) temperatures after argon ingress, DataQuality027. Riser plan view shading corresponds to thermocouple grouping	211
106	Comparison of identical transition sequence procedure, argon and air gas compositions	214
107	Density and temperature relationship for elevated air temperatures	216
108	System wide reverse flow observed during failed Run016 created dangerous temperatures at inlet	218
109	Impact extended into overall system and caused degraded heat removal and elevated temperatures	218
110	Impact on otherwise calm cool-down period after Run018 from a sudden wind gust	220
111	Drop in riser outlet gas temperatures from wind gust	221
112	Early warning signs via wall temperatures	221
113	Gap between butterfly valve and inner ductwork. Average gap across entire circumference of 0.125-in	227

114	Picture of 1/12, chimney duct-work only, forced flow mini-NSTF	231
115	New (left) and existing (right) NSTF outlet chimney caps	232
116	Installation of new caps	233
117	New caps installed, Bldg. 308	233
118	Temperature profiles (normalized dimensions) across KAERI, UW, and ANL facilities for 'I-NERI Test Case 1'	237
119	Radar map of the current testing envelope by ANL and collaborators for RCCS concept	238
120	Rust from riser ducts collected in inlet plenum. 13.86 g over 100 day period	240
121	Removed south chimney section of air-based NSTF	249
122	Exposed riser ducts (outlet) after removal of upper plenum, August 2016	249
123	Timeline for air- and water-based NSTF program	250
124	NE Division, Engineering Development Labs Organization Chart	257

This page was intentionally left blank.

List of Tables

1	Summary of audits performed of the NSTF program at Argonne	6
2	Features of standard GA-MHTGR [10]	9
3	Scaling similarity parameters and ratios	12
4	Geometric scaling comparison between full GA-MHTGR and model NSTF	14
5	Scaling of heat removal specifications for full GA-MHTGR and model NSTF	14
6	High level testing summary - Accepted cases	16
7	High level testing summary - Failed and trending cases	17
8	Ducting segment types and equiv. lengths for horizontal and vertical flow paths	39
9	Material and thermal specifications for NSTF insulation	50
10	Summary of adjustable features on the NSTF	52
11	Summary of National Instruments data acquisition devices	57
12	Summary of NSTF instrumentation with listed accuracy	58
13	Summary of heat flux sensors on risers. Procured from iTi Inc., model BHT	74
14	Device specifications for Davis VantageVue weather station	77
15	Differential pressure device specifications	80
16	Inlet mass flow meter specifications	83
17	Inlet plenum humidity probe specifications	83
18	Specifications of Luna ODiSi A-10	93
19	Unique requirements for LUNA fibers	96
20	TC vs LUNA recorded temperatures during steady-state Run015 (26 kW _t)	118
21	Dimensional numbers for convection within the downcomer, risers, and chimney. Dimensionless number subscripts indicate specific characteristic length used	126
22	Riser Nusselt number and convective coefficients for varying correlations. Dimensionless number subscripts indicate specific characteristic length used	127
23	Parametric study variables examined in RELAP5	140
24	Span of available data collected at zero power conditions	149
25	Scaling ratios and resulting values for full and NSTF scales	154
26	Peaking factors for cosine power profiles	157
27	Summary of air-based testing - Data Quality runs	164
28	Summary of air-based testing - Separate Effects & Scoping runs	165
29	Pre-test zero flow system parameters for Run011	167
30	Summary of weather conditions during full test window of Run011	167

31	Testing conditions for repeat baseline cases performed	172
32	Measured values across steady-state periods for all performed baseline test cases . .	176
33	Power skews at source and sink, 1-D steady-state thermal	181
34	Test log for Run014 - GA-MHTGR summer	183
35	Summary of steady parameters for GA-MHTGR Run014	184
36	Summary of weather conditions for two GA-MHTGR tests, winter and summer . . .	185
37	Summary of GA-MHTGR accident scenario averaged thermal hydraulic parameters .	186
38	Summary of steady-state period during Run017 (prior to break area)	187
39	System behavior with varying amounts of chimney short-circuit break areas	189
40	System segment flow rates during 33% break area between inlet & outlet chimneys .	190
41	Summary of scale test facilities at collaborating institutions	192
42	Target testing conditions, INERI testing series Case I and Case II	193
43	Acceptance criteria and results for INERI test cases, Run023	194
44	Test log for Run015 - Performance testing with block riser tubes	198
45	Acceptance criteria and system parameter summary over four stages in Run015 . . .	198
46	Physical Properties of Dry Air and Argon at STP (0 °C, 101.325 kPa)	201
47	Physical Properties of Elevated Temperature Dry Air and Argon	202
48	Oxygen Sensor Specifications	203
49	Installed Oxygen Sensors	203
50	Measurement values used for acceptance criteria during Run027 prior to injection . .	206
51	Before, During, and After Injection quasi-steady-state values, Run027	212
52	Summary of major improvements to test facility	226
53	Influence on system flow rate due to varying levels of air ingress past damper valve .	228
54	Measured (original) and corrected values, sample baseline case	228
55	Summary of scale test facilities at collaborating institutions	236
56	Elevations of inlet and exhaust ports, all dimensions in meters	241
57	Geometric ratios of loop segments. ℓ_i refers to all inlet ductwork, ℓ the heated length, and ℓ_{exit} the exit chimney length	242

Foreword

The following report serves as a comprehensive summary of the accomplishments from the air-based portion of the Natural convection Shutdown heat removal Test Facility (NSTF) program at Argonne National Laboratory (Argonne). Previously published materials have been included to ensure completeness and allow a single point of reference of the work performed. Details of the test facility design and data acquisition have been transferred from ANL-SMR-8 [41], topics pertaining to experiment methodology and early testing results transferred from ANL-ART-22 [40], and topics related to computational analysis from ANL-ART-14 [22] and ANL-ART-46 [33].

This page was intentionally left blank.

Chapter 1

Introduction

Under support of the Department of Energy (DOE) Office of Advanced Reactor Technologies (ART), a program was established¹ at Argonne National Laboratory (Argonne) to develop technologies to improve the reliability and safety of new reactor designs. Of the solutions under consideration for passive decay heat removal, the Reactor Cavity Cooling System (RCCS) stands as a leading concept. To examine the feasibility of this solution, an experimental test assembly, the Natural convection Shutdown heat removal Test Facility (NSTF), was constructed at Argonne and is the focal point of the content presented in this report.

The RCCS concept aims to provide a means of achieving passive decay heat removal and safe reactor shutdown during accident scenarios, with recent designs tailored to the latest generation of High Temperature Reactors (HTR). The design is appealing given its relatively simplicity, reliance on natural forces, and potential for high levels of performance. However, the inclusion of an RCCS in the safety portfolio of future reactor installations is contingent on its ability to guarantee the following requirements [1]:

1. Maintain the vessel wall at safe limits during normal operation and accident conditions, which in turn must ultimately ensure safe peak core fuel temperatures (i.e. retain a solid form) across all design basis scenarios.
2. Maintain the reactor cavity concrete and support structures at safe limits during normal operation and accident conditions to prevent concrete materials degradation and possible failure.
3. Sustain intended function and performance across the 40-year life span of a reactor installation.
4. Accomplish the above functions without human intervention, active systems (e.g. AC or DC power), at all foreseeable reactor construction sites, domestically and abroad.

¹Office of Advanced Reactor Concepts under contract number DE-AC02-06CH11357

The top-level objective of the program at Argonne was to obtain experimental data which could be utilized to support licensing of safety features in advanced reactor designs. The validation data obtained by this program has been collected in compliance with the 2008 / 2009a Nuclear Quality Assurance (NQA)-1 plan and contains the necessary documentation, traceability, and quality standards to support these licensing purposes. The overarching design of the NSTF centered on a philosophy of flexibility which facilitated multiple operating conditions to best-reflect full scale concepts, along with ease in accommodating alternative test section designs. Ultimately, the project has provided benchmark data for validation and verification of safety related codes, and through multi-parameter studies, will aid in the optimization of the design concept for passively safe decay heat removal.

Construction of the test section was completed in September 2013, after which the focus was shifted to facility shakedown and checkout activities which extended through the remaining calendar year. Since the start of data collection in early 2014, the NSTF has seen over 2,250 hours of active operation over the course of thirty-five scheduled runs. As of July 1st 2016, experiment based testing with the air-based NSTF has concluded and facility operations have transitioned to disassembly and long term storage of air-based components. The project has completed the requirements of the air-based testing program including original objectives and those action items identified during the data review meeting held on January 26th 2016 with participation from the DOE, NRC, INL, AREVA, GA, and US Universities.

A review of the test facility and data acquisition will be provided in brief, followed by a description of the experimental method and procedures used for test operations. The primary focus will then be on the results obtained from the full set of air-based test operations, followed by a discussion on the feasibility of a full scale RCCS installation.

1.1 Management of NQA-1 Requirements

The Quality Assurance Program Plan (QAPP) is based on the requirements set forth in the American Society of Mechanical Engineers (ASME) NQA-1-2008 (with 1a 2009 addenda) Quality Assurance (QA) requirements for nuclear facility applications [2]. It is consistent with QA plans adopted by Argonne [3][4] and the Argonne Nuclear Engineering (NE) division [5], and the QAPP for the Next Generation Nuclear Plant Project (NGNP) at the Idaho National Laboratory (INL) including INL PLN-2690 [6] and 10 CFR Part 50, App. B [7].

In accordance with this program, a graded QA approach is desirable and the requirements of ASME NQA-1-2008 (with 1a 2009 addenda), Subpart 4.2 [8] may be used as guidance for Research and Development activities. Under this graded approach, current NGNP Research and Development (RD) work at the INL is classified as Applied Research. With this general background and in accordance with the Argonne QAPP, this task is assigned a QA level C with a level of detail consistent with the graded approach. The RD activities of this experimental program under the control of this QAPP are designed to provide reliable, reproducible, and timely data on the effects of the reactor cavity cooling system on the heat removal from the reactor vessel wall.

All controlled documents within the QAPP are uniquely identified in the following format: ANL-NSTF-0000000-CCCCC-XXX(-RYY)(-AZZ), where CCCCC is a maximum five character string representing the particular document category, XXX is a three digit number that uniquely identifies each document, RYY identifies the revision number, and when required, AZZ refers to the addenda documents. A tabulated list of the program's control records is provided in the Appendix. To maintain compliance with NQA-1, the NSTF program has regular reviews including external audits, formal internal audits, and informal management assessments (MA). An overview of all the audits performed is provided below in Table 1.

Table 1: Summary of audits performed of the NSTF program at Argonne

Date	Audit Type	Lead Auditor	Summary
Mar. 18-20, 2014	External	Kirk Bailey (INL)	Instruction provided to support future compliance, 27 recommendations and 4 weaknesses
Feb. 16-18, 2015	M.A.	Roberta Riel (ANL)	Verified observations from Bailey audit were effectively implemented
Jul. 20-23, 2015	Internal	Roberta Riel (ANL)	Six observations
Nov. 3-5, 2015	External	Alan Trost (INL)	Compliance established, 6 recommendations
Jan. 21, 2016	M.A.	Roberta Riel (ANL)	Verified recommendations from Trost audit were effectively implemented
Jun. 29-30, 2016	Internal	Roberta Riel (ANL)	One observation

1.2 Legacy NSTF

Originally built to study air-side performance of the General Electric (GE) Power Reactor Innovative Small Module (PRISM) Reactor Vessel Auxiliary Cooling System (RVACS), the first NSTF program at Argonne successfully provided experimental data during the later portion of the 1980's [9]. This NSTF was established to examine the performance of an ex-vessel, natural circulation driven, decay heat removal system, a purpose closely aligned to the current work scope. The last (on-record) test was performed in November of 1988, after which the facility sat idle until 2010. The facility was then revisited as part of the current NSTF work scope, aiding the current team through past experience and lessons learned. Some design choices were re-used, e.g. heated plate thermocouple mounting method, however the majority of the facility was re-designed to better reflect the newer concept for the NGNP. Of the physical components from the original experimental facility, only the heater plates were salvaged while all other component were replaced or re-designed to accommodate advances in data acquisition and measurement technology.

(Figure 1 has been deleted)

Figure 1: Original NSTF dimensions and design [9]

(Figure 2 has been deleted)

Figure 2: Original NSTF test section cross-section [9]

1.3 Design Basis

The General Atomics (GA) Modular High Temperature Gas cooled Reactor (MHTGR) was chosen as the full scale basis for the NSTF. Developed in the United States, this gas-cooled reactor uses helium as the primary coolant with prismatic fuel elements in a hexagonal core. GA proposed a four-unit plant with two steam turbine generators, and a net power output of approximately 560 MW_e [10]. This reactor was selected primarily on the basis that the design follows similar characteristics to the more recent NGNP, but moreover the passive cooling system received considerable attention and resulted in engineering design details that are readily available. Features of the standard MHTGR can be found in Table 2, a graphical illustration of a single module and steam generator in Figure 3, and a sketch of the RCCS piping network within the reactor building in Figure 4.

Table 2: Features of standard GA-MHTGR [10]

Fuel	UCO + ThO ₂	Power per module	140 MW _t / 87.5 MW _e
Moderator	Graphite	Fuel temperature	1,060°C (max), 677°C (avg)
Coolant	Helium	Coolant temperature	259°C (in), 687°C (out)

Of key interest in the GA-MHTGR design is the Reactor Cavity Cooling System (RCCS), which serves as a fully passive decay heat removal system. Natural convection drives air from the atmosphere, which flows through a series of standpipes that line the concrete containment to remove heat from the reactor pressure vessel (RPV) through radiation (primarily) and convection. The design consists of an array of 227 tubes, 2.5 cm wide by 25 cm deep that line the concrete containment [10]. A redundant series of concentric chimney ducts allows air to be both drawn in and exhausted to the atmosphere, which join via manifolds to form plenums near the inlet and outlet of the riser tubes. The supply air rises up through these risers, which surround the exterior of the vessel, and remove heat by a combination of convection and radiation before rejecting the heat to the outside environment, Figure 4. This system is attractive since it is completely passive and can remove decay heat indefinitely while maintaining acceptable system temperatures.

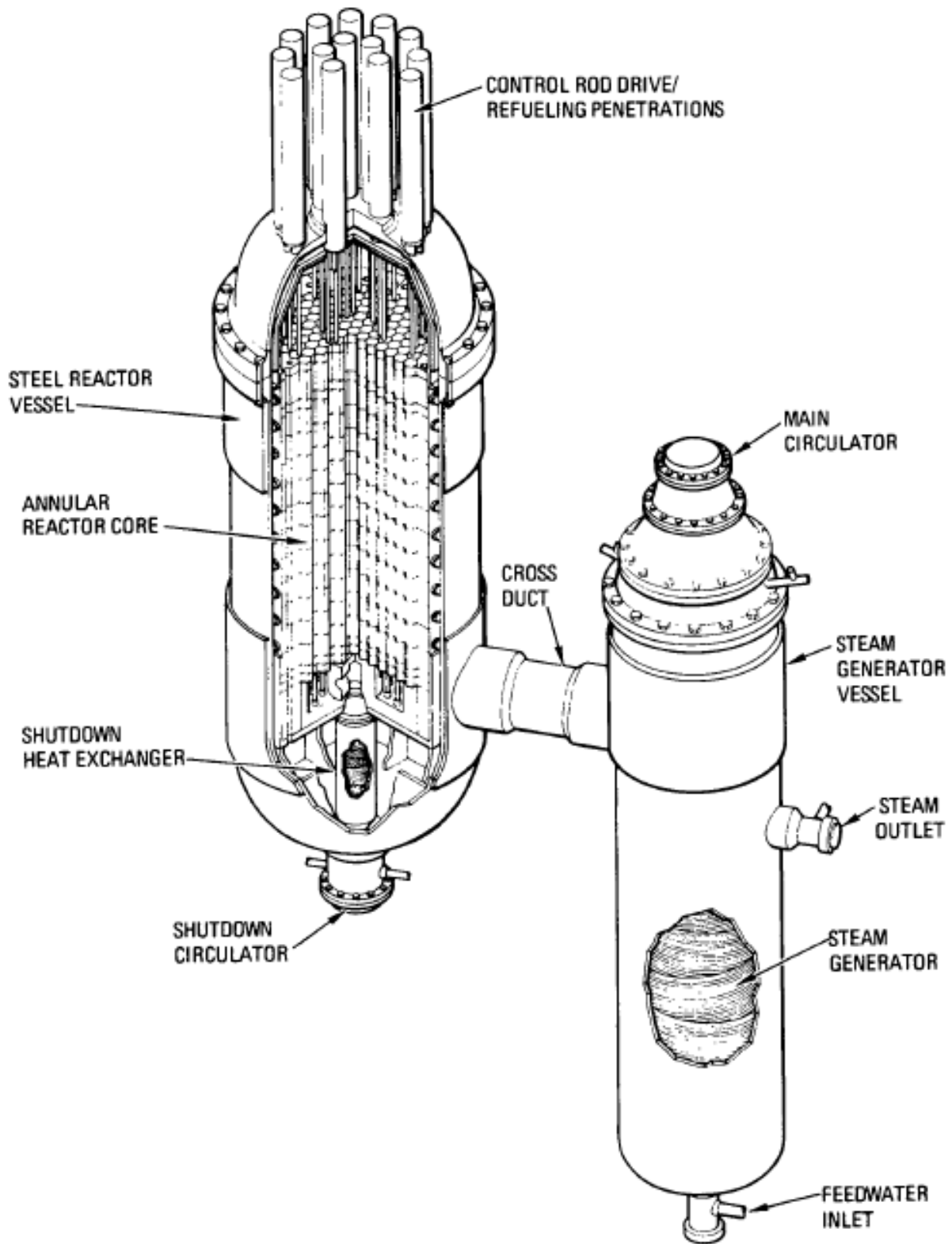


Figure 3: GA-MHTGR concept, single module shown [10]

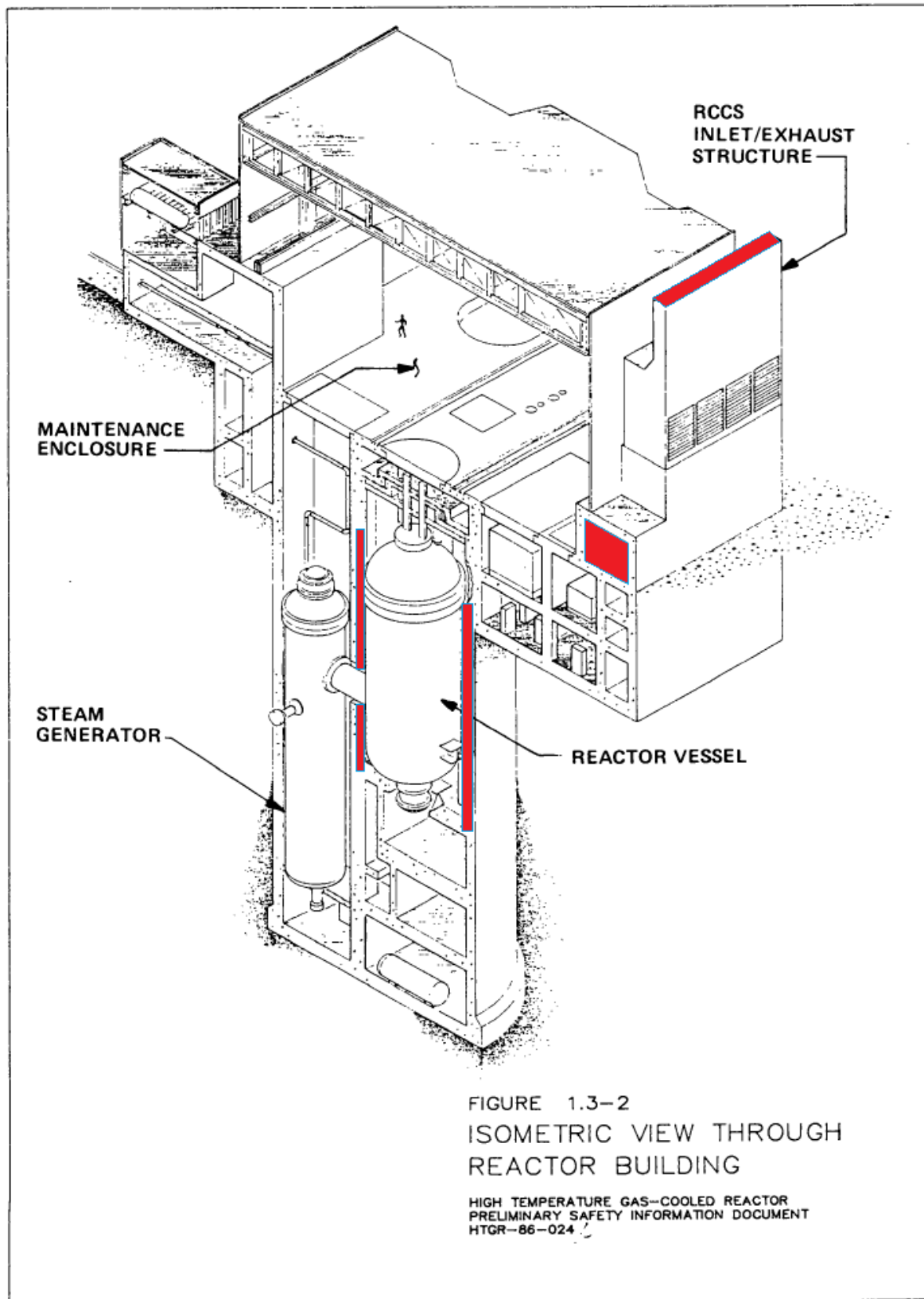


Figure 4: Sketch of GA-MHTGR reactor building. RCCS highlighted in red [10]

1.4 Scaling

A scaling evaluation of an air-cooled RCCS system was performed based on openly available literature on the RCCS design for the GA-MHTGR. A top-down scaling approach was used for the non-dimensional conservation equations describing the response of RCCS during steady-state and transient operations. These equations were developed into scaling laws to minimize distortions between scaled experiments and prototype operation, Table 3. The primary criterion to the air-cooled RCCS scaling was selecting the cold inlet to the hot riser duct as the reference location and that the cold atmosphere air is at the same condition for all scales and experiments, thus preserving the temperature rise across the heated section, $\Delta T_R = 1.0$. An overview of primary scaling similarity ratios is provided in Table 3, with a full analytical derivation and accompanying analysis detailed in previous works ?? [11].

Table 3: Scaling similarity parameters and ratios

Parameter	Scaling Ratio	Similarity Parameter	Values for $l_R = 0.5$
Material thickness	δ_R	1	1
Area	A_R	1	1
Air velocity	U_R	$\sqrt{l_R}$	0.707
Time ratio	T_R^*	$\sqrt{l_R}$	0.707
Heated temperature rise	ΔT_R	1	1
Reference temperature	T_R	1	1
Heat flux	q_R''	$l_R^{-0.5}$	1.414
Integral power	\dot{Q}_R	$\sqrt{l_R}$	0.707
Heat transfer coefficient	h_R	$l_R^{0.4}$	0.758
Reynolds number	Re_R	$\sqrt{l_R}$	0.707
Richardson number	Ri_R	1	1
Stanton number	St_R	$l_R^{0.9}$	0.536
Biot number	Bi_R	$l_R^{0.4}$	0.758

1.4.1 Top-down Scaling

The top-down scaling approach preserves integral behavior for mass and energy balances, however does not capture local behavior such as 3-dimensional mixing phenomena within the plenum. Furthermore, it does include behavior involving multiple riser ducts and parallel channel interactions. Natural circulation flow patterns, especially at low flow rates and small density differences (e.g. air driven systems), exhibit complex behavior and are difficult to predict with confidence. However, the discharge of hot jets from the riser ducts can be scaled based on a maximum ceiling height X_m for jet penetration. Turner [12] conducted experiments on a negative buoyant jet for an axisymmetric case, and is a considerable simplification over the behavior in an RCCS, which sees an initially positive buoyant jet that eventually reaches neutral or even negative buoyancy. Based on Turners work, the jet penetration depth, D_{jR} is proportional to the jet Froude number, Fr_{jR} , Eqn. 1.

$$\frac{X_m}{D_j} \propto Fr_j^{0.5} \quad (1)$$

Using the notation of integral scaling parameters, this can be re-written as Eqn. 2.

$$X_{mR} = D_{jR}^{0.5} l_R^{0.5} \quad (2)$$

For the 1/2 scale test facility at Argonne, where $D_{jR} = 1$ and $l_R = 0.5$, this yields $X_{mR} = 0.707$. Thus, the elevation of the scaled model hot outlet plenum, or the distance between the exit of the riser ducts and the ceiling of the exit plenum, was built to the scale of 0.707 of the full scale prototype.

1.4.2 Scaling Summary

As built, the NSTF reflects the primary design features of the full scale GA-MHTGR RCCS. The facility features twelve riser ducts at $1/2$ axial scale (l_R). Based on the full design basis of 227 total riser ducts, the resulting configuration reflects a 19.03° sector slice (\angle). A summary of the geometric and thermal hydraulic scaling parameters as applied to the model NSTF in comparison to the full scale GA-MHTGR prototype is provided in Tables 4 and 5, respectively.

Table 4: Geometric scaling comparison between full GA-MHTGR and model NSTF

Parameter	GA RCCS	ANL $1/2$ scale	Scaling Ratio
Height Scaling	1:1	2:1	l_R
Total RCCS Height	55.2 m	26 m	l_R
Heated Riser	13.86 m	6.82 m	l_R
Outlet Plenum Ceiling	1.83 m	1.47 m	$\sqrt{l_R}$
Heated Area	311.2 m ²	8.82 m ²	\angle, l_R
Riser Duct Count	$x227$	$x12$	\angle

Table 5: Scaling of heat removal specifications for full GA-MHTGR and model NSTF

Parameter	Scaling Ratio	Scenario	GA RCCS	ANL $1/2$ scale
Decay Power	$\angle, \sqrt{l_R}$	Peak, accident	1.5 MW _t	56.07 kW _t
		Normal	700 kW _t	26.16 kW _t
Heat Flux	$l_R^{-0.5}$	Peak, accident	4.82 kW/m ²	6.82 kW/m ²
		Normal	2.25 kW/m ²	3.18 kW/m ²
Heated ΔT	1	Peak, accident	121°C	121°C
		Normal	67°C	67°C
System Flow Rate	$\angle, \sqrt{l_R}$	Peak, accident	12.2 kg/s	0.456 kg/s
		Normal	10.6 kg/s	0.396 kg/s

1.5 Testing Program

Across a 33-month testing period, performance metrics were assessed by varying parameters of integral power, power profile, chimney configurations, discharge elevations, and inclement weather. Off-normal testing was performed to establish a performance envelope during scenarios of blocked riser channels, chimney by-pass leakages, and non-air gas ingress. Lastly, special considerations were made to include full-scale features and operating conditions, such as adjacent chimney roles, cosine power shaping, and the full time history of one Safety Related Design Condition (SRDC-II).

Each test averaged 82 hours in duration, and testing was performed year-round to capture a wide range of ambient weather conditions. Across the full series, the project examined system behavior with ambient outdoor temperatures as low as -18.1°C and as high as 32.1°C . A total of 2,250 hours of active test operations were conducted and resulted in 16 accepted test cases. However, not all test cases were successful in meeting the target objectives; out of the 27 total performed, 11 were unable to meet the full stated objectives. These cases were classified as either “trending” if usable data could still be preserved, or “failed” if the test as a whole was unable to add any meaningful data to the test records. Failure mechanisms included hardware faults, weather induced instabilities, or energy balance deficiencies.

A summary of all the test cases completed by the project conclusion is provided for those accepted in Table 6, and those failed or trending in Table 7.

Table 6: High level testing summary - Accepted cases

Test Type	Test Number	Date	Duration	Classification	Primary Objectives	Flow Path
Baseline	DataQuality004	April 2014	49h 52m	Accepted	Test series kick-off	Natural, Dual vertical
	DataQuality011	January 2015	52h 47m	Accepted	Mid-project baseline	Natural, Dual vertical
	DataQuality020	September 2015	52h 8m	Accepted	Hot weather baseline	Natural, Dual vertical
Scaling	DataQuality005	May 2014	30h 05m	Accepted	Low power study	Natural, Dual vertical
	DataQuality008	July 2014	51h 09m	Accepted	Reduced chimney discharge	Natural, Reduced discharge
Chimney roles	DataQuality017	June 2015	58h 38m	Accepted	Adjacent chimney study	Natural, Adjacent
	DataQuality024	April 2016	145h 50m	Accepted	Single chimney	Natural, Single vertical.
Power Shaping	DataQuality013	March 2015	72h 05m	Accepted	Mid-plane cosine	Forced, Reduced discharge
	DataQuality022	January 2016	120h 8m	Accepted	Bottom-peaked cosine	Natural, Dual vertical
	DataQuality026	May 2016	97h 38m	Accepted	Azimuthal, 65/35%	Natural, Dual vertical
GA-MHTGR	DataQuality014	April 2015	130h 28m	Accepted	SRDC-II, winter months	Natural, Dual vertical
	DataQuality018	August 2015	129h 55m	Accepted	SRDC-II, summer months	Natural, Dual vertical
Performance	DataQuality015	May 2015	82h 53m	Accepted	Blocked riser tubes	Natural, Single vertical
	DataQuality027	June 2016	30h 07m	Accepted	Heavy gas (argon) ingress	Natural, Single vertical
Weather	DataQuality007	June 2014	13h 28m	Accepted	Inclement weather start-up	Natural, Reduced discharge
Collaboration driven	DataQuality023	February 2016	190h 20m	Accepted	INERI test series	Forced, Reduced discharge

Table 7: High level testing summary - Failed and trending cases

Test Type	Test Number	Date	Duration	Classification	Primary Objectives	Failure Mode
Baseline	DataQuality001	February 2014	28h 10m	Failed	Test series kick-off	Energy balance (inadequate insulation)
	DataQuality002	February 2014	49h 46m	Trending	Test series kick-off	Energy balance (inadequate insulation)
	DataQuality003	March 2014	50h 02m	Trending	Test series kick-off	Mechanical (fan loft discrepancy)
	DataQuality019	August 2015	9h 08m	Failed	Hot weather baseline	Electrical (cDAQ failure)
Chimney roles	DataQuality006	May 2014	52h 45m	Trending	Single chimney	Electrical (heater load failure)
	DataQuality016	June 2015	9h 06m	Trending	Adjacent chimney study	Weather (unable to establish flow)
Power Shaping	DataQuality009	August 2014	48h 27m	Trending	Mid-plane cosine	Weather (reversal)
	DataQuality010	August 2014	50h 12m	Failed	Mid-plane cosine	Weather (reversal)
GA-MHTGR	DataQuality012	March 2015	116h 26m	Trending	SRDC-II, summer months	Electrical (heater load failure)
Performance	DataQuality025	May 2016	9h 8m	Failed	Heavy gas (argon) ingress	Weather (early reversal)
Collaboration driven	DataQuality021	October 2015	56h 21m	Trending	INERI test series	Energy balance (inadequate electric power)

This page was intentionally left blank.

Chapter 2

Experiment Method

The intent of the testing program at ANL is to generate Type-A data, as defined by the INL Data Qualification guidelines [13], for licensing and code validation purposes. Not including shakedown and scoping tests, those tests performed for the purposes of data generation per NQA-1 guidelines began with the drafting and formal review of a procedural document. This control document identifies the test objectives, details the step-by-step operator actions, and provides the required acceptance criteria. Attached to each procedure is a full collection of data acquisition channel listings, engineering drawings identifying the location of each instrument, and a print-out of the relevant software and computer configurations. Additionally, the calibration of each sensor was verified to be valid prior to the start of every data quality test. At the conclusion, these documents were archived into the control document set of the NSTF project, and the run was classified according to the following metrics [13]:

Accepted Data - Test was performed fully within scope and defined procedures. Submit for data qualification and Type-A evaluation.

Trend Data - Some aspects of the test fell outside the intended scope and defined procedures, however still performed within NQA-1 guidelines. Data set may still be valuable for an intended use.

Failed Data - Test was not successful and fell well outside the intended scope and defined procedures. Likely the test was not realized through completion. Discard data.

The naming of each test was chosen based on the purpose and quality level required for the testing objective:

DataQuality0NN - formal test for data collection per NQA-1 guidelines

Run0NN - alternate name for DataQuality0NN, common for figures and analysis

SPEF0NN - formal test for the purposes of generated data for separate effects testing, geared directly towards supporting analysis development

Scoping0NN - informal testing used to examine new configurations or procedures

BakeOut0NN - informal testing used to prepare materials and facility components

2.1 Primary Testing Objectives

Data quality testing, defined as tests conducted with full verification of procedures and calibrated instrumentation by NQA-1 standards, was initiated early 2014 and extended through late 2015. The following section outlines the parameters of primary interest and also provides a test matrix outline. Each test spans approximately 2 weeks, which is largely due to the exhaustive quality assurance procedures to be performed at the start and conclusion of each test. The actual test itself spans duration between 24 - 96 hours.

Of primary interest are areas of heat flux variation (integral levels and profiling), scaling verification, mimicking of a typical accident scenario, investigations of chimney roles, and performance testing. Within the subset of chimney roles we are particularly interested in the start-up procedure as initial scoping tests suggested a strong sensitivity to ambient weather conditions during system start up. Thus certain tests have been repeated as weather conditions change and sometimes preceded other scheduled tests, altering the proposed testing order. Additionally, the effect of varying chimney roles has been studied, including a prototypic scenario where one chimney serves as the fresh air intake while the other as a traditional exhaust (adjacent chimney roles). An outlined summary of our primary testing parameters is provided on the following page.

1. Shakedown/Calibration
 - (a) Conduct electrical, power, and instrumentation system shakedown tests, carry out insulation and ceramic heater bake-out procedure
 - (b) Verify gross system mass flow rate measurement methodology
 - (c) Isothermal facility characterization (e.g. frictional losses)
 - (d) Separate effects turbulence data for modeling efforts and analysis program
 - (e) System energy balance verification tests and characterization of facility heat loss
2. Baseline testing
 - (a) Conduct a baseline test at nominal conditions: 1) full exit plenum elevation, 2) flat profile, 1.5 MW_t scaled power, 3) full stack cross-section and height, and 4) nominal riser tube setback
3. Scaling
 - (a) Integral heat source variation
 - i. Steady state heat removal (700 kW_t)
 - ii. Accident decay heat power (1,500 kW_t)
 - (b) Heat source profiling
 - i. Cosine power profile
 - ii. Azimuthal power profile
 - (c) Reduced chimney discharge elevation
4. GA-MHTGR accident scenario
 - (a) Seasonal influence (summer, winter)
5. Variations of chimney roles
 - (a) Single chimney configuration
 - (b) Adjacent inlet / outlet chimney roles
6. Performance Testing
 - (a) Blocked riser channels
 - (b) Short-circuit inlet and outlet ducting
 - (c) Non-air gas ingress
 - (d) Forced flow testing at baseline conditions
7. Start-up procedure investigations
 - (a) Time varying loafer position
 - (b) Inclement weather start-up
8. Repeatability and collaboration driven testing
 - (a) Repeatability of baseline test case at regular intervals
 - (b) I-NERI work scope, driven by international collaborators

2.2 General Test Procedure

Independent of the specific test objective, each test (run) shared a similar procedure that is heavily guided by NQA-1 best practices for experimental test operation. A detailed test procedure (e.g. ANL-NSTF-000000-TEST-0NN) is drafted prior to the start of each test, and includes requisites for personnel training, test objectives, instrumentation records, etc. Along with up-to-date drawings, data acquisition channel listings, calibration reports, and software configurations, these documents are bundled together in formal test report that is archived with each test. An outline of the typical procedure is given below:

1. Administrative prerequisites
 - (a) Review of primary testing objectives and training of involved personnel
 - (b) Documentation of facility configuration, including engineering drawings, data acquisition channel listings, software configuration, and calibration records
 - (c) Notification of personnel in laboratory space
 - (d) Designated of access control areas
2. Pre-test verification
 - (a) Establishment of a stagnation period of no less than 5 days to ensure that any residual heat was dissipated from the structure and that the facility was allowed to reach thermal equilibrium with the ambient surroundings
 - (b) Check of working operation of all data acquisition channels, including documenting any abnormal sensors or open thermocouples
 - (c) Characterization of the isothermal facility by establishing zero-flow conditions
 - (d) Verification of working operation of anticipated engineering controls / user input

3. Hold point

- (a) Critical point in test procedure that ensures all prior steps must be completed prior to commencing active test operations

4. Power on and active test operation

- (a) Initialization of active heater system and deployment of power ramp, typically 120 minutes to desired electric power as to prevent thermal shock and allow gradual rise in system temperatures
- (b) Steady-state observations, including monitoring key system parameters to identify test acceptance criteria that typically state stable operation for a period of 6 hours
- (c) Upon reaching acceptance criteria, initiating power down ramp

5. Post-test operation

- (a) Verification on data acquisition channels, and documentation of any new sensors that appear abnormal or deviated from pre-test verifications
- (b) Archiving of generated data sets and verification that data has been properly logged
- (c) Characterization of isothermal facility by establishing cold-shutdown, zero-flow conditions

6. Post-test review

- (a) Documentation of testing results in a Preliminary Test Acceptance Report (PTAR)
- (b) Review and signing of control documents (TEST, PTAR) by key project personnel

This page was intentionally left blank.

Chapter 3

Test Assembly Description

The following sections detail the engineering specifications, design features, and dimensions of the test facility at Argonne. Details of structural and mechanical systems will be presented first, followed by ducting components, heated cavity, and finally a stand alone section on the various insulating materials used. Relevant engineering drawings have been included after each section in their original format.

3.1 Base Support and Cavity Framework

The structural base assembly that supports the primary test assembly components was manufactured from W12x65 I-beam sections and weighs approximately 30,000 lbs. Base supports, six in total, extend to the concrete floor and are secured by four 1.25” bolts. The total height of the assembly is 6’ tall, Figure 5.

Resting on top of the base support is a U-channel framework that serves as the structural support for the heavy steel assemblies that make up the heated cavity, Figure 6. Built in two sections; each is constructed of ASTM A36 channels, four MC12x45 and two MC6x18, that join onto 1” steel plates to makeup the skeletal framework.



Figure 5: Base support



Figure 6: Lower skeleton framework

3.2 Flow Path Ducting

3.2.1 Inlet Downcomer

The air supply to the NSTF enters through an inlet downcomer, an uninsulated 24” diameter duct that provides a means to stabilize and measure the incoming flow, Figure 7. The inlet downcomer begins with a vertical straight length, 90° elbow, and finally horizontal straight, which combined span an equivalent length (distance along centerline of ducting segments) of 184.5”.

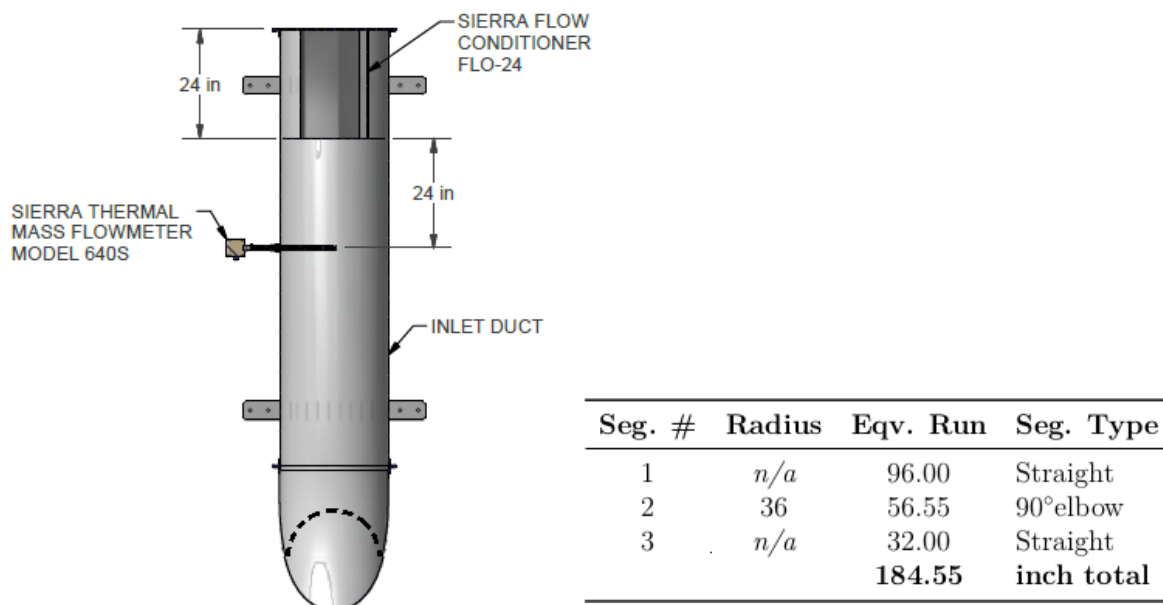


Figure 7: Inlet downcomer (front view) and equivalent segment lengths

We have positioned a Sierra flow conditioner, Figures 8 - 9, which sits at the top edge of the duct and extends 24” deep as a means to establish a fully developed inlet flow profile. Along with the entrance and exit lengths, these design choices are driven by an experimental requirement to accurately measure the inlet flow conditions.



Figure 8: Flow conditioner

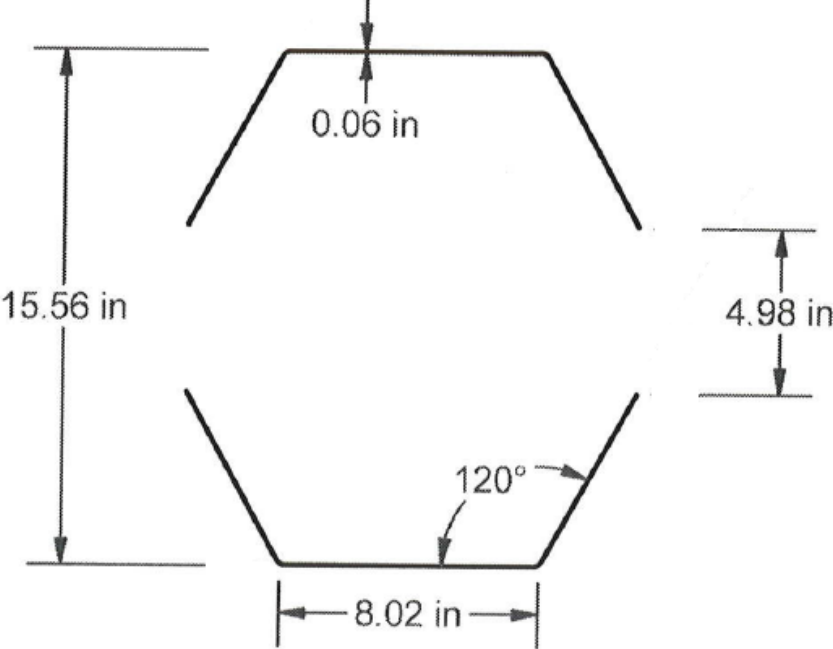


Figure 9: Geometric dimensions (plan view)

3.2.2 Inlet Plenum

The inlet plenum is a large volume that provides an essentially zero pressure boundary condition for the incoming air from the downcomer to distribute among the twelve riser channels, Figure 10. The assembly is constructed from 1/8" thick aluminum alloy 3003. The total available volume of the inlet plenum is 78 ft³ (2.21 m³). A divider plate reduces the available area for air flow to 41.7 ft³ (1.18 m³). The unused back cavity is insulated and available for access should maintenance be required.

The configuration of the inlet plenum mates the downcomer ducting to the center of the west plenum wall. There are also two additional potential inlet ports, one each on the North and South walls of the inlet plenum. These are blanked off in the current configuration. The centerline of each of the three inlet ports measures 16" from the bottom, and all are centered along their respective widths (33" for the north and south ports, 52" for the primary west port).

To facilitate instrument placement for measurement of the inlet flow conditions into twelve riser tubes, the ducts extend 7" below the ceiling of the inlet plenum. The inlet plenum ceiling contains twelve slots for this purpose, and the slotted joint is sealed against air leakage by a Kevlar wrap. The purpose of this slotted design is to allow unconstrained movement due to thermal expansion, as a fixed support would induce significant stress onto the steel riser ducts. During steady-state experimental operating temperatures the riser ducts will expand upwards approximately 1-cm.

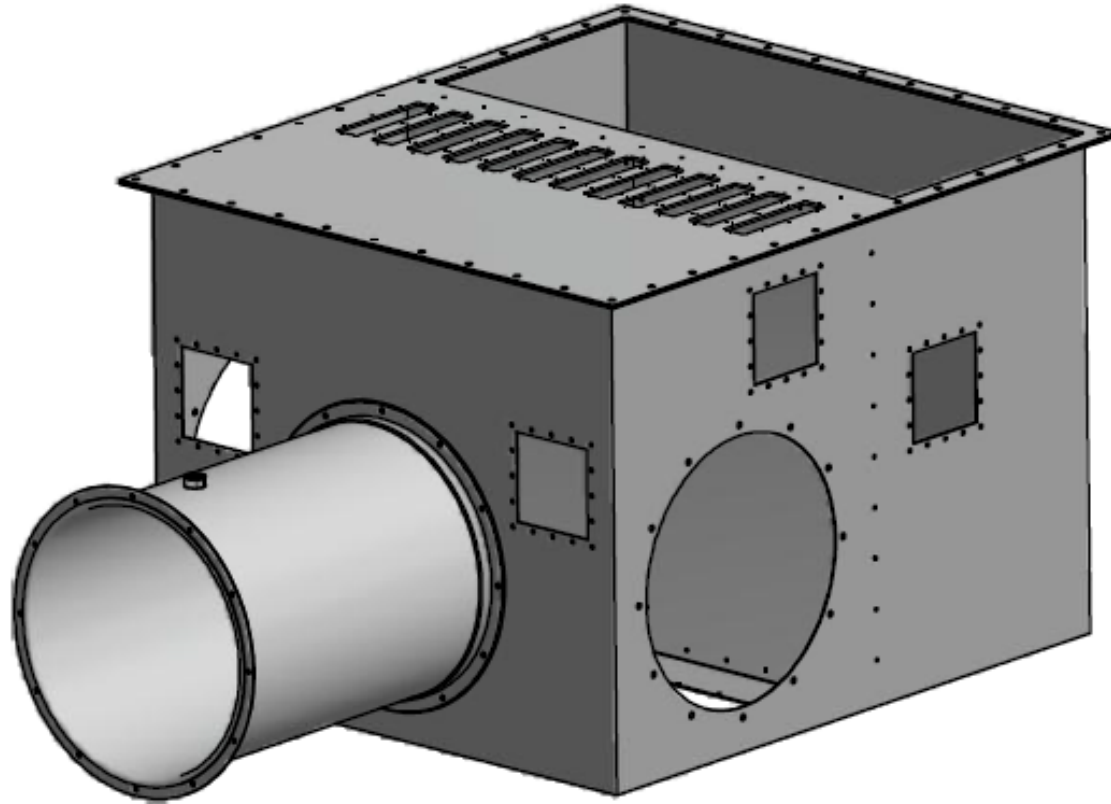


Figure 10: Inlet plenum. Duct stub shown connects to inlet downcomer, rectangular slotted holes connect to riser ducts. Interior volume measures 44" tall, 51.75" width (parallel to riser slots), and 59.75" deep, of which only 31.75" is available for the working gas due to the present of the false back wall.

3.2.3 Riser Ducts

The NSTF houses twelve riser ducts as the primary flow area test section, and are constructed from welded structural rectangular steel tubing, ASTM A 500 Grade B. The cross-section dimensions are duplicate of the full scale GA-MHTGR design, and measure 10"x2"x0.188", at an approximate weight of 385 lbs / riser, Figure 11. The length of each duct measures 295"; however, only 272" resides within the heated cavity due to the 7" extension below into the inlet plenum and 16" above into the outlet plenum.

The combined weight of the twelve tubes totals 4,620 lbs and required creative mounting methods to omit the need for rigging the full assembly. Each riser tube features a 3/8" plate that has been welded 16" below the top lip as a means to support the individual tubes. The installation process required hoisting above the outlet plenum, and dropping each duct through a slotted support plate into the heated cavity. The plate, manufactured from 1" thick ASTM A 36 steel and weighing approximately 1,820 lbs, bears the full load of the ducts and is secured to the support structure, Figure 12.

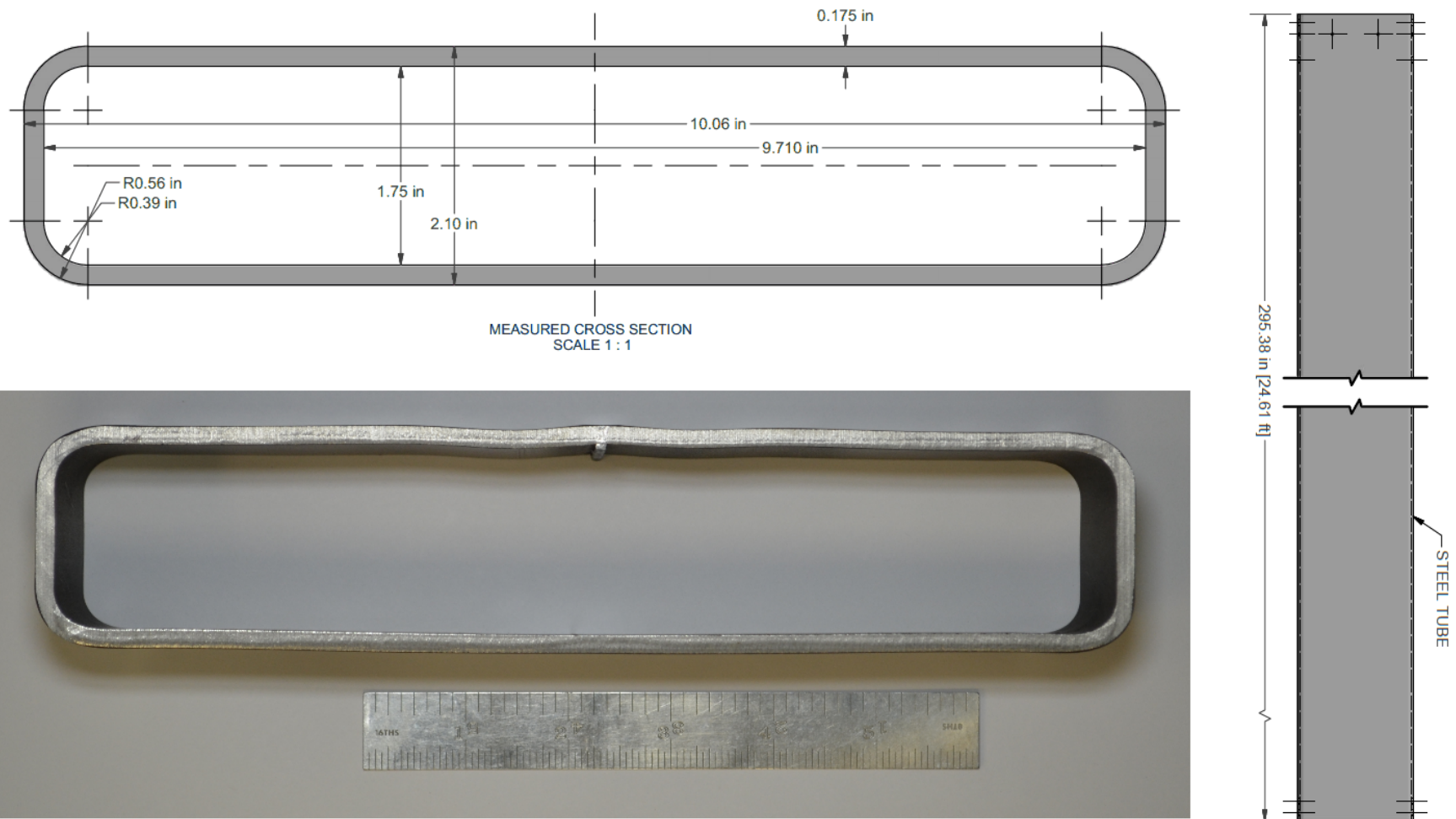


Figure 11: Cross section of riser ducts (dimensional drawing above, picture below)



Figure 12: Top plate which bears the weight of the twelve riser ducts

3.2.4 Outlet Plenum

Upon exiting the riser individual riser ducts, heated gases combine in the upper plenum and exhaust into the dual symmetric chimneys, Figure 13. The riser tubes protrude 16" past the floor of the outlet, allowing access to the instrumentation ports. Additionally, this extended length reduces the effort when installing a false-floor, since the riser tubes can be kept in their position without reconfiguration.



Figure 13: View into the outlet plenum from opened east wall. False west wall visible behind riser tubes

The plenum interior measures 74" tall, 87" east/west, and 64" north/south. The plenum features adjustable false-floors and walls as a means to adjust the inside volume. The as-built design consists a false wall on the westward side, reducing width (west - east) from 87" to 74". The interior volume measures 203.8-ft³ (5.77-m³), which is reduced by the false west wall from the total available volume of 240-ft³ (6.79-m³). The 24" diameter ports, which

serve as the entrance into the chimney ductwork on the north and south facing walls, are positioned at the plenum centerline (east-west) and elevated 56.5" from the plenum floor, or 40.5" above the top surface of the riser tube end. The centerline of the riser tubes is offset westward by 16.5" from the chimney ports center. With the added 3" of insulation, the riser ducts exit face extend 13", and the centerline of the chimney ports 53.5", above the insulated floor.

The exterior paneling on the outlet plenum consists of five similarly designed sub-assemblies, which are constructed in the same fashion as the heated cavity west wall panels: a steel angle (L3x2x1/4") framework that contains 6" of insulation, and is protected on both inside and outside facing walls by 1/8" thick aluminum sheets. Each panel weighs approximately 800 lbs., and has mounting provisions for hoisting and lifting operations. An exploded view of the north and south panels is shown below in Figure 14, and an east-west cross section of the entire outlet plenum and paneling in Figure 15.

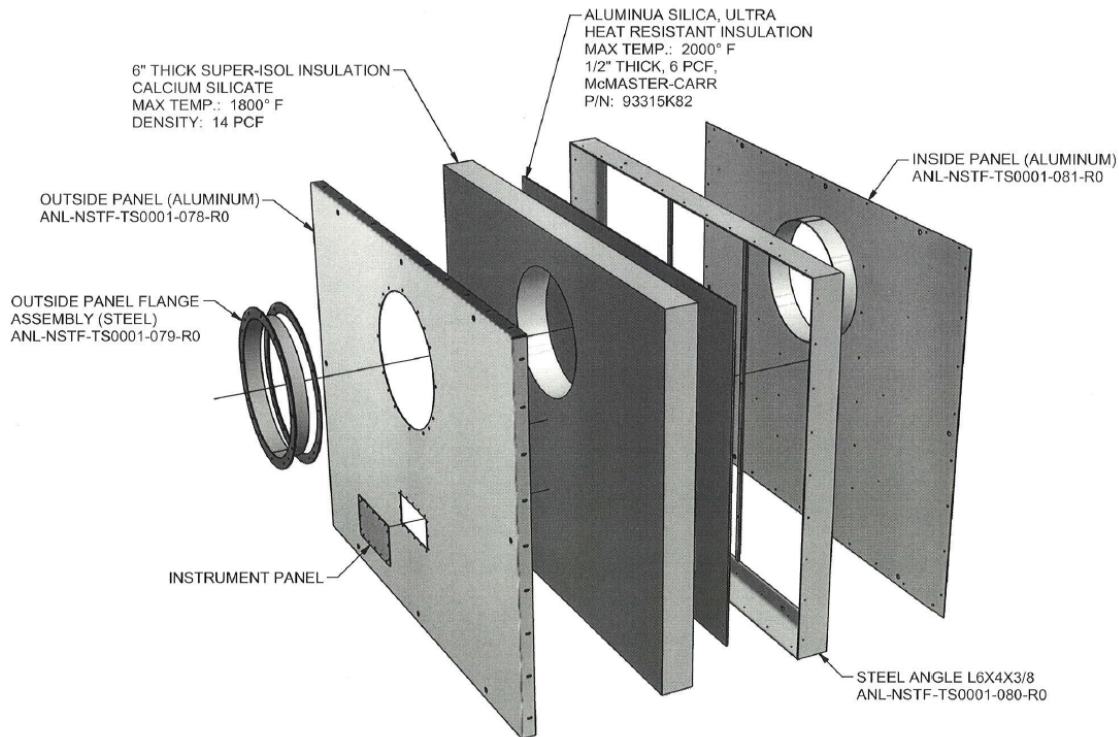


Figure 14: Exploded view of north/south panels on outlet plenum

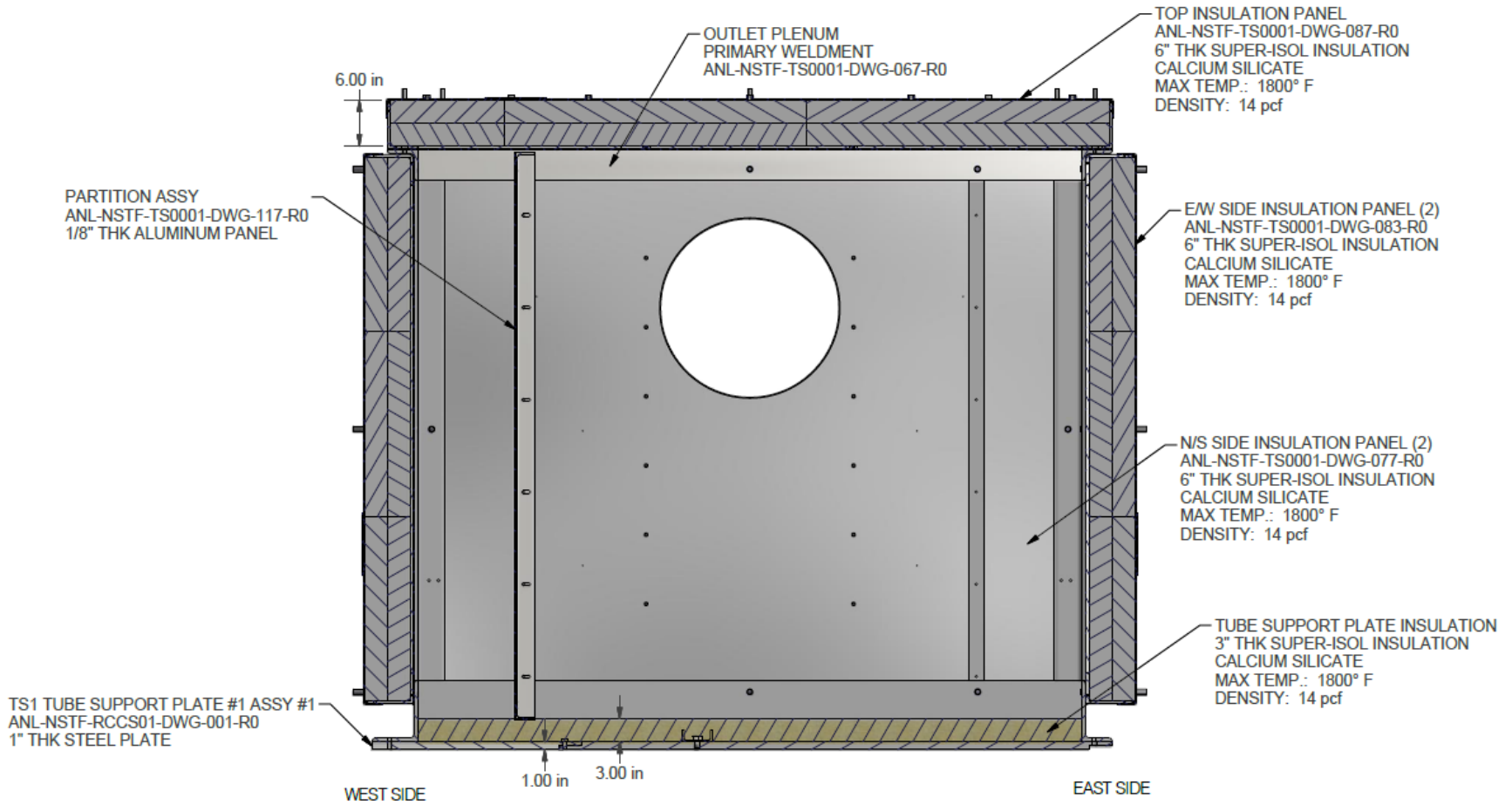


Figure 15: Cross section (east/west) of outlet plenum and surrounding insulation panels

3.2.5 Chimney Stacks

The chimney in the NSTF consists of dual ductwork assemblies that provide the necessary driving head and chimney effect to transport the heated gases to the outside environment. The ducts, constructed from 24" diameter, 14 gauge galvanized steel, and are wrapped in 3" of mineral wool followed by a 0.016" protective aluminum jacket. The ductwork model was designed to preserve the thermal hydraulic flow patterns observed in full scale simulations while also catering to the physical requirements of the building space. Thus, the end product is an intricate flow path that includes multiple elbows of varying degrees, vertical, horizontal, and sloped duct runs. A design priority was placed on flexibility in forming alternative networks for varying flow path configurations. Included are five butterfly valves (loafers) and two forced fan loft blowers for isothermal testing, Figure 16.

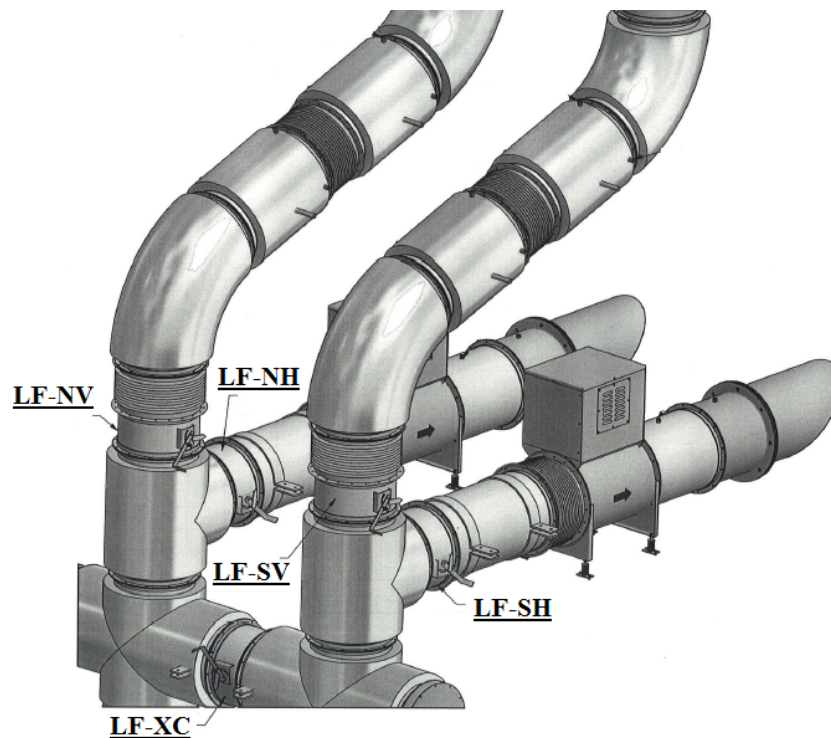


Figure 16: Variable component locations on chimney ducting. Five butterfly valves and dual forced blowers

The five butterfly valves are mounted with electronic actuators, Honeywell MS7520A2205, to allow remote positioning of the valves by an operator. The actuator units receive a 2 - 10 volt DC control signal and proportionally adjust the position of the damper blade within the valve. They are able to control positions between 0 and 90° in 3° increments, and require 90 seconds to traverse a full rotation. The flow area as a function of actuator position is shown in Figure 17.

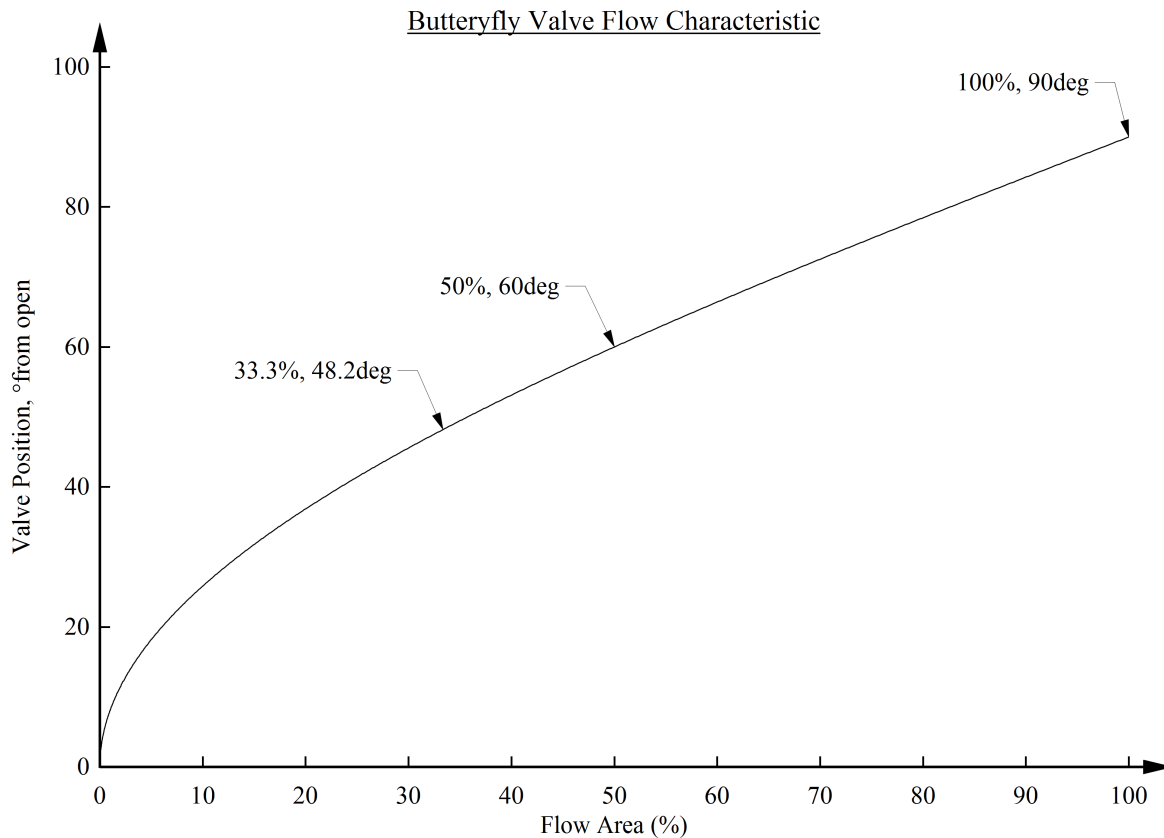


Figure 17: Valve position and resulting chimney duct flow area

Vertical and Horizontal Exhaust Configurations

The standard or baseline configuration for the chimney duct work removes the heated gas via both north and south segments along the full elevation of the network piping, ultimately exiting from the vertical stacks extending through the building’s roof. The alternative configuration, which is used during isothermal benchmarks or at a reduced atmospheric discharge, closes the vertical stack dampers and vents air through the building’s east wall. Either flow path runs through a network of segments, comprised of elbows, straight lengths, bellows, damper valves, and etc..

The equivalent flow paths, as measured from the exit of the outlet plenum, measures 826.13” for the vertical and 470.37” for the horizontal configurations. A detailed breakdown of the various network segments for both configurations is provided in Table 8.

Table 8: Ducting segment types and equiv. lengths for horizontal and vertical flow paths

Seg. #	Radius	Eqv. Run	Seg. Type	Seg. #	Radius	Eqv. Run	Seg. Type
1	36” in	56.55”	90°elbow	1	36”	56.55”	90°elbow
2	36in	28.27	45°elbow	2	36	28.27	45°elbow
3	<i>n/a</i>	22.00	Straight	3	<i>n/a</i>	22.00	Straight
4	36	28.27	45°elbow	4	36	28.27	45°elbow
5	<i>n/a</i>	13.75	Bellows	5	<i>n/a</i>	13.75	Bellows
6	36	56.55	90°elbow	6	36	56.55	90°elbow
7	<i>n/a</i>	13.75	Bellows	7	<i>n/a</i>	13.75	Bellows
8	<i>n/a</i>	42.00	4-way	8	<i>n/a</i>	42.00	4-way
9	<i>n/a</i>	40.00	Tee (straight thru.)	9	20	31.42	Tee (side port)
10	<i>n/a</i>	12.00	Valve	10	<i>n/a</i>	12.00	Valve
11	<i>n/a</i>	13.75	Bellows	11	<i>n/a</i>	43.00	Straight
12	36	44.61	90°elbow	12	<i>n/a</i>	13.75	Bellows
13	<i>n/a</i>	36.13	Straight	13	<i>n/a</i>	31.06	Fan blower
14	<i>n/a</i>	13.75	Bellows	14	<i>n/a</i>	30.00	Straight
15	<i>n/a</i>	36.13	Straight	15	<i>n/a</i>	48.00	Tapered straight
16	36	44.61	90°elbow			470.37	inch total
17	<i>n/a</i>	324.00	Straight				
		826.13	inch total				

3.2.6 Forced Blower Fans

Two fan loft blowers, model 24 AFB-H purchased from Air Products Equipment Co., are powered by 3-phase 460VAC power and controlled by a variable frequency drive (VFD) up to 1,725 RPM. They are able to withstand temperatures up to 500°F, and thus suitable for active heating operation in the NSTF. The primary purpose of these blowers is to obtain isothermal flow to benchmark and verify the working state of instrumentation. They also provide a safety mechanism in the event of an overheated temperature condition. A relation to the flow rate and driven frequency of the twin fan loft blowers is provided in Figure 18.

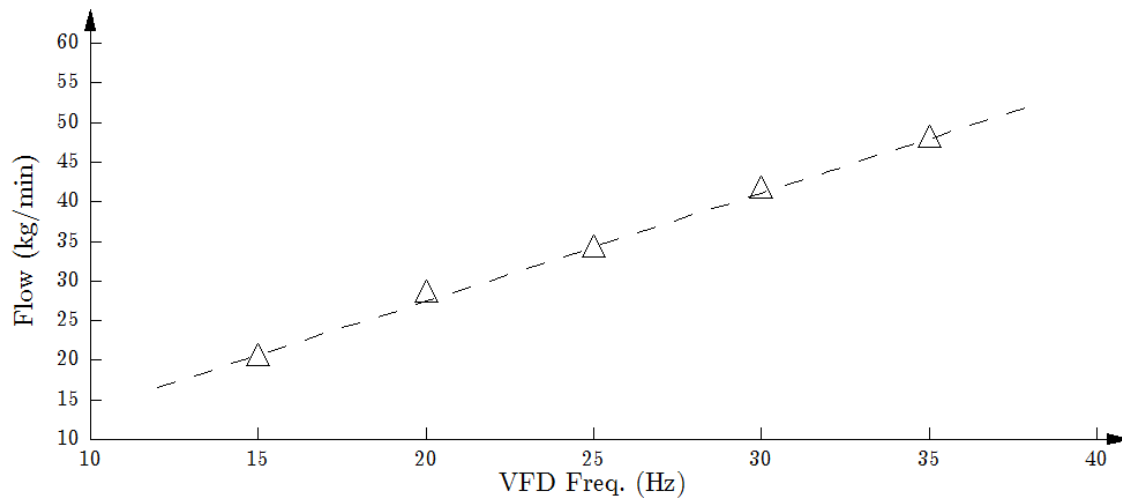


Figure 18: Flow vs frequency for dual fan loft blowers

3.3 Heated cavity

The primary test section of the NSTF is an insulated enclosure that provides a means of heat transfer from the radiant heater source (simulated reactor vessel) to the twelve riser ducts, and is built around the U-channel structural framework. The other three sides are adiabatic. This heated enclosure has an overall height of 22-ft (6.7-m), a width of 52" (132-cm) and has an adjustable cavity depth that can range from 17.7" to 59" (45 to 150-cm) in increments of 1" (2.5-cm), Figure 19. The spacing between the front facing surfaces of the riser tubes and heated plate used for the first round of test operations measures 27.82" (706.55 mm), and the area for heat transfer off the primary heated plate measures 109.6 ft² (10.18 m²).

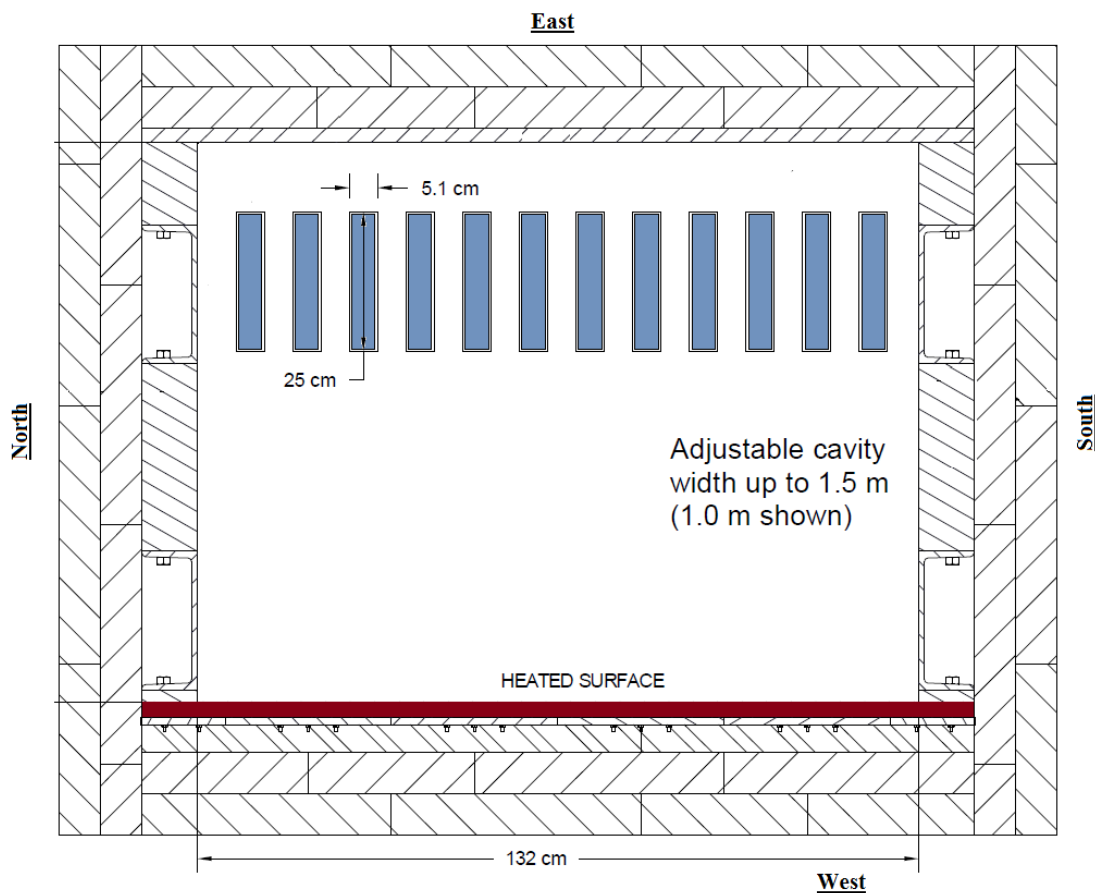


Figure 19: Plan view of NSTF heated cavity and test section. Heater surface is shown in red, riser ducts in blue. Hatched perimeter denotes insulated areas

3.3.1 Unheated Paneling

The insulated panels on the north and south walls are placed on hinges that facilitate removal and access without needing to perform a major disassembly. Twenty-four panel assemblies are required to cover the full area of the north and south walls. Each panel measures 67"x21", and is constructed from 6" of insulation (facing inward), and protected by 16 gauge aluminum alloy #3000, on the outward surface. The hook and groove mounting channels secure to 1/2"-13 steel spacing studs placed across the width of each U-channel, and when fully installed allow for complete enclosure and isolation of the heated interior from the ambient surroundings.

The four panels on the west wall are constructed from a steel angle (L3x2x1/4") framework that contains 6" of insulation, and is protected on both inside and outside facing walls by 1/8" aluminum. Each panel weighs approximately 267 lbs., and has mounting provisions for hoisting and lifting operations.

3.3.2 Heated Wall

The heated east wall comprises a nine-layer composite to provide the necessary structural support for the massive steel plate, provide an efficient means for heat transfer, and also insulate the system from parasitic heat losses. These nine layers were constructed and installed as three separate sub-assemblies: two vertical primary plates, four rows of heater sub-panels, and four rows of outside insulation panels. An air gap separates the 1st and 2nd, and a thin buffer layer of insulation separate the 2nd and 3rd.

3.3.3 Primary Heated Plate

To accurately represent the heat flux condition off the walls of a prototypic RPV, the primary heat source in the NSTF (electrically powered radiant heaters, detailed in later sections) are placed behind a 1" steel plate as a means to smooth any sharp temperature gradients from the hot coils while also providing the necessary emissivity for radiation heat transfer to the riser tubes. Figure 20 shows the lower plate in preparation for installation, including temporary eye bolts needed to hoist the 2,230 lb plate onto the structural framework.

This plate is fabricated from SAE 1020 low carbon steel which has stated ladle composition limits given as 0.18% - 0.23% C, 0.30% - 0.60% Mn, 0.040% P_{max} , 0.50% S_{max} , and Fe being the remaining constituent. The surface condition of the back plate is mill scale oxidized so that its emissivity was initially in the 0.7 to 0.9 range. This emissivity was measured prior to test operations and was found to average 0.78 - 0.79 [14] The same plates were used from the early PRISM/RVACS work, a project at ANL which investigated a similar concept for passive decay heat removal. Early reports have mentioned that the researchers hand selected these plates based on uniformity and surface condition which had a thin surface scale that was an electrically nonconducting oxide with a dull dark-purple coloration. Furthermore, they add that surface deformation by grinding for welding and thermocouple spot welding was kept at a minimum.

The primary heated plate has enlarged mounting holes to allow for thermal expansion in all directions. The plate is hung to structural support structure, separated by 2" spacers and insulation, so that the heater plate subassembly is allowed to expand horizontally and vertically. Figure 21 shows dimensions and mounting points for the lower plate.

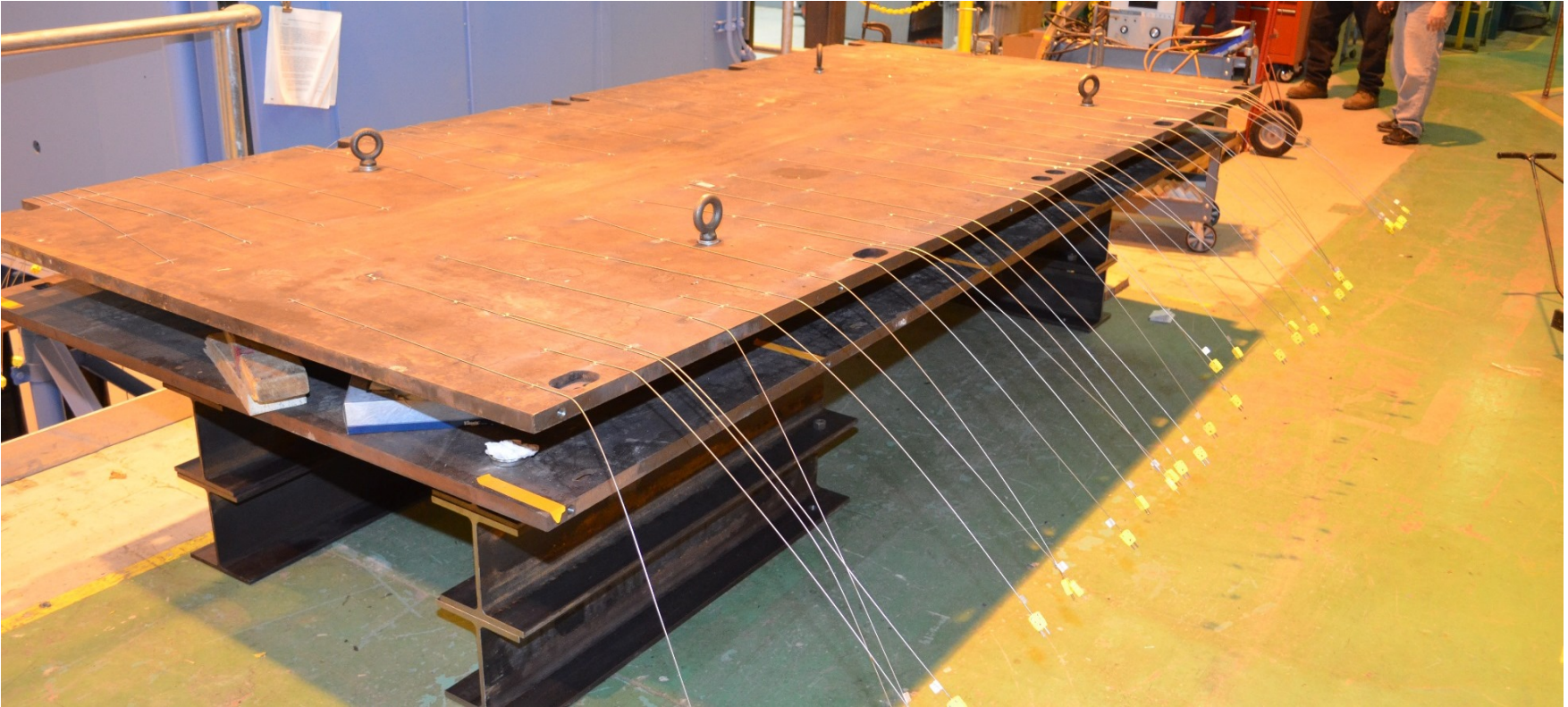


Figure 20: Lower heated plate prior to installation. Eye hooks were temporarily installed for lifting, thermocouples visible

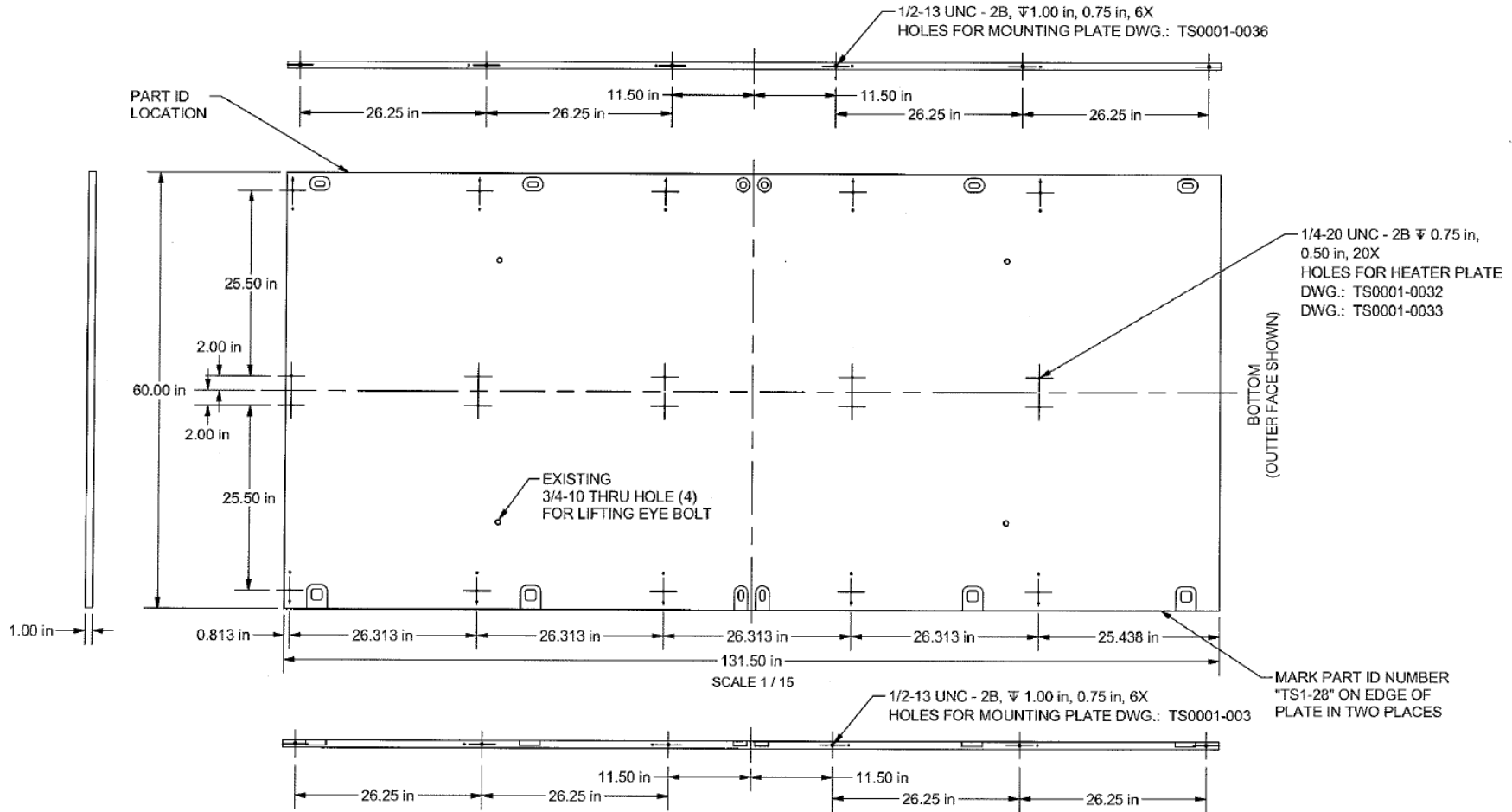


Figure 21: Dimensions and mounting hole specifications of primary heated plate (top shown)

3.3.4 Heater Subpanels

The heater sub-panels, ten in total, serve as the primary area for power control, heat transfer, and insulation for the 220 ceramic heater plates. The mounting system, Figure 23, positions the radiant coils of the heaters away from the test section as a means to provide uniformity in the heat flux across the plate. This setup also minimized the risk of electrically shorting out the heater coils against any neighboring conductive materials.

The stainless steel sheets were sandblasted and then heat treated to 1900°F to relieve internal and surface stresses. The sandblasting process was performed to enhance the surface emissivity of the sheets from about 0.25 to about 0.90 uniformly over both sides of the sheets, significantly improving heat transfer and temperature uniformity, and thereby reducing the chance of warping the stainless steel sheet. The ceramic heaters (detailed in the following section) are fastened to the steel sheet with 10-32 size studs that are welded to the steel sheets. Each heater subassembly contains twenty ceramic plate electric heater elements (6-in x 12-in). The 16 central heater elements are one heater zone, and the four edge heater elements compose the second heater zone on the 2-ft x 5-ft heater plate subassembly.

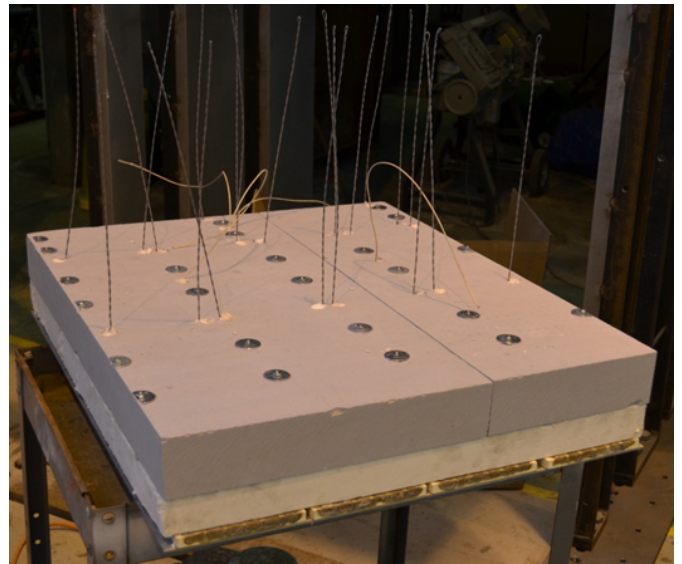
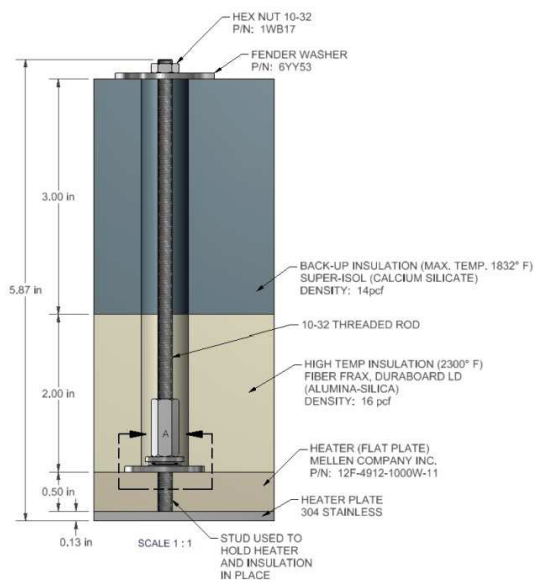


Figure 22: Heated wall, heater subpanel assembly

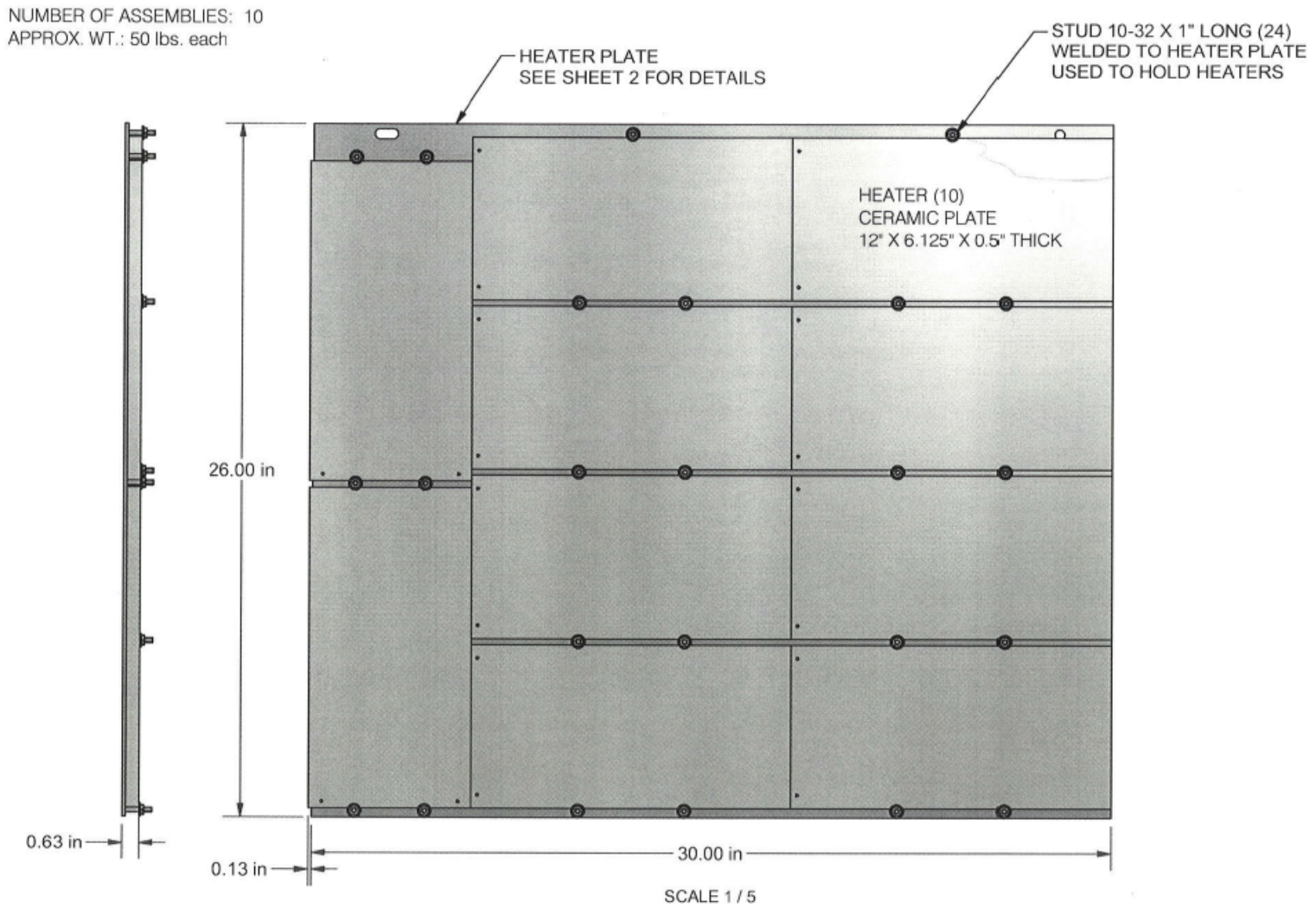


Figure 23: AutoCAD drawing of heater subpanel with ceramic heaters outlined

3.3.5 Ceramic Heaters

The heat source within the NSTF comprises an array of radiant heaters powered by 480 and 240 VAC. 200 individual ceramic heaters, each measuring 6"x12"x0.5", are capable of supplying up to 1,100 W each, totaling a maximum available power of 220 kW_e. These 200 individual plates are grouped into 40 control zones, 20 designated as the "main" and 20 as the "guard" zones. Each "main" consists of 8 ceramic heater plates, while each "guard" consists of two ceramic heater plates, Figure 24. The parallel series connections of each Main and Guard result in 120 VAC across any individual heater element.

These 40 control zones produce a power distribution that provides 80% of the total from the Main and the remaining 20% from the Guard zones. For the purposes of test operations, power is primarily supplied to the Main zones while the Guards are adjusted to maintain a uniform temperature distribution across the heated plate, minimizing thermal gradients and reducing stresses.

3.3.6 Heated Wall Insulation Panels

The outside insulation panels on the heated wall, installed in four vertical rows, are constructed from framed assembly that is similar to the opposing cold wall insulation panels. A sheet metal framework houses two stacks of 3" insulation (6" in total), and is protected on the exterior surface by 1/8" aluminum sheet metal panel. Each panel weighs approximately 270 lbs., and has mounting provisions for hoisting and lifting operations.

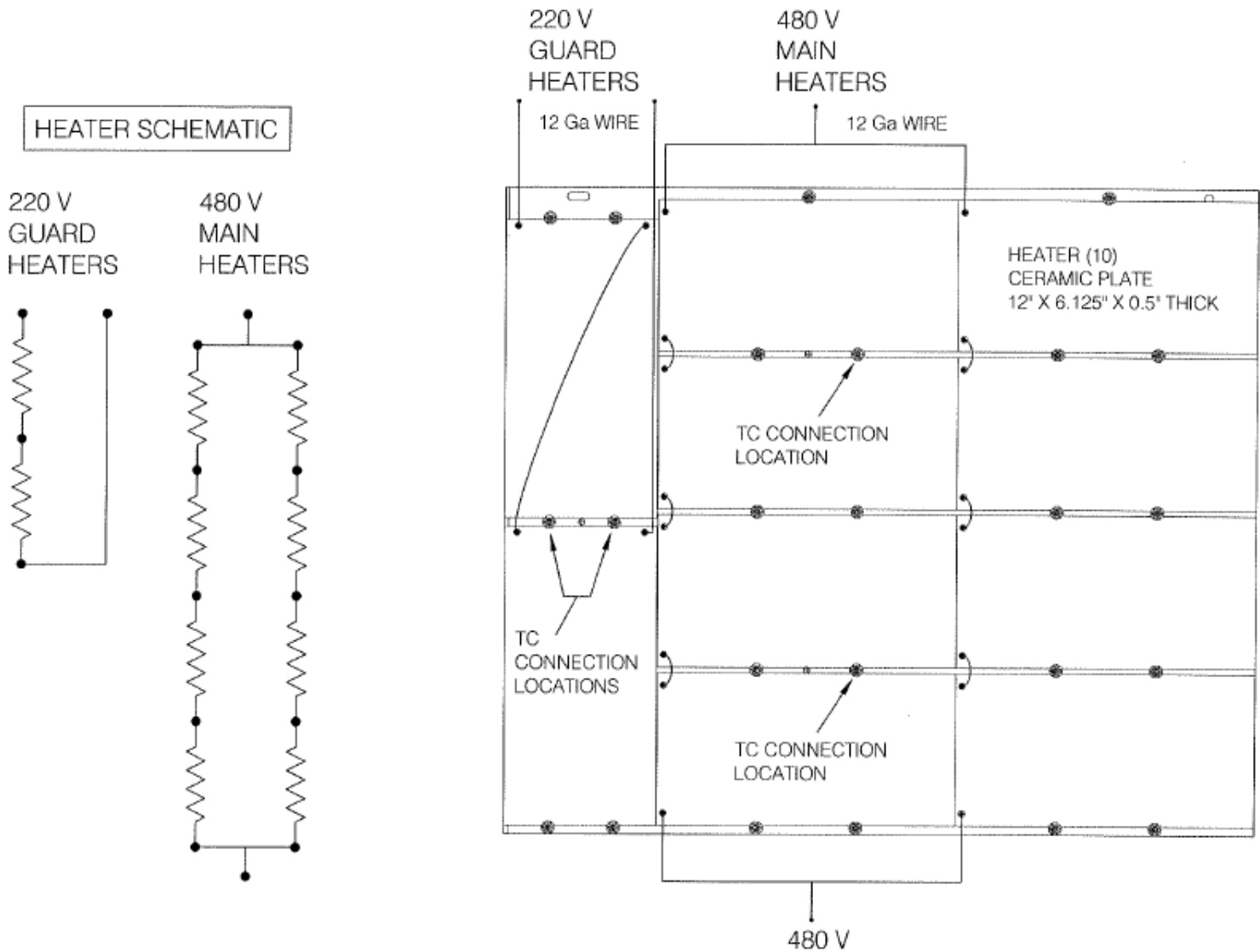


Figure 24: Electrical detail of Main and Guard heating zones

3.4 Insulation

In an effort to reduce heat losses to the ambient surroundings, the NSTF is heavily insulated in primary control areas at or after the heat source. Non-insulated areas include the inlet downcomer, inlet plenum, and horizontal chimney ducts. SuperIsol[®] was used on all test section insulated panels and walls. Duraboard LD[®] was used as the backing for the ceramic heaters. Energywrap 80[®] was used for the chimney ductwork. Durablanket S[®] was used as filler and patchwork in smaller areas throughout. Thermal specifications and properties of the insulation materials used are provided in Table 9.

Table 9: Material and thermal specifications for NSTF insulation

Name	Thickness	Max Temp	Density	Thermal Conductivity (BTU-in/hr-ft ² -°F)		
Super Isol [®]	3"	1,800 °F	16 pcf	400 °F 0.416	750 °F 0.554	1100 °F 0.693
Duraboard LD [®]	2"	2,300 °F	16 pcf	400 °F 0.55	1000 °F 0.847	1600 °F 1.339
Durablanket S [®]	1"	2,150 °F	8 pcf	600 °F 0.56	1000 °F 0.977	1600 °F 2.003
Energywrap 80 [®]	3"	1,200 °F	8 pcf	200 °F 0.30	400 °F 0.42	600 °F 0.59

Figure 25 shows a north facing cross section of the heated cavity, which identifies the various types of insulation and thicknesses used to retain thermal energy within the enclosure. The north and south walls (not shown) are of similar construction to the west wall, and ultimately include the same 6" thickness of Duraboard LD[®] insulation. The east (heated) wall comprises a matrix of different materials, which was necessary to ensure compliance with the elevated temperatures found nearest the ceramic heaters. Insulation on the 24" ductwork is included for all duct length with the exception of the inlet piping and horizontal fan loft forced blower segments. Nominally 24" inner diameter, a layer of 3" thick mineral wool insulation surrounds the bare ducts, which is covered by a 0.016" aluminum jacket.

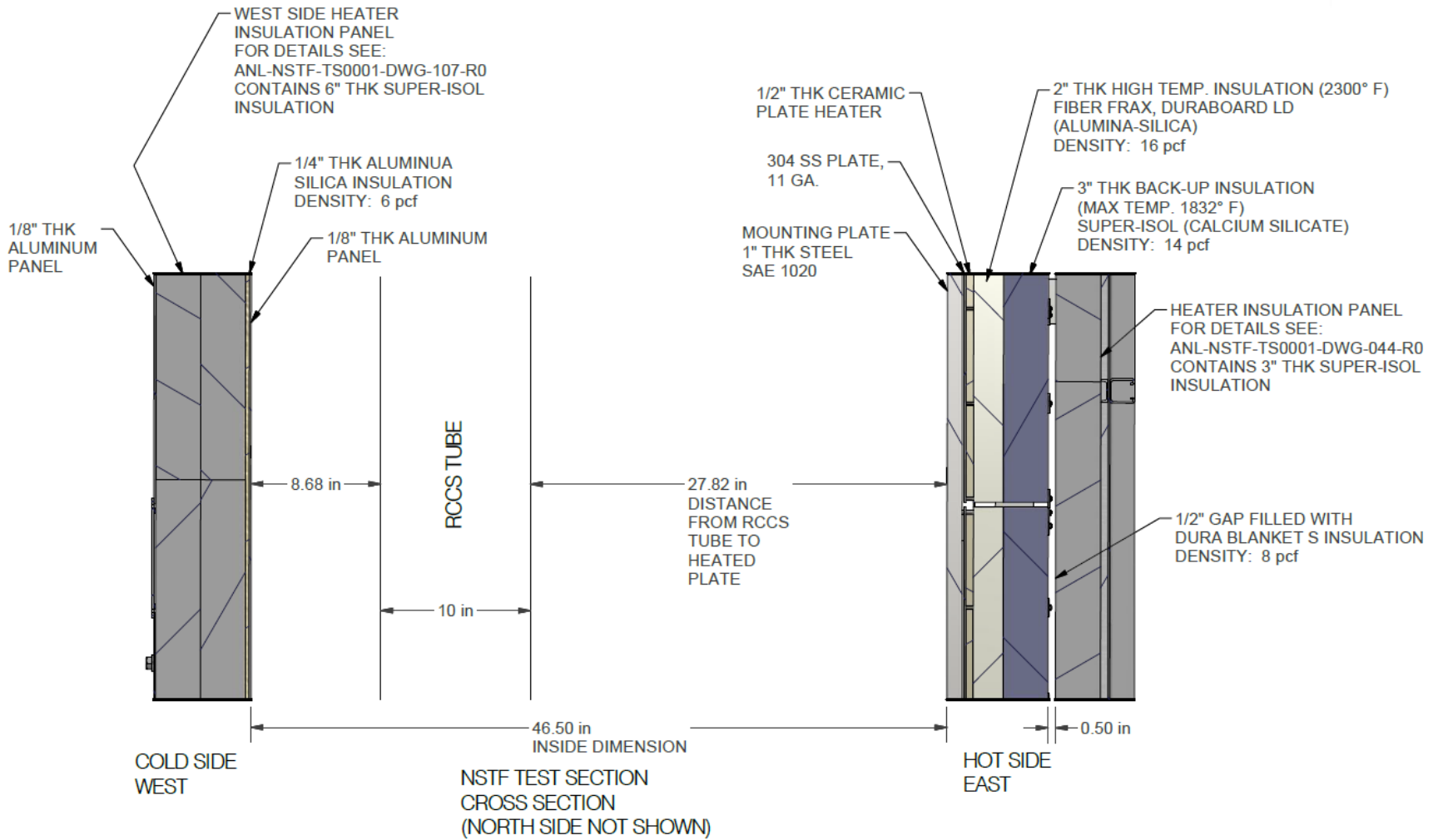


Figure 25: Cross section of heated cavity outlining areas of insulation. Viewed from a north facing perspective

3.5 Operating Flexibility

The initial design philosophy of the NSTF has resulted in a high level of flexibility in the available configurations for testing. Since a final design for an air-based RCCS has not yet been constructed on a full scale, nor has an exact design been decided upon by US vendors, this flexibility has allowed the project to maintain relevance as the RCCS design and technology matures. Furthermore, it has allowed the project to create a diverse range of testing conditions. In addition to the normal boundary conditions of power and spatial profiling of the heater surface, other areas for reconfiguration include the floor and wall spacing of the outlet plenum, heated plate to riser setback depth, chimney flow routing, among others.

Arrays of valves allow for an experiment operator to introduce alternative flow path routing. Across the testing performed, the NSTF saw four primary configurations: baseline, reduced discharge, single chimney, and adjacent chimney roles. A summary of the components or features that can be adjusted to alter the configuration are summarized below in Table 10, along with a diagram depicting the possible chimney flow paths in Figure 26.

Table 10: Summary of adjustable features on the NSTF

Component	Ranges	Baseline Value
Heater Power	0 - 220 kW_e	78 kW_e
Heater Profile	Arbitrary across 40 zones	Linear
Flow operation	Natural, forced	Natural
Forced flow	0 - 1 kg/s	n/a
Riser - heater spacing	0.45 - 1.5 m	0.71 m
Riser flow area	0.078 - 0.155 m	0.155 m
Outlet plenum floor spacing	0 - 0.41 m	0.41 m
Outlet plenum depth	1.88 - 2.2 m	1.88 m
Chimney discharge height	7.7 - 19.6 m	19.6 m
Chimney flow area	0 - 0.58 m ²	0.58 m ²

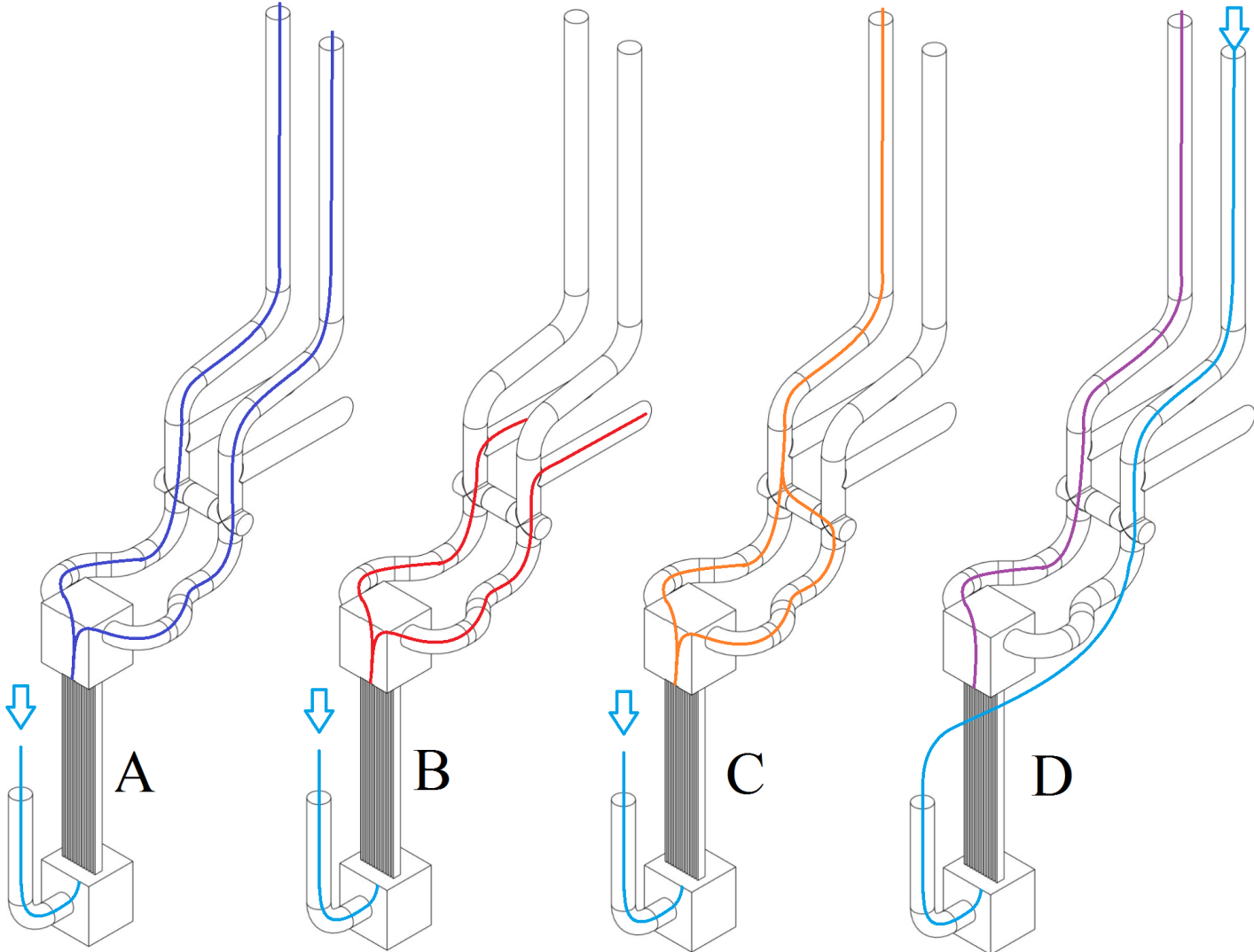


Figure 26: Facility configurations of chimney ductwork, arrow denotes air inlet. Blue (left): baseline, dual vertical, Red (left,center): reduced chimney discharge, Orange (right-center): single chimney vertical, Purple (right): adjacent inlet/outlet

3.6 As-built Summary

Described in sections above, the NSTF is a highly flexible experimental apparatus that can be re-configured to different testing states with minimal or reduced effort. The areas that have been designed specifically for reconfiguration include the heated wall to riser tube horizontal spacing, the extension of the riser ducts into the outlet plenum, and the presence of false walls on both the inlet and outlet plenum. These four areas are the primary variables that will be reconfigured in future test operations, but in their present state define the ‘as-built’ configuration of the NSTF, Figure 27.

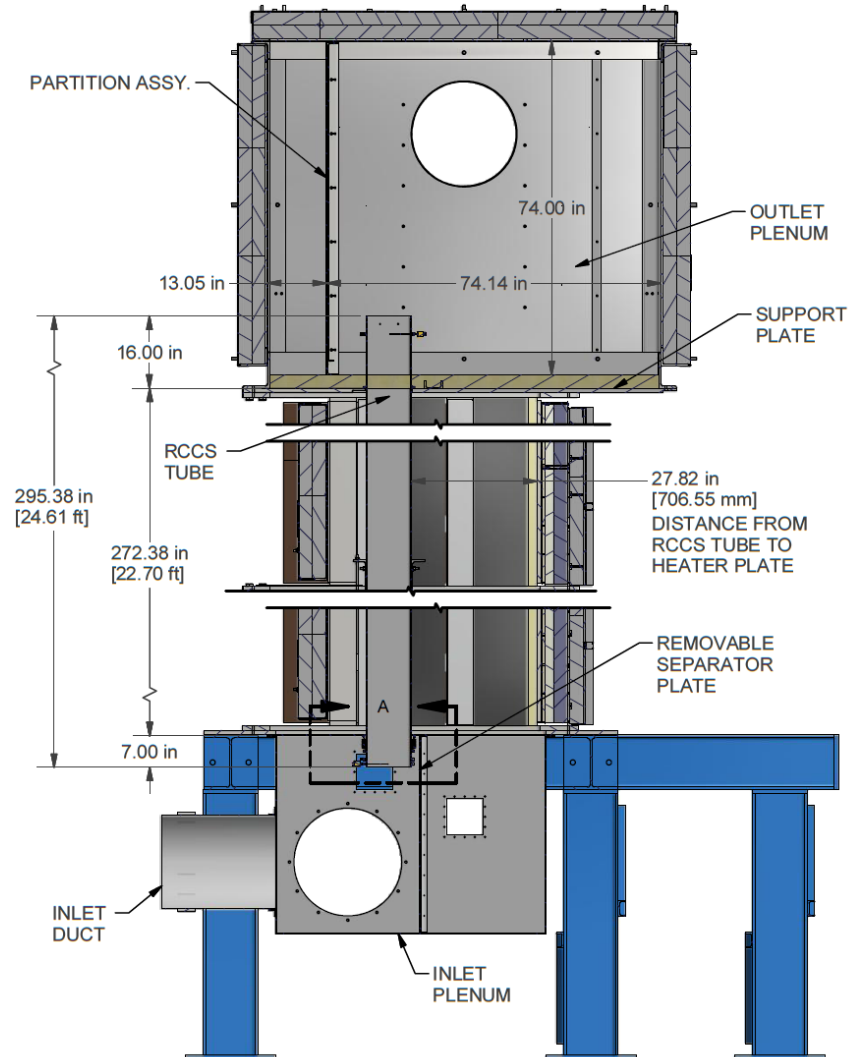


Figure 27: Primary areas of flexibility, dimensions shown for ‘as-built’ configuration

Chapter 4

Test Assembly Sensors & Control

The NSTF features a sophisticated suite of data acquisition and instrumentation for test operations in a dedicated control room, Figure 28. The data acquisition boards are placed at four points alongside the test section and routed to the central control station.

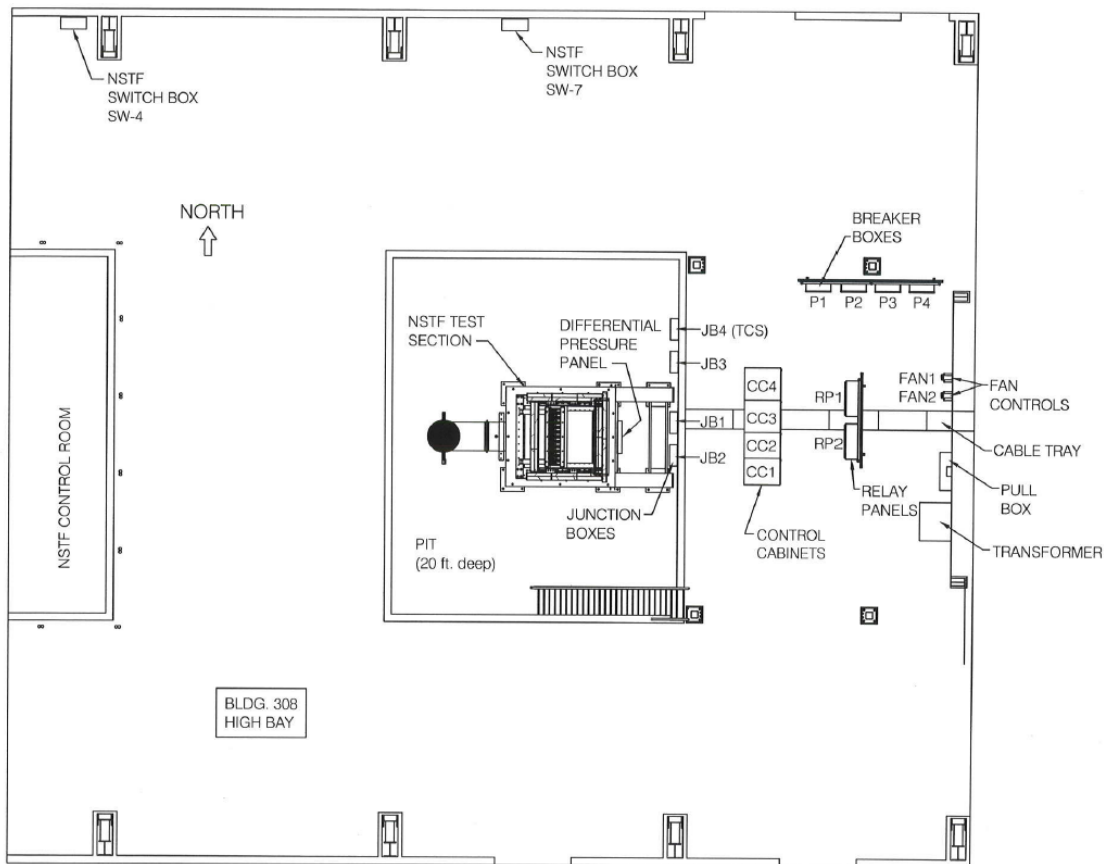


Figure 28: Plan view of Building 308 and NSTF test operations

4.1 Data Acquisition

The data acquisition and control suite comprises several individual devices that have all been linked to the primary control computer via TCP/IP and a central switch, Figure 29. This network was created to facilitate data logging and ensure synchronization across disparate devices. The control software is LabVIEW 2012, which interacts with all devices except the LUNA fiber optic system. The computational demands of the fiber hardware require a dedicated system, although remote viewing, control, and data file access are still possible during test operations.

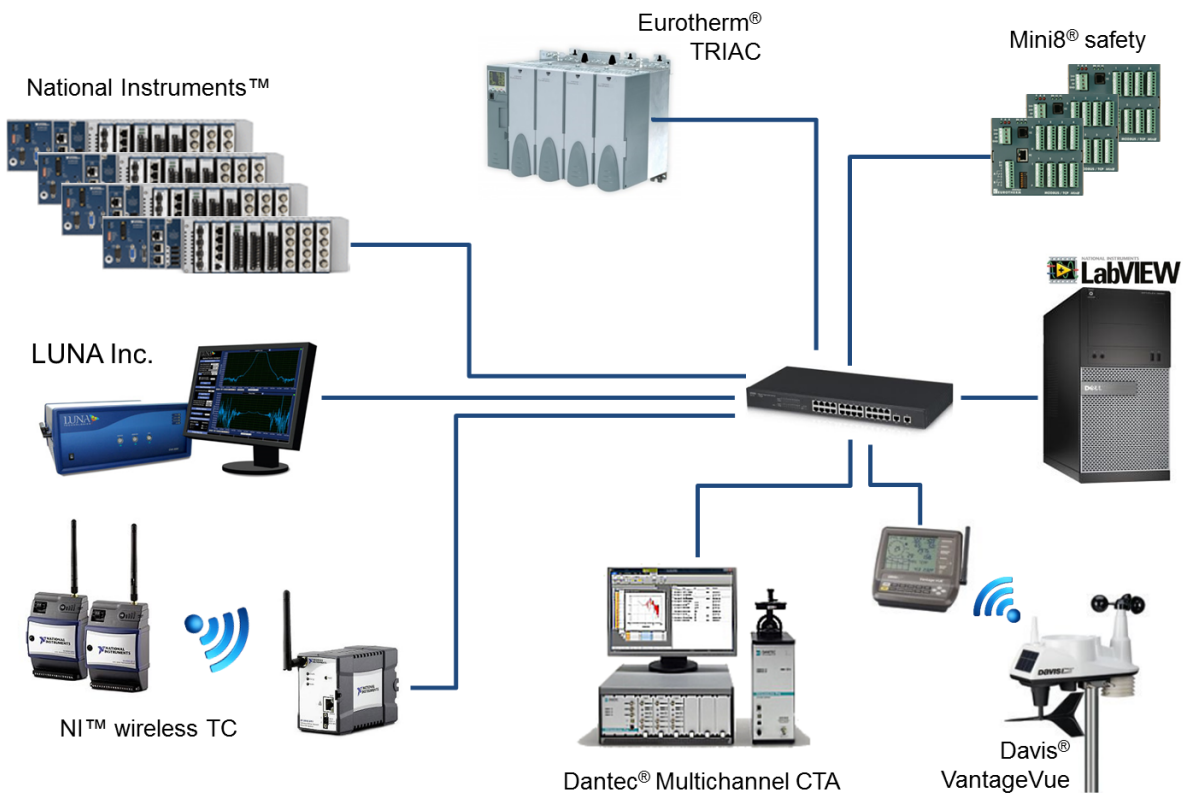


Figure 29: Communications overview

The core of the data acquisition system is four A/D converters housed in cDAQ chassis (cDAQ-9188 from National Instruments) which provide access to all the thermocouples, heat flux sensors, and analogue flow transmitters installed on the NSTF. Each cDAQ can be filled with up to eight cards for various analogue input/output requirements. The NSTF

is currently fitted with twenty-six NI-9214 cards, each able to read sixteen high-resolution thermocouple input channels. Additionally, two NI-9205 cards provide sixteen -10-10 VDC analogue input channels, and one NI-9265 provides four analogue output (4-20 mA) for control of the chimney damper actuators. To measure temperatures along the chimney duct work, we have installed four wireless thermocouple transmitters, National Instruments model WSN-3212, which can monitor and relay a total of eight thermocouples back to a wireless receiver and read into the primary LabVIEW software. A summary of these National Instrument devices is provided in Table 11.

Table 11: Summary of National Instruments data acquisition devices

Qty.	Model	Description
x4	cDAQ-9188	8 slot cDAQ chassis
x26	NI-9214	16-Channel Isothermal Thermocouple Input Module
x2	NI-9205	32-Ch ± 200 mV to ± 10 V, 16-Bit, 250 kS/s Analog Input Module
x4	WSN-3212	4 Ch, 24-Bit, Programmable Thermocouple Input Node
x1	NI-9265	4-Channel, 100 kS/s, 16-Bit, 0 to 20 mA Analog Output Module

4.2 Sensors

Sensors positioned along the test assembly measure local surface temperatures, local and bulk air temperatures, air volumetric and mass flow rates, the total normal radiative and convective components of the total heat flux, the electric power input to the heaters, and the local and total or bulk heat flux. These data will be used to evaluate the heat removal performance for particular configurations and testing conditions. The primary measurement objective is to determine the local and bulk heat flux transport rates and associated heat transfer coefficients.

The following sections will supply detailed information about the instrumentation, which consists of thermocouples, differential pressure transducers, radiation and heat flux transducers, mass flow meters, and the wind monitor and humidity instrumentation. An overview summary is provided in Table 12.

Table 12: Summary of NTSF instrumentation with listed accuracy

Measurement	Instrument	#	Range	Accuracy
Power	Eurotherm EPower	x40	0 - 12 kW	$\pm 1\%$
Heat flux	iTi Inc., model BHT	x16	0 - 300 kW/m ²	$\pm 5\%$
Temperature (Type-K TC)	Gas space	x34	0 - 1,250°C	$\pm 1.1^\circ\text{C}$ or 0.4%
	Riser wall	x32	0 - 1,250°C	$\pm 1.1^\circ\text{C}$ or 0.4%
	Heated plate	x125	0 - 1,250°C	$\pm 1.1^\circ\text{C}$ or 0.4%
	Insul. wall	x193	0 - 1,250°C	$\pm 2.2^\circ\text{C}$ or 1.1%
	Ceramic heater	x40	0 - 1,250°C	$\pm 2.2^\circ\text{C}$ or 1.1%
Mass flow rate	Sierra 640s	x1	0 - 1 kg/s	$\pm 1\% + 0.3\text{kg}/\text{min}$
Chimney velocity	Dwyer 160F	x2	$\pm 0 - 45\text{m}/\text{s}$	$\pm 8.3\%$
Riser ΔP	Dwyer 668-11	x8	$\pm 64\text{Pa}$	$\pm 1\%$
Chimney ΔP	Dwyer 607-0B	x2	$\pm 24\text{Pa}$	$\pm 0.5\%$
Humidity	Dwyer RHP	x1	3 - 95 %RH	$\pm 2\%$
Wind speed	Davis Vantage Vue	x1	1 - 80 m/s	$\pm 5\%$
Wind direction	Davis Vantage Vue	x1	0 - 360°	$\pm 3^\circ$
Outdoor humidity	Davis Vantage Vue	x1	1 - 100 %RH	$\pm 3\%$
Outdoor temperature	Davis Vantage Vue	x1	-40° - +65°C	$\pm 0.5^\circ\text{C}$
Rainfall	Davis Vantage Vue	x1	0 - 6553 mm	$\pm 4\%$
Barometric pressure	Davis Vantage Vue	x1	410-820 mmHg	$\pm 0.8\text{mmHg}$

4.2.1 Wall Thermocouples

The NSTF thermocouples (a total of 424) are type-K with an accuracy of $\pm 2.2^{\circ}\text{C}$ or 0.75% of measured temperature. Others, such as the riser inlet and outlet gas temperature, along with the heated plate surface temperature, are calibrated to special limits of error (SLE) and have an accuracy of $\pm 1.1^{\circ}\text{C}$ or 0.4%. The vast majority of these sensors are located on the heated plates and surrounding insulated panels. Sensors are flush-mounted for accurate measurement of surface temperatures without disruption of the flow field.

Figure 30 shows the installation method used for the heated plate TCs. Sensor wires were passed through the plates from the opposite side of the 1-in thick steel plates through a 5/32-in. dia. hole that is countersunk 90° to a 1/4-in. opening. A high-temperature thermal cement is used to bond junctions to the plate. Note that the wires are not joined at the junction and so the electrical circuit is completed through the steel plate. This allows detachment of the wire from the plate to be detected as an open circuit, which is not the case if the wires are bonded together at the junction as in conventional configurations.

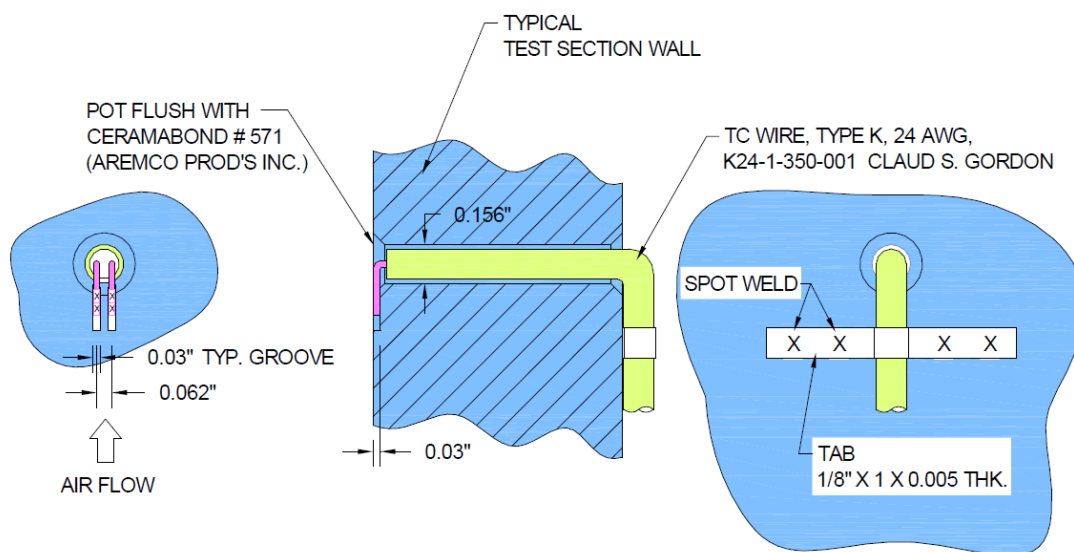
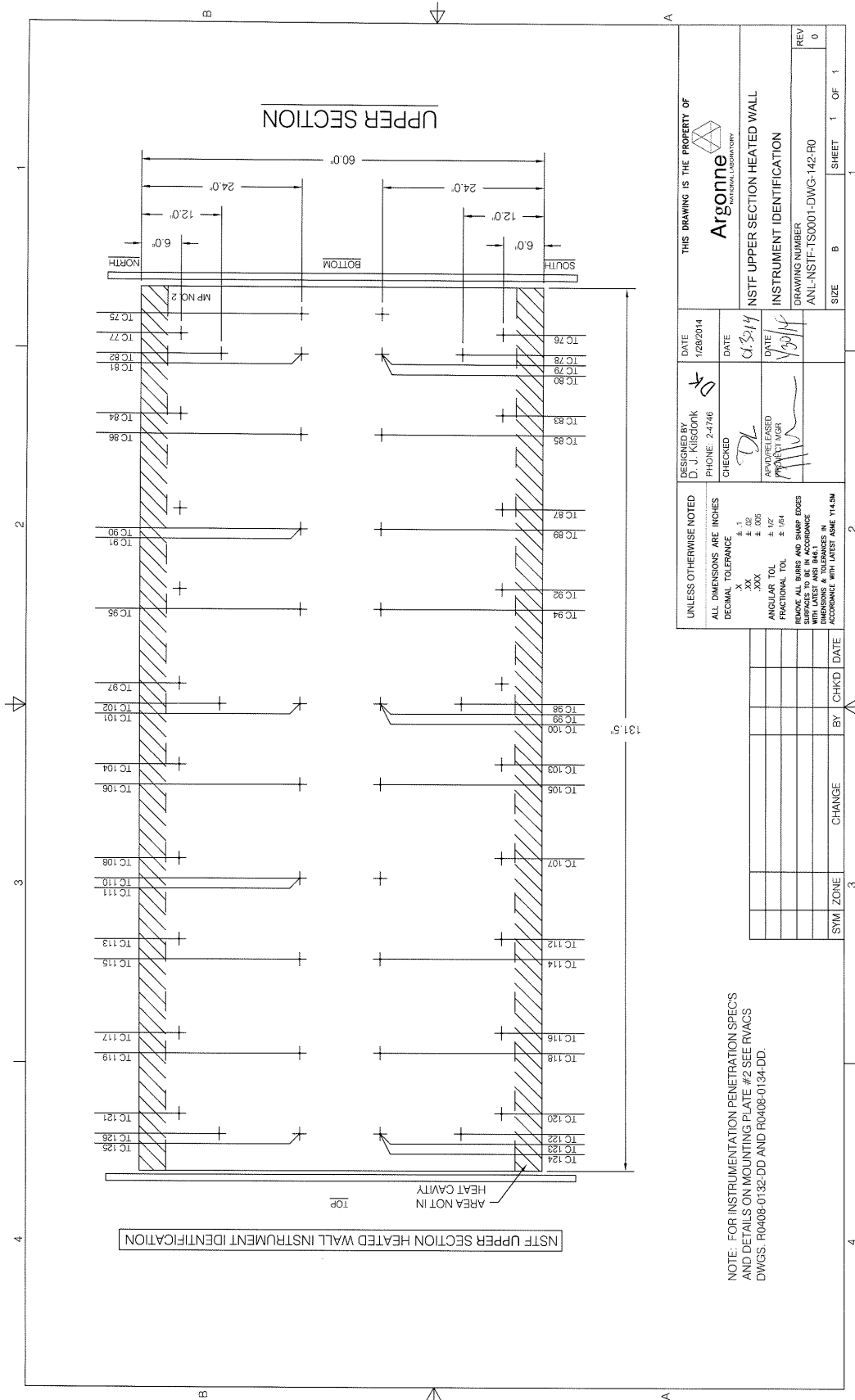
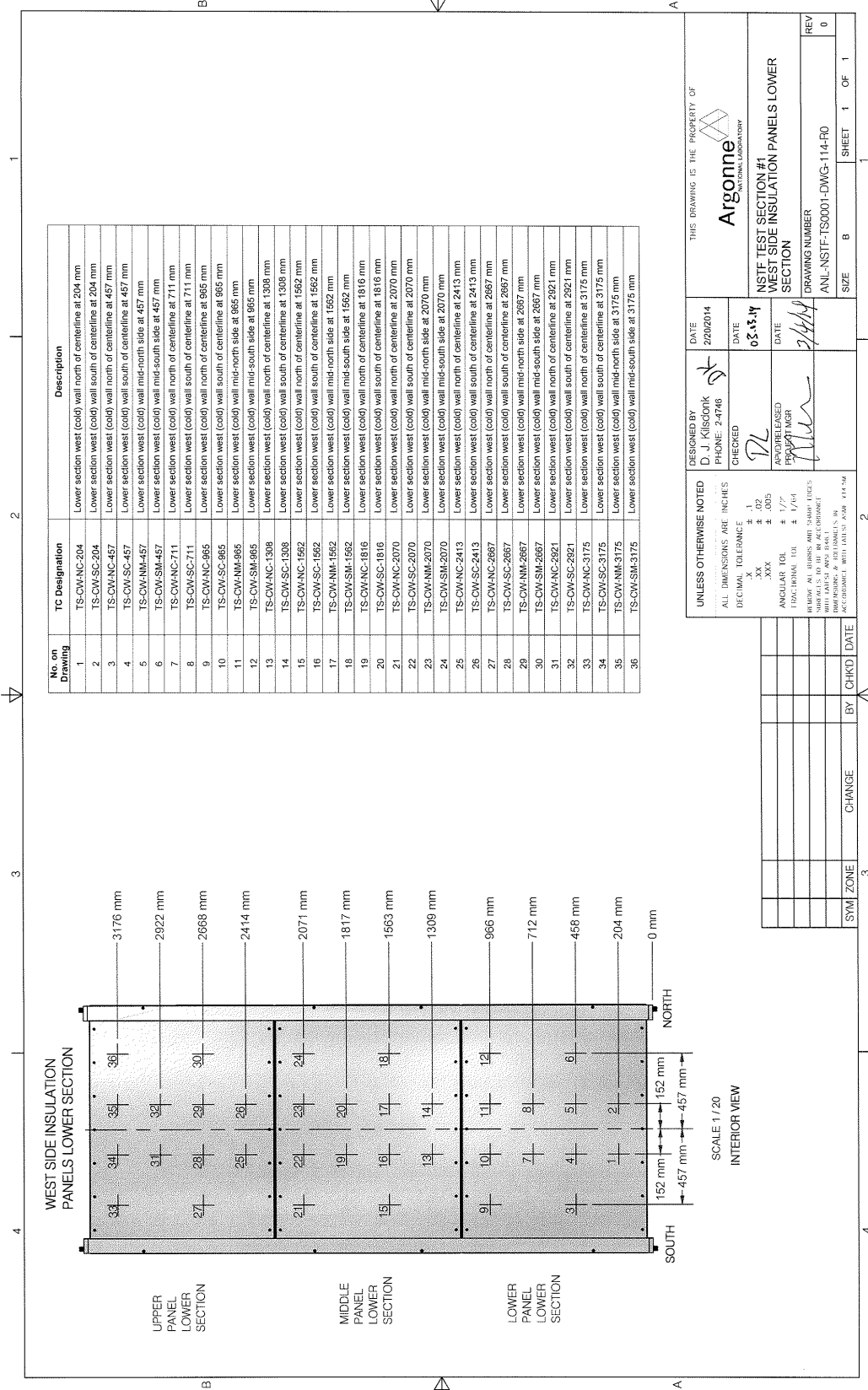


Figure 30: Heated plate thermocouple mounting method





No. on Drawing	TC Designation	Description
1	TS-CW-NC-204	Lower section west (cold) wall north of centerline at 204 mm
2	TS-CW-SC-204	Lower section west (cold) wall south of centerline at 204 mm
3	TS-CW-NC-457	Lower section west (cold) wall north of centerline at 457 mm
4	TS-CW-SC-457	Lower section west (cold) wall south of centerline at 457 mm
5	TS-CW-NM-457	Lower section west (cold) wall mid-south side at 457 mm
6	TS-CW-SM-457	Lower section west (cold) wall mid-north side at 457 mm
7	TS-CW-NC-711	Lower section west (cold) wall north of centerline at 711 mm
8	TS-CW-SC-711	Lower section west (cold) wall south of centerline at 711 mm
9	TS-CW-NC-965	Lower section west (cold) wall north of centerline at 965 mm
10	TS-CW-SC-965	Lower section west (cold) wall south of centerline at 965 mm
11	TS-CW-NM-965	Lower section west (cold) wall mid-south side at 965 mm
12	TS-CW-SM-965	Lower section west (cold) wall mid-north side at 965 mm
13	TS-CW-NC-1308	Lower section west (cold) wall north of centerline at 1308 mm
14	TS-CW-SC-1308	Lower section west (cold) wall south of centerline at 1308 mm
15	TS-CW-NC-1562	Lower section west (cold) wall north of centerline at 1562 mm
16	TS-CW-SC-1562	Lower section west (cold) wall south of centerline at 1562 mm
17	TS-CW-NM-1562	Lower section west (cold) wall mid-south side at 1562 mm
18	TS-CW-SM-1562	Lower section west (cold) wall mid-north side at 1562 mm
19	TS-CW-NC-1816	Lower section west (cold) wall north of centerline at 1816 mm
20	TS-CW-SC-1816	Lower section west (cold) wall south of centerline at 1816 mm
21	TS-CW-NC-2070	Lower section west (cold) wall north of centerline at 2070 mm
22	TS-CW-SC-2070	Lower section west (cold) wall south of centerline at 2070 mm
23	TS-CW-NM-2070	Lower section west (cold) wall mid-south side at 2070 mm
24	TS-CW-SM-2070	Lower section west (cold) wall mid-north side at 2070 mm
25	TS-CW-NC-2413	Lower section west (cold) wall north of centerline at 2413 mm
26	TS-CW-SC-2413	Lower section west (cold) wall south of centerline at 2413 mm
27	TS-CW-NC-2687	Lower section west (cold) wall north of centerline at 2687 mm
28	TS-CW-SC-2687	Lower section west (cold) wall south of centerline at 2687 mm
29	TS-CW-NM-2687	Lower section west (cold) wall mid-south side at 2687 mm
30	TS-CW-SM-2687	Lower section west (cold) wall mid-north side at 2687 mm
31	TS-CW-NC-2921	Lower section west (cold) wall north of centerline at 2921 mm
32	TS-CW-SC-2921	Lower section west (cold) wall south of centerline at 2921 mm
33	TS-CW-NC-3175	Lower section west (cold) wall north of centerline at 3175 mm
34	TS-CW-SC-3175	Lower section west (cold) wall south of centerline at 3175 mm
35	TS-CW-NM-3175	Lower section west (cold) wall mid-south side at 3175 mm
36	TS-CW-SM-3175	Lower section west (cold) wall mid-north side at 3175 mm

THIS DRAWING IS THE PROPERTY OF
Argonne
NATIONAL LABORATORY

DESIGNED BY: D. J. KISGOOLK
PHONE: 24746
CHECKED: *PL*
DATE: 02-15-14

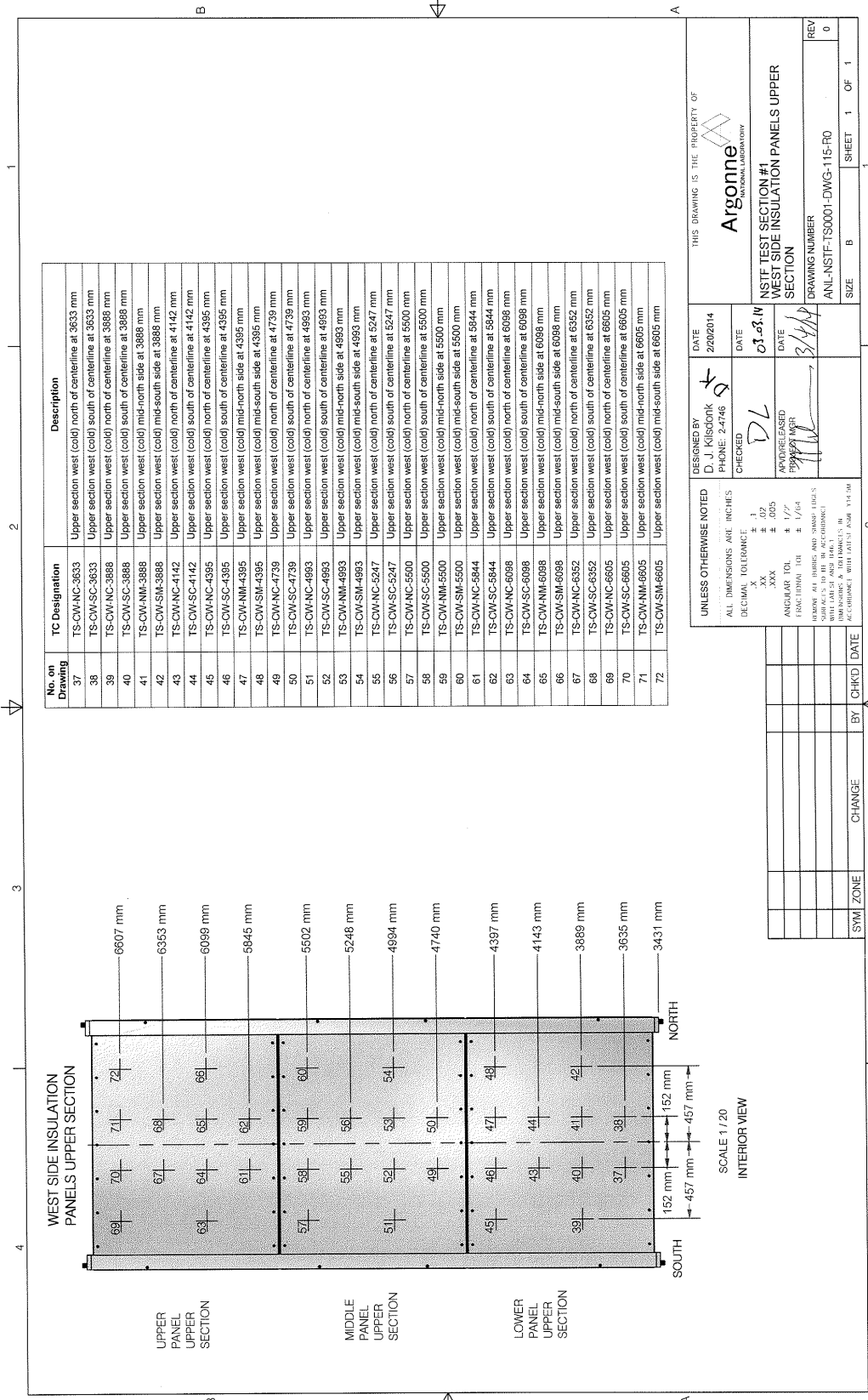
APPROVED/RELEASED: *PLM*
DATE: 2/14/14

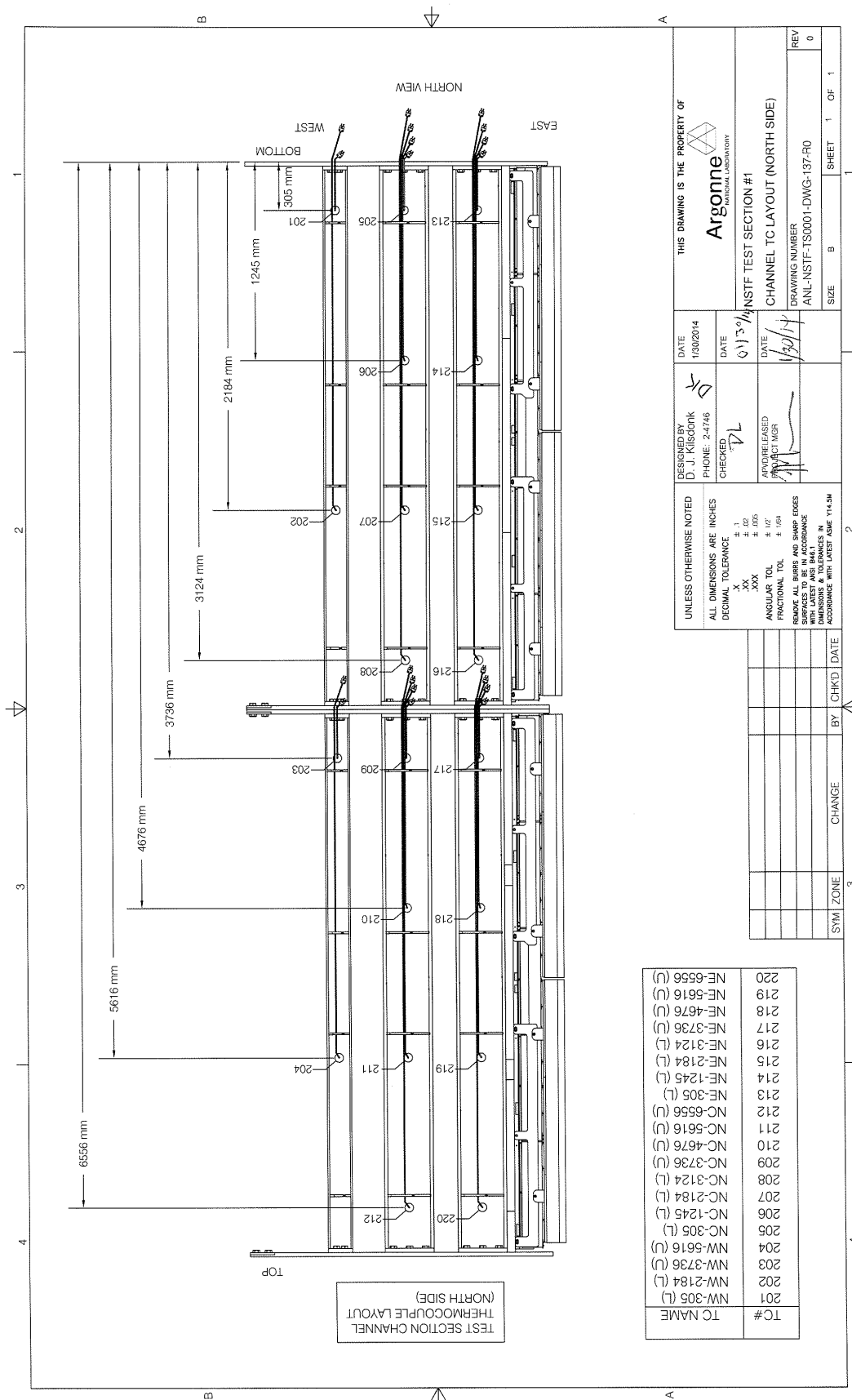
NSIF TEST SECTION #1
WEST SIDE INSULATION PANELS LOWER SECTION

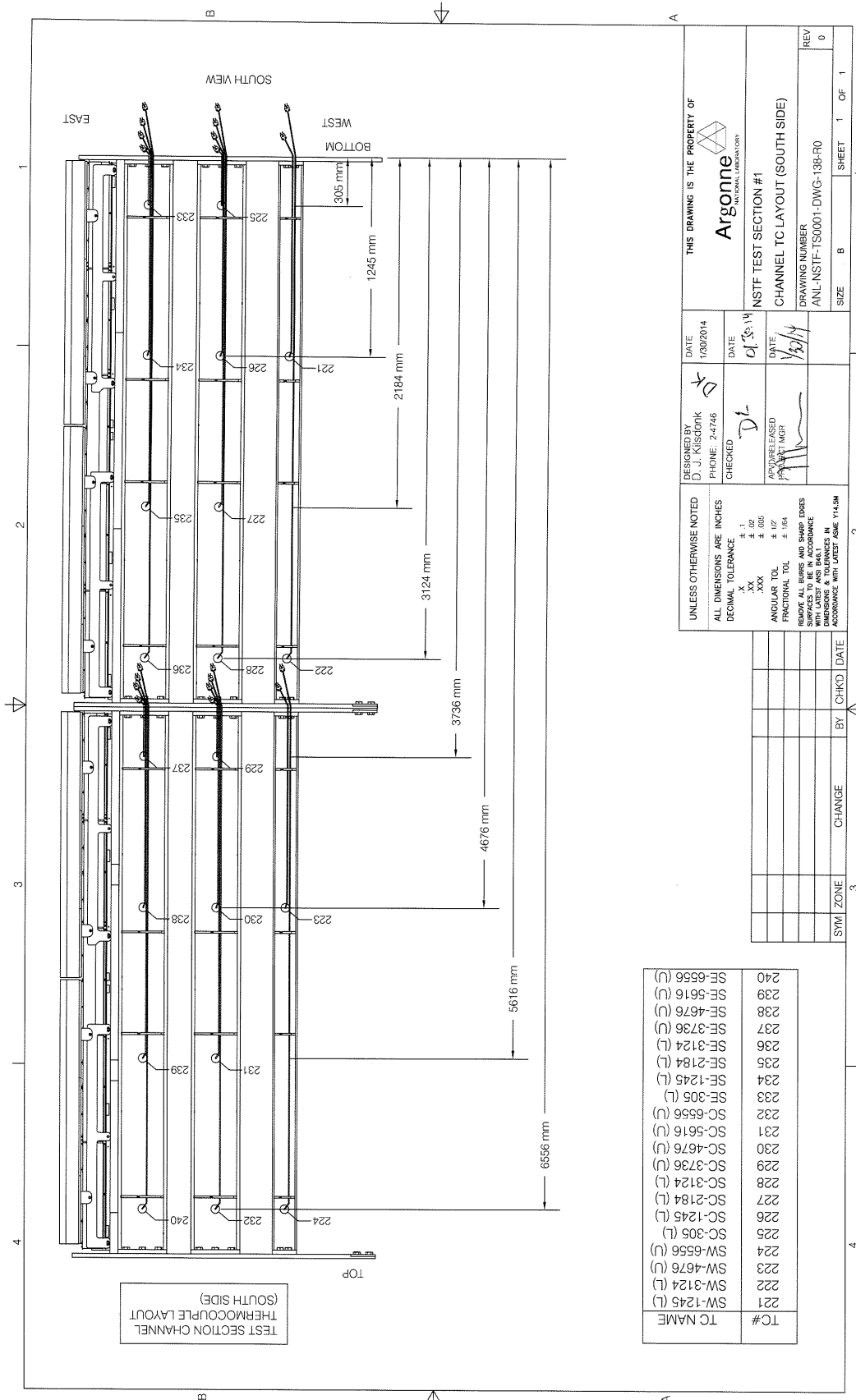
DRAWING NUMBER: ANL-NSTF-TS0001-DWG-114-RO
REV: 0

SIZE: B
SHEET 1 OF 1

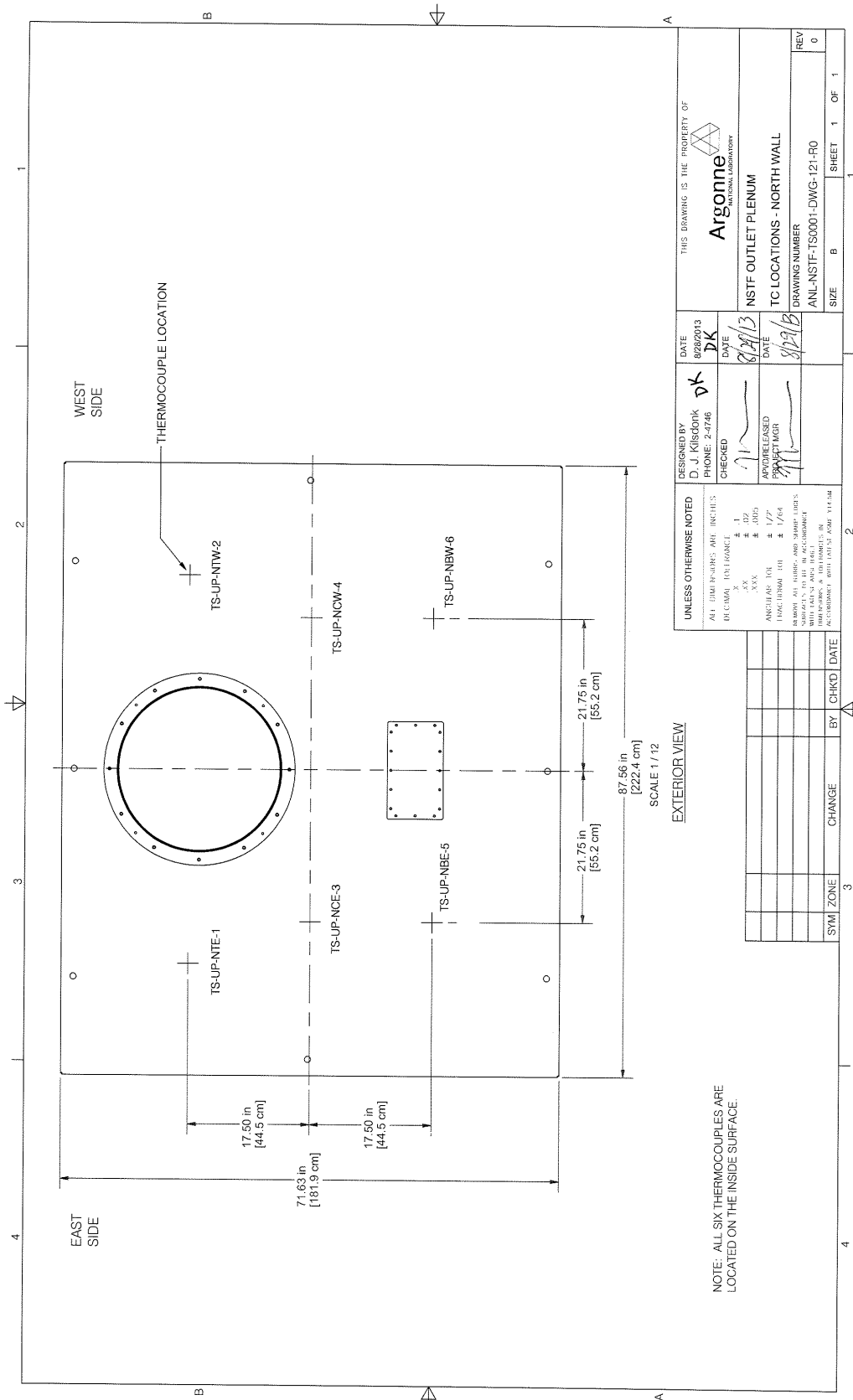
UNLESS OTHERWISE NOTED
ALL DIMENSIONS ARE IN INCHES
DECIMAL TOLERANCE
X .00
XX .005
XXX .005
ANGULAR TOL ± 1/2°
FRACTURAL TOL ± 1/64
HOLD ALL DIMS AND START LINES
UNLESS TO THE REVERSE
DIMENSIONS & TOLERANCES IN
PARENTS WITH LATEST ASME Y14.5M

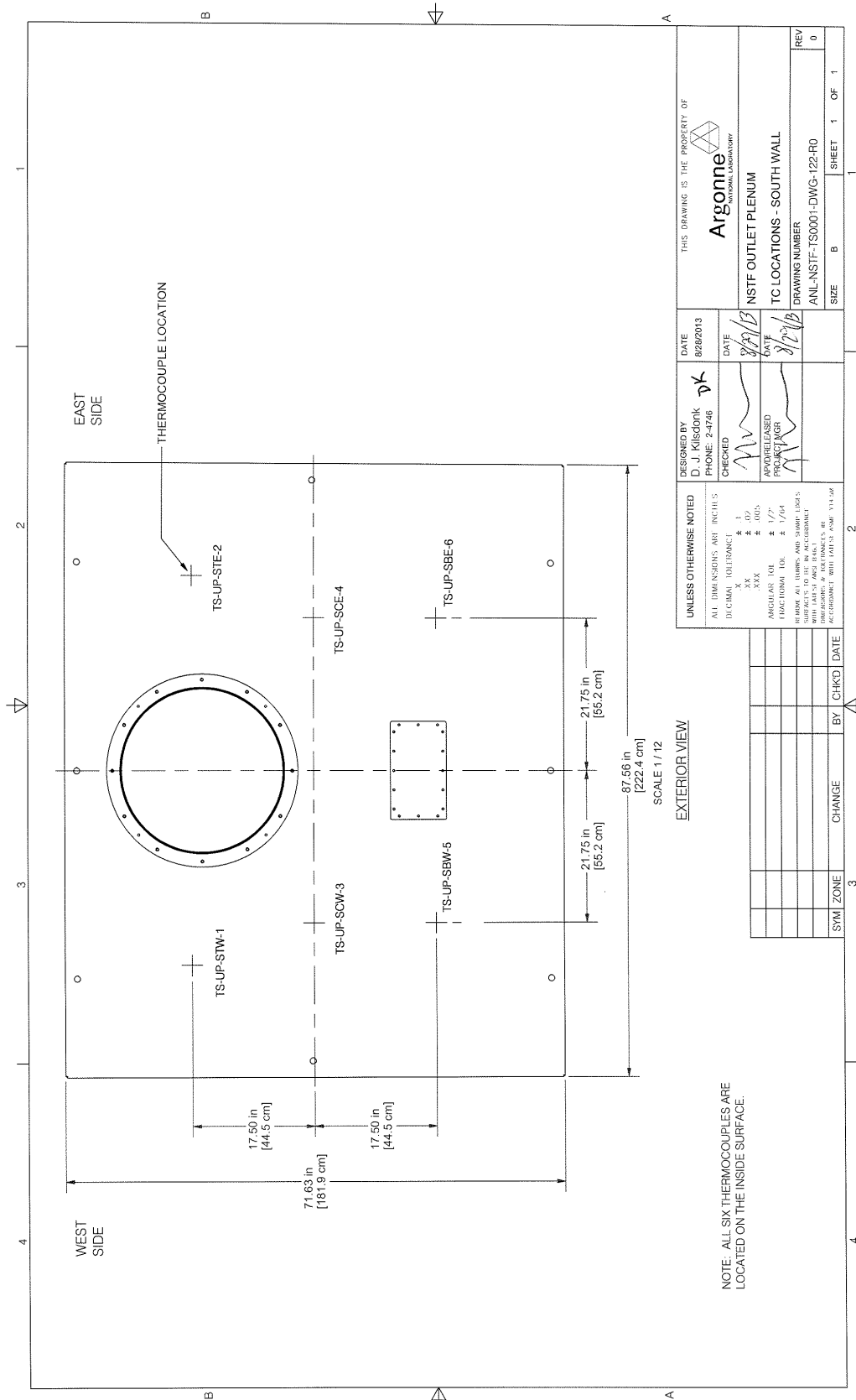


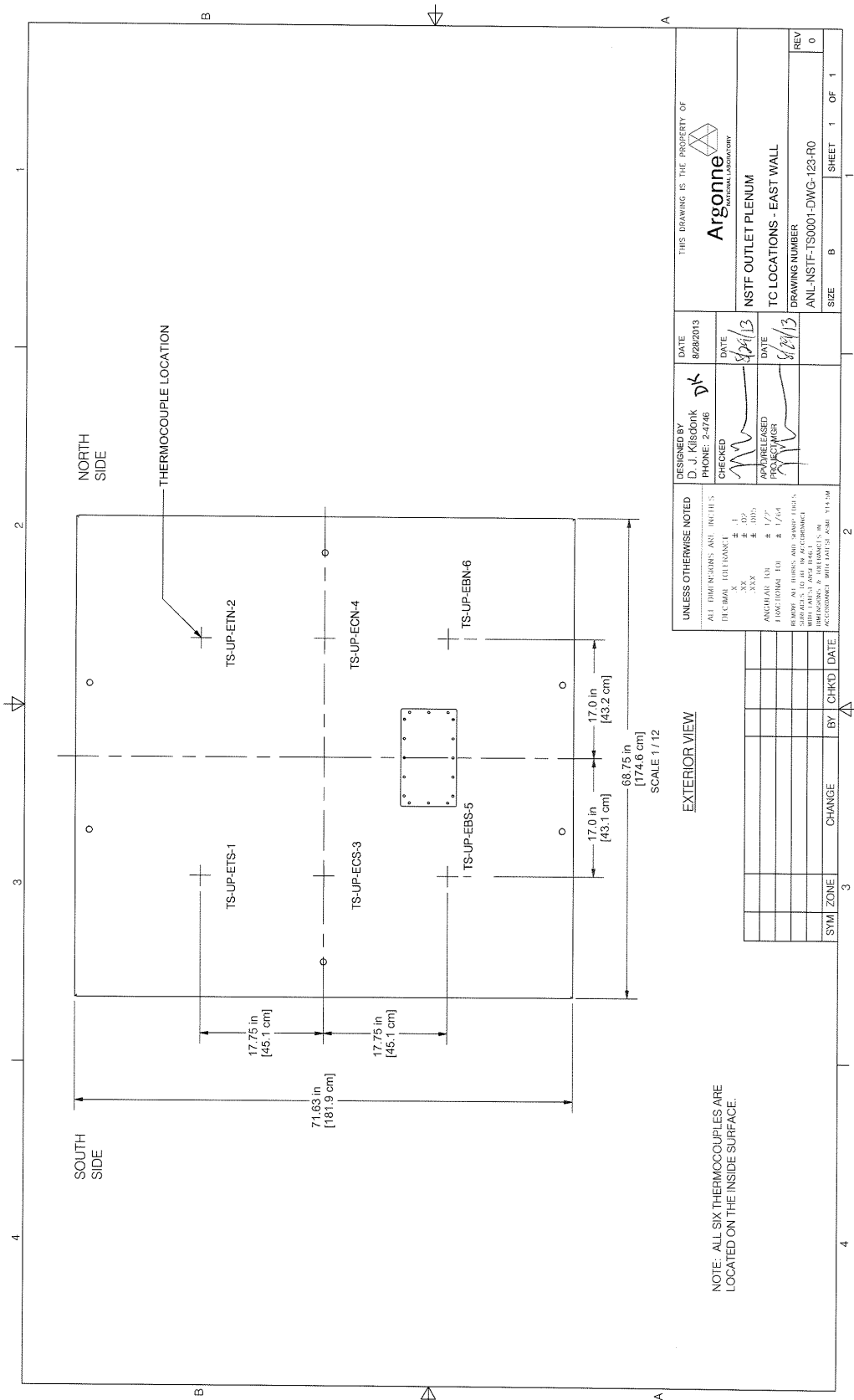




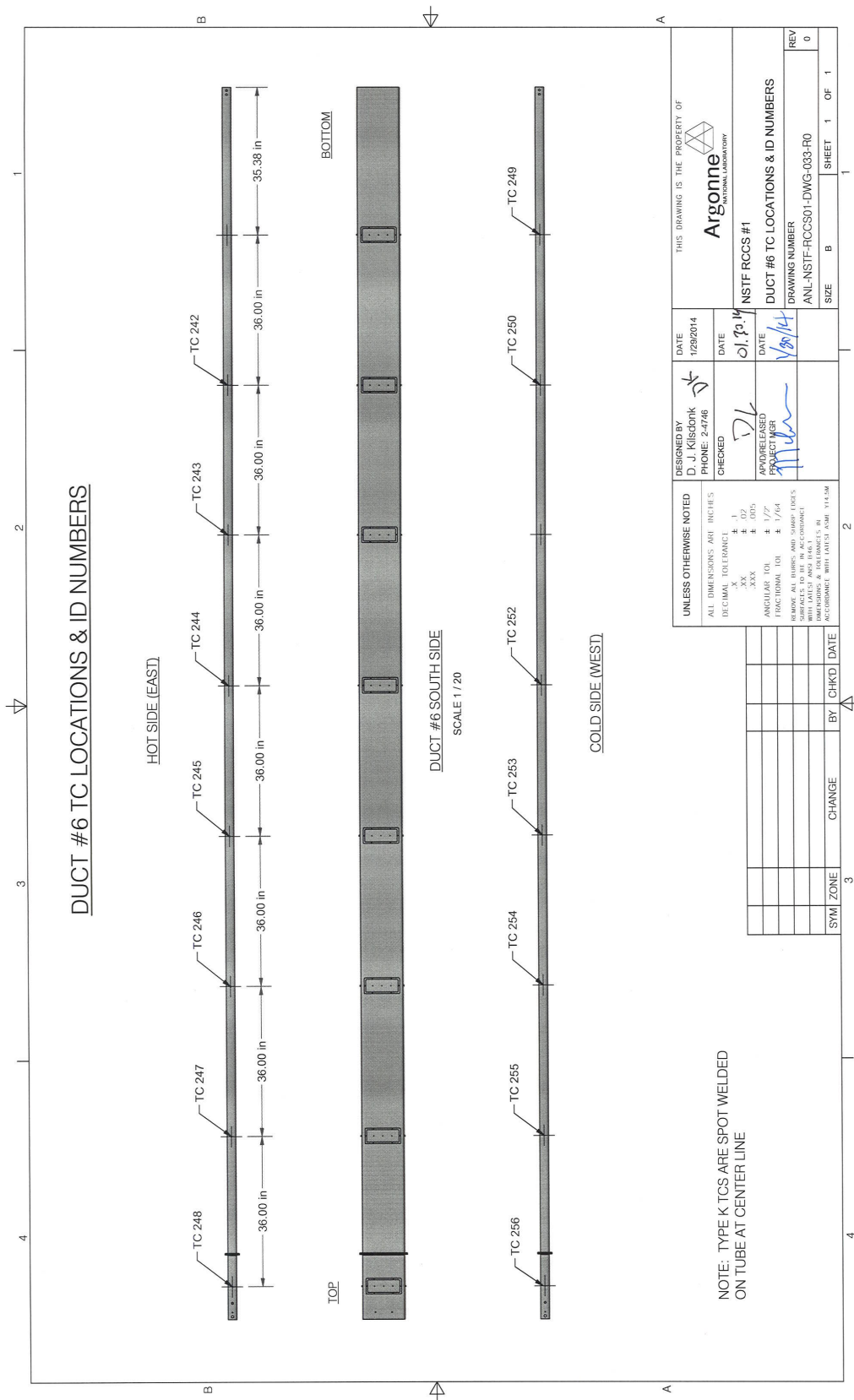
TC#	TC NAME
221	SW-1245 (L)
222	SW-3124 (L)
223	SW-4676 (U)
224	SW-6556 (U)
225	SC-305 (L)
226	SC-1245 (L)
227	SC-2184 (L)
228	SC-3124 (L)
229	SC-3736 (U)
230	SC-4676 (U)
231	SC-5616 (U)
232	SC-6556 (U)
233	SC-305 (L)
234	SE-1245 (L)
235	SE-2184 (L)
236	SE-3124 (L)
237	SE-3736 (U)
238	SE-4676 (U)
239	SE-5616 (U)
240	SE-6556 (U)







DESIGNED BY D. J. KISCOONIK PHONE: 2-4746		DATE 8/28/2013	THIS DRAWING IS THE PROPERTY OF Argonne NATIONAL LABORATORY	
CHECKED <i>[Signature]</i>	DATE 8/28/13	NSTF OUTLET PLENUM		
APPROVED <i>[Signature]</i>	DATE 8/28/13	TO LOCATIONS - EAST WALL		
DRAWING NUMBER ANL-NSTF-TS0001-DWG-123-R0		REV 0		
SYN ZONE		CHANGE	BY	CHKD DATE
3				
2				
1				
SIZE		SHEET 1 OF 1		



4.2.2 Heat Flux Sensors

Heat flux meters are used to measure the heat transfer from the heated plate to the riser ducts, and have been positioned along various riser tubes on both the cold and hot facing walls. The principle of the measurement is the same as that for a pair of thermocouples measuring the temperature difference across a conductor with a known thermal conductivity. Instead of thermocouples, the heat flux sensor uses a pair of thermopiles, which greatly amplifies the signal generated by the temperature difference. The relationship between the signal and heat flux is obtained through NIST traceable calibration.

Sixteen sensors were purchased from iTi Inc, and are of Model BHT with additional polyimide HFT, NIST-calibrated for 5% accuracy, rated for a maximum temperature of 300°C, Figure 31.

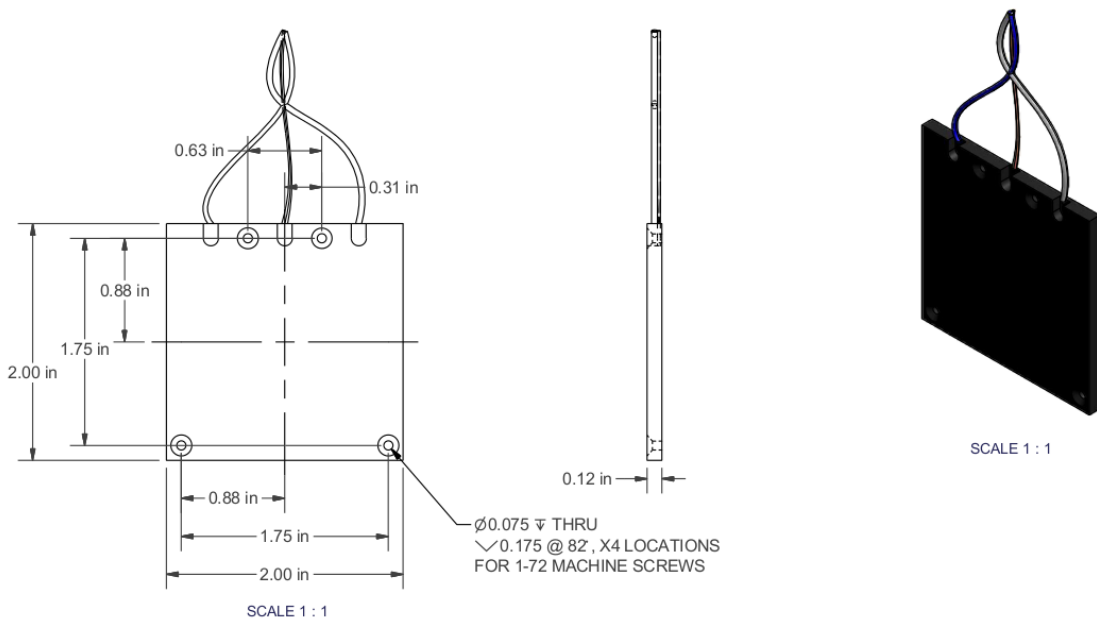


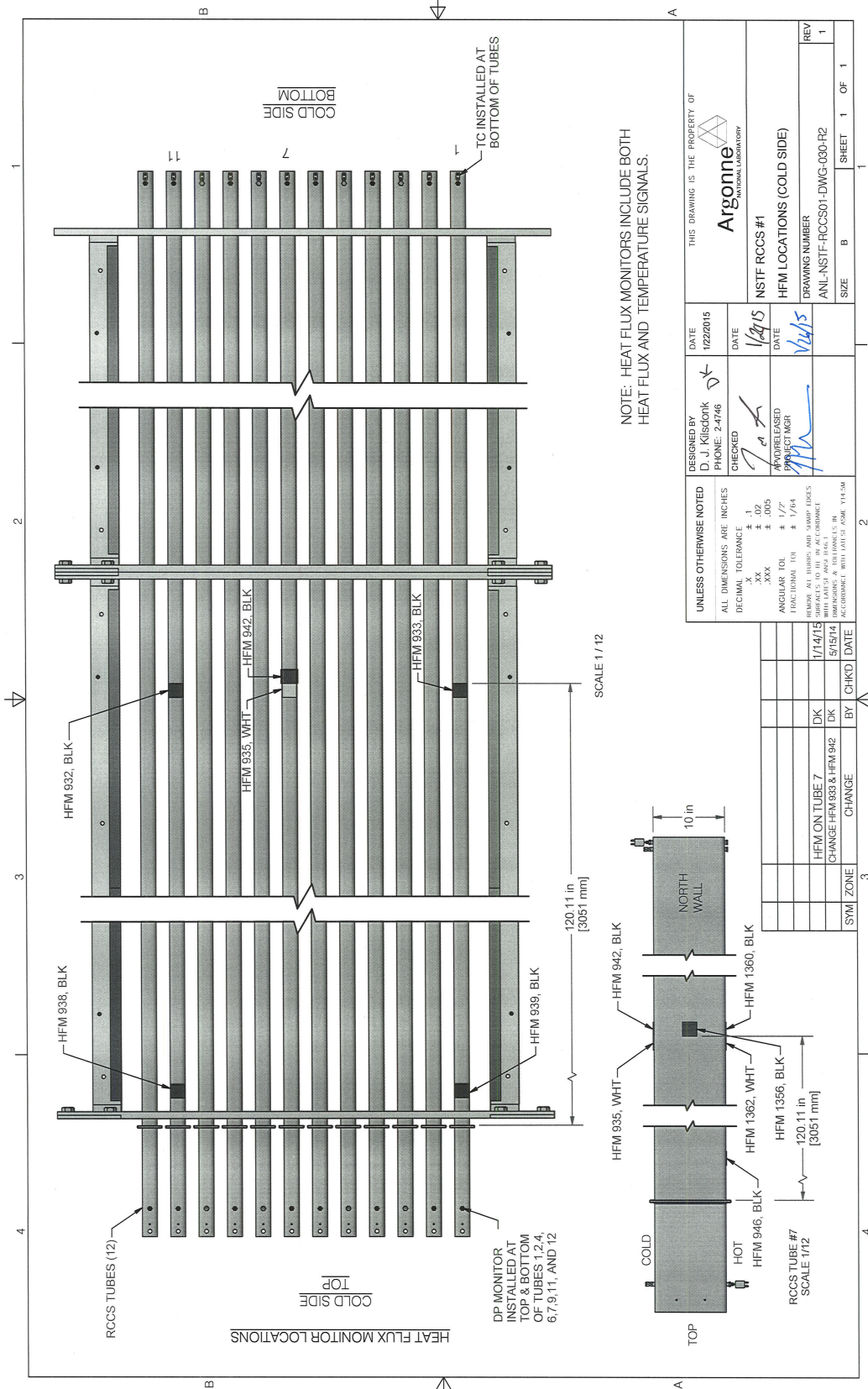
Figure 31: iTi model BHT, 300 °C Polyimide HFT

Two types of sensors were purchased: one featuring a matte black surface, and the other a high reflectivity golden surface by means of a polyimide HFT coating. The combination of separate matte black surfacing ($\varepsilon \approx 1.0$) and silver reflective surfacing ($\varepsilon \ll 1.0$) allows extraction of the split between convective and radiative heat transfer modes from the heated wall. Specific sensitivities and description of locations are provided below in Table 13, and reference drawings on the following pages.

Across the life of the heat flux sensors, performance of the “shiny” or convective-only units were found to degrade with time. Given their mode of operation strongly depends on maintaining a low surface emissivity, gradual oxidation of the surfaces (an observed phenomenon) can alter the output signals and provide readings outside of the original tolerance and calibration. Quantification of this degradation is in-progress by in-house calibrations and will be published in supplemental reports by the project team.

Table 13: Summary of heat flux sensors on risers. Procured from iTi Inc., model BHT

#	Sensor ID	$K_{radiative}$ (W/m ² , mV)	Surface finish	Location
1	950	20.20	matte	Hot side of duct 1 at 100 mm
2	951	65.72	reflective	Hot side of duct 1 at 100 mm
3	948	21.59	matte	Hot side of duct 1 at 3500 mm
4	1358	15.92	matte	Hot side of duct 1 at 7000 mm
5	933	21.73	matte	Cold side of duct 1 at 7000 mm
6	939	18.15	matte	Cold side of duct 1 at 7000 mm
7	1360	15.12	matte	Hot side of duct 7 at 3500 mm
8	1362	41.07	reflective	Hot side of duct 7 at 3500 mm
9	946	19.11	matte	Hot side of duct 7 at 7000 mm
10	942	18.55	matte	Cold side of duct 7 at 3500 mm
11	935	52.97	reflective	Cold side of duct 7 at 3500 mm
12	940	24.68	matte	Hot side of duct 11 at 3500 mm
13	941	22.07	matte	Hot side of duct 11 at 7000 mm
14	936	62.43	reflective	Hot side of duct 11 at 7000 mm
15	932	19.77	matte	Cold side of duct 11 at 350 mm
16	938	22.88	matte	Cold side of duct 11 at 700 mm
17	1355	15.54	matte	South side of duct 7 at 3500 mm
18	1356	15.24	matte	North side of duct 7 at 3500 mm
19	1359	44.62	reflective	Hot side of duct 1 at 7000 mm



4.2.3 Meteorological

Ambient conditions can have a significant effect on RCCS performance and so it is necessary to monitor meteorological conditions near the stack outlet. A weather station, model Davis VantageVue, was selected for this purpose, providing barometric pressure, temperature, humidity, wind speed, and wind direction. All measurements except wind direction have been calibrated to NIST standards.

The weather station is mounted on the building roof and linked to a console station in the control room via wireless transmissions. The console is able to store up to 2,560 records on internal storage before it begins overwriting the oldest data. The console has been configured to poll and store 1 data record every minute, which limits its total capacity to 1.75 days or 42 hours. To work around this, given the three day or longer test operations, the software has been configured to automatically download and store all available records every 24 hours. Time synchronization across the devices is routinely performed to ensure accurate data. Details of the different meteorological measurements for the Davis VantageVue weather station are provided below in Table 14, and a reference to its physical mounting location in Figures 32 and 33.

Table 14: Device specifications for Davis VantageVue weather station

Function	Resolution	Range	Accuracy (\pm)
Barometric Pressure	0.1 mmHg	410 - 820 mmHg	0.8 mmHg
Humidity	0.01	1 - 100%	0.03
Rainfall	0.2 mm	0 - 6553 mm	0.04
Temperature	0.1 °C	-40 to 60 °C	0.5 °C
Wind direction	1°	0 - 360°	3°
Wind speed	0.1 m/s	1 - 80 m/s	0.05
Wind run	0.01 km	<i>unlimited</i>	0.05

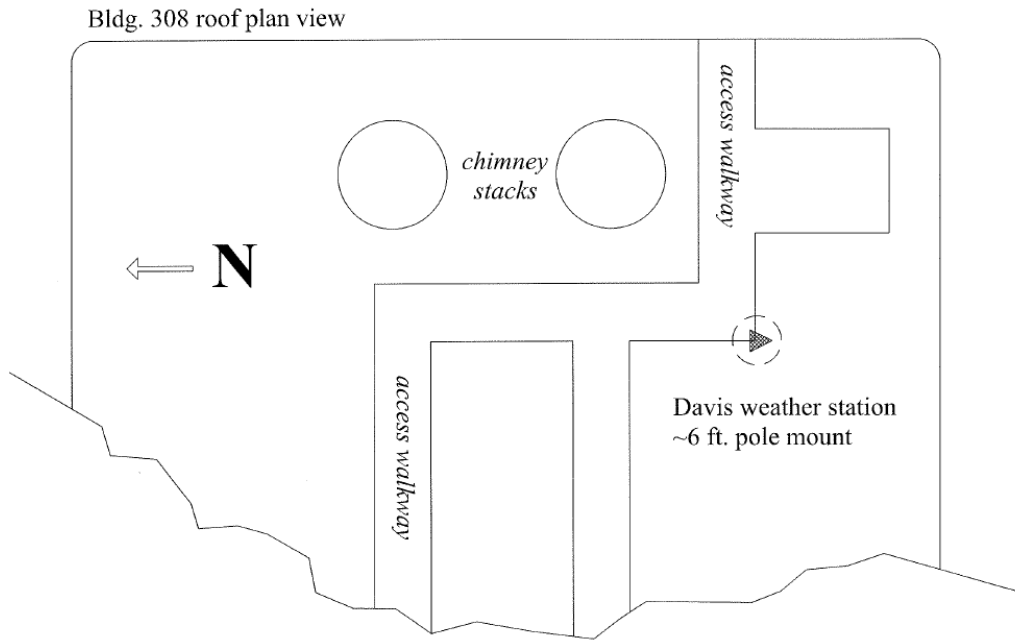
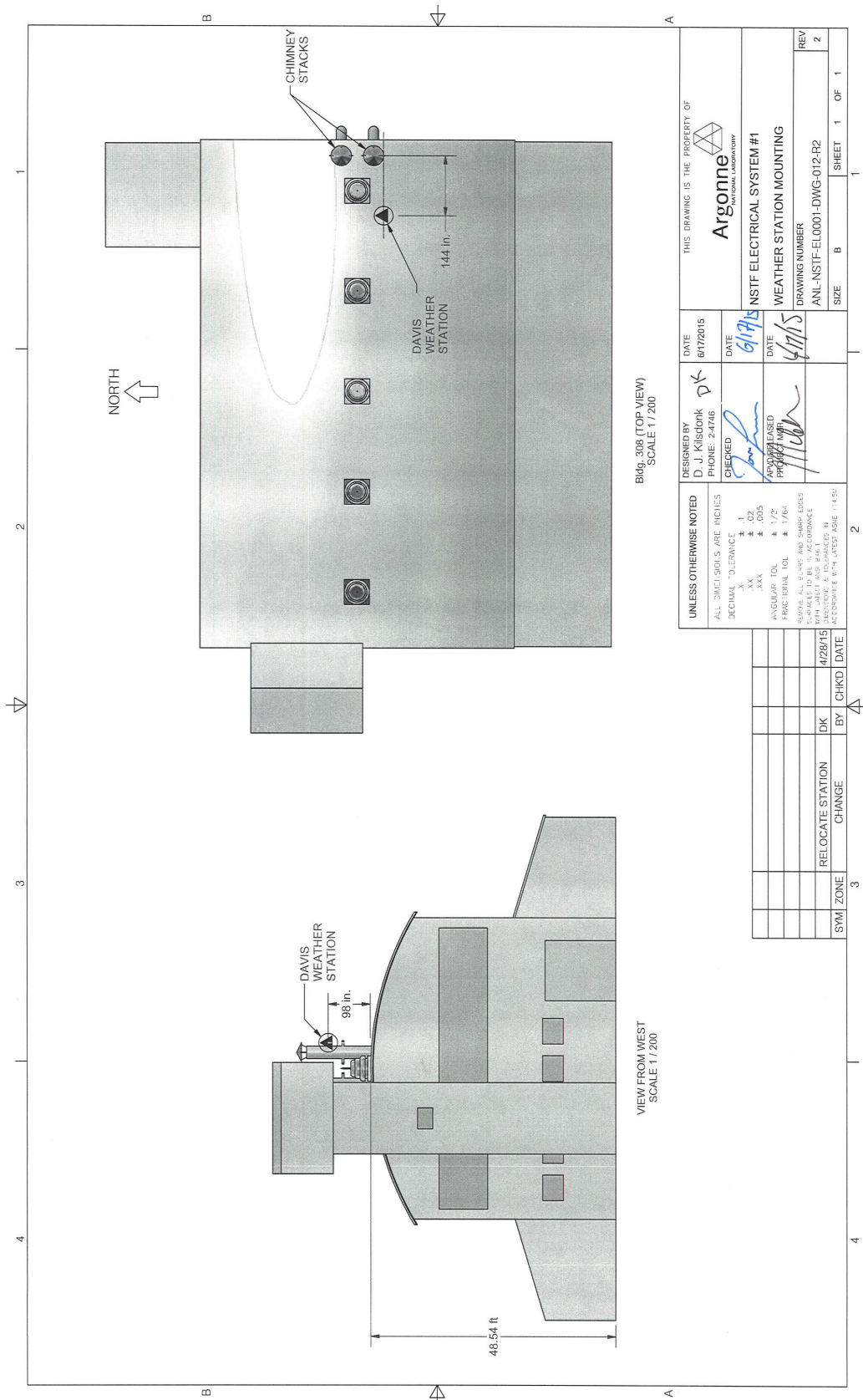


Figure 32: Position of weather station of Bldg. 308 roof top



Figure 33: Picture of weather station of Bldg. 308 roof top

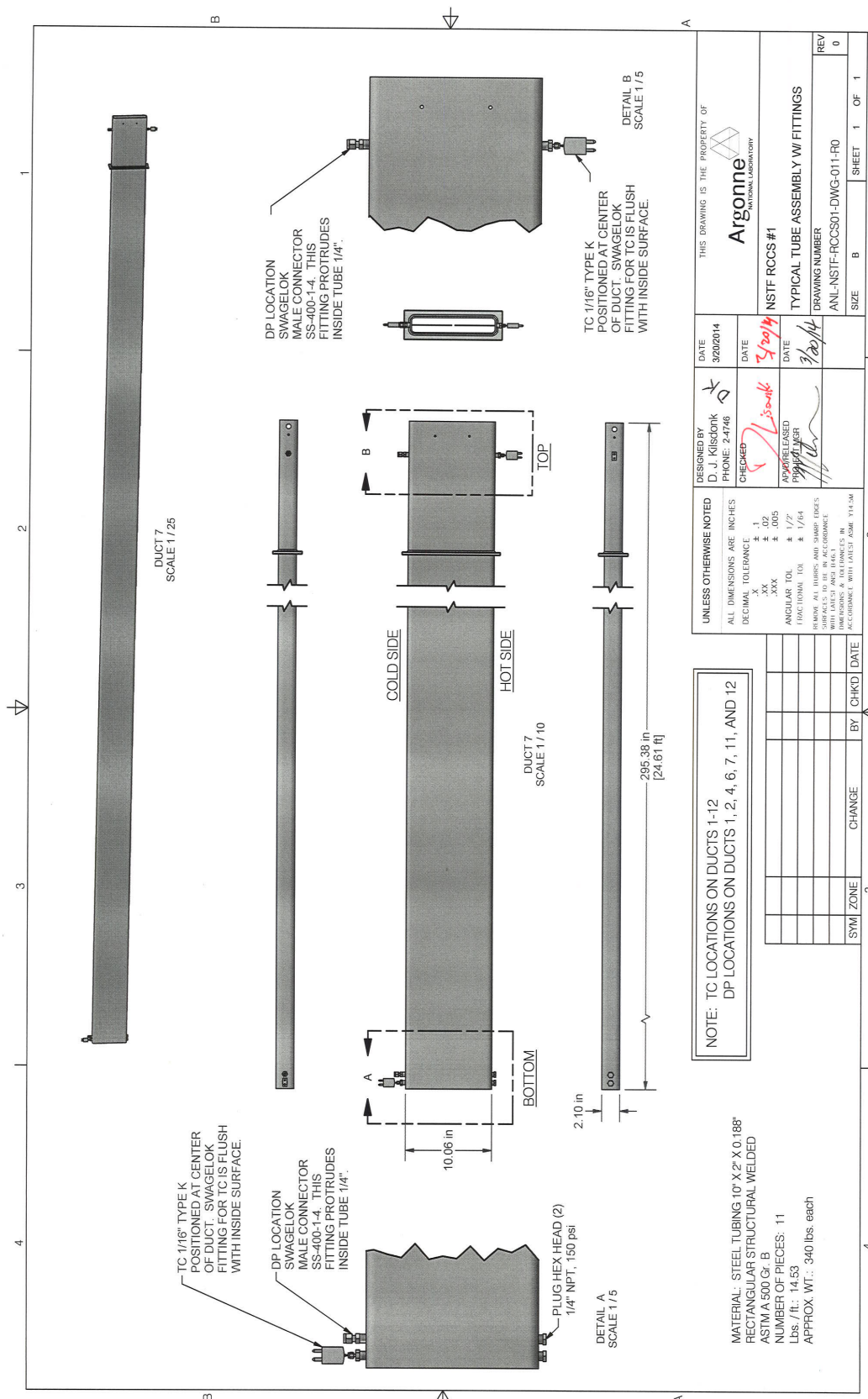


4.2.4 Differential Pressure

Differential pressure transmitters are installed across eight of the riser ducts (3, 5, 8, and 10 omitted), and across both chimney networks. The total pressure drop can be defined by the sum of frictional, gravitational, and minor losses. To separate the gravitational (density) influences, thermocouples are positioned alongside each tap point and references to isothermal baseline measurements. Influences from ambient temperature gradients are minimized by tightly bundling impulse lines, selecting bundle runs that avoid surfaces at elevated temperatures, and shielding the transmitters from large temperature swings. Eight of the transmitters positioned across the riser ducts were purchased from Dwyer, model 668 which features bidirectional capabilities with a span of $\pm 0.25''$ H₂O (64 Pa). Two additional transmitters across the chimney segments were also purchased from Dwyer, but high accuracy and resolution model 607 were selected, which features bidirectional capabilities with a span of $\pm 0.1''$ H₂O (24 Pa).

Table 15: Differential pressure device specifications

	Dwyer 668-11	Dwyer 607-0B
NSTF Location	Riser tubes	Chimney ducts
Range	0 to $\pm 0.25''$ w.c.	0 to $\pm 0.10''$ w.c.
Accuracy	$\pm 1\%$ of full scale (RSS)	$\pm 0.5\%$ F.S.
Long Term Stability	not rated	$\pm 0.5\%$ F.S.O./yr
Temperature Limits	0 to 150°F (-18 to 65°C)	-20 to 160°F (-29 to 71°C)
Pressure Limits	10 psig (0.69 bar)	10 psig (0.69 bar)
Operating Temp.	0 to 150°F (-18 to 65°C).	35 to 135°F (2 to 57°C)
Thermal Effects	0.033% FS/°F (0.18% FS/°C)	$\pm 0.015\%$ F.S./°F
Supply Voltage	12-30 VDC	12-36 VDC
Output	4 to 20 mA, 2-wire	4 to 20 mA DC, 2-wire
Response Time	<60 msec	250 msec max
Loop Resistance	0-800 ohms	0 to 1045 ohms
Housing	Fire retardant glass polyester	300 Series stainless (NEMA 2)
Weight	3 oz (85 g)	1.04 lb (472 g)
Agency Approval	CE	CE



THIS DRAWING IS THE PROPERTY OF
Argonne
 NATIONAL LABORATORY

DESIGNED BY: D. J. KISDOBK
 PHONE: 2-4746

CHECKED: [Signature]

APPROVED: [Signature]

DATE: 3/20/14

DATE: 3/20/14

DATE: 3/20/14

NSTF RCCS #1

TYPICAL TUBE ASSEMBLY W/ FITTINGS

DRAWING NUMBER: ANL-NSTF-RCCS01-DWG-011-R0

REV: 0

SIZE: B

SHEET 1 OF 1

UNLESS OTHERWISE NOTED
 ALL DIMENSIONS ARE IN INCHES

DECIMAL TOLERANCE: ± .005

ANGULAR TOL: ± 1/2°

FRACTIONAL TOL: ± 1/64

REWORK: ALL DIMS AND SHARP EDGES SHALL BE TO ACCORDANCE WITH THE LATEST ASME Y14.5M

BY: [Signature]

DATE: []

CHANGE: []

BY: []

DATE: []

SYMBOL ZONE: []

4.2.5 Inlet Flow and Humidity

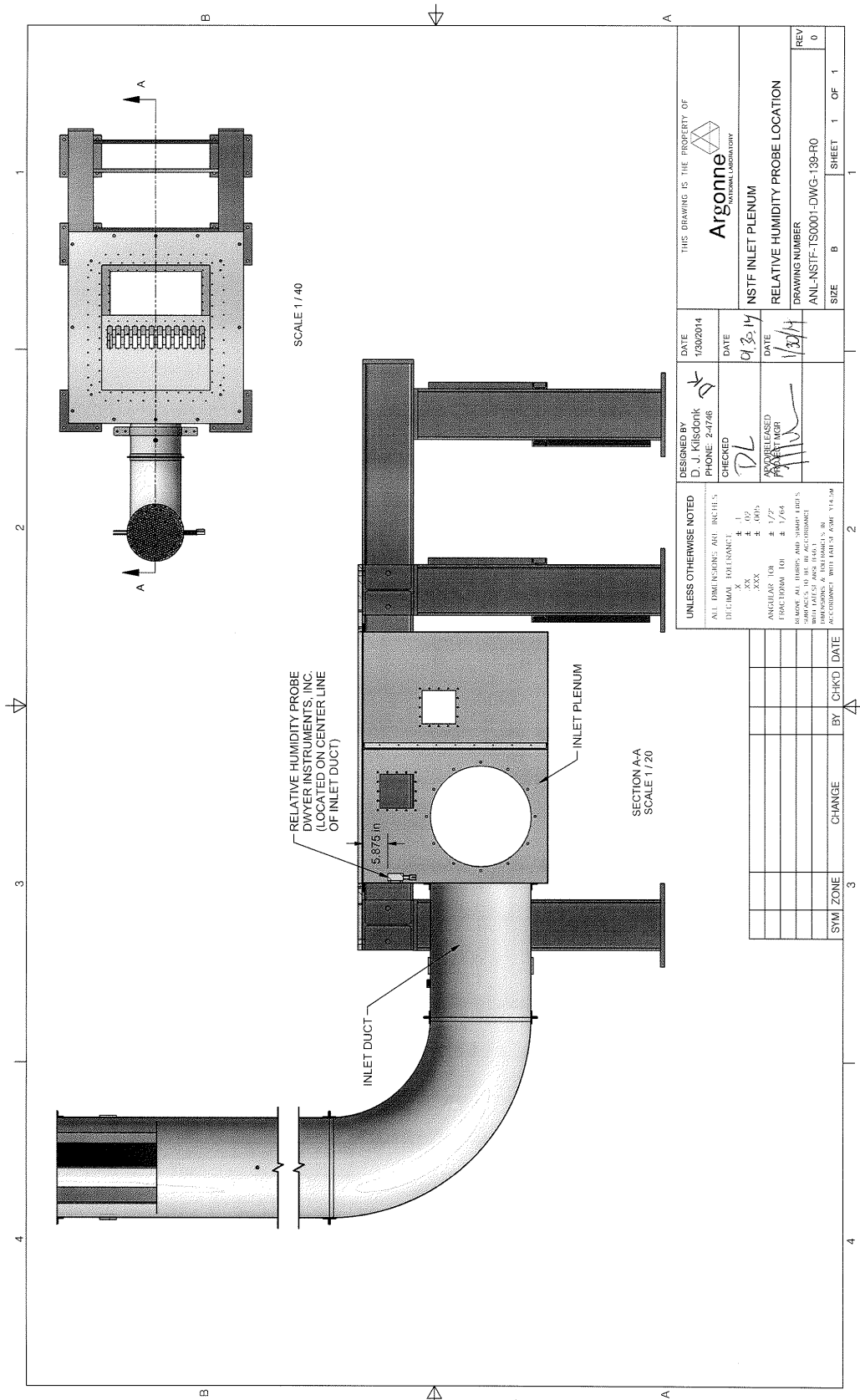
A Sierra 640S thermal mass flow meter is located 24” past the end of the flow conditioner and extends to the centerline of the duct. This instrument provides measurement of temperature compensated mass flow rates and is the first measurement parameter of the incoming air supply. Measurement of bulk humidity is made by a single humidity probe, Dwyer RHP-2011, which is positioned 24” above and at the centerline of the 24” diameter entrance area.

Table 16: Inlet mass flow meter specifications

Sierra 640S	
NSTF Location	Inlet downcomer
Accuracy of Point Velocity	$\pm 1\%$ of reading + 0.5% of full scale
Repeatability	$\pm 0.2\%$ of full scale
Temperature Coef.	$\pm 0.06\%$ per $^{\circ}\text{C}$ within $\pm 25^{\circ}\text{C}$ to 50°C of calibration
Pressure Coef.	0.02% per psi for air, consult factory for other gases
Response Time	One second to 63% of final velocity value
Pressure Drop	Negligible for pipes three inches in diameter or larger

Table 17: Inlet plenum humidity probe specifications

Dwyer RHP 20-11	
NSTF location	Inlet plenum
Relative Humidity Range	0 to 100% RH
Temperature Range	-40 to 140°F (-40 to 60°C)
Accuracy	$\pm 2\%$ 10-90% RH @ 25°C
Hysteresis	$\pm 1\%$
Repeatability	$\pm 0.1\%$ typical
Temperature Limits	-40 to 140°F (-40 to 60°C)
Response Time	15 seconds
Drift	$< 1\%$ RH/year



4.2.6 Hot-wire Probes

A suite of Dantec hot-wire, or constant temperature anemometer (CTA) probes have been procured and added to the NSTF. The probes are miniature straight-wires with a 3-mm OD body and 10- μm tungsten wire, Figure 34, capable of measuring velocities between 0.2 and 500 m/s at a maximum process temperature of 300°C. Each probe is calibrated to a range of known velocities prior to test operations to obtain a 5th order polynomial fit curve, and operate at a constant wire temperature of 242°C. Probes are simultaneously sampled at 50 kHz, and feature a co-located thermocouple to allow for temperature correction during post-processing [15].

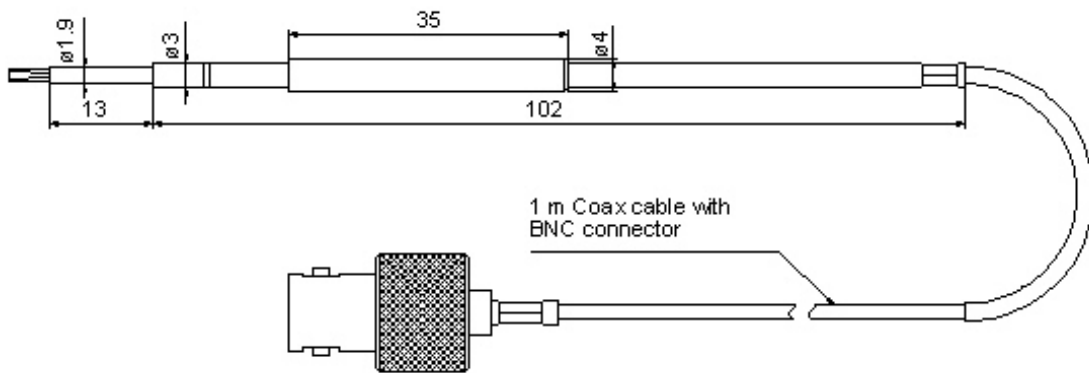


Figure 34: Diagram of miniature hot-wire probe, units in mm

The turbulence intensity was calculated from RMS velocity measurements [16] from the hot-wire probes, Eqns. 3 - 5. The numbers of samples per acquisition totaled 250,000 points and were taken at a rate of 50 kHz.

$$U_{mean} = \frac{1}{N} \sum_1^N U_i \quad (3)$$

$$U_{rms} = \left(\frac{1}{N-1} \sum_1^N (U_i - U_{mean})^2 \right)^{0.5} \quad (4)$$

$$I = \frac{U_{rms}}{U_{mean}} \quad (5)$$

4.2.7 Pitot Tubes

Testing performed during 2014 produced high-quality measurements of the differential pressure drop within the riser ducts. However, measurements within the chimney region were dominated by gravitational effects and thus provided little insight into the frictional effects. To isolate the effects of friction only, two pitot tubes, Model 160F from Dwyer instruments, Figure 35 were added to the suite of instrumentation and served as replacements for the chimney differential pressure measurements. While convention recommends a minimum flow length of 10 L/D, this was not possible within the current chimney configuration. Thus, their installation position will require their output signals to be treated as relative flow velocities between the dual chimney ducts, and not as absolute measurements of the flow velocity.

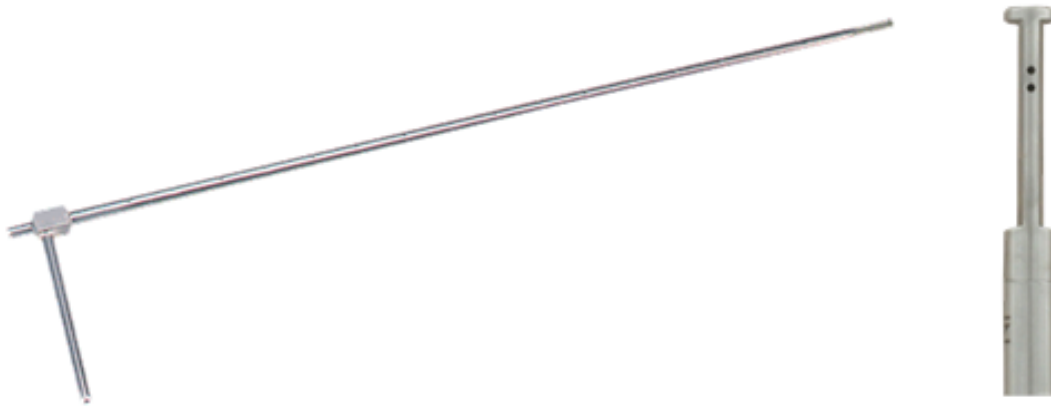


Figure 35: Dwyer 160F pitot tubes installed along chimney ductwork. Right figure shows air ports that translate air velocity into fluid pressure

The pitot tubes are constructed from 304 SS, are characterized by a K-factor, K_p of 0.81, and claim an accuracy of $\pm 2\%$ of the full scale range, from 0 - 45 m/s. The full uncertainty, however, requires a propagation of error from their defining velocity correlation, Eqn. 6. As an example for baseline testing conditions, where measured differential pressures average 1.5 Pa and gas temperatures of 100 °C, the calculated velocity would be 1.44 ± 0.12 m/s, or $\pm 8.3\%$.

$$V_{pitot} = K_p \sqrt{\frac{2\Delta P}{\rho}} \quad (6)$$

4.2.8 Gas Temperature

Within each riser, Type-K thermocouples are placed and extend to the length wise (10") duct centerline, Figure 36. These thermocouples were purchased from ARI industries, and are of model T-22N-12BK8A-96(MOD). The inlet thermocouple is placed 0.75" from the bottom lip on the cold side, and the outlet placed 4.0" below the top lip from the hot side.

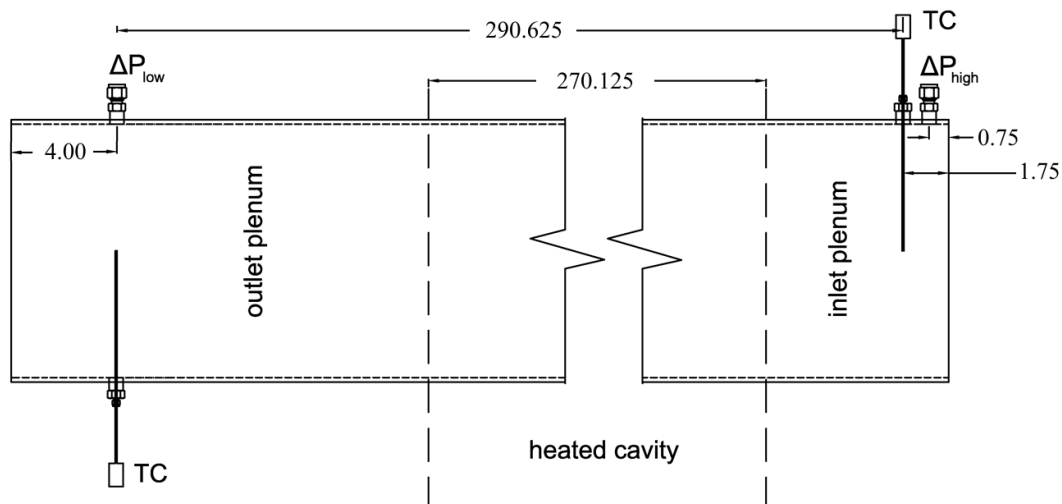
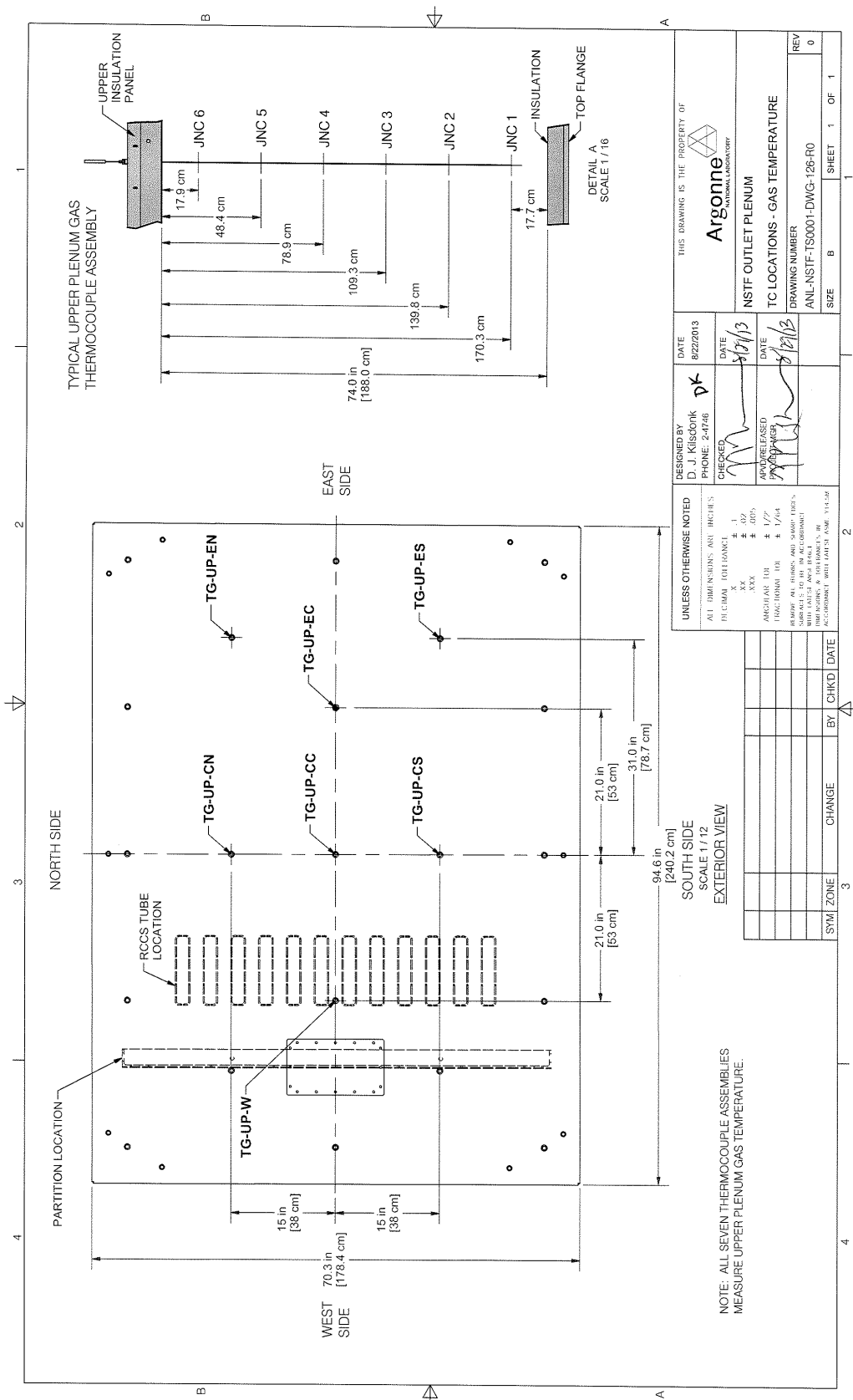
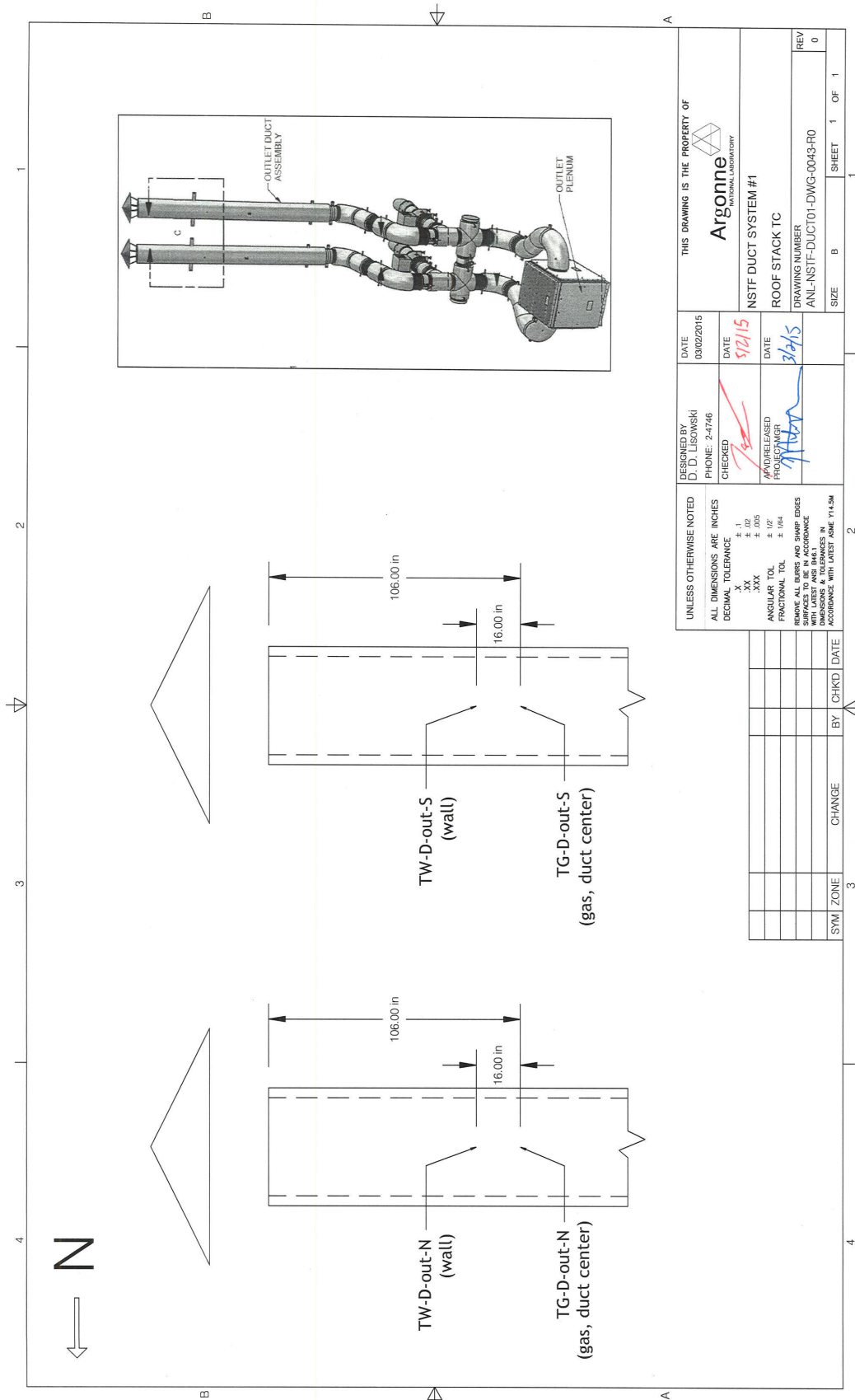


Figure 36: Placement of inlet and outlet instruments for riser

The outlet plenum features five instrumented insulation panels. The four adjacent vertical sides (north, south, east, and west) contain six embedded interior wall thermocouples, while the fifth top ceiling panel contains identical wall thermocouples in addition to seven thermocouple rakes for gas temperature measurements within the bulk volume of the plenum. Each rake measures six junctions along its length, extending a 170-cm along the total 188-cm height of the plenum.





UNLESS OTHERWISE NOTED ALL DIMENSIONS ARE INCHES		DESIGNED BY D. D. LISOWSKI PHONE: 2-4746	DATE 03/02/2015	THIS DRAWING IS THE PROPERTY OF Argonne NATIONAL LABORATORY	
DECIMAL TOLERANCE	± 1 .XX .XXX	CHECKED <i>[Signature]</i>	DATE 5/21/15	NSTF DUCT SYSTEM #1	
ANGULAR TOL	± 1/2	APPROVED FOR RELEASED PROJECT MGR <i>[Signature]</i>	DATE 3/2/15	ROOF STACK TC	
FRACTIONAL TOL	± 1/4	DRAWING NUMBER ANL-NSTF-DUCT01-DWG-0043-R0		SIZE	B
SHOW ALL EDGES AND SHARP EDGES WITH LATEST ANS B46.1 DIMENSIONS AND TOLERANCES ACCORDANCE WITH LATEST ASME Y14.5M		BY CHKD DATE		SHEET	1 OF 1
SYMBOL	ZONE	CHANGE	BY	CHKD	DATE

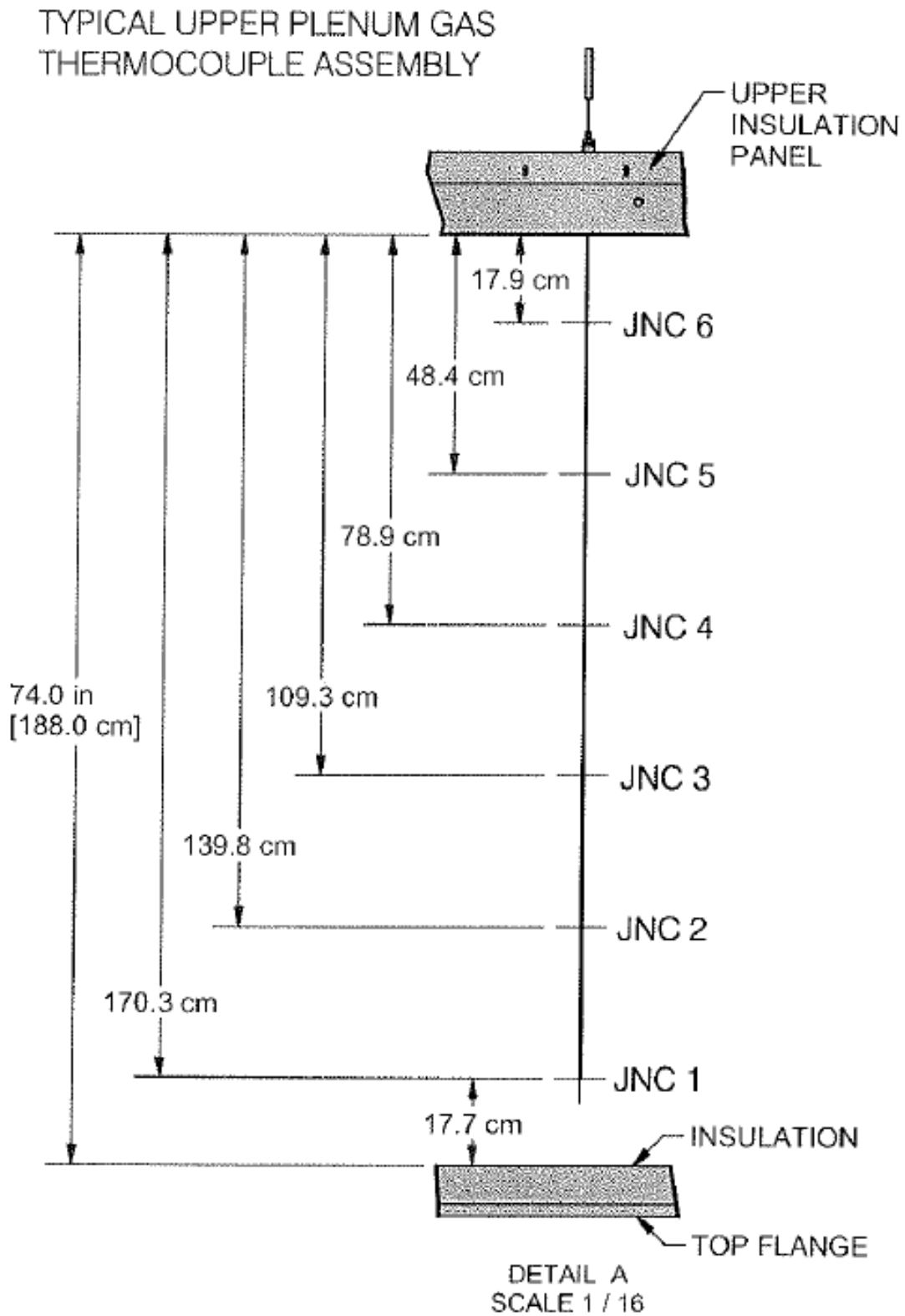


Figure 37: Typical rake junction locations, placed along upper plenum top panel and extending downward

4.2.9 Luna Fiber Optic Temperature

The NSTF is outfitted for fiber optics, notably a distributed sensing system by Luna Technologies that can provide the necessary data density for validation of CFD tools. Distributed fiber optic temperature sensing is a technique based upon distributed strain sensing and enables the acquisition of thousands of temperature measurements from a single optical fiber [17]. The fiber temperature sensors used here exploit Rayleigh scattering losses from structural inhomogeneities and impurities at the molecular level of ordinary telecom fibers [18]. The ODiSi A-10 from Luna Technologies has been used at other facilities at Argonne [19], and also was used for measurements in the NSTF.

Table 18: Specifications of Luna ODiSi A-10

Parameter	Specification
Model	A10
Maximum Sensing Length	10 m
Acquisition Rate ¹	5 Hz
Minimum Sensor Spacing	0.4 mm
Minimum Gage Length ²	1 mm
Wavelength Accuracy ³	1.5 pm
Strain	
Range	±13,000 μ Strain
Single Scan Pepeatability ^{1 4 5}	±2 μ Strain
Temperature	
Range ⁶	-50 to 300 °C
Single Scan Pepeatability ^{1 4 5}	±0.2 °C

¹For the default measurement range of ±1,250 μ Strain or ±200 °C

²Minimum gage length is achievable using the largest measurement range, having a single scan repeatability of ±17.0 μ Strain or ±2.0 °C

³Accuracy maintained by an internal NIST - traceable HCN gas cell

⁴Temperature and strain measurements are calculated from the spectral shift of scattered laser light. Using the default conversion coefficients of 1 GHz = 0.8 °C = 6.58 μ Strain, the accuracy of temperature and strain are 0.15 °C and 1.25 μ Strain

⁵For the default gage length of 1 cm

⁶Based on material properties of the standard sensor: polyimide - coated, low - bend - loss optical fiber

The fibers are made of 155 μm polyimide-coated single-mode commercial telecom fiber (Specialty Photonics CL POLY 1310) that has been tested for accuracy and repeatability to 150°C [17]. The system can generate temperature measurements every 10-mm at 1 Hz for a total of 9,750 data point/s along each 7.5 m fiber. This initial installation has been limited in facility inclusion because the measurement technique is relatively new; this is the first time it has been used in a large-scale test facility.

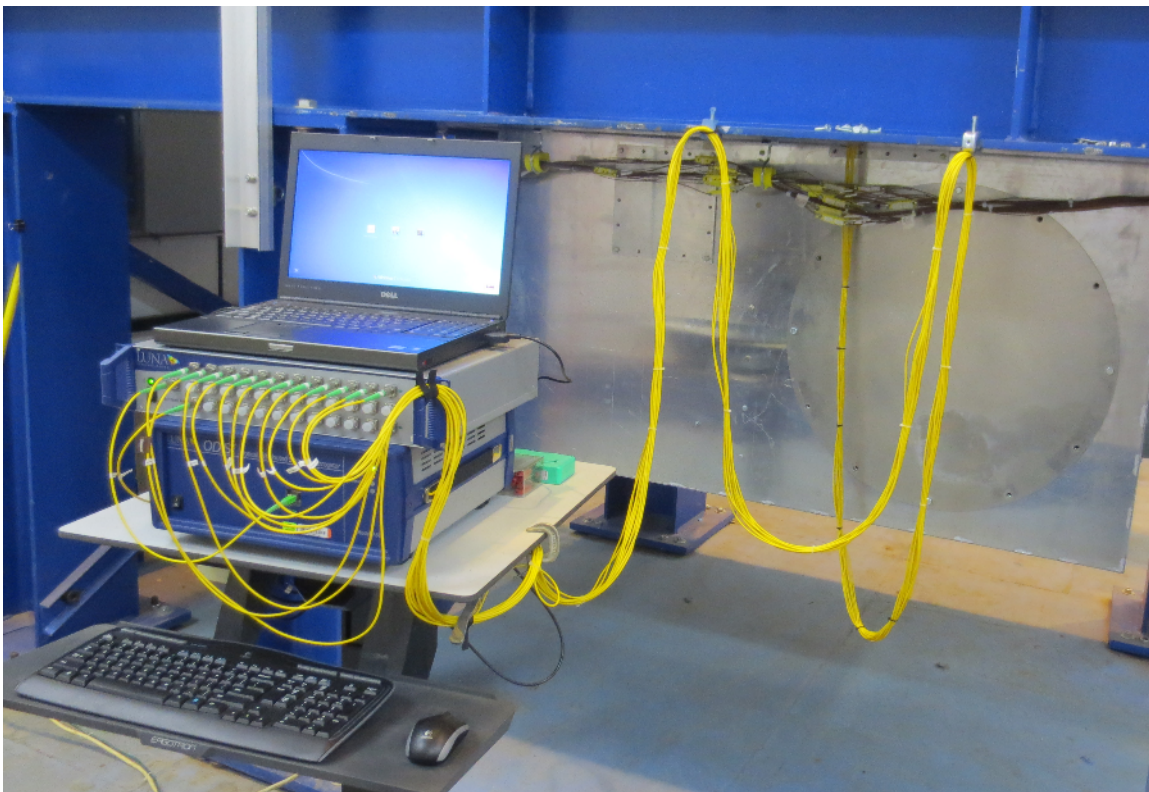


Figure 38: Luna fiber setup, near base mount and fed from inlet plenum

Inherent in their design, these sensors are unable to distinguish between strain and temperature: either will influence the measured signal. To overcome this, fibers were installed within 1/16" OD x 0.030 ID stainless steel capillaries, and secured (via heat shrink tubing) to only the head, nearest the insertion point, Figure 39.

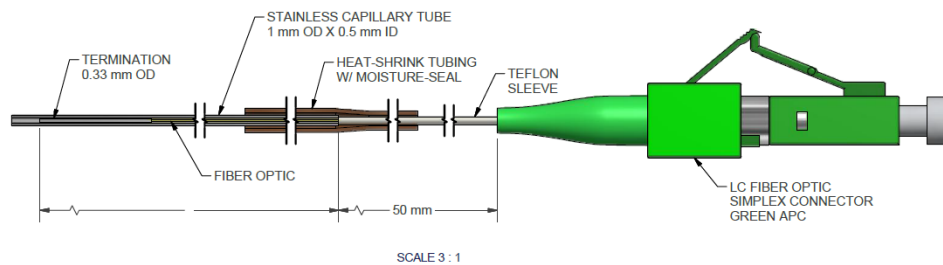


Figure 39: Method of Luna fiber optic cables securement to capillary support tubes

This configuration allows the fiber to freely expand up the capillary when heated, thus preventing any internal strain. Two riser ducts, #6 and #9, have been outfitted with these fibers: 6 on the outside wall and 5 within the gas space. These capillaries have been secured to the duct wall with spot welded bands, and within the gas space by routing through 8-32 brass fillister head screws.

The Luna fiber optic temperature measurement system requires a baseline calibration, as the actual measurements are in the form of a temperature *difference* from a known baseline, and not an absolute value themselves. Thus, sixteen (x16) NIST-calibrated Type-K wall thermocouples have been positioned along the duct walls for purposes of calibrating the LUNA fiber optic cables during baselines. These have been placed in a similar fashion to the wall capillaries - they extend along the length and are secured with spot welded bands to the riser tubes. Furthermore, an in-house calibration was performed to derive a polynomial fit for as-measured LUNA temperature to actual physical temperatures (as reference to a calibrated thermocouple), Figure 40. Details of this calibration procedure have been published in earlier works by the authors [19].

Given the relatively recent introduction of these sensors to the industry, they cannot be treated with the same maturity and reliability as conventional thermocouples. The successful installation and use requires a number of unique considerations. These are discussed briefly in Table 19, with further details available in other works by the authors [20].

Table 19: Unique requirements for LUNA fibers

Practice	Remarks
Thermal expansion	For measurement of temperature, the installation method shall be free from mechanical induced strain caused by thermal expansion. Thus, the fibers must be positioned in a manner that allows free expansion and contraction without restriction
Calibration	A representative sample fiber, construction from the same fiber type and termination connectors, must be calibrated against a known reference to obtain reference curves
Humidity	Changes in humidity influence fiber performance, and must be accounted for during post-processing. Observations from the NSTF testing program found, on average, a 0.15°C shift per % change in RH. This influence can be avoided if the fibers are housed in capillaries, purged with an inert gas and then sealed
Annealing	Upon final installation, the fibers must be annealed or cycled from room temperature, to the maximum anticipated operating point, and back to room temperature. This step is critical for collection of reliable, repeatable, and accurate data

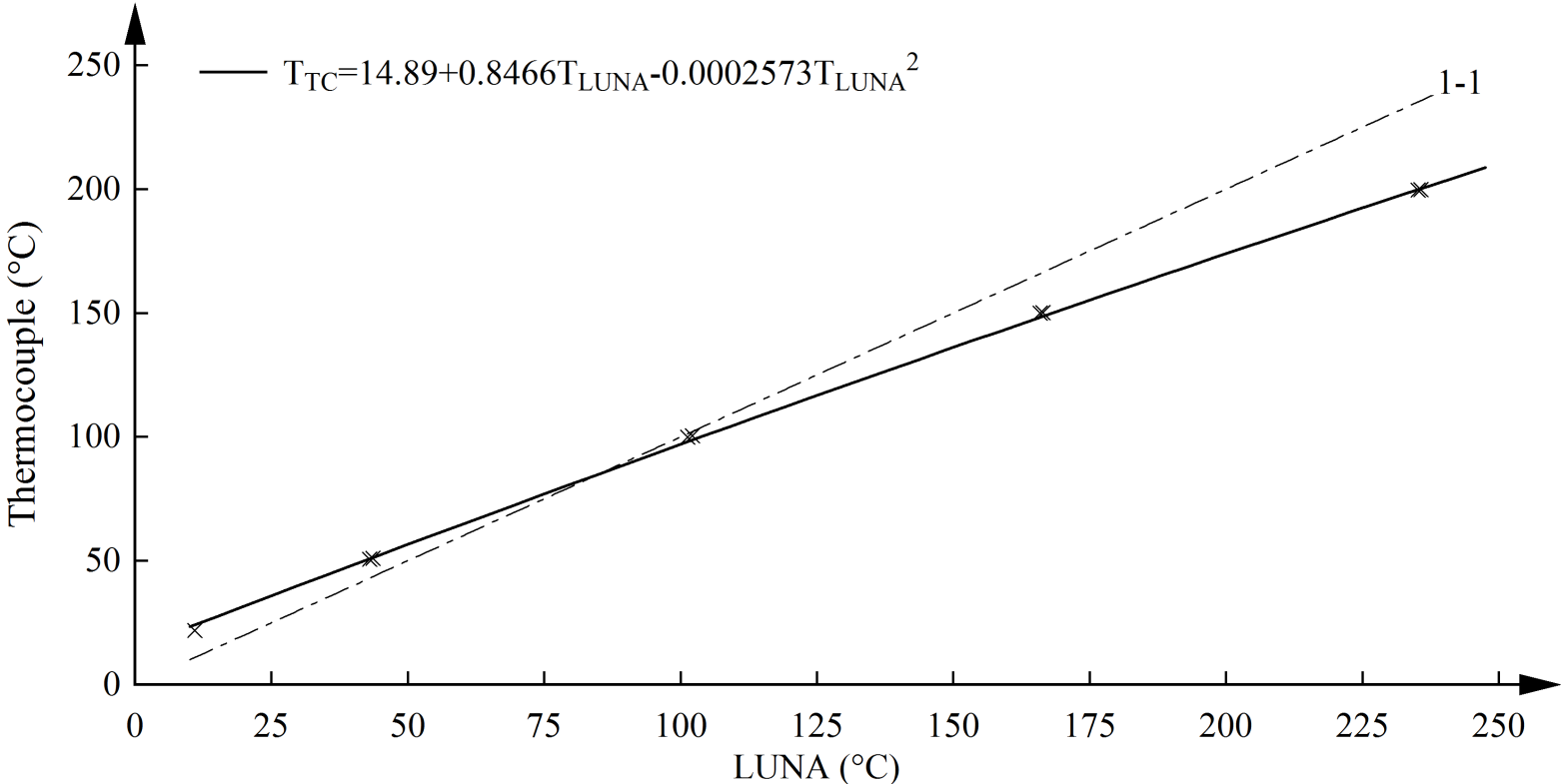
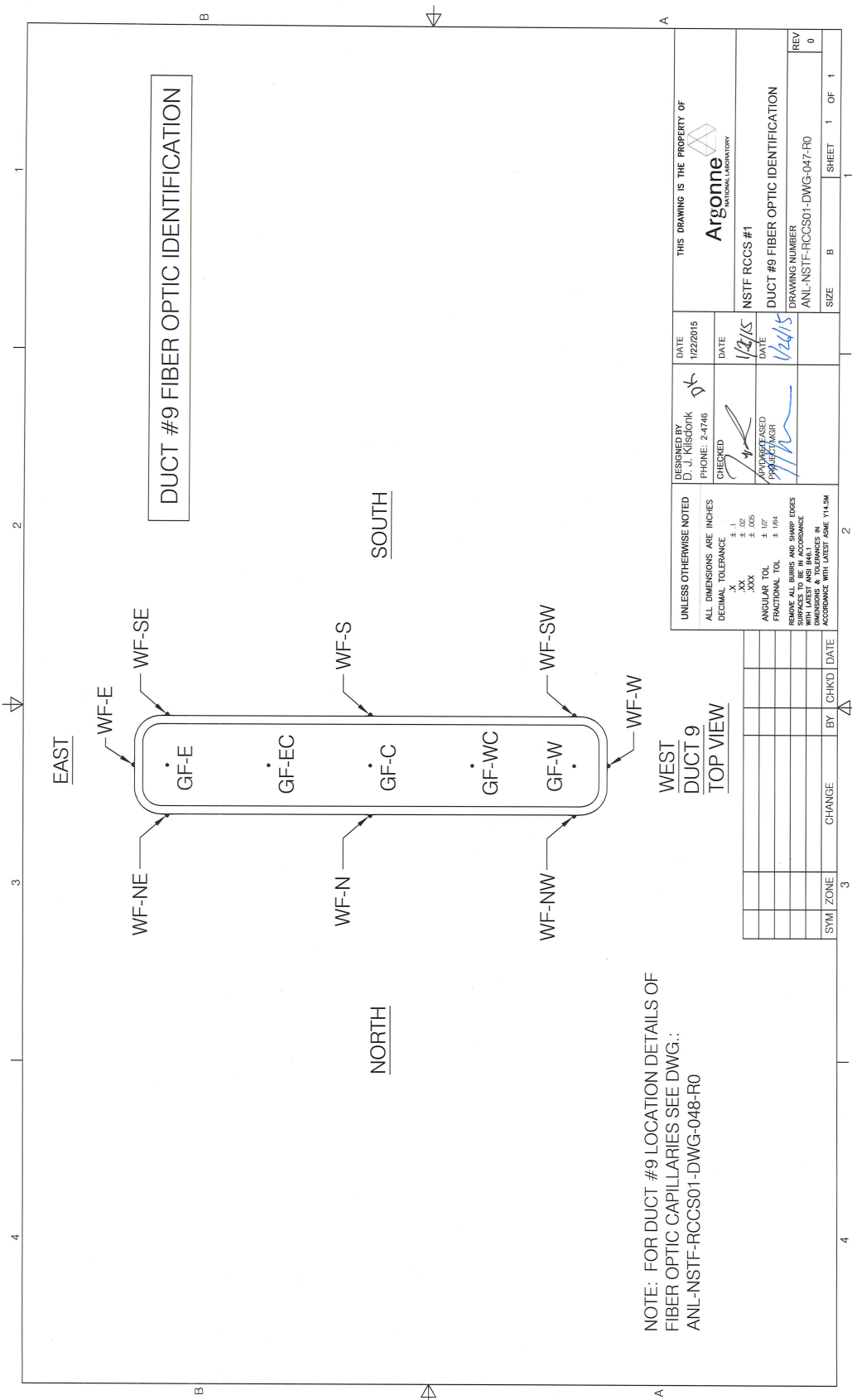
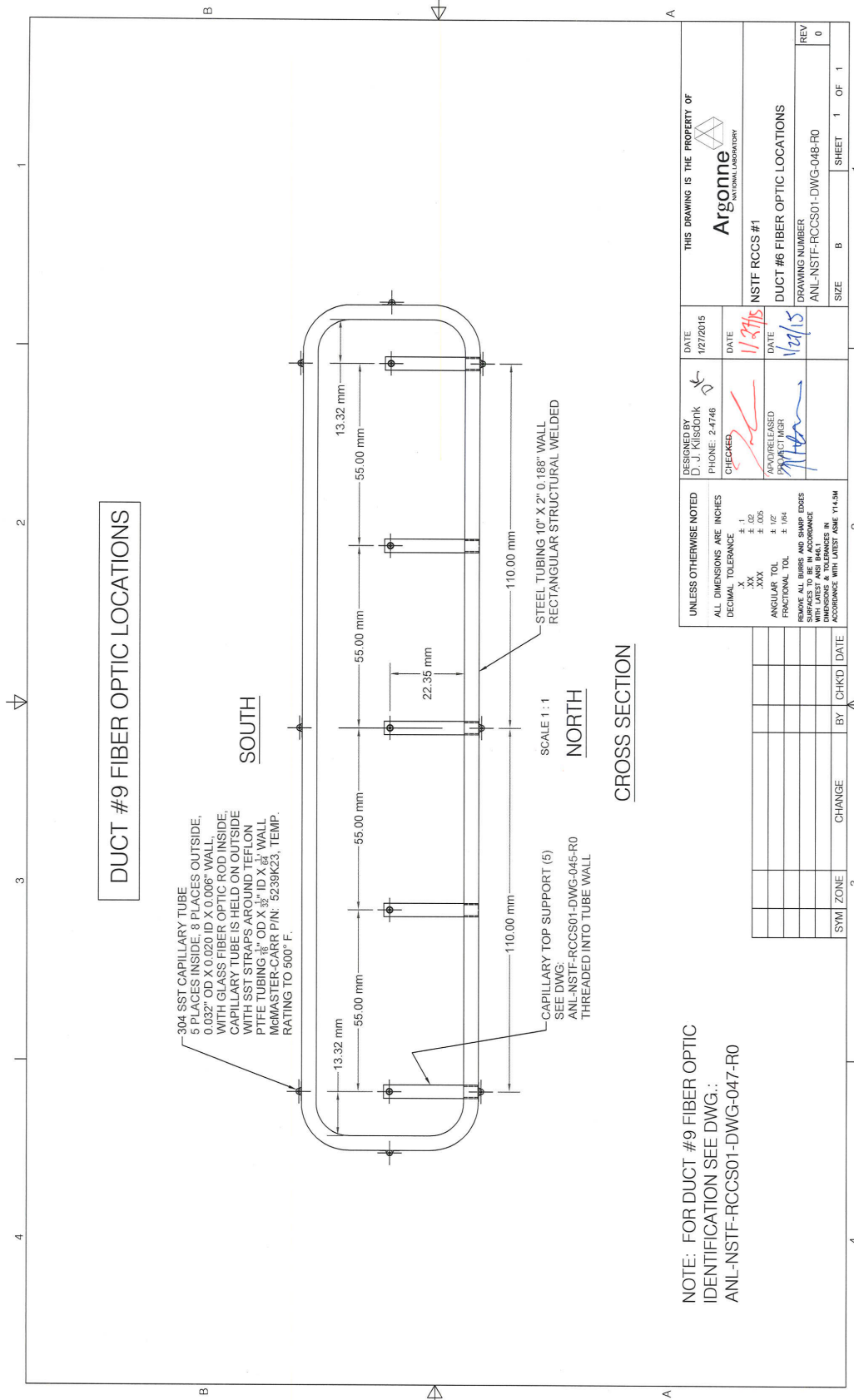


Figure 40: Calibration curve for polyimide LUNA fibers, reference to thermocouple standard





4.3 Heater Power Control

The heated section can be operated in one of three different modes: i) constant heat flux (21.6 kW/m² maximum), ii) constant temperature (677°C maximum), or iii) an arbitrary combination of these two modes. The 220 radiant heaters have been zoned into 40 control zones, 20 designated as the *main* and 20 as the *guard* zones, and produce a power distribution that provides 80% of the total from the *main* and the remaining 20% from the *guard* zones. The temperature and/or heat flux can be spatially controlled due to the fact that the heaters are zoned; the overall height is broken down into ten 67-cm long axial segments, while there are four azimuthal control zones at each axial elevation (two central zones plus two guard heater zones) yielding 40 control zones in total.

The zones are powered by 40 Eurotherm EPower controllers, rated for 600 VAC at 50A. The units maintain target power within $\pm 1\%$ of full scale during any moderate variations in line voltage, load impedance, and ambient temperature. Controllers perform real time measurements of actual delivered power via internal measurements of supply voltage and current, which are both accurate to within $\pm 1\%$. These have been configured in 5 primary banks, each with 4 substations, and communicate directly with the central control station via the iTools control software. Each of the 40 Eurotherm controllers and accompanying heated zones is hard wired to a Mini8 temperature controller that is programmed to a prescribed temperature set point. Should the thermocouple at this zone reach the safety trip set points it will automatically trigger a signal to deactivate the related contactor and thus shut off all main power to the individual zone. A top-level wiring diagram of the heater power system and control is provided in Figure 42.

The forty Eurotherm power controllers were initially configured for a Phase Angle mode of power control, which varies the amount of each cycle which is applied to the load by switching the controller thermistor on part-way through the cycle. However, this method comes with a number of drawbacks. First, high order harmonics are often introduced that

can create noise on nearby signals. Furthermore, it can deliver high di/dt (current spikes) which may reduce the life of a heater. Thus, later portions of the testing program switched to a Burst Firing mode of power control. This is the ideal mode of control since it provides a stable and smooth means of power delivery. To allow accurate measurement and calibrated verification of the power controllers, a NIST calibrated oscilloscope was procured as part of the testing program. Modifications were made to the heater calibration panel which allows measurement of each of the forty circuits and monitoring of the waveform by the oscilloscope, Figure 41. These waveforms can be readily read into LabVIEW and true power measurements calculated. The oscilloscope is Keysight model DSOX2004A, and features 4-channels capable of sampling at rates up to 70MHz. The AC/DC current probe, model Keysight 1146B, allows measurement of amperage ranging from 0.5 - 40 amp, while the voltage probe, model Keysight N2791A, allows measurement of voltages up to 700VAC.

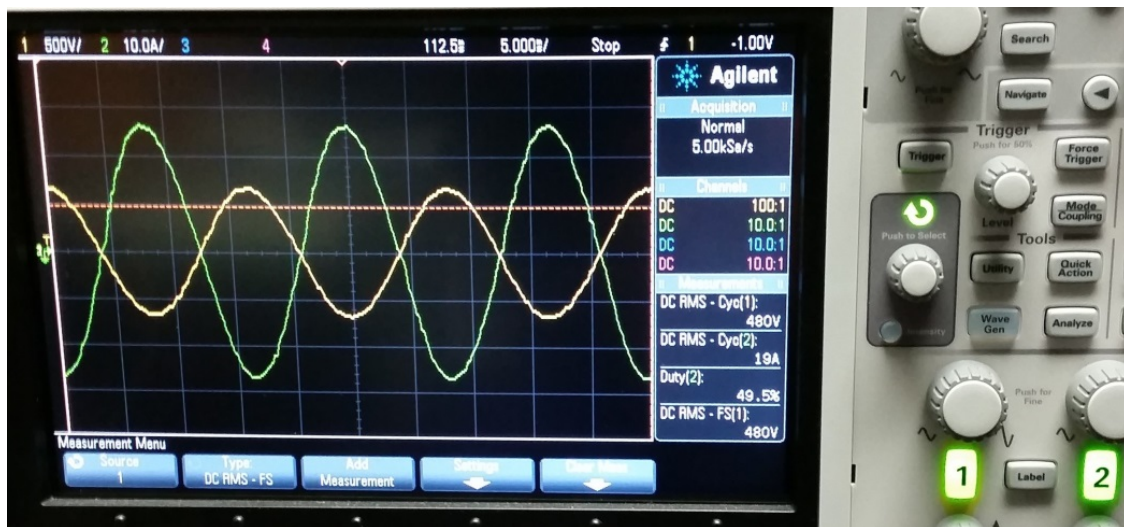


Figure 41: Voltage (yellow) and current (green) phases from 480VAC heater circuit

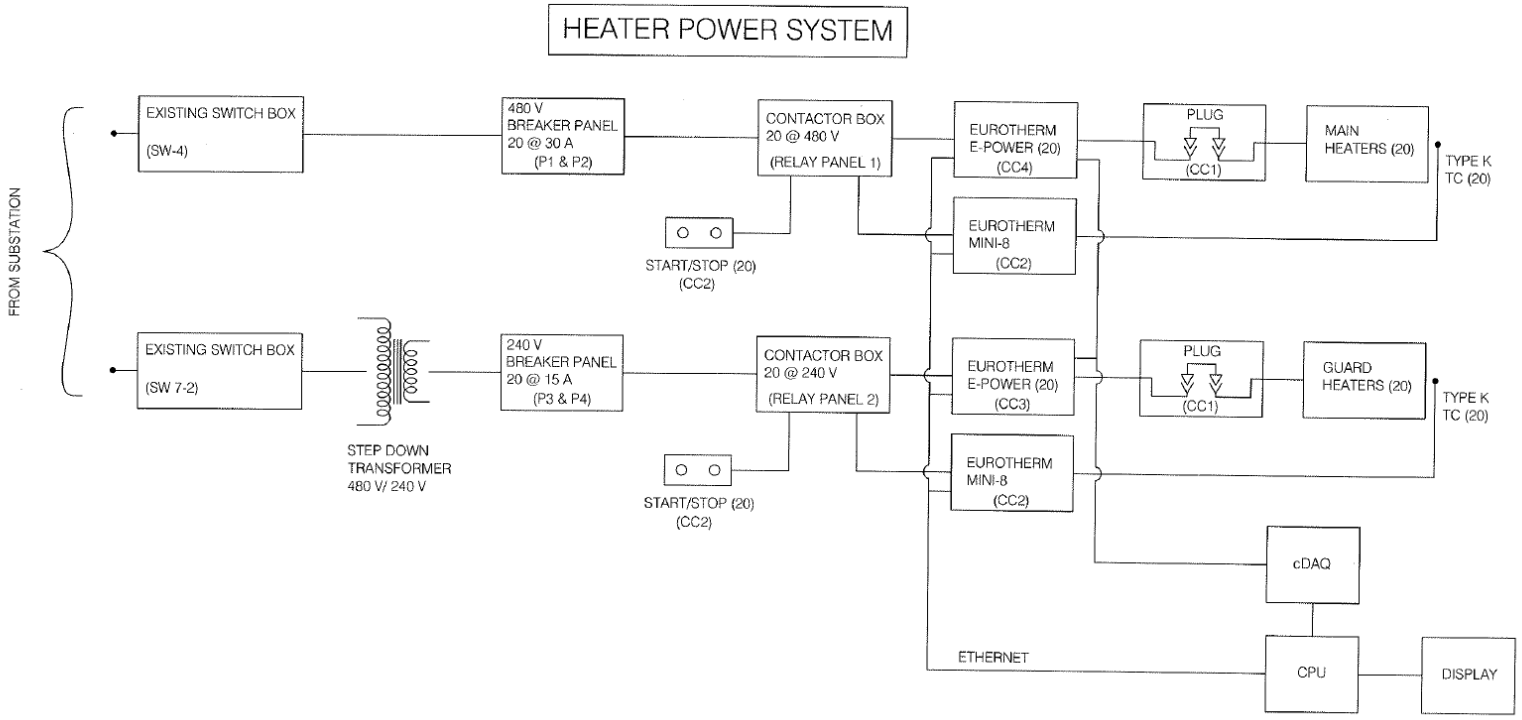


Figure 42: Eurotherm power and Mini electrical wiring

This page was intentionally left blank.

Chapter 5

Test Assembly Characterization

Unique to natural circulation systems are extended unheated chimney lengths and very low frictional losses; features that are critical to drive the chimney effect and establish system flows. However, given the sensitive nature inherent with natural circulation systems, those wishing to reproduce this work must repeat not only the prescribed boundary and initial conditions but also specific details to the geometry and material selection. Following best practices, the details presented in the following section will quantify the frictional form losses, parasitic heat losses, and closure of energy balances.

Several of the newest additions to the instrumentation suite within the experimental test facility have been directly for the purposes of characterizing the facility while also supporting computational modeling. Parameters such as turbulence intensity, frictional losses, and velocity profiles are critical to accurately capturing physical phenomena for documentation purposes and implementation within a computer based model.

5.1 Isothermal Velocity Profile & Frictional Losses

In-house calibration of the hot-wire sensors was verified by comparison to a NIST calibrated thermal flow meter, Model 640S from Sierra Instruments. The flow meter is able to measure flow rates between 0 - 1 kg/s with 1% uncertainty. Across the range of measured velocities, Figure 43, the two sensors differ by an average of 3.16%, and have suggested that reliable performance can be expected. This sensor was then mounted on a linear traversing system and used to map the velocity distribution across the inlet downcomer, Figure 44. The probe was positioned 2" past the flow conditioner, and highlighted the edge effects of the flow conditioner. As shown in Figure 44, "tails" of higher velocities can be observed near the outer edges of the inlet downcomer and are attributed to dimensional tolerances of the flow conditioner. The outer diameter (OD) of the honeycomb plate used to achieve the flow conditioner is not exactly the inner diameter (ID) of the ductwork, thus small gaps exist. However since the flow sensor was calibrated in this exact geometry, the non-uniform velocity is known to the sensor and thus does not introduce additional uncertainty into the measurements.

Testing was performed at isothermal conditions to quantify the frictional losses at varying points along the flow path. A high-resolution differential pressure transmitter, Dywer Model 668-11, was used and is capable of measuring pressure differentials between ± 62.25 Pa with 1% uncertainty. The losses across the exhaust chimney ducts, Figure 45, and inlet downcomer, Figure 46, were measured and in some cases converted to parameters such as the K-factor to facilitate integration into computational codes. Similar efforts were made to quantify the average loss across the full length of the riser ducts, which has been converted to the friction factor, f , to facilitate integration into computational codes, Figure 47.

During heated operations, the system sees flow rates that average 0.5 kg/s. Thus, isothermal testing was performed over a span of 0.2 - 0.8 kg/s, which translates to Reynolds numbers between 35,000 and 95,000 for the inlet downcomer, and 6,000 and 24,000 for the riser ducts.

This testing was performed to characterize the turbulence intensity and velocity profiles of the inlet and riser ducts within the NSTF.

The inlet downcomer experiences a turbulence intensity that averages 9.7% at the range of Reynolds numbers typically observed during test operations, Figure 48. Across the riser ducts, Figure 49, this value is reduced to 5.36%, which stems from the longer length of the riser tubes and thus greater distance for the flow to become fully developed.

The high turbulence values at the downcomer inlet can be primarily attributed to the placement of a flow conditioner and otherwise lack of an extended length for flow development. The flow conditioner, a wire-mesh type device, is commonly used to establish a known velocity profile when spatial constraints do not allow required length to establish fully developed flow for flow sensors. The resulting profile is flat and known, to which our flow sensors are calibrated against.

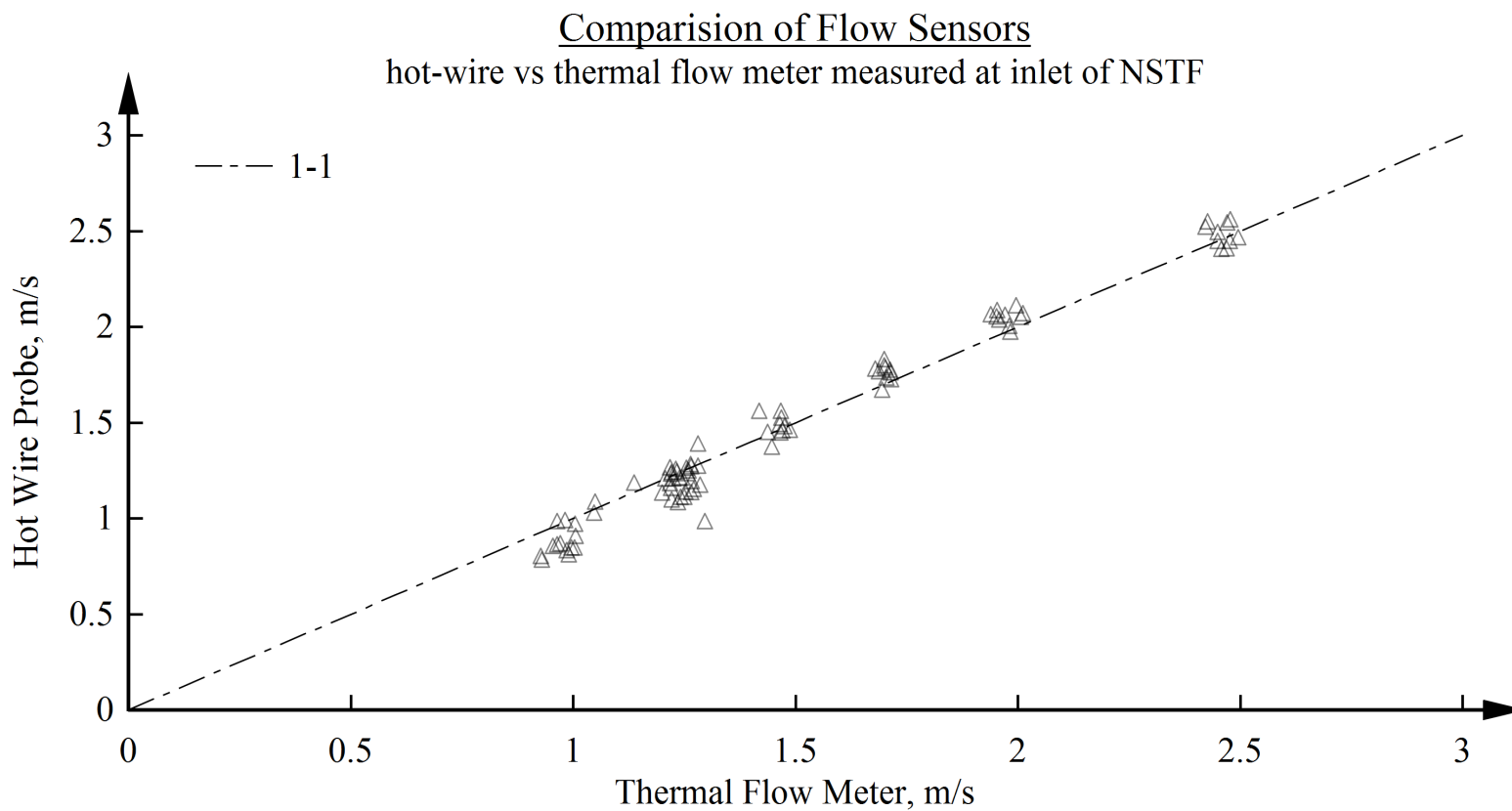


Figure 43: Comparison of velocities as measured by flow meter (x-axis) and hot-wire (y-axis)

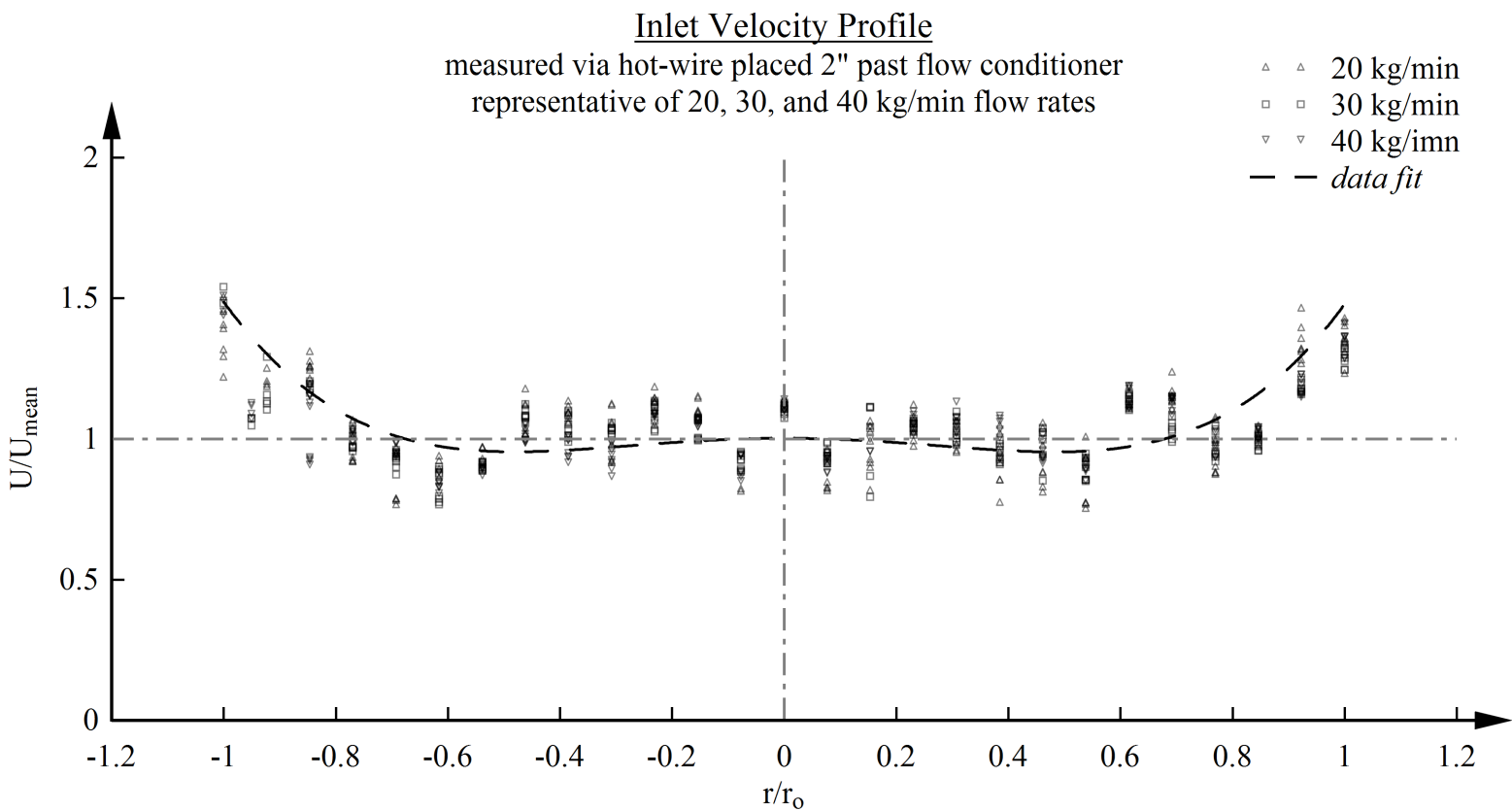


Figure 44: Velocity profile of inlet downcomer via hot-wire probe. Tails near radial extremes are due to leakage past honey-comb grating of flow straightener

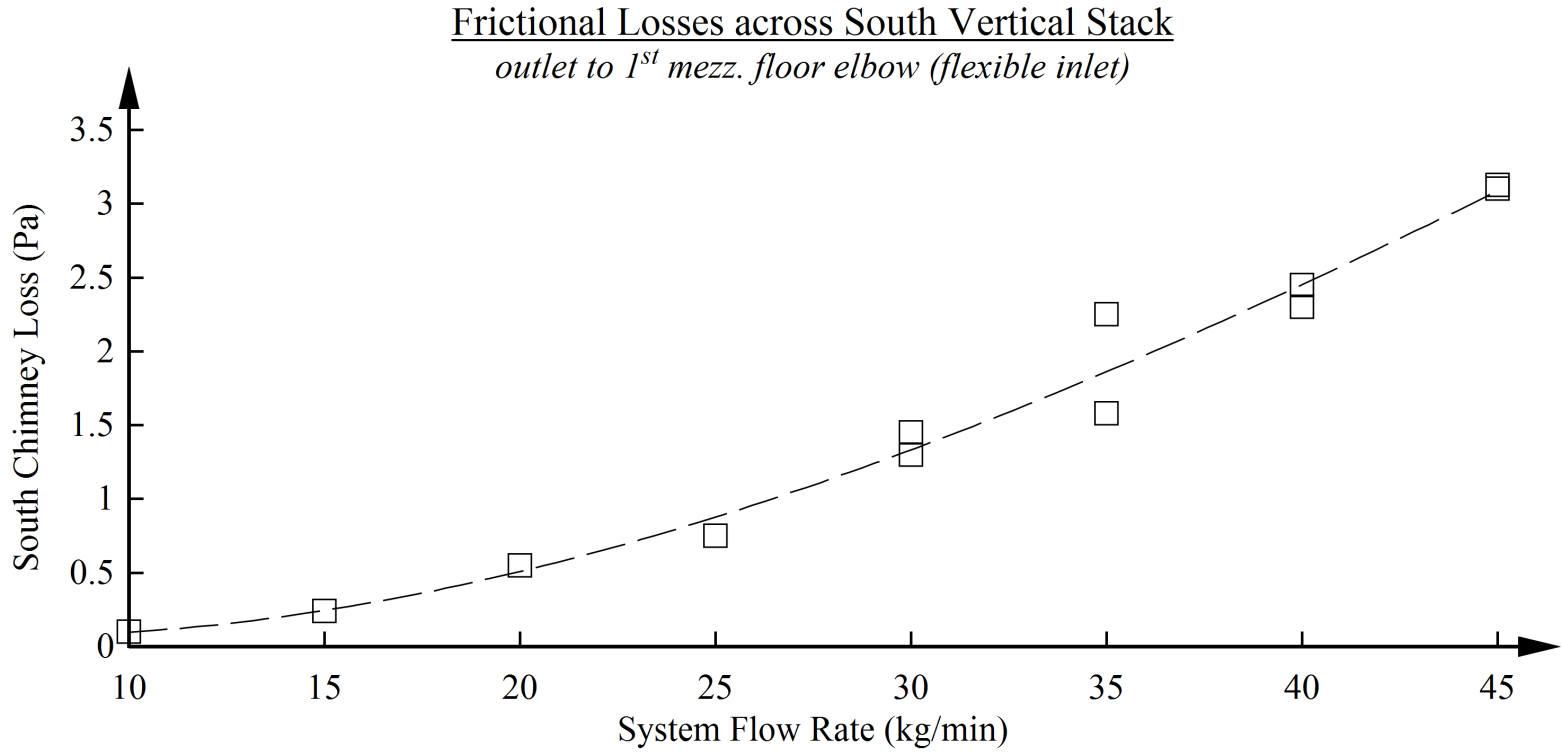


Figure 45: Frictional losses across a single chimney flow path, shown in raw units of Pascals

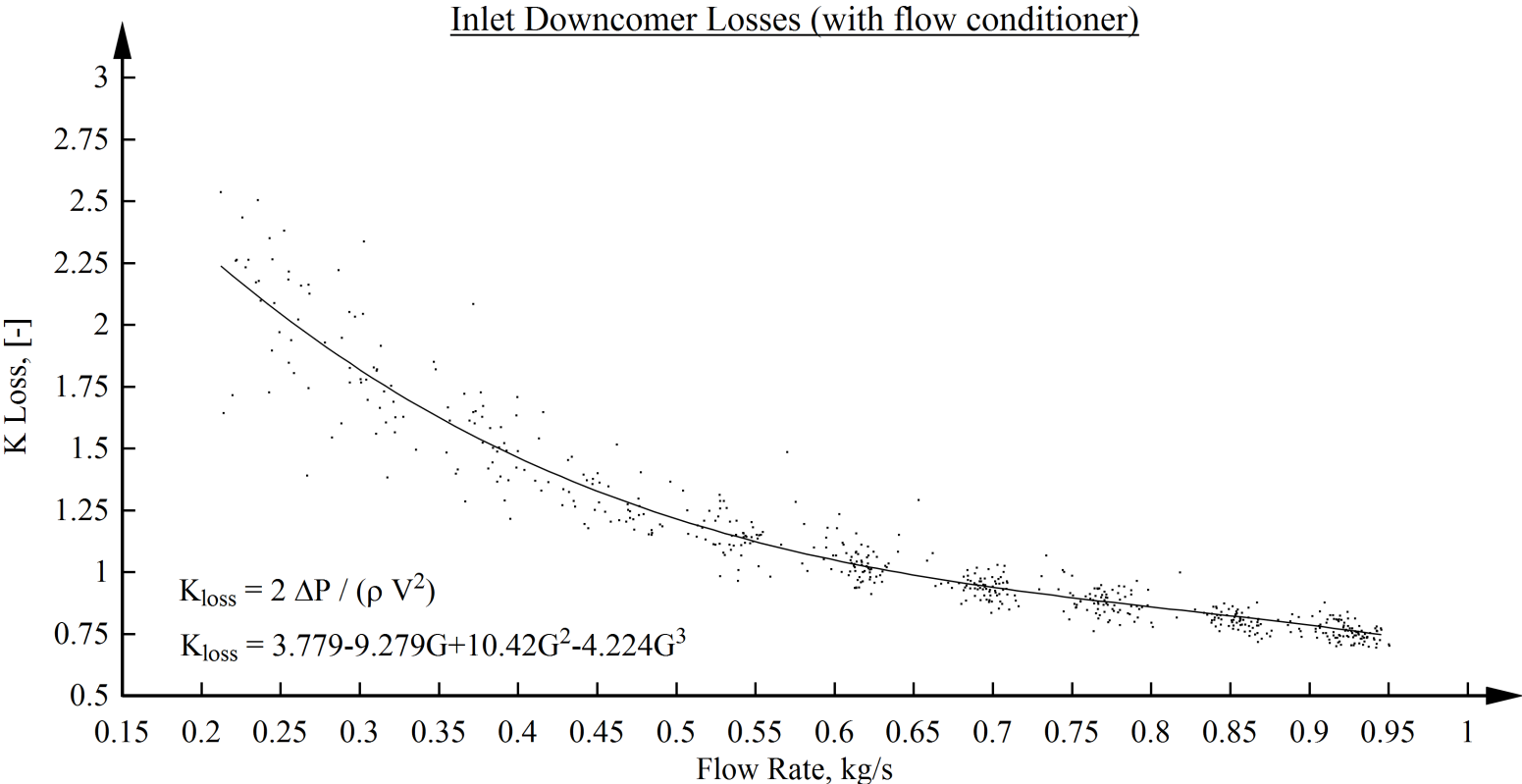


Figure 46: Frictional losses across inlet downcomer, in terms of K-factor

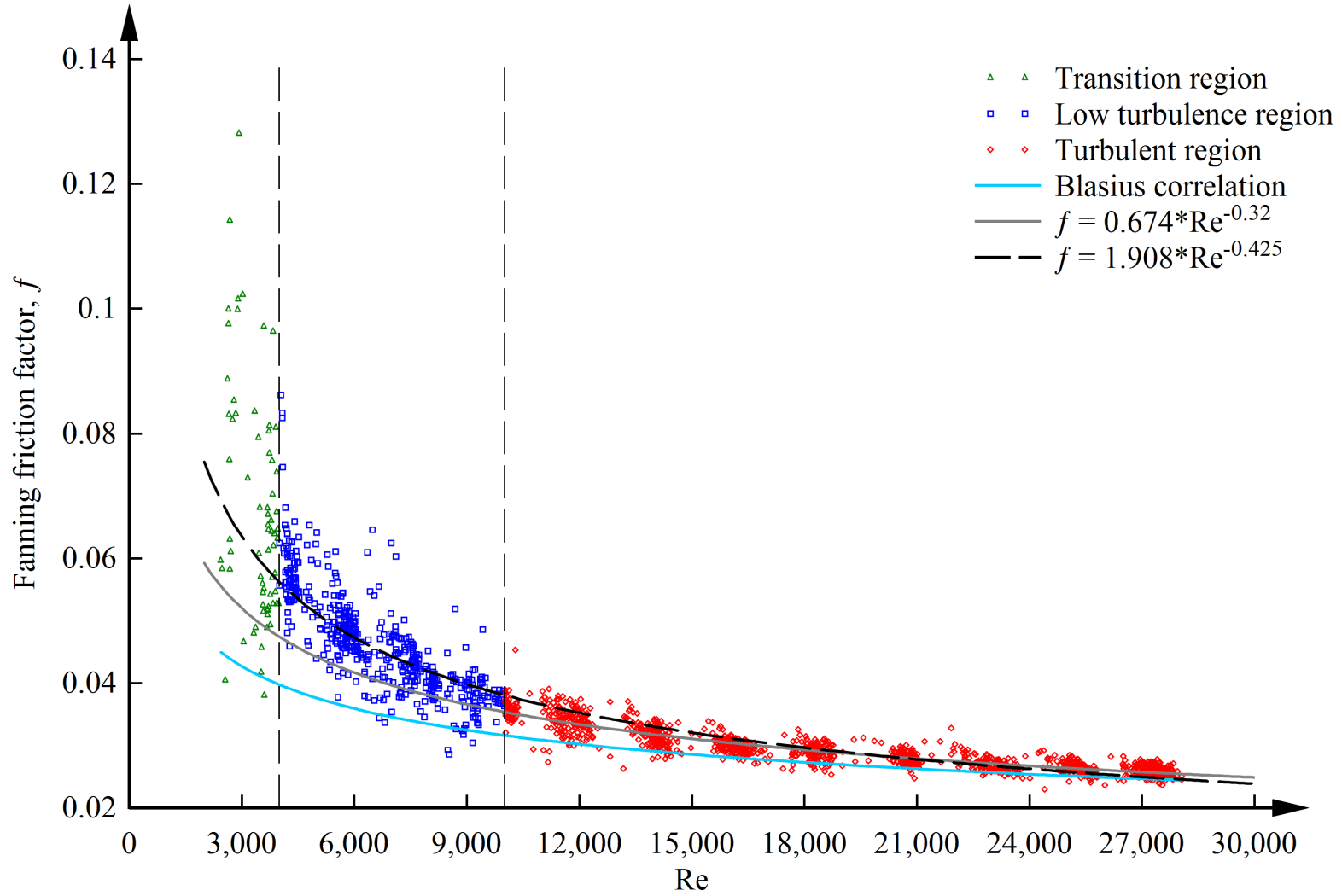


Figure 47: Isothermal losses across riser ducts in terms of fanning friction factor, f

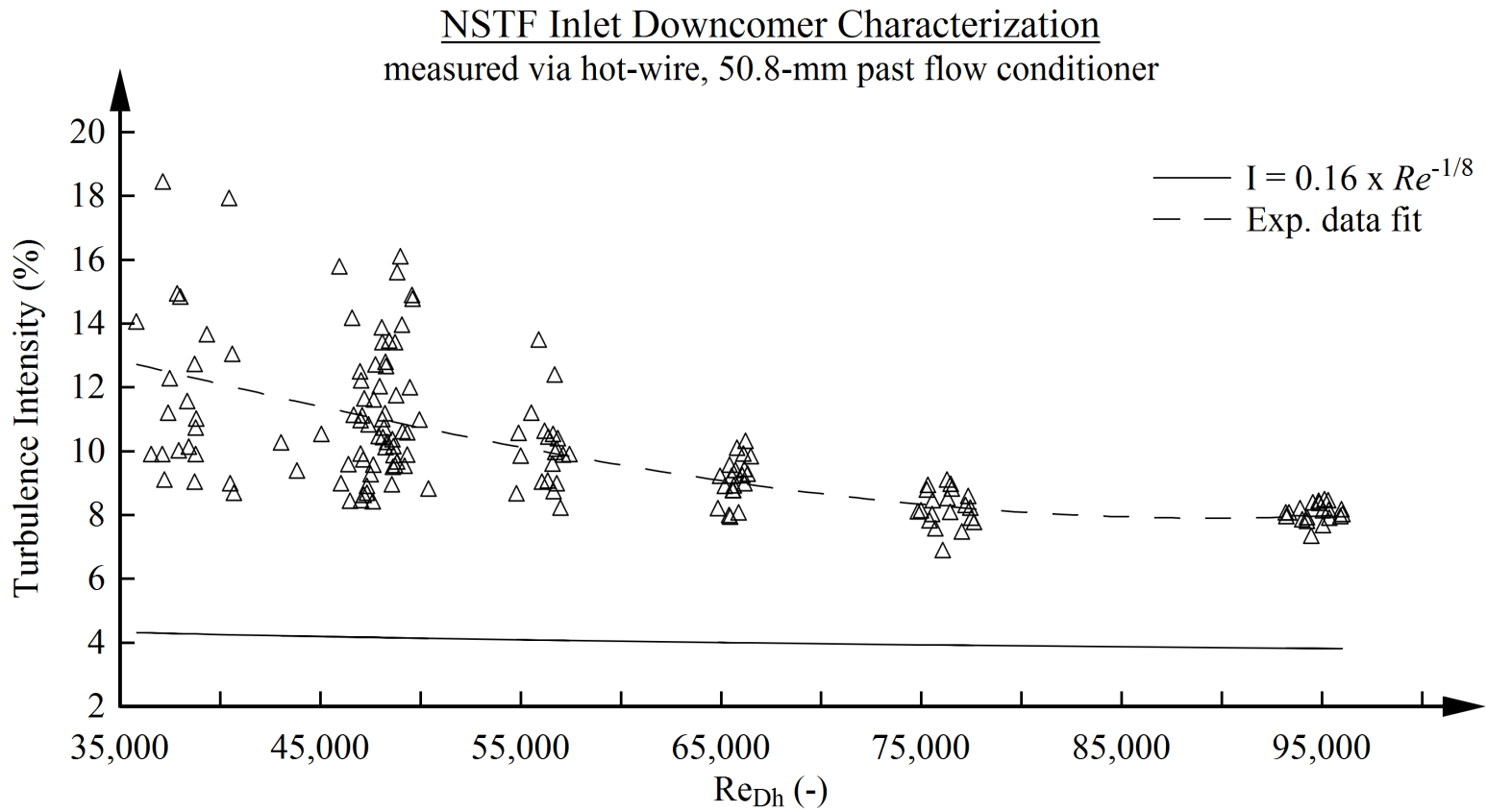


Figure 48: Turbulence intensity at inlet conditions measured via hot-wire probes. Scatter at low Re-numbers occurs due to the very large duct diameter and relatively low velocities, which creates large fluctuations in the flow

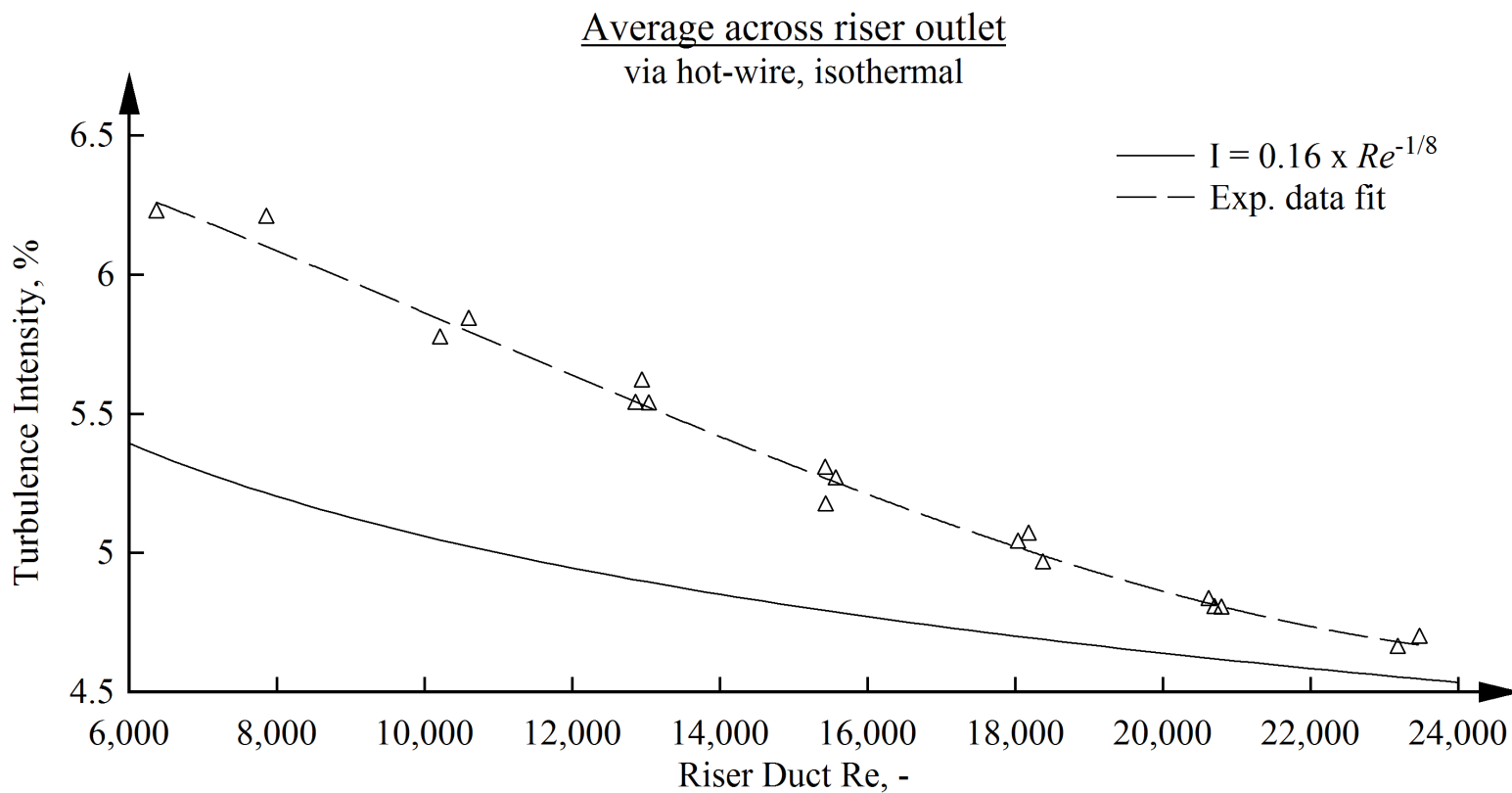


Figure 49: Turbulence intensity at riser outlet conditions measured via hot-wire probes

5.2 Temperature Profiles

The primary sensors used to measure the temperature rise across the heated test section, or the gas temperatures at the inlet and outlet of the riser ducts, have relied on 1/16" type-K thermocouples positioned at the center-line of the ducts. These gas measurements have served as the main means of calculating thermal energy balances and characterizing the air temperature leaving the riser ducts. However, newly installed LUNA fiber cables, positioned across the duct area at the outlet as shown in Figure 50, have provided greater temperature detail and enabled new performance observations, Figure 51.



Figure 50: New LUNA fiber sensors installed across 10-inch width of one riser duct (outlet)

The temperature profile at the exit face of the risers was observed to vary moderately with the power levels, but highly with system flow rates, Figure 52. During CaseII of the INERI test series, where a low flow (0.22 kg/s) and high temperature ($\Delta T = 98^{\circ}\text{C}$) operating state was required, a flattened temperature gradient is visible within the core of the risers and transitions through a sharp rise near the wall. The majority of other observed cases, which are representative of baseline testing conditions, exhibit a more gradual gradient that follows a relatively smooth transition from the core to the walls.

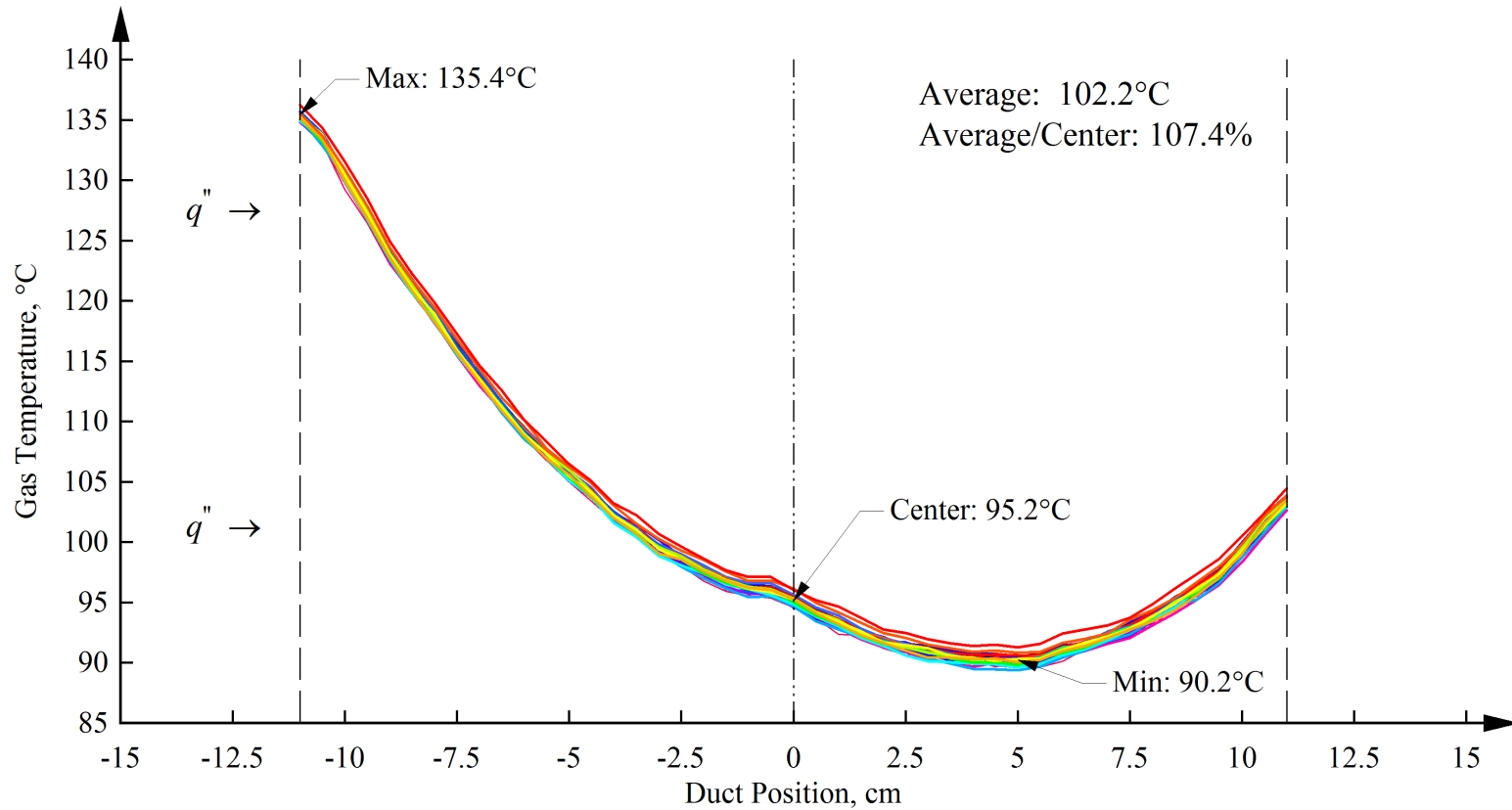


Figure 51: Continuous temperature profile as measured at the exit plane of the riser ducts. Heat source originates from the left side of the figure, and the cold wall on the right side

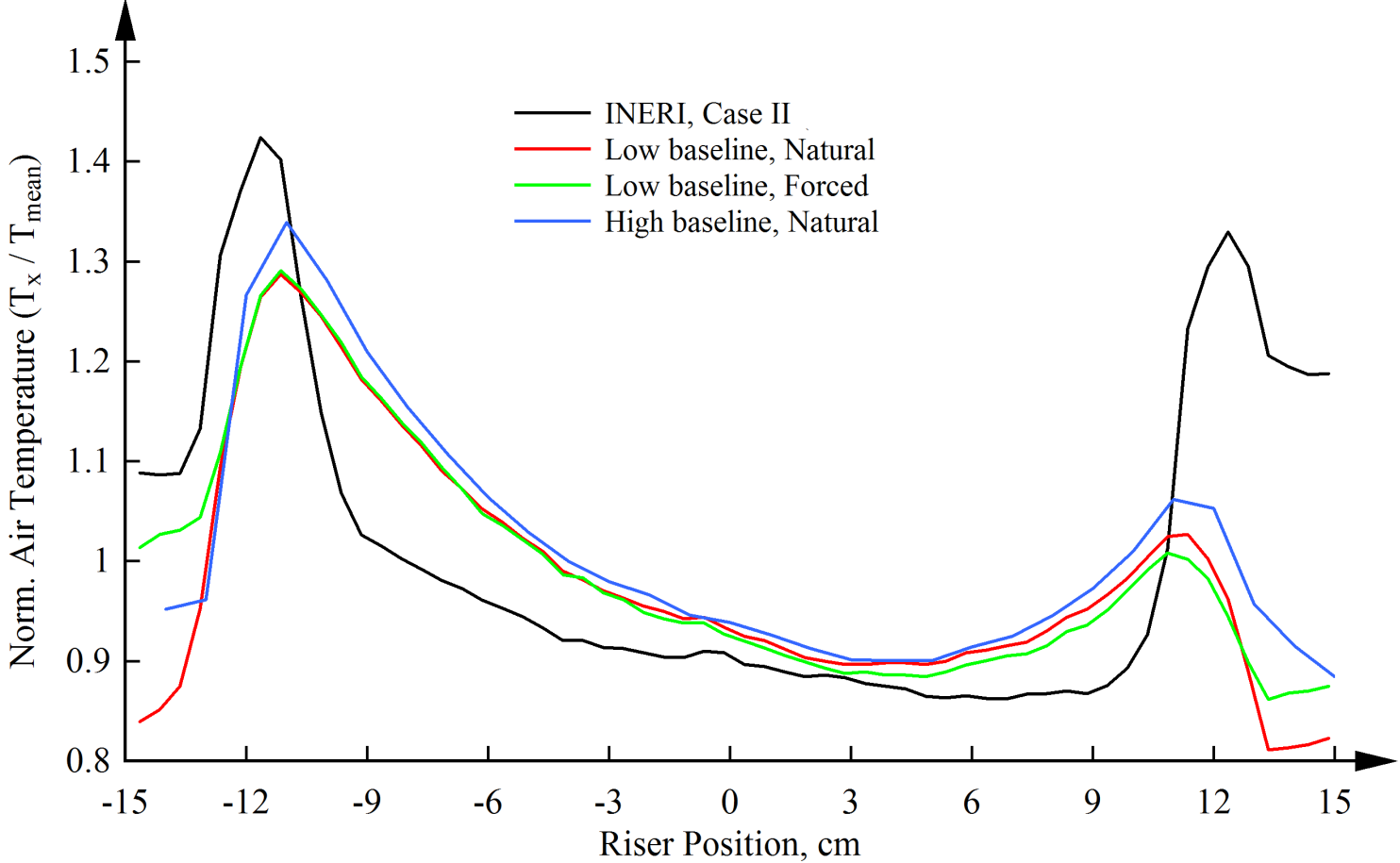


Figure 52: LUNA temperature profile across riser outlet face for varying conditions

For a sample set of conditions (initial steady-state period of Run015, which was the baseline configuration at the steady-state residual heat load of 26 kW_t), the temperatures indicated by the thermocouples only give a partial picture, Table 20. These results suggest that, on average, the entire duct-average gas temperature is on the order of 112% greater than the center-point temperature as measured by the TCs. This result is strongly dependent on the system flow rate and heater power, and will be the focus of future testing.

Table 20: TC vs LUNA recorded temperatures during steady-state Run015 (26 kW_t)

Sensor	Position	Temperature
1/16" TC	Duct center	76.53 °C
LUNA	Duct center	76.64 °C
LUNA	Duct maximum	107.49 °C
LUNA	Duct averaged	85.76 °C

Other installations of the LUNA fibers included the riser gas space and wall surfaces. The original installation within riser #6, coined *SuperDuct*, exhibited some short-comings that introduced artifacts in the temperature data and was subsequently improved during a 2nd iteration within riser #9, coined *SuperDuct 2.0*. The new installation omitted the multi-point mounting and instead fixed the fibers within a capillary near the outlet of the riser, and used springs to tension the lower end. This served two purposes: ensure that no conduction heat transfer was introduced along the length of the gas space, and allow free expansion of the stainless capillary as the facility experienced heated test operations. The improved method generated high-quality data that proved valuable in direct comparisons against CFD models. The old duct was then painted and mounted on display for tours in the high bay of building 308.

Lastly, two 8.5-m fibers were installed within the gas space of the outlet plenum which provided high-fidelity temperature profile across the full volume of the outlet plenum. This specific installation proved challenging, given the demanding requirements of strain-free installation for valid temperature measurements. The team ultimately constructed mounting jigs that allowed the stainless steel capillary to be pre-formed into the desired S-shape, which was then transferred by a light-weight vehicle for installation in-situ, Figure 53. The task of mapping physical locations to points along the fiber was performed and the resulting figures gave new insight into temperature distributions.

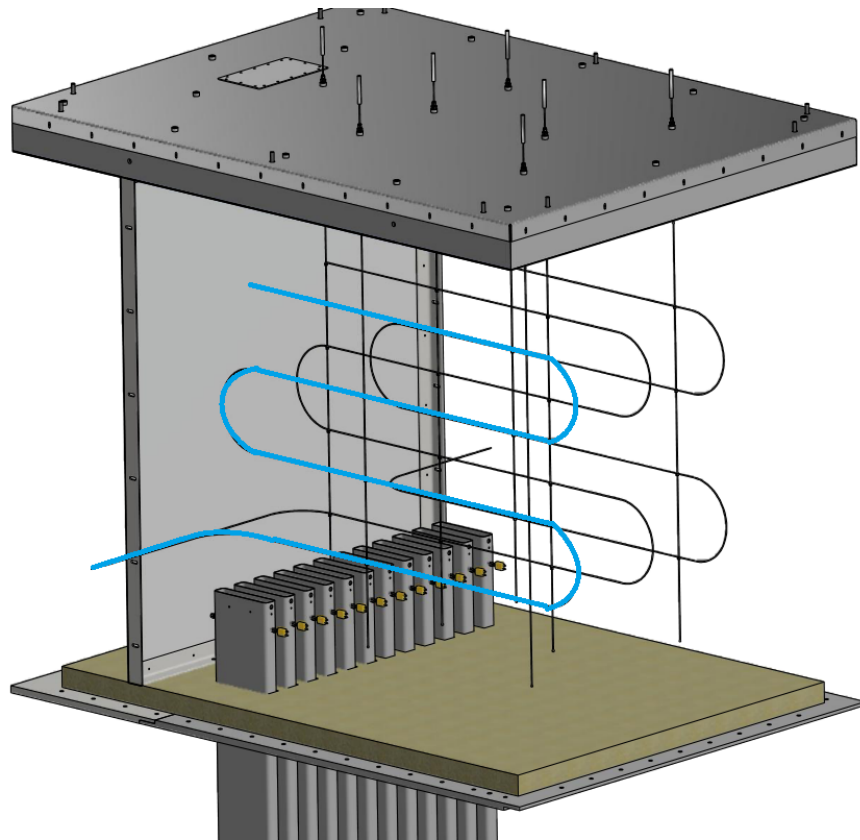


Figure 53: Mounting of LUNA fibers within outlet plenum gas space

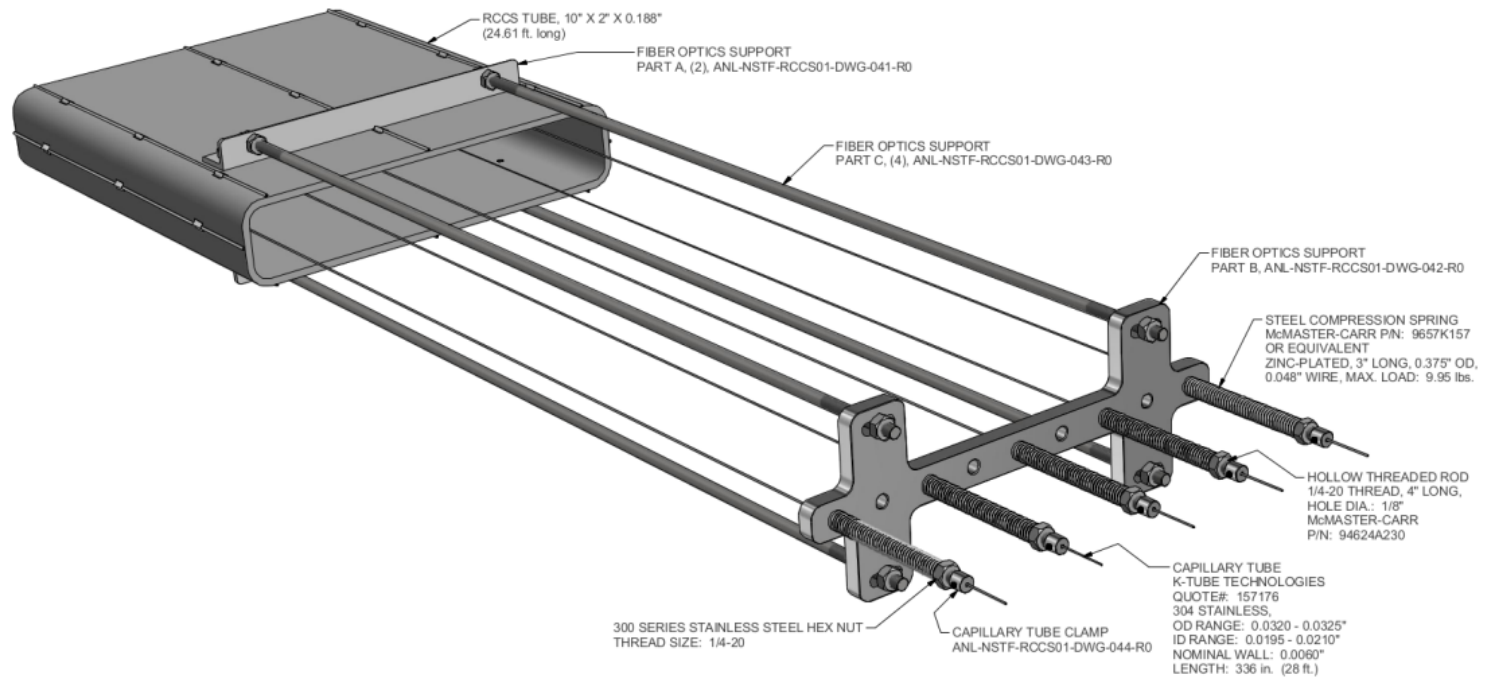


Figure 54: Riser #9, SuperDuct 2.0, gas fiber mounting method

5.3 Heat Losses

The knowledge of true power removed by the riser ducts within the NSTF is a critical parameter for assessment of the facility performance across the testing conditions performed. Due to physical imperfections, e.g. the inability to create a truly adiabatic wall, thermal losses are unavoidable. While these do not detract from the overall quality of the testing, it is important to accurately quantify these to obtain knowledge of the true thermal power within the test section.

The power supplied to the electric heaters is controlled from a set of industrial power controllers, with details available in earlier works by the authors [22]. Their ability to control voltage and current levels to the resistive heaters is one basis for determining thermal losses. The path of heat transfer for electric power from the heaters to the working fluid within the riser ducts includes a complex route of conduction, convection, and radiation. During this process a portion of the originating power is removed as parasitic losses across the insulated walls, back cavity, and other paths of leakage around the heated enclosure. The efficiency of this thermal network was determined through a separate effects study that examined a range of electric powers and system flow rates, with comparisons to the measured thermal power removed by the risers, Figure 55.

The calculated power has included the true average temperature of the outlet gas via LUNA measurements, and indicated that the NSTF operates at a nominal 65% thermal efficiency from the original electric power to the heaters. With this knowledge, testing procedures can be refined to include best estimates of the required electric power to achieve a desired test section heat removal rate, along with more accurate inputs to computational modeling.

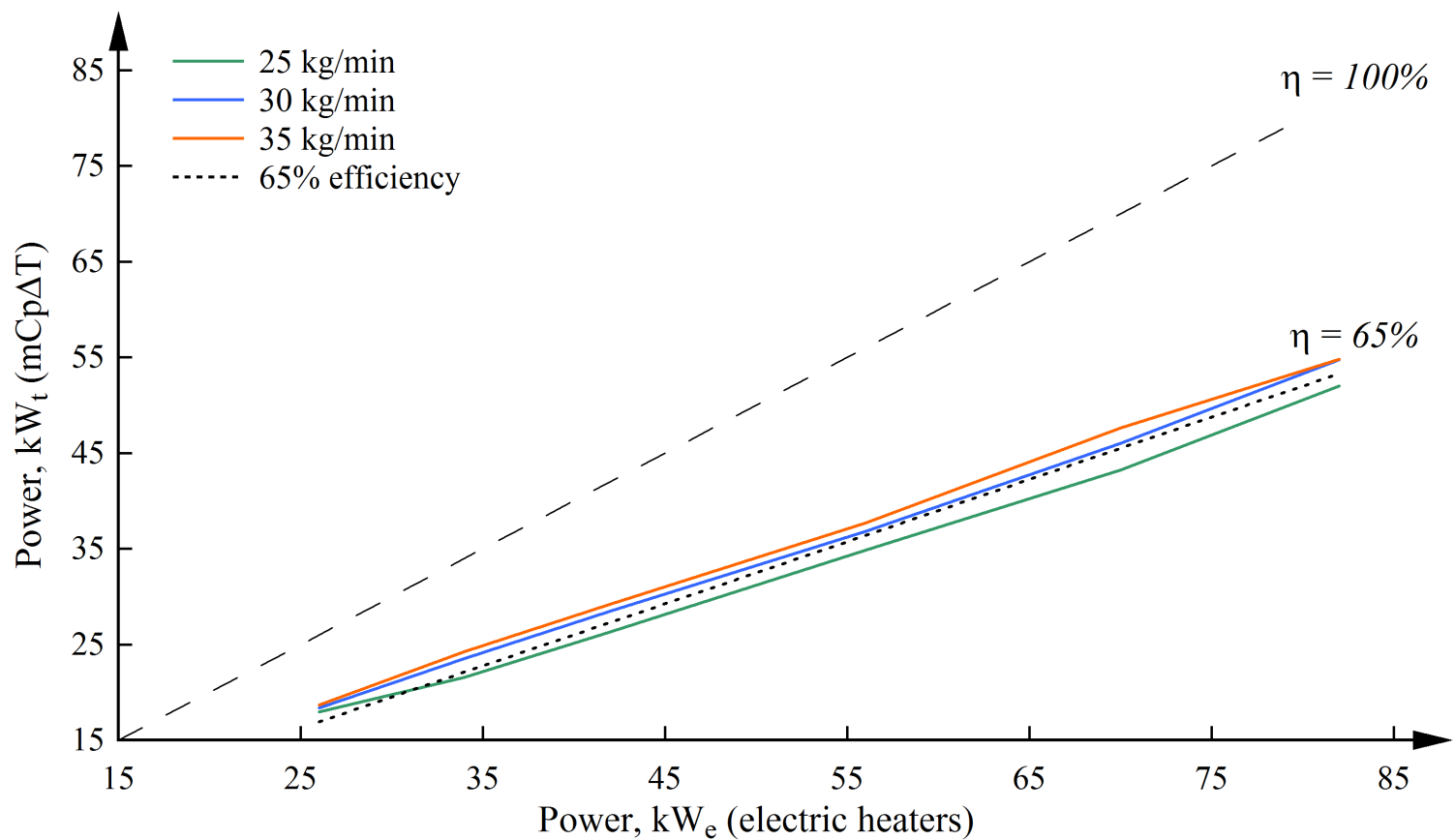


Figure 55: Thermal efficiency of the NSTF, determined by separate effects testing at varying electric powers and flow rates

5.4 Physical Properties

The thermal-hydraulic behavior of the NSTF is a complex system driven by multiple heat transfer mechanisms. One region of particular interest is the convective heat transfer within the riser tubes. Given that the system fundamentally operates on natural circulation to achieve its heat removal function, it is of interest to quantify the mode of convection. Dimensionless numbers such as the Reynolds, Rayleigh, Nusselt, etc. can provide insights into the physical behavior and aid in the overall understanding.

Characteristic flow parameters, along with related dimensionless numbers have been identified for the span of observed behavior across the NSTF testing program. To obtain values for the various dimensionless numbers such as the Nusselt number, one must first identify the correct empirical correlation which is dependent on a characteristic length and flow regime. The riser duct geometry, a tall slender vertical cylinder, lends itself to discussion on the appropriate characteristic length used in determining these dimensionless numbers.

Perhaps the most common dimensionless parameter, the Reynolds number, Eqn. 7, describes the ratio of inertial to viscous forces and is a primary means of identify the flow regime. For internal pipe geometries, the flow regime can be classified as laminar when $Re < 2,300$, turbulent when $Re > 4,000$, and transition when values fall between these two ranges. Fluid properties are evaluated at the mean fluid temperature, $T_m = (T_{inlet} + T_{outlet})/2$, and the characteristic length is the diameter for circular ducts $L_c = D$, and the ratio of flow area to wetted perimeter for square or rectangular ducts, $L_c = 4A_c/P_w$.

$$Re = \frac{\rho U_{\infty} L_c}{\mu} \quad (7)$$

Thermally, natural convection along a heated vertical cylinder leads to the development of a boundary layer that grows along the cylinder axis, or direction of fluid movement. These two geometries can however be treated equally when the boundary layer thickness along a vertical cylinder is much smaller than the cylinder diameter. If this relation holds

true, then the curvature of the cylinder is insignificant in the heat transfer mechanisms and can be idealized as a flat plate. More specifically, a vertical cylinder can be treated as a vertical plate in a free convection system when the following relationship, Eqn. 8, holds true. The Grashof number, defined by Eqn. 9, represents the ratio of buoyancy to viscous forces and is analogous the Reynolds number for free convection systems. It can also provide an indicator of the flow regime, and when also considering inertial forces, can define the type of convection.

$$\frac{D_h}{L} \geq \frac{35}{Gr^{0.25}} \quad (8)$$

$$Gr = \frac{g\beta(T_s - T_\infty)L_c^3}{\nu^2} \quad (9)$$

For the test cases spanning the measured ranges of NSTF testing, the flat plate approximation was found to be not applicable ($0.01 \not\geq 1.2$), thus requiring use of cylinder or enclosure specific correlations for free convection parameters.

Identifying the characteristic geometry for natural convection within a heated riser is strongly dependent on the specific flow conditions and duct dimensions. The characteristic flow patterns can be modeled as either a cylinder, plate flat, enclosure, or parallel channel. Enclosures are defined by relatively large aspect ratios in either direction, of sufficient spacing to allow circulation flow patterns to develop, thus not applicable to the slender riser geometry of the NSTF. Previous discussions indicate that a vertical plate is not appropriate, thus only a vertical cylinder and parallel channel remain for consideration.

Vertical parallel channels exhibit similar behavior to internal forced convection conditions because growing boundary layers are inherently bounded by the side walls. There exists a developing region with boundary layer growth, followed by a fully developed region with bounded layers. For developing regions greater than the total length of a channel, the flow can be accurately modeled using correlations for a vertical plate. However, if the ratio of

channel length to space is large, the flow will quickly become fully developed and parallel plate specific correlations must be used [23].

The Rayleigh number for free convection between parallel plates is based on a characteristic length defined by the plate spacing, S . For symmetrically heated, isoflux surfaces, a modified Rayleigh number is given by Eqn. 10, with fluid properties evaluated at a modified film temperature, $\bar{T} = (T_{S,L} + T_{\infty})/2$.

$$Ra_S = \frac{g\beta q_S'' S^4}{k\alpha\nu} \quad (10)$$

Moreover, when combined with the Reynolds number to consider inertial forces, this ratio, termed the Richardson number, Eqn. 11, represents the ‘importance’ of natural to forced mechanisms of heat transfer in mixed convection systems. Typically, forced convection dominates when the $Ri \ll 1$, natural convection dominates when $Re \gg 1$, and both contribute when the $Ri \approx 1$.

$$Ri = \frac{Gr}{Re^2} \quad (11)$$

A number of test cases were examined in detail, and selected to provide a representative span of the ranges observed across NSTF test cases. Lowest system flow rates were measured during the I-NERI (Run023) and Adjacent Chimney (Run017) test cases, and highest flow rates during cold weather baseline testing (Run022). Based on calculated dimensionless thermal and hydraulic parameters, Table 21, all cases were determined to fall in the turbulent flow regime ($Re_{D_h} > 4,000$), with free convection effects assumed to be negligible compared to forced convection ($Ri \ll 1$). This is further confirmed by a mapping of the regimes through vertical tubes, Figure 56, valid for $10^2 < Pr(D/L) < 1$, [23].

Table 21: Dimensional numbers for convection within the downcomer, risers, and chimney. Dimensionless number subscripts indicate specific characteristic length used

	Downcomer		Chimney	Riser			
	\dot{m} (kg/min)	Re_D	Re_D	Re_{D_h}	Ra_S	Gr_{D_h}	Ri_{D_h}
Run023	13.6	9,735	19,470	5,883	1.49E+06	2.14E+06	0.062
Run017	21.3	14,726	29,452	8,944	2.10E+06	3.01E+06	0.038
Run020	28.1	19,733	39,466	11,910	2.66E+06	3.81E+06	0.027
Run022	36.3	26,687	53,373	16,136	4.03E+06	5.77E+06	0.022

The convective heat transfer from the riser walls to the working fluid can be described by an average or local Nusselt number, which allows calculation of a characteristic heat transfer coefficient, h_{conv} . Combining relations for developing and fully developed flow regimes within vertical parallel channels, Bar-Cohen and Rohsenow [25] obtained a Nusselt number correlation applicable to the complete range of S/L for isoflux conditions, Eqn. 12.

$$Nu_{S,L} = \left[\frac{48}{Ra_S S/L} + \frac{2.51}{(Ra_S S/L)^{(2/5)}} \right]^{-0.5} \quad (12)$$

As a comparison, other Nusselt correlations for varying flow regimes and geometries will also be considered. The Dittus-Boelter correlation [26], Eqn. 13, is valid for fully turbulent forced convection systems, while the Churchill-Chu correlation [27], Eqn. 14, is valid for free convection off a vertical plate. Lastly, the Elenbaas correlation [28], Eqn. 15, is valid for symmetrically heated, isothermal vertical plates.

$$Nu_D = 0.023 Re_D^{4/5} Pr^n, \quad \text{where } n = 4 \text{ for heating} \quad (13)$$

$$\overline{Nu}_L = \left(0.825 + \frac{0.387 Ra_L^{1/6}}{[1 + (0.492/Pr)^{9/16}]^{8/27}} \right)^2 \quad (14)$$

$$\overline{Nu}_S = \frac{1}{24} Ra_S \left(\frac{S}{L} \right) \left[1 - \exp \left(-\frac{35}{Ra_S (S/L)} \right) \right]^{3/4} \quad (15)$$

A summary of the Nusselt numbers and convective heat transfer coefficients is provided in Table 22. Values averaged in the range of 3 - 5 W/m²-K for the vertical plate and parallel channel correlations, suggesting that specific considerations for geometry are not highly sensitive and reasonable results can be obtained through multiple approaches. The Dittus-Boelter correlation stands as an outlier, however is expected based on the explicit form and applicability to only forced turbulent internal pipe flow.

Table 22: Riser Nusselt number and convective coefficients for varying correlations. Dimensionless number subscripts indicate specific characteristic length used

	Elenbaas		Churchill-Chu		Dittus-Boelter		Bar-Cohen	
	\overline{Nu}_S	\bar{h}_S	\overline{Nu}_L	\bar{h}_L	Nu_{D_h}	h_{D_h}	$Nu_{S,L}$	$h_{S,L}$
Run023	6.13	4.28	14.97	6.27	20.66	8.65	3.92	2.73
Run017	6.68	4.85	13.69	5.96	28.88	12.58	4.22	3.06
Run020	7.08	5.05	13.71	5.86	36.31	15.53	4.44	3.17
Run022	7.86	5.32	14.33	5.82	46.32	18.82	4.85	3.29

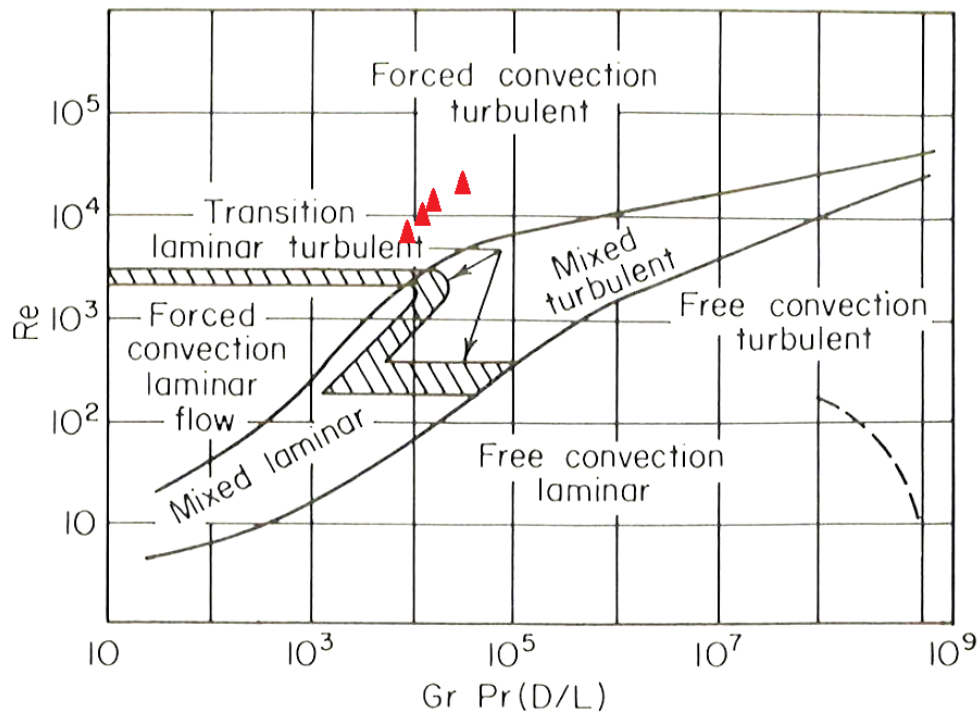


Figure 56: Regimes for free, forced, and mixed convection through for flow through vertical tubes, [29]. Red triangles indicate NSTF measured points for Run017, Run020, Run022, and Run023

Chapter 6

Computational Models & Analysis

6.1 Computational Codes

Parallel modeling and simulation efforts were revitalized in FY15 [22] to support the design, operation, and analysis of the natural convection systems. Updates to prior models [11][30][33] were made to reflect changes in the final “as-tested” design of the NSTF. The primary objective of the NSTF analyses is to assess the limitations in typical approaches for modeling this type of natural circulation RCCS systems, and validate the analysis methods and computer codes which can be used in licensing support. Both system-level thermal-hydraulics (STH) and computational fluid dynamics (CFD) codes were utilized in this effort. RELAP5-3D [31] and STAR-CCM+ [32] code analyses were performed to gain a complete understanding of the complex flow and heat transfer phenomena in natural convection systems. Additionally, the NSTF analyses aided in the RCCS design optimization, and supporting experiment activities, i.e. helping assure that the experimental procedures, setup, and measurements were performed as planned. Throughout the course of model development and code benchmark, the computational effort evolved to strengthen the experimental program. This mutually beneficial relationship has become integral to the overall program objective of examining the heat removal performance of the RCCS concept.

6.1.1 Experiment Support

To support the experimental program, computational modeling was performed using both 1-D system-level and 3-D CFD codes. Throughout the course of computational model developments, the computational effort has evolved to also play a major role in strengthening the experimental program, including improvements on the instrumentation, test procedures, and the physical construction of the test facility. The analysis effort for experiment support is briefly summarized here, while the details can be found in [22].

A large number of new measurements were added to the facility for code comparison and better facility characterization, including measurements for characterizing facility heat loss, stratified building temperatures, turbulence intensities of key flow regions, and distributed temperature measurements in key locations. The inclusion of high fidelity instruments was intended to not only supplement existing sensors, e.g. thermocouples, flow meters, but also to provide new information on the local details of thermal-hydraulic phenomena. One such example was the installation of the DTS fibers across the 10-inch exit faces of the riser ducts.

Over the course of the experimental testing program, a number of improvements were made to the physical construction of the test facility. Several of these were the result of observations made by the analytical team during review of previous data, and ultimately proved valuable in strengthening the overall impact of the experimental program. As an example, the sealed loft damper valves, which caused leakage of air past the fan loft damper valves, was a significant finding and addressed within the programs Quality Assurance Plan (QAP), ANL-NSTF-000000-DAR-005-R0. The chimney damper (butterfly) valves used to close the flow paths along the horizontal loft segments allowed a portion of fresh air ingress due to a 0.125-in gap between the valve disk and inside duct walls. A study was performed to quantify the amount of air leakage/ingress at the fan loft damper. This was supplemented by RELAP5 simulations with a parametric sensitivity study on the air-ingress flow rate, which allowed high confidence in quantifying the impact of the leak on previous data.

Finally, computational modeling and simulation is also very valuable in defining the test

configurations, boundary conditions, and procedures in the air-based NSTF experiments. An example is to determine the azimuthal power distribution in one NSTF test to mimic the power skew in the full-scale RCCS, in which the non-uniformity in the temperature and power distributions of the full-scale reactor vessel wall is expected. Analyses of the radiation heat transfer view factors in both MHTGR and NSTF cavities have been performed with the CFD software STAR-CCM+, which includes a ray-tracing model to calculate the surface-to-surface view factors. Based on the simulation results of the view factor distributions and power peaking factors in MHTGR and NSTF cavity, the two azimuthal zone power distributions in NSTF were determined to mimic the power skew of the MHTGR cavity in NSTF.

6.1.2 System Level Modeling

As part of the modeling effort conducted during this project, a RELAP5-3D model was developed for the NSTF to perform transient analysis and focused primarily on simulating the integral system performance of the facility. The analysis results have demonstrated to be very useful to confirm the experiment tests were performed as expected or to identify areas of the facility where improvements could be implemented.

To analyze the ability of the model to predict important performance metrics of the facility (such as the air mass flow rate), comparisons were made between experimental test data and code simulation results. After initial comparisons and the assessments of the experimental results of several repeated baseline tests, it became apparent that modeling ambient effects on the facility would be necessary to properly simulate the overall system performance. These effects were due to the temperature differences between indoor and outdoor air and wind speeds, both of which varied (significantly during some tests) throughout each test. These ambient conditions can drastically affect the mass flow rate of air through the facility. To simulate these conditions in the model, virtual volumes were added to account for the temperature effects on the facility, while wind effects were simulated by controlling the pressure difference between the inlet and outlet of the facility [33].

The final RELAP5-3D model, Figure 57, was calibrated to results from a single experimental test (Run022) to accurately account for flow resistances in the facility as well as air entering the NSTF building. Following calibration, the model was used to simulate additional experimental tests (Run011, Run020, and Run024) over a range of operating and ambient conditions. The simulation results compared well with experimental data for all of the tests for the overall system mass flow rate (the average absolute error was less than 5% in all of the simulations) and the average temperature rise of air within the riser ducts (the average absolute error was less than 6% in all of the simulations). These simulation results demonstrate the ability of the code to capture the integral behavior of the system as well as the effects of ambient conditions on the performance of the facility (for outdoor

temperatures ranging from -22.3°C to 33.4°C and wind speeds ranging from 0 m/s and 8.5 m/s). However, differences were identified between experimental data and the simulation results for certain pressure and velocity measurements. These are most likely due to the location of the instrumentation in the facility and limitations of 1-D systems codes (such as RELAP5-3D) to capture local versus averaged quantities.

The RELAP5-3D model was also utilized to perform sensitivity analyses to investigate how the NSTF performs during different operating and ambient conditions. The following parameters were investigated during the sensitivity study: power, outdoor air temperature, facility inlet air temperature, wind speed, and form loss coefficient. The effects on the system mass flow rate and temperatures were analyzed to examine the performance of the facility under a wide range of operating conditions.

It is demonstrated that 1-D system codes such as RELAP5-3D can simulate the integral behavior of the system responses while the effects of ambient conditions on the behavior of the NSTF are modeled or accounted for. This provides confidence that its usage can provide insights into the efficiency of the RCCS under various operating conditions, which would be required during reactor licensing. Overall, the ability of RELAP5-3D to capture the performance of natural circulation airflow systems, such as the NSTF, demonstrates that it is an appropriate tool for use in transient analyses of air-cooled passive systems such as the RCCS.

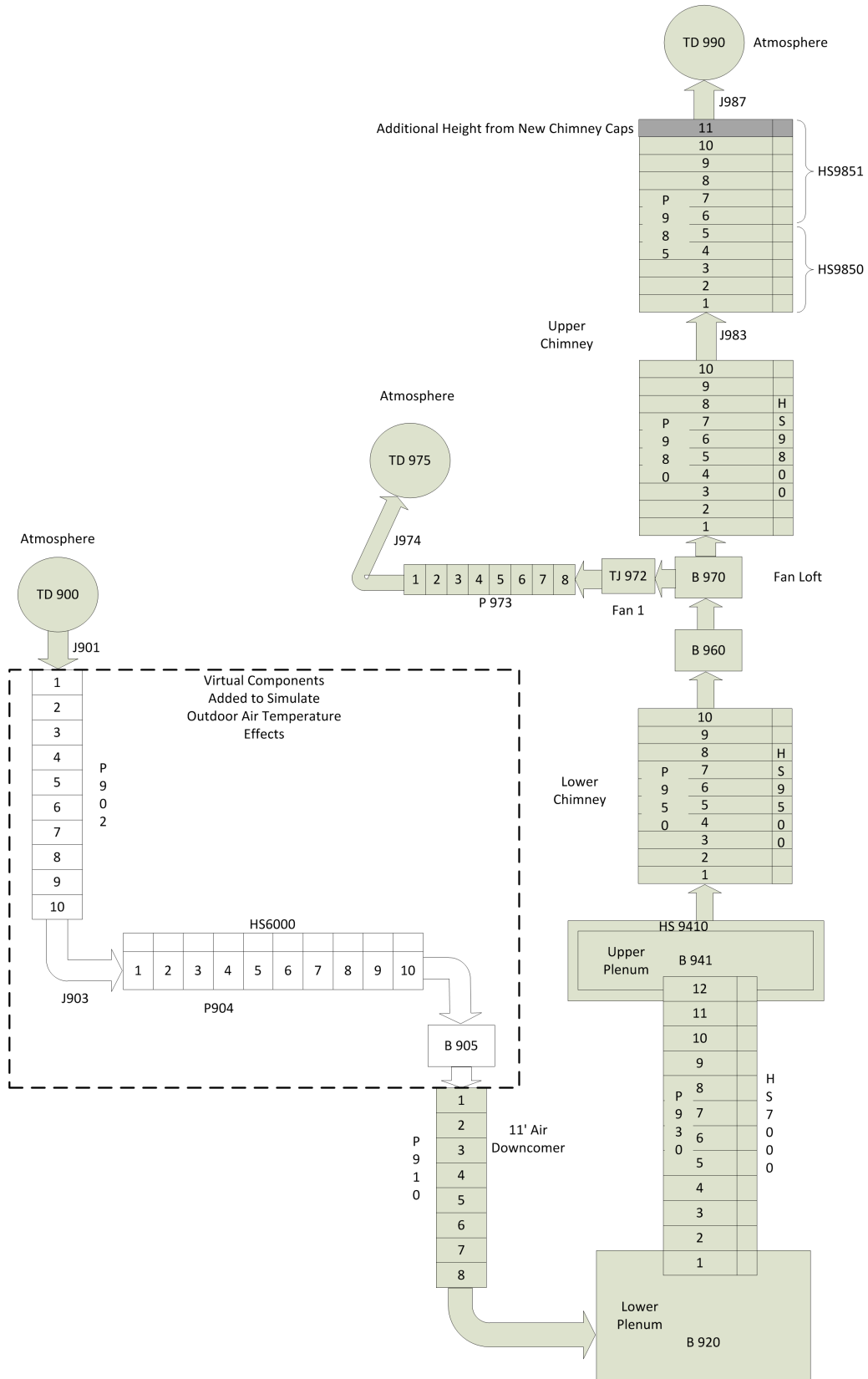


Figure 57: Nodalization diagram of NSTF model in RELAP5-3D

6.1.3 Computational Fluid Dynamics Modeling

The CFD analysis of the NSTF in STAR-CCM+ has progressed significantly since the program's inception. CFD (as well as RELAP and analytical methods) was used at the very onset of the project to aid in the design of the NSTF. This included confirmations of the scaling methodology and suggestions for where to place instrumentation. Sensitivity studies were performed for changes in flow geometry in certain areas, such as the extension length of the risers and the inlet pipe configuration, which directly influenced the geometry of the constructed NSTF system. Many meshing and physics modeling studies were performed which were very beneficial to the later studies of the system.

After the initialization of NSTF testing, CFD analysis was resumed. The computational model was updated from the "as-designed" to the "as-tested" geometry, which involved some changes in the plenum false wall locations and heated cavity dimensions. The availability of experimental data also provided for a more rigorous evaluation of the computational methods used in the CFD analyses. In turn, CFD and system code results helped to improve instrumentation requirements and the procedures used in the experiments themselves.

Initial simulations of the "as-tested" geometry, Figure 58, applied methods similar to those used in early work, with relatively simple boundary conditions. All runs were steady-state. Radiation and convection were modeled within the cavity in all simulated cases. A uniform heat flux boundary condition was applied at the heated East cavity wall that was equivalent to that removed by the main air flow, with adiabatic conditions applied to the other cavity walls. Conjugate heat transfer was modeled between the cavity air, riser ducts, and main air.

The simulations were started as forced-flow cases, with the inlet flow rate and temperature fixed to the values found in the experiment. These methods performed adequately for predicting the global system behavior when compared with the experimental data. The methods were then tested on a fully natural convection-driven model, which required only the ambient temperature, applied heat flux, and system geometry as specifications. Thus

this was essentially an *a priori* test, and provided a more rigorous benchmark for evaluating the simulation approach. These were performed for both the baseline and low power test conditions. The bulk air flow rate was predicted within 10%, indicating that a basic CFD approach could yield good results for global flow and temperature quantities for multiple test cases. An important conclusion of this CFD modeling, which was in agreement with experiment, was that the main system flow rate has only a small impact on the heated surface temperatures. This bodes well for the applicability of the RCCS concept during a wide range of weather conditions.

After establishing the basic framework for CFD simulation of the NSTF, extensive investigations were undertaken to assess the impact of various modeling approaches. First, the importance of heat loss modeling was assessed. Initial simulations attempted to use the specified thermal conductivity of the insulation along the cavity walls, but severely underestimated the true heat losses. To improve this, thermal imaging of the external NSTF surfaces was used to estimate the heat loss distribution in the system. Results showed improved predictions of cavity wall temperatures compared to the adiabatic cases, with relatively similar predictions for the RCCS air flow. While the methods to obtain the data are sound, they were only tested for one specific case. Future work could extend these to model the heat loss appropriate to a range of system flow rates and power levels.

Detailed meshing and turbulence modeling studies were also undertaken. These included studies of both the duct flow and the cavity flow, and took full advantage of the DTS fibers installed in the ducts. These were performed for Run023, with baseline test conditions but forced-flow operation for better control of the boundary conditions. These actually indicated that some models that were tested in prior work, namely the Xu Two-Layer $k-\varepsilon$ model and the SST $k-\Omega$ model, over-predicted the turbulent diffusion when used with a coarse wall mesh. This led to under-predictions of the local duct wall temperatures. The Xu model, although specifically developed for natural convection-driven flows, was also found to give poor results with mesh refinement. The Wolfstein model was found to give better predictions

of temperatures and flow rates for similar computational cost.

An important finding of the turbulence modeling studies was that prediction of local quantities, such as the temperature distribution along the duct air, was improved through the use of a refined wall mesh. This will yield a more accurate result for the heated surface and duct wall temperatures. However, this significantly increases the computational mesh size and computational cost. It was also found that the refinement of the wall mesh was, generally speaking, more impactful on the results than the choice of specific turbulence model. Thus it was recommended that for design of RCCS systems, two levels of approach be performed. The first could include scoping and design calculations using the Wolfstein model and coarse wall meshes. These provide good general estimates of the performance of the RCCS system. Once the general design of the system has been established, some detailed calculations could be performed using the Low-Re $k-\varepsilon$ model with refined wall meshes for better estimates of local surface temperatures.

A final area of study was the impact of the weather conditions on the RCCS performance. In prior models, only the ambient temperature effects were included. Zero-power experimental tests were performed to gauge the impact of the weather without any confounding variables. Correlations were established that took into account both the stack effect (i.e. the pressure difference due to temperatures inside and outside of the NSTF building) as well as the influence of wind speed. The losses from air entering the building were also correlated. The CFD model was modified to incorporate an inlet/outlet pressure difference to account for these effects. Results showed significant improvement in the predicted flow rate for two test cases at different powers and ambient conditions. The high-power case changed from slight over-prediction to slight under-prediction, while the low-power case changed from a 9% under-prediction to 2% under-prediction of mass flow rate.

In conclusion, a CFD analysis framework was established for simulating the buoyancy-driven flow of the NSTF. Relatively straightforward methods can be used to assess global quantities such as the heat removal capability of the RCCS. These were tested *a priori*

with success. Simple implementation of weather effects can improve these predictions even further. Assessment of local quantities can be improved through the use of refined meshing and turbulence modeling, as well as more accurate heat loss boundary conditions. Overall, the results from the modeling effort give confidence that CFD can be used as a predictive tool in the design and analysis of the air-based RCCS systems.

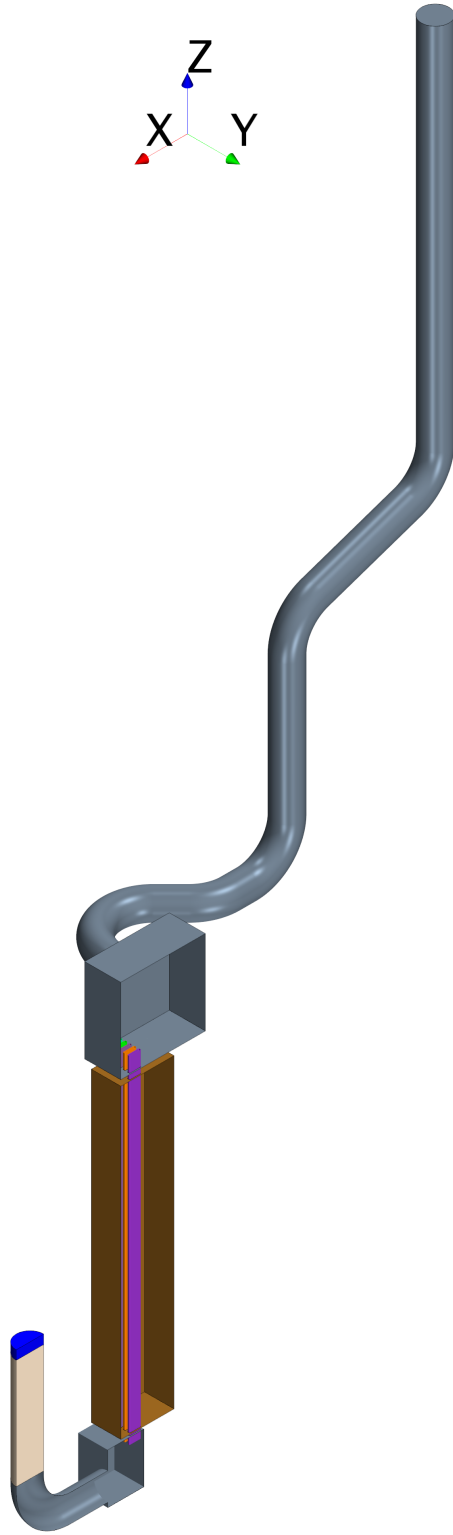


Figure 58: Solid model of NSTF in STAR-CCM+

6.2 System Trends

To determine the influence of certain variables on the performance of the NSTF, a sensitivity study was performed using the RELAP5-3D model of the facility. The variables investigated include: power, outdoor air temperature, facility inlet air temperature, wind speed, and form loss coefficient. Steady-state reference values for each variable, shown in Table 23, are from Run022 when the facility was operating at full power in the normal chimney configuration. The range for each variable was selected to cover the expected operating range of the facility along with some bounding values (e.g. outdoor air temperature equal to 60°C).

Table 23: Parametric study variables examined in RELAP5

	Reference Value	Range	Increment
Power	49.05 kW _t	20 - 100 kW _t	20 kW _t
Outdoor Air Temperature	-9.6°C	-40 - 60°C	20°C
Facility Inlet Air Temperature	17.5°C	-10 - 50°C	10°C
Wind Speed	0.15 m/s	0 - 20 m/s	5 m/s
Flow Restriction	20 [-]	0 - 40 [-]	10 [-]

Steady-state RELAP5-3D simulations were performed to determine the facility air mass flow rate, the average riser air temperature rise, and the average riser peak wall temperature. The results for each of these metrics over the range of each variable are provided in Figure 59 through Figure 63.

As the power of the facility is increased, the mass flow rate of the facility, the average riser air temperature rise, and the average riser peak wall temperature all increase due to the increased heat load. For increasing outdoor air temperatures, the mass flow rate of the facility decreases due to the reduced density of the air. Denser (colder) outside air temperatures provide a higher driving head and therefore increase the airflow rate through the facility. As the flow rate of air decreases, the average riser air temperature rise and the average riser peak wall temperature increase due to the reduced heat transfer in the facility at lower mass flow rates.

Similarly, with an increase in the facility inlet air temperature, the mass flow rate of the system subsequently rises. This is due to the density difference between the air passing through the facility and the outside air. The increase in mass flow rate corresponds to a decrease in average riser air temperature rise and an increase in the average riser peak wall temperature (the increase in wall temperature is mainly due to the increase in inlet air temperature, not the performance of the facility). With increase in the form loss coefficient of the NSTF, the mass flow rate of air through the facility decreases. This leads to an increase in both the average riser air temperature rise and the average riser peak wall temperature.

Wind creates pressure differences between the inlet and outlet of the facility, which affects the flow rate of air through the facility. As the wind speed increases, so too does the pressure difference between the inlet and outlet of the facility and therefore the mass flow rate of air in the NSTF. This increase in mass flow rate corresponds to a decrease in both the average riser air temperature rise and the average riser peak wall temperature.

Lastly, as the form loss coefficient of the NSTF increases, the mass flow rate of air through the facility decreases. This leads to an increase in both the average riser air temperature rise and the average riser peak wall temperature.

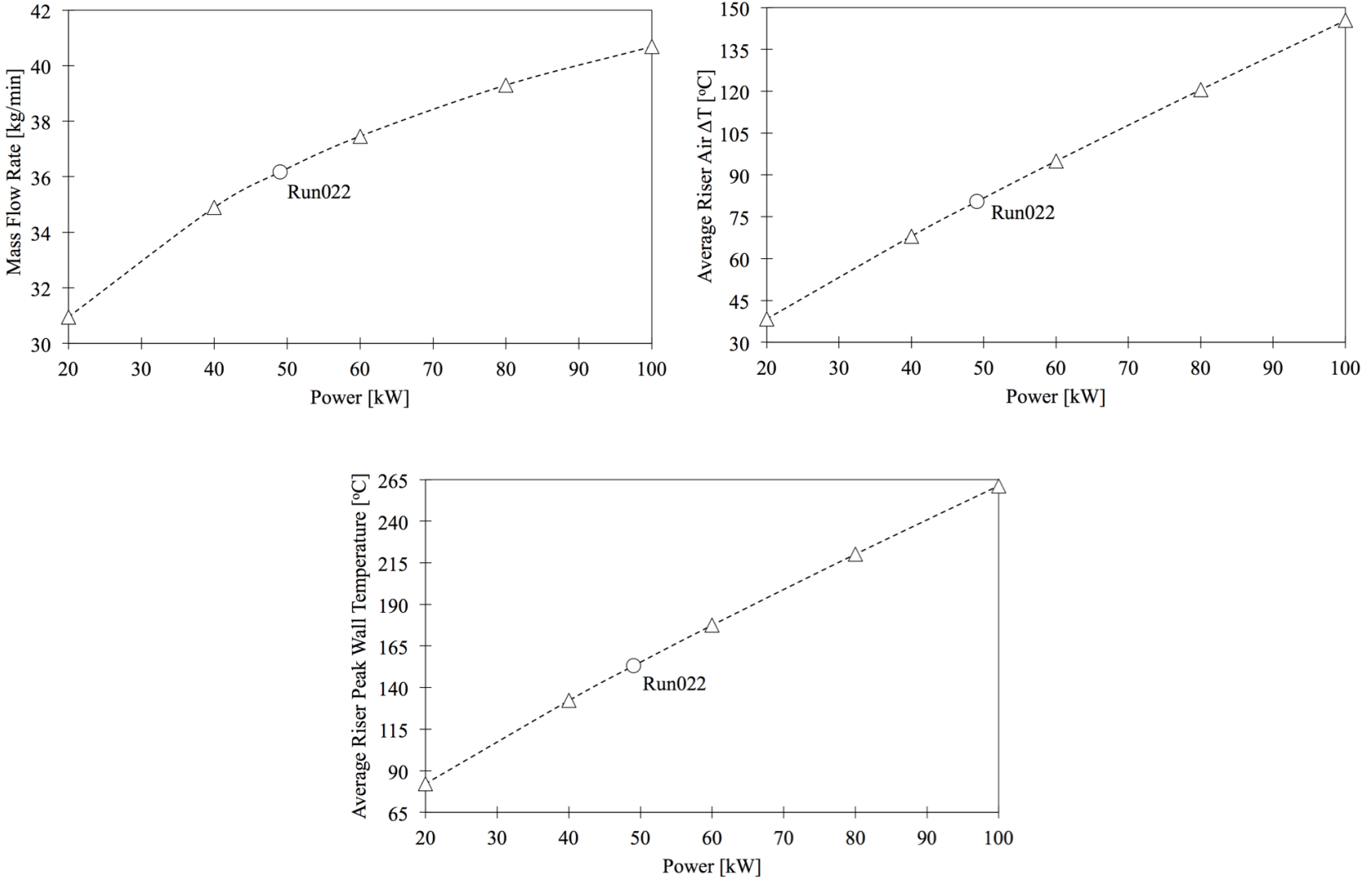


Figure 59: RELAP5 response of system parameters for variations in actual thermal power

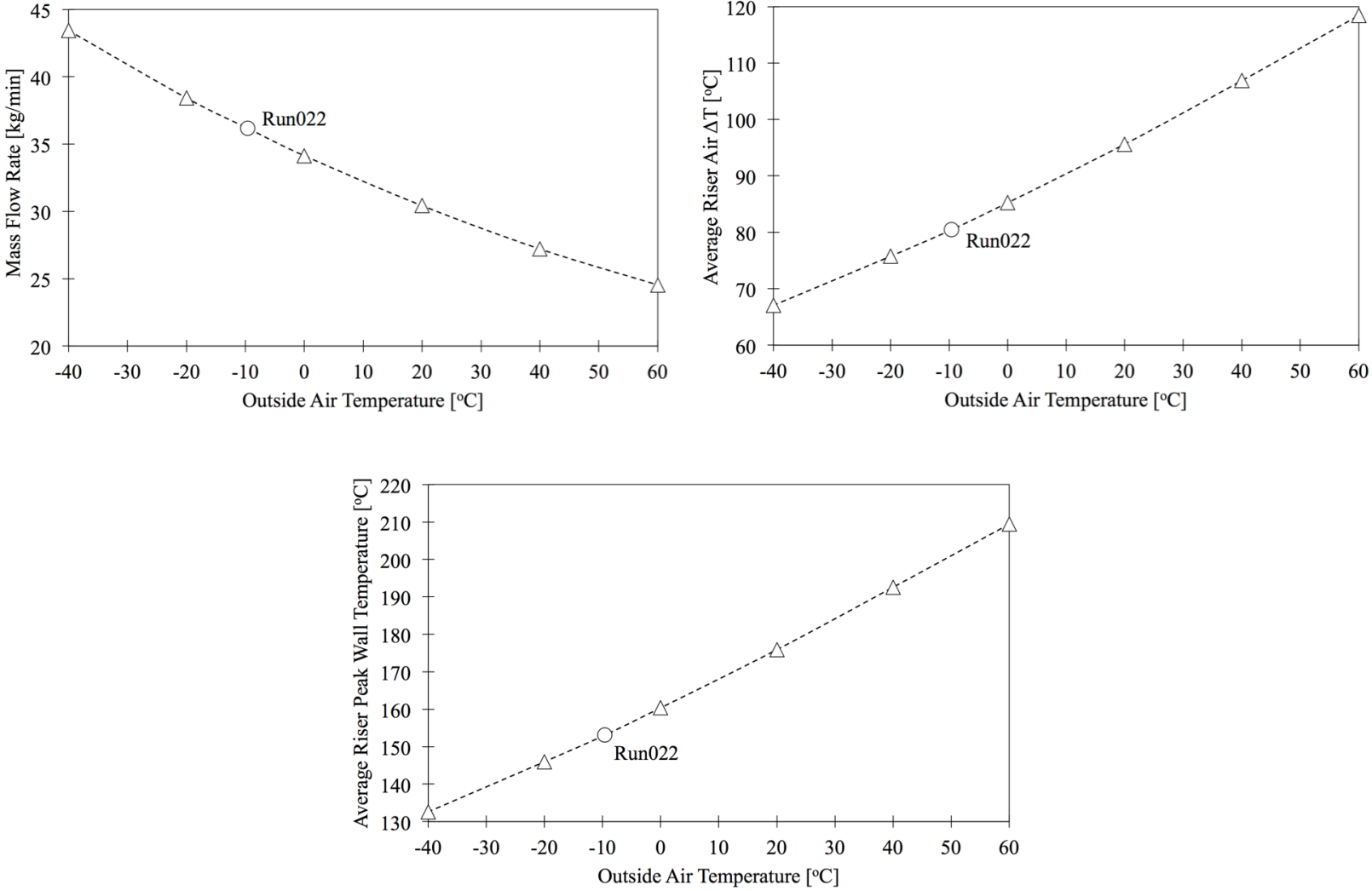


Figure 60: RELAP5 response of system parameters for variations in outdoor air temperature

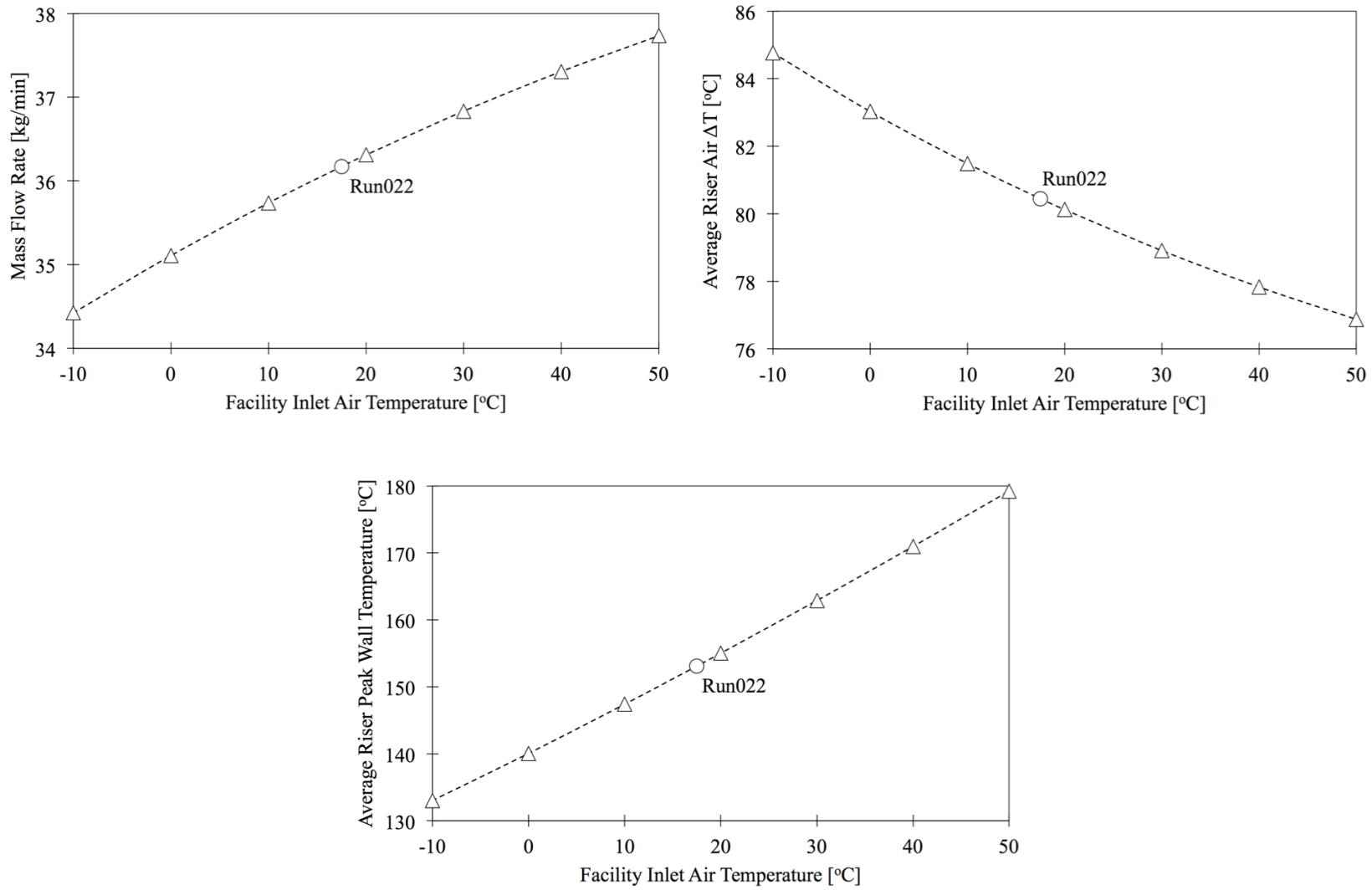


Figure 61: RELAP5 response of system parameters for variations in inlet air temperature

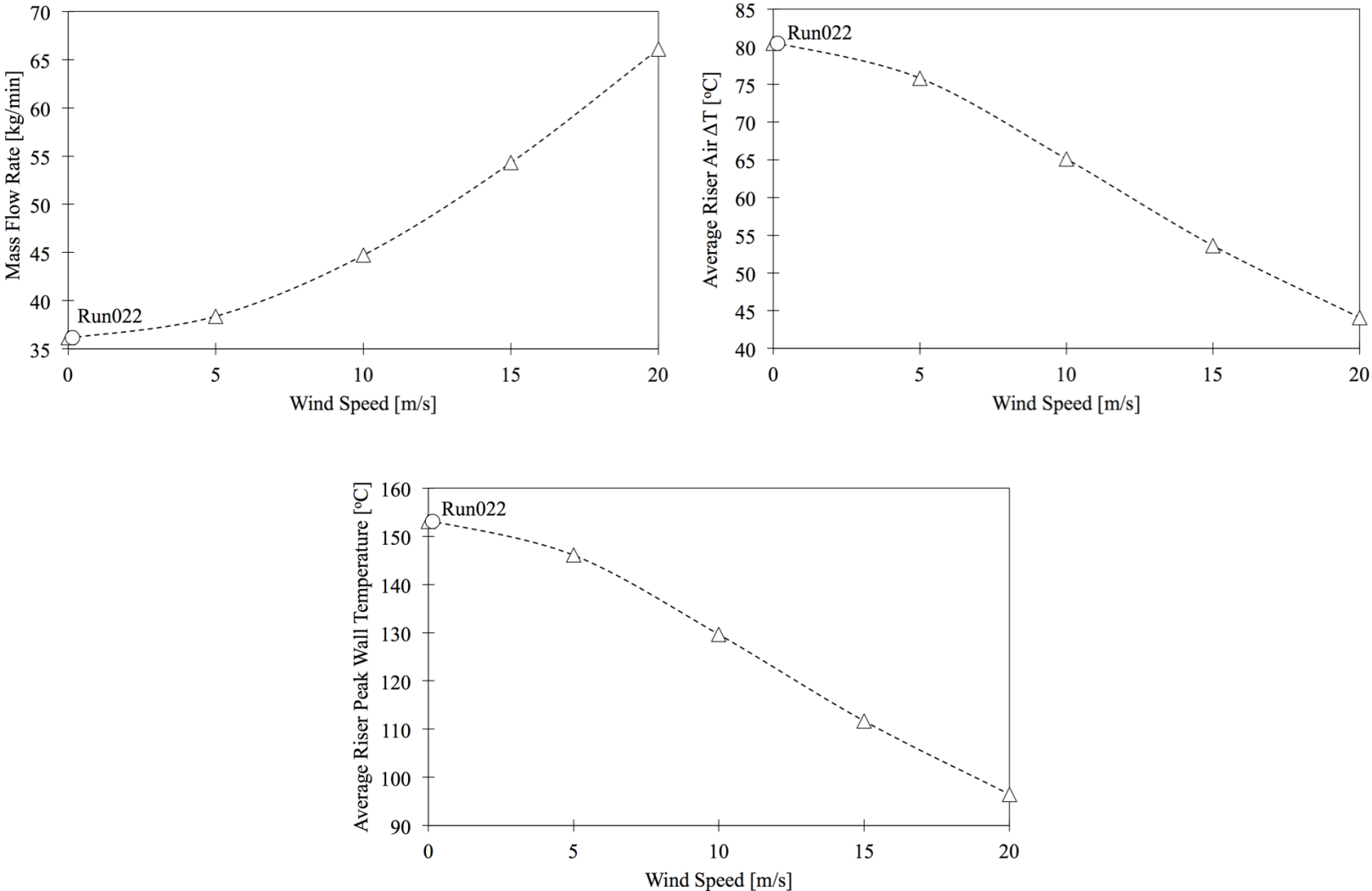


Figure 62: RELAP5 response of system parameters for variations in wind speed

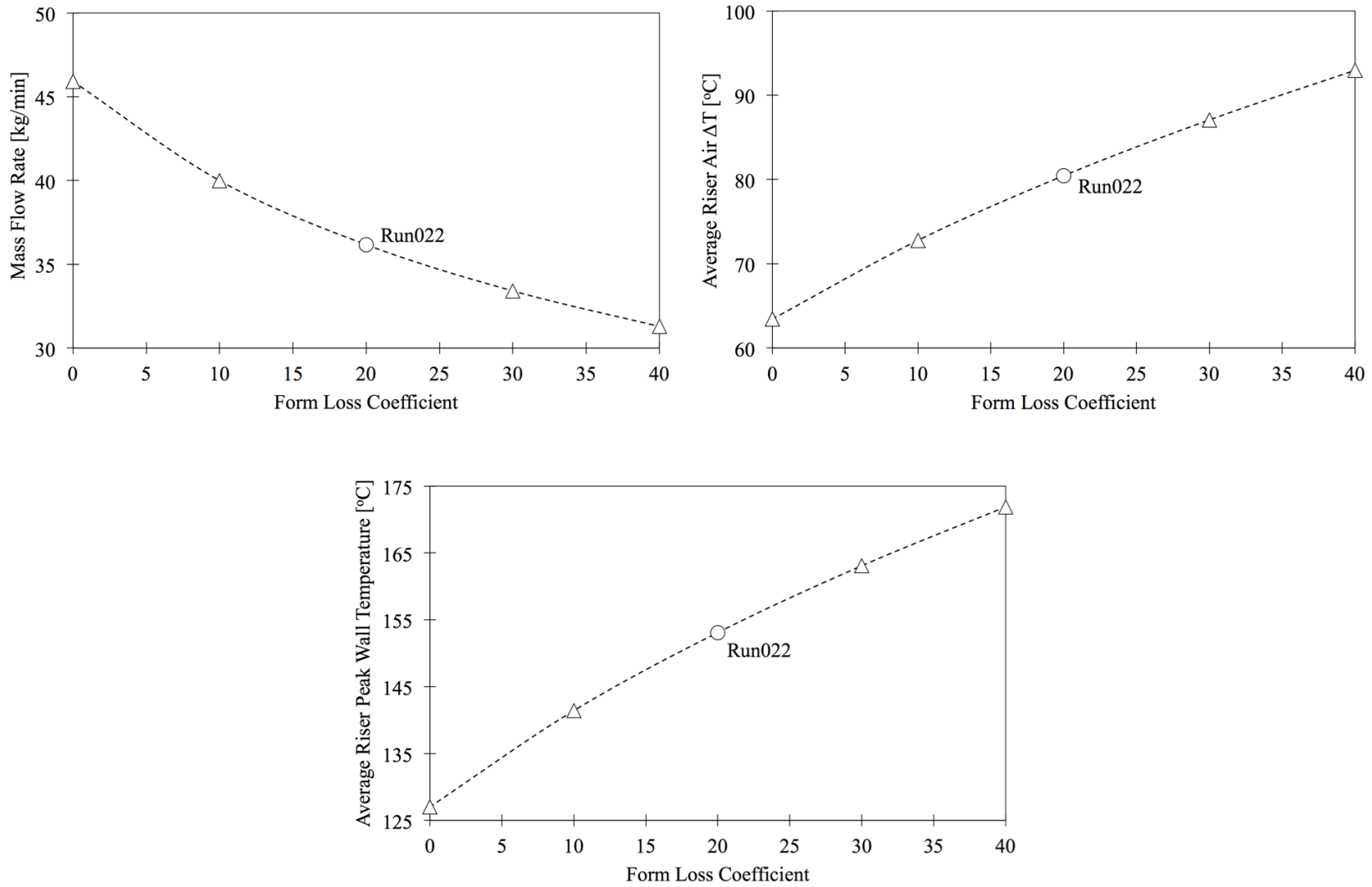


Figure 63: RELAP5 response of system parameters for variations in form loss coefficient

6.3 Ambient Correlations

To aid development of computational models and gain confidence in the predictive capabilities based on physical measurements, a correlation was derived to estimate the induced flow within the NSTF as a function of weather conditions. The primary inputs were riser inlet temperature, ambient outdoor temperature, and ambient wind speed. To facilitate coefficient fitting, a simple model of this natural draft was derived from basic principles. This model is intended to be a general description, and represents relative scaling of key variables. The wind effects, for example, can be related to a velocity pressure head with a 2nd order dependence (V^2) while temperature effects can be related to a hydrostatic head pressure and follow a 1st order differential temperature dependence (ΔT).

Even without active power, natural ventilation will occur due to a temperature differential across axial extents of the chimney ductwork, a phenomenon commonly known as the ‘stack effect’. For a geometry of height h , inlet temperature T_{in} , and outlet temperature T_{out} , the driving stack pressure can be defined by Eqn. 16, where the maximum pressure is at P_{stack} where $h = H$.

$$P_s(h) = \rho_{out}gh \frac{T_{in} - T_{out}}{T_{in}} \quad (16)$$

Furthermore, wind blowing around the building produces a positive pressure zone on the windward side, and negative pressure zone on the leeward side. These pressures act on the building envelope and influence the driving head described previously. The flow of wind across the exit face of the chimney stacks will also produce a low pressure region that assists pulling air from the chimney region. However, assuming the largest leakage path of the system is through the chimney region, the wind will always enhance the flow the NSTF. The effect of wind on the driving pressure can then be modeled by Eqn. 17, where C_w is the wind effect factor and V_w is the wind speed.

$$\Delta P_w = C_w P_{wind} = \frac{C_w \rho_{out} V_w^2}{2} \quad (17)$$

Combining the stack and wind effects, the total driving pressure can be modeled as Eqn. 18, where β is the air expansion coefficient and H is the height between the NSTF chimney outlet and the inlet.

$$\Delta P_{total} = P_s + \Delta P_w = \beta \rho (T_{in} - T_{out}) g H + \frac{C_w \rho_{out} V_w^2}{2} \quad (18)$$

This approach models the full air flow path from the outside of the building, infiltrating to the inside of the building at the ground level, entering into the NSTF downcomer, passing through NSTF piping, and leaving the NSTF duct system through the chimney outlets. The total driving force would be balanced by the pressure losses in all parts of the system. The total pressure loss can be correlated with the system flow rate, Eqn. 19, where K_i is the form loss coefficient and f_i the frictional coefficient.

$$\Delta P_{loss} = C_L \dot{m}^n = \sum (K_i \frac{1}{2} \rho v_i^2 + f_i \frac{L}{D} \frac{1}{2} \rho v_j^2) \quad (19)$$

The friction factor can be determined from the Blasius correlation [23] one of the earliest and simplest forms for determining the (Darcy) friction factor, Eqn. 20, and expressed as a function of only the Reynolds number. This correlation is applicable given the turbulent flow rates typically observed within the NSTF ductwork.

$$f = \frac{0.316}{Re^{0.25}} \quad (20)$$

Combining Eqns. 18, 19, and 20 results in a correlation (Eqn. 21) that contains two fitting coefficients, C_a and C_b . By using experimental data to determine these coefficients, the result provides a physical basis for predicting the induced flow rate as a function of ambient temperature and wind conditions.

$$\dot{m} = (C_a \Delta T + C_b V^2)^{9/5} \quad (21)$$

Relevant data generated at zero power conditions was compiled and prepared into a format that would allow fitting of these two coefficients. These data sets included pre-testing zero flow values along with additional separate effects tests conducted without electric heating. The span of available data is summarized below in Table 24.

Table 24: Span of available data collected at zero power conditions

	$T_{inlet}, ^\circ\text{C}$	$T_{outdoor}, ^\circ\text{C}$	$\Delta T, ^\circ\text{C}$	Wind Speed, m/s	Flow Rate, kg/min
Minimum	15.85	-16.7	0.44	0.04	0.12
Maximum	25.77	27.97	32.93	11.2	37.19

A fitting program was then scripted in MATLAB that iterated over values of constants C_a and C_b , compared the resulting mass flow rate against actual values, and identified best fit values based on a minimum root-mean-squared-error (RMSE). Both constants were given a range from 0 to 20 at 0.01 increments. Results for best-fit values found 5.53 and 3.75 for C_a and C_b , respectively. The correlation was then compared first against existing data sets, Figure 64. Given that this data was included in determining these constants, the high level of agreement is expected. To ensure validity of this predicative capability, a new test was performed in the test facility that generated data not used in the fitting correlation. The results are shown in Figure 65, further confirming confidence in the findings. Finally, a response surface was generated showing the calculated flow rate as a function of temperature and wind speeds, Figure 66.

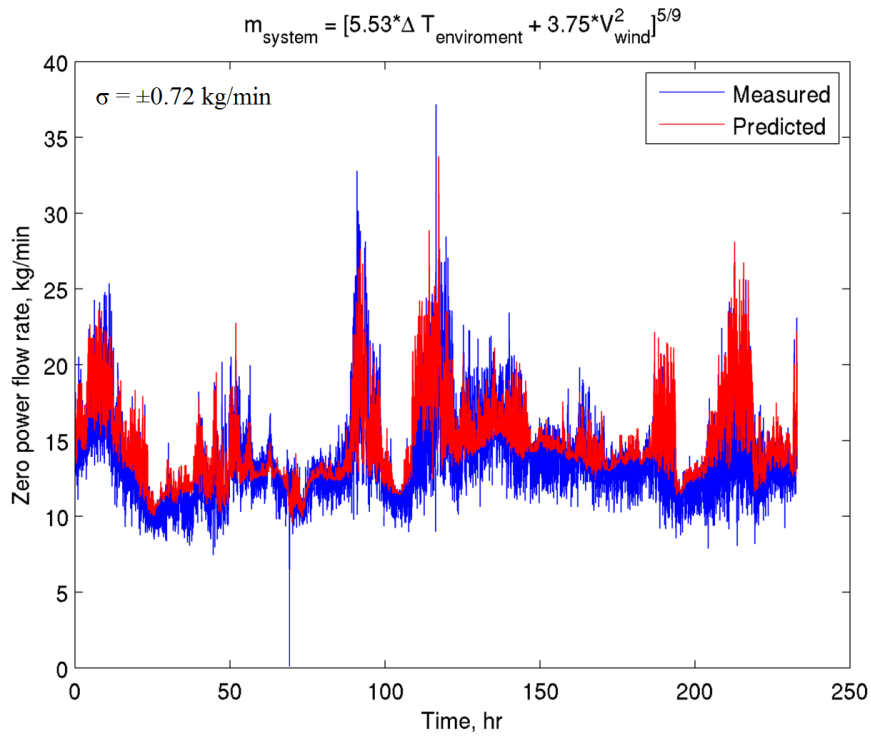


Figure 64: Fitting correlation, comparing existing data SPEF005

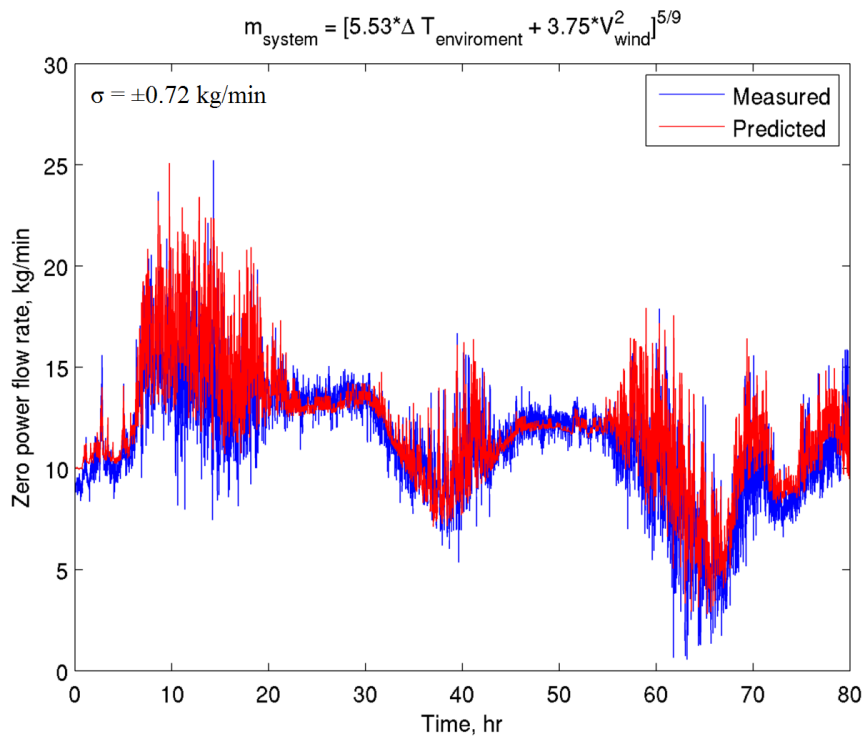


Figure 65: Fitting correlation, comparing new data SPEF007

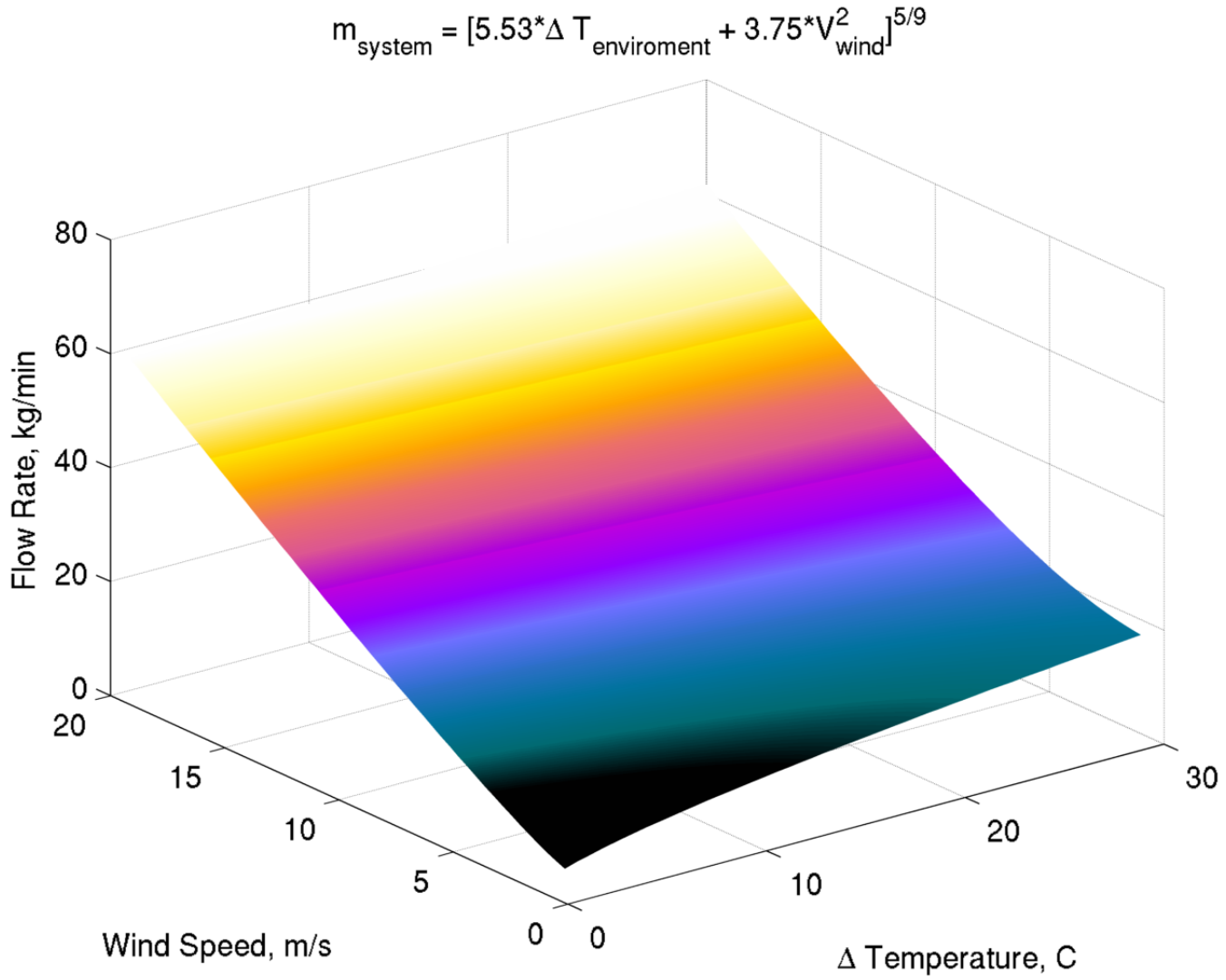


Figure 66: Response surface of fitting correlation

6.4 Prototypic Testing Conditions

6.4.1 GA-MHTGR Accident Scenario

The ability to accurately mimic the heat flux profile from the walls of a prototypic reactor pressure vessel (RPV) during an accident scenario is of high interest for the NSTF. Of the proposed test series, one specific subset calls for a hypothetical accident scenario. The following sections provide an overview of the methods used to determine the experimental boundary conditions in the NSTF.

Reference Basis

The full scale design for the NSTF is based off the General Atomics (GA) Modular High Temperature Gas Reactor (MHTGR), which has published openly available literature on the heat removal specifications of their reactor cavity cooling system (RCCS). Section 5.5-16 in Amendment 13 of the Preliminary Safety Evaluation [10], provides details of these operating conditions, Figure 67. They specify that the RCCS steady-state performance during normal plant operation imposes 700 kW_t heat loss onto the RCCS. Then, during a Depressurized Conduction Cooldown (DCC) with Small Primary Leak, the time history of conditions imposed onto the RCCS are shown in Figure 68:

Integration to the NSTF

The data set for ‘RCCS Removal’ in Figure 68 was digitized, normalized to values of unity along the y-axis for peak values of 1.5 MW_t, and fitted to a 10th order polynomial curve fit. The fitted coefficients are provided below, which require a power factor, P_{scale}, to yield engineering units in Watts. This data was then scaled according to the similarity parameters derived in earlier works [11], Table 25.

$$P_{watt,electric} = [C(00) + C(01) \times t_{min} + \dots + C(10) \times t_{min}^{10}] \times P_{scale}$$

$$P_{scale} = 90 \text{ (estimated to yield 56 kW}_t\text{)}$$

RCCS heat removal is a function of vessel temperature and ambient air temperature. A constant 43°C (110°F) ambient air temperature is assumed for this analysis. For the depressurized cooldown accident, there is very little convective heat transfer from the core to the top head. Decay heat is primarily removed by conduction horizontally through the reflector to the vessel sidewall. Vessel temperature peaks at 441°C (826°F) just above the core midplane at 120 hours after shutdown. All major RCCS parameters also peak at 120 hours. Peak RCCS parameters are as follows:

RCCS heat removal	1.50 MW
Air flow rate	12.2 kg/sec (9.68 x 10 ⁴ lbm/hr)
Maximum panel temperature	219°C (426°F)
Air outlet temperature	164°C (326°F)

Figure 67: GA documented decay heat load during DCC with small primary leak [10]

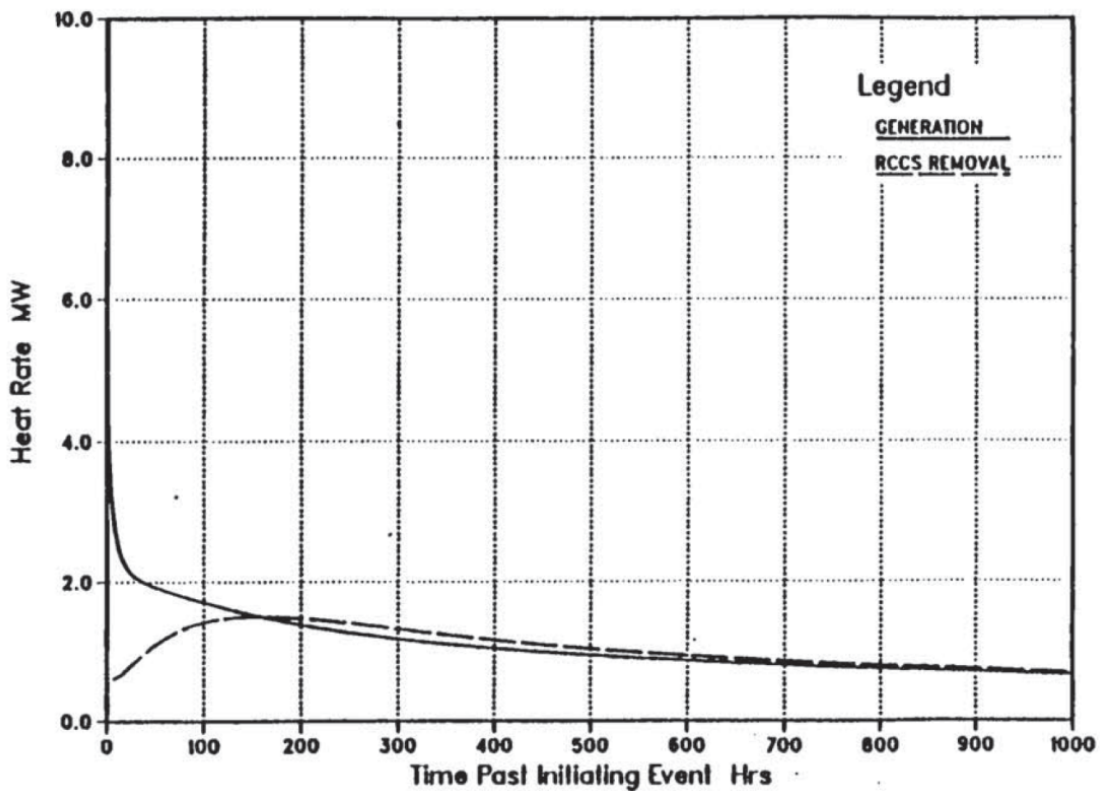


Figure 68: Heat rate for RPV generation and RCCS removal, GA-MHTGR DCC [10]

$$\begin{aligned}
 C(00) &= 466.531039994; & C(05) &= -1.27606140005e-014; \\
 C(01) &= 0.078631095079; & C(06) &= 2.04789514471e-018; \\
 C(02) &= 0.000170562320568; & C(07) &= -2.08318254453e-022; \\
 C(03) &= -1.28449427566e-007; & C(08) &= 1.29530038954e-026; \\
 C(04) &= 5.09424812301e-011; & C(09) &= -4.48601180685e-031;
 \end{aligned}$$

Correlation coefficient is 0.999958043125

Standard error about the line = 1.46350115015

Table 25: Scaling ratios and resulting values for full and NSTF scales

Parameter	Scaling Ratio	Full Scale	ANL $1/2$ scale
Power (normal)	$\dot{Q}_R = \sqrt{l_R}$	700 kW _t	26.16 kW _t
Power (DCC accident)	$\dot{Q}_R = \sqrt{l_R}$	1,500 kW _t	56.07 kW _t
Time	$T_R^* = \sqrt{l_R}$	120 hr	84.85 hr

Thus, the final resulting power profile that will be programmatically supplied by LabVIEW is shown below in Figure 69. A comparison of the digitized GA-MHTGR decay heat curve (in black, left Y-axis) and the resulting NSTF decay heat curve (in red, right Y-axis) is shown as an overlay in Figure 70.

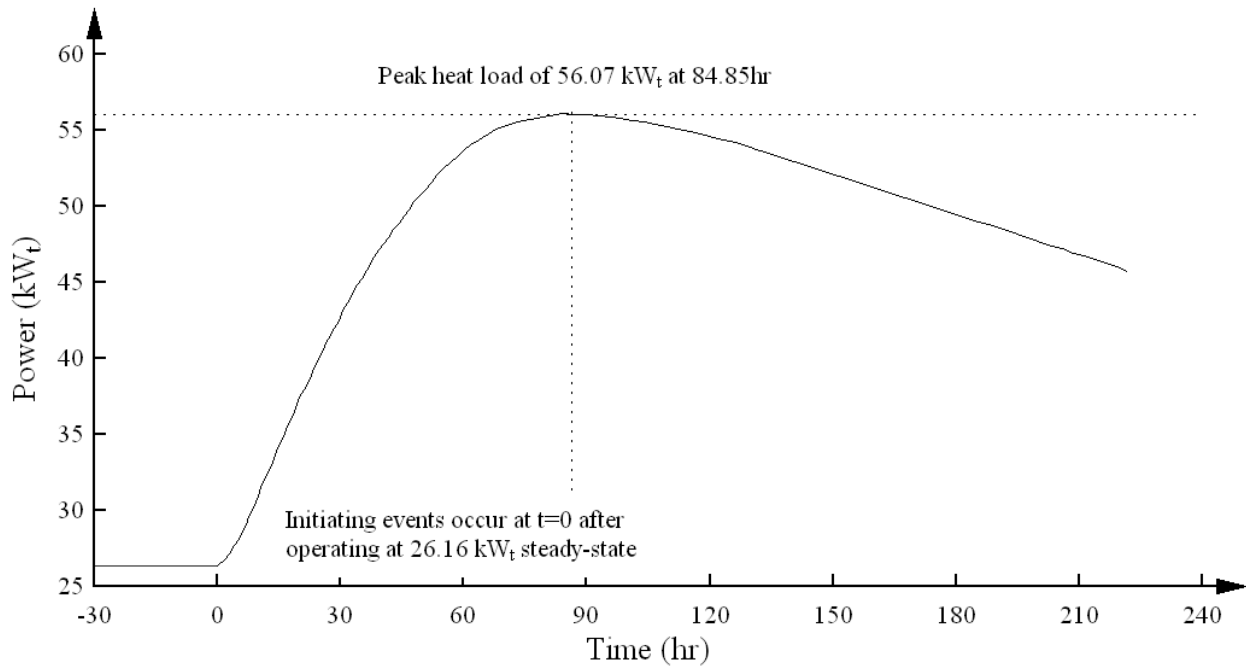


Figure 69: Decay heat curve scaled for NSTF operation

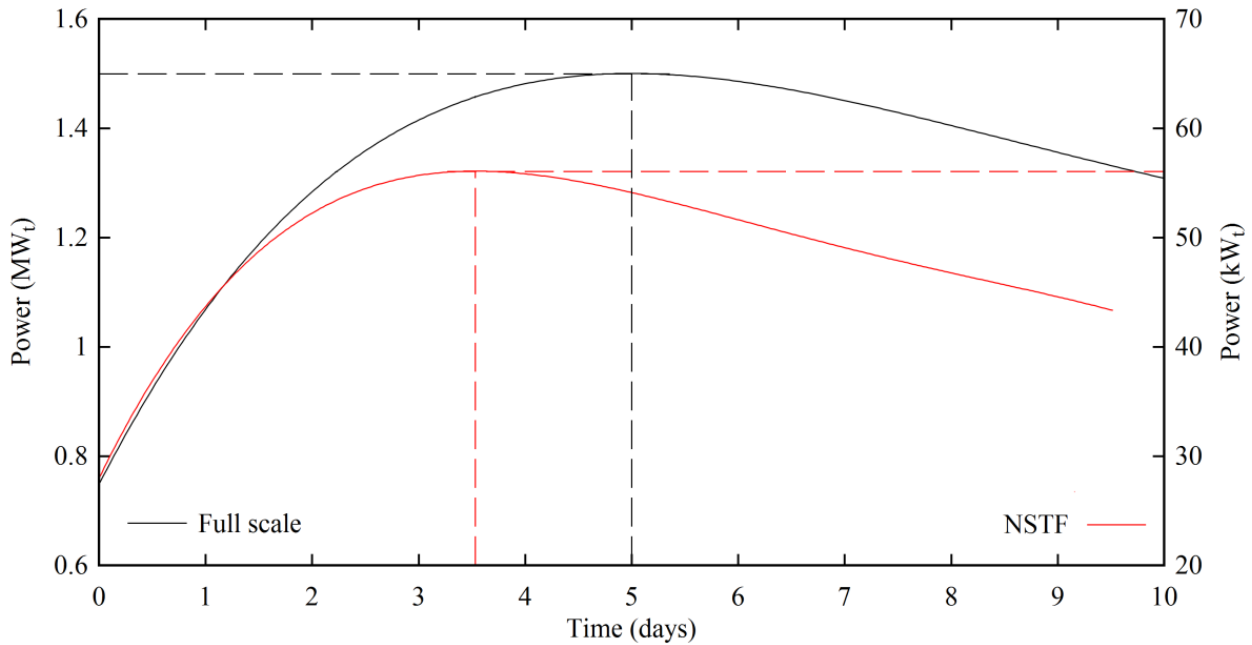


Figure 70: Overlay of GA-MHTGR and NSTF decay heat

6.4.2 Cosine Power Profile

The ability to accurately mimic the heat flux profile from the walls of a prototypic reactor pressure vessel (RPV) is of high interest for the NSTF. Of the proposed test series, one specific subset calls for a cosine power shaping profile along the axial direction.

Since the accident scenario specifies a depressurized condition with heat transfer primarily in the horizontal direction, the power density within the core can serve as a valid surrogate for the heat flux distribution off the walls of the pressure vessel. Since the GA literature does not quantify the exact power profile, other available references provide information for a generic high temperature reactor (HTR). J.P. Simoneau [34] gives the axial distribution as a function of peak power for a HTR and H. Haque [35] provides a typical axial power density in the core for a generic MHTGR, Figure 71. Furthermore, to examine variations in the axial power profile during early life stages of a reactor core, an additional profile was developed that featured a skew peaked near the bottom.

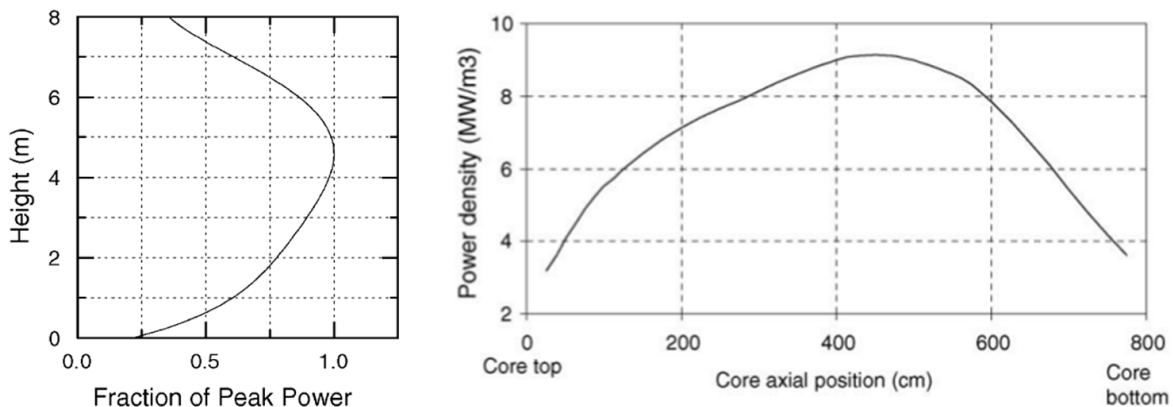


Figure 71: Axial distribution for an typical HTR [42]

Each of these data sets was normalized to values of unity for both x- and y-scales, verified that their integration summed to unity, and compared against the curve of a true cosine distribution, Figure 72. The peak occurs at exactly the mid-point for the true cosine, 0.575 for the MHTGR, which is similar to the suggested GA position of “just above the core midplane” [10], and 0.25 for the bottom peaked cosine, a position that provides an lower

bound on early life RPV power profiles. To apply these skews to the NSTF test operations, the forty available control zones were fitted to this skewed cosine distribution by iterating over the available power levels while ensuring that the summation matched the expected integral power. A summary of the as-tested peaking factors is provided in Table 26.

Table 26: Peaking factors for cosine power profiles

NSTF Zone	Peaking Factor (P_n / P_{linear})		
	Linear	Bottom Peak	Mid-Plane
Zone1	1.0	1.225	0.498
Zone2	1.0	1.325	0.831
Zone3	1.0	1.425	1.010
Zone4	1.0	1.375	1.140
Zone5	1.0	1.275	1.248
Zone6	1.0	1.150	1.313
Zone7	1.0	0.900	1.294
Zone8	1.0	0.650	1.157
Zone9	1.0	0.450	0.904
Zone10	1.0	0.225	0.605

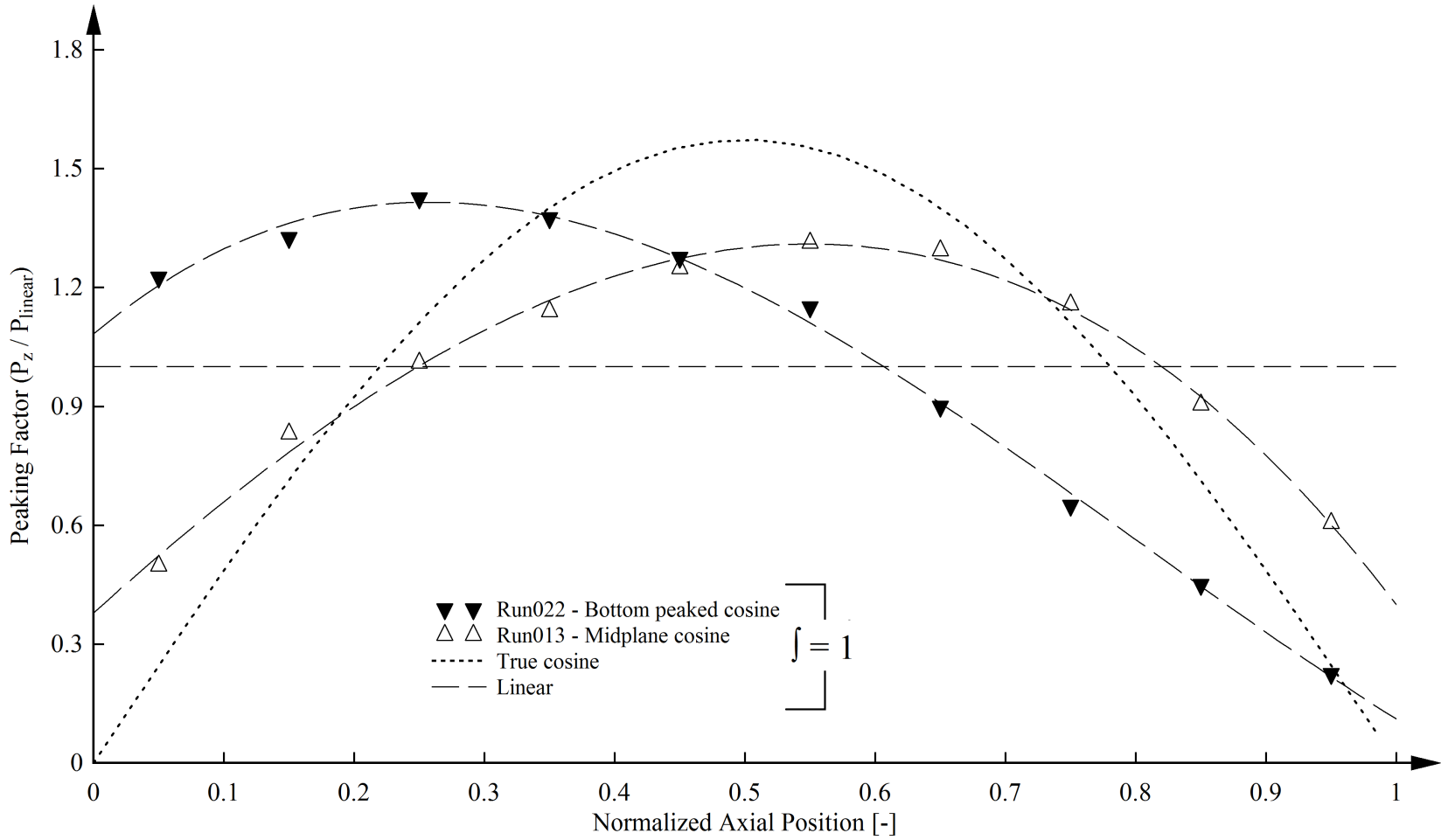


Figure 72: Cosine power skews with linear reference, GA mid-plane and bottom peaked

6.4.3 Azimuthal Power Skew

During the air-based data review meeting, a discussion was made on the most probably full-scale temperature effects on riser ducts within a reactor containment cavity with influences from skewed radiation view factors. Corner mounted riser tubes, along with physical obstructions such as RPV support mounts and steam lines, would cause a real RCCS to experience some level of power skew in the azimuthal direction. To examine this experimentally, an analysis of the radiation heat transfer view factors was performed for both MHTGR and NSTF cavities. The simulations were performed with the CFD software STAR-CCM+, which includes a ray-tracing model to calculate the surface-to-surface view factors. As the objective is to find the peak view factor per riser duct, all the surfaces (front, side, and back surfaces) are combined for each riser. Based on STAR-CCM+ results, the view factors from the vessel wall to the riser ducts are very non-uniform. The normalized peak view factor is ~ 1.84 for the peak riser duct, which is highlighted in Figure 73. However, it was found that one sidewall of this peak riser duct has a very large view factor facing the vessel wall, and large gaps exist in the array of riser ducts due to the vessel support structures and piping. Banks of riser ducts extend the length of the heated cavity, and are separate by gaps to avoid interfacing with RPV support structures. In consultation with industry experts [21], it was emphasized that the MHTGR and NGNP designs were only pursued to conceptual level, and therefore detailed design around cross ducts have not been addressed. In order to minimize azimuthal variation on vessel temperatures, it is necessary to have RCCS cooling panels above the structures and would have been addressed during the preliminary and final phases of the designs. One likely approach is illustrated in Figure 75, which uses an octagonal plenum around the structures to connect the riser ducts from the bottom plenum to top plenum. Given that a full scale RCCS was never constructed by GA, this approach is a best-attempt guess and likely would exhibit some amount of differences from an actual installation.

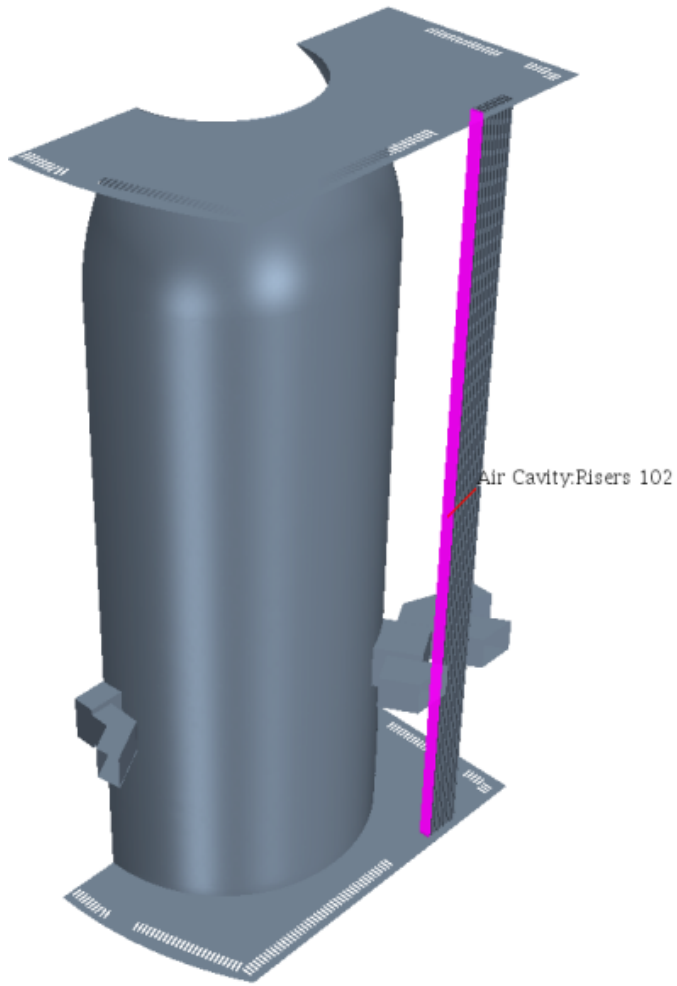


Figure 73: Group I

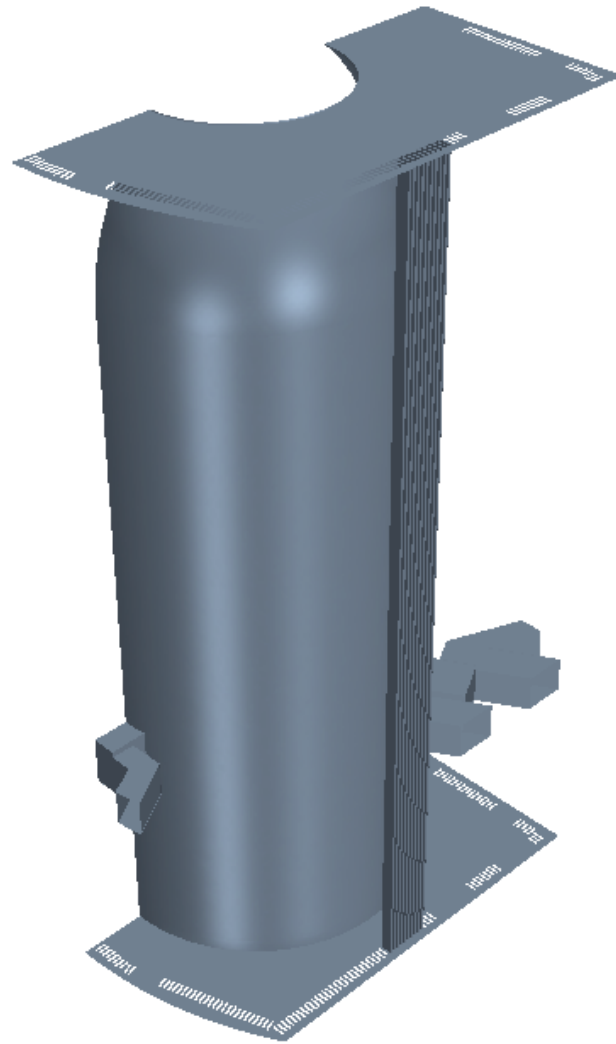


Figure 74: Group II

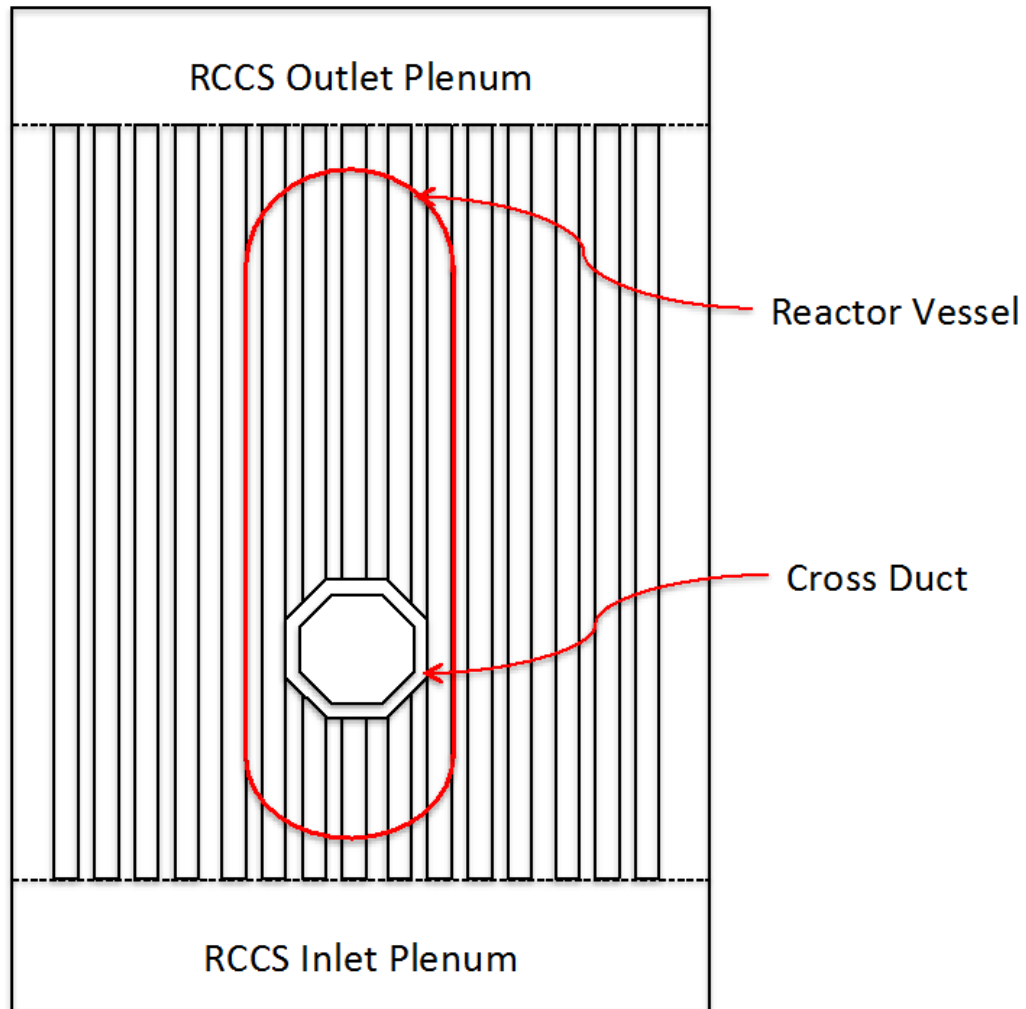


Figure 75: Schematic for air risers behind cross ducts [21]

Assuming that RCCS cooling panels will be more evenly distributed in the later phases of the design, the focus was then shifted towards the riser ducts with high view factors but not next to those cross-duct structures. The top ten riser ducts with high view factors (but away from the cross-duct structures) are the closest bank immediately adjacent to the RPV, and exhibit normalized view factors ranging between 1.29 and 1.31. Note that this peaking factor would be reduced if additional risers were placed in the current gap space.

The view factors in NSTF between the heated surface and the riser surfaces are also calculated using the STAR-CCM+ ray-tracing model. It is found the peak normalized view factors are 1.13 for the two central riser ducts (#6 and #7). However, the cavity sidewalls

(with emissivity at 0.2 and not existing in the full-scale MHRGR cavity) in NSTF may have significant impacts on the actual power distribution among all the risers. The power distributions among all the risers were calculated in the CFD simulation of one NSTF baseline test, and the edge riser duct has a peaking factor ~ 1.06 .

NSTF only has two azimuthal zones to control the power distribution. To mimic the azimuthal power skew of the MHTGR cavity in NSTF, the needed power peaking would be $1.31/1.06=1.24$. A power peaking of 125% vs. 75% was thus used for the two zones of heaters in NSTF.

Chapter 7

Testing Results

The following chapter details the tests completed within the air-based NSTF program at Argonne. Spanning a 33-month period, a total of 2,250 hours of active test operations were conducted. A high-level summary of each test's purpose, date completed, varied parameter, and classification is first provided by Tables 27 and 28. Following, a detailed discussion including testing conditions, facility configuration, and results will be provided on selected tests of primary interest.

Table 27: Summary of air-based testing - Data Quality runs

Test Name	Date	Duration	Purpose	Power,	Profile	Flow Path	Mode	Classification
DataQuality001	02/12/14-02/13/14	28h10m	Baseline	1,500	Linear	Dual vertical	Natural	Failed
DataQuality002	02/24/14-02/26/14	49h46m	Baseline	1,500	Linear	Dual vertical	Natural	Trending
DataQuality003	03/10/14-03/12/14	50h02m	Baseline	1,500	Linear	Dual vertical	Natural	Trending
DataQuality004	04/09/14-04/11/14	49h52m	Baseline	1,500	Linear	Dual vertical	Natural	Accepted
DataQuality005	05/01/14-05/02/14	30h05m	Low power	700	Linear	Dual vertical	Natural	Accepted
DataQuality006	05/27/14-05/29/14	52h45m	Chimney roles	1,500	Linear	Single vertical	Natural	Trending
DataQuality007	06/30/14-07/01/14	13h28m	Inclement weather	700	Linear	Reduced discharge	Natural	Accepted
DataQuality008	07/24/14-07/26/14	51h09m	Reduced discharge	700	Linear	Reduced discharge	Natural	Accepted
DataQuality009	08/05/14-08/07/14	48h27m	Power shaping	700	Cosine	Dual vertical	Natural	Trending
DataQuality010	08/26/14-08/28/14	50h12m	Power shaping	700	Cosine	Dual vertical	Natural	Failed
DataQuality011	01/28/15-01/30/15	52h47m	Baseline	1,500	Linear	Dual vertical	Natural	Accepted
DataQuality012	03/02/15-03/07/15	116h26m	GA-MHTGR accident scenario	variable	Linear	Dual vertical	Natural	Trending
DataQuality013	03/23/15-03/26/15	72h05m	Mid-cosine	700	Cosine	Reduced discharge	Forced	Accepted
DataQuality014	04/06/15-04/11/15	130h28m	GA-MHTGR accident	variable	Linear	Dual vertical	Natural	Accepted
DataQuality015	05/19/15-05/22/15	82h53m	Blocked riser tubes	700	Linear	Single vertical	Natural	Accepted
DataQuality016	6/22/2015	9h06m	Adjacent chimney roles	1,500	Linear	Adjacent	Natural	Trending
DataQuality017	06/25/15-06/27/15	58h38m	Adjacent chimney	1,500	Linear	Adjacent	Natural	Accepted
DataQuality018	08/13/15-08/18/15	129h55m	GA-MHTGR accident	variable	Linear	Dual vertical	Natural	Accepted
DataQuality019	8/25/2015	9h08m	Baseline (repeat)	1,500	Linear	Dual vertical	Natural	Failed
DataQuality020	09/05/15-09/07/15	52h8m	Baseline	1,500	Linear	Dual vertical	Natural	Accepted
DataQuality021	10/07/15-10/10/15	56h21m	I-NERI Test Series	1,000	Linear	Loft blowers	Forced	Trending
DataQuality022	01/17/16-01/22/16	120h8m	Bottom cosine	1,500	Cosine	Dual vertical	Natural	Accepted
DataQuality023	02/15/16-02/23/16	190h20m	INERI test series	1,000	Linear	Reduced discharge	Forced	Accepted
DataQuality024	04/08/16-04/14/16	145h50m	Single chimney	1,500	Linear	Dual / Single vert.	Natural	Accepted
DataQuality025	5/11/2015	9h8m	Heavy-gas (argon) ingress	700	Linear	Single vertical	Natural	Failed
DataQuality026	05/16/16-05/20/16	97h38m	Azimuthal	1,500	Linear / Azim.	Dual vertical	Natural	Accepted
DataQuality027	06/13/16-06/14/16	30h07m	Heavy gas (argon) ingress	700	Linear	Single vertical	Natural	Accepted

Table 28: Summary of air-based testing - Separate Effects & Scoping runs

Test Name	Date	Duration	Purpose	Power	Heated Profile	Flow Path	Mode	Type
BakeOut001	9/4/2013	12h40m	Heater & insulation bake out	-	-	-	-	Bakeout
BakeOut002	9/9/2013	05h25m	Heater & insulation bake out	-	-	-	-	Bakeout
Scoping001	9/23/2013	09h20m	New instrumentation shakedown	-	-	-	-	Scoping
Scoping003	02/09/15- 02/12/15	87h51m	Scoping for forced flow	-	-	-	Forced	Scoping
Scoping005	06/15/15- 06/17/15	46h30m	Scoping for flexible duct	-	Linear	Adjacent	Natural	Scoping
SPEF001	07/27/15- 07/30/15	71h21m	Chimney break	1,500	Linear	Adjacent	Natural	Separate Effects
SPEF002	10/12/2015	171h6m	Multi-parameter power/flow	variable	Linear	Loft blowers	Forced	Separate Effects
SPEF003	10/27-15 - 10/29/15	54h3m	Wind study / baseline	1,500	Linear	Dual vertical	Natural	Separate Effects
SPEF004	01/09/16- 01/15/16	54h3m	Chimney cap scoping	700	Linear	Dual vertical	Natural	Separate Effects
SPEF005	01/29/16- 02/08/16	232h58m	Zero power flow study	-	n/a	Dual vertical	Natural	Separate Effects
SPEF006	03/01/16- 03/09/16	197h28m	Zero power flow study	-	n/a	Dual vertical	Natural	Separate Effects
SPEF007	04/22/16- 04/25/16	79h56m	Zero power flow study	-	n/a	Dual vertical	Natural	Separate Effects
SPEF008	6/27/2016	4h08m	Isothermal characterization	-	n/a	Reduced discharge	Forced	Separate Effects

7.1 Baseline Test Cases

A baseline test case was established to serve as a common reference for parametric studies and also to monitor system repeatability. These conditions simulated the depressurized conduction cooldown (DCC) accident scenario decay heat load of the GA-MTHGR, which defined a peak power removal by the RCCS of 1.5 MW_t . When scaled using similarity parameters derived in earlier sections, the resulting heat load on the NSTF is 56 kW_t . Thus, our baseline test case began with a power ramp to 56 kW_e , then a 2^{nd} ramp to a higher power that, with heat losses considered, would result in nominally 56 kW_t within the heated test section. The operating state for the test, hereby referred to as ‘baseline’ conditions, defines the configuration of facility in terms of a select number of user-adjustable components:

1. Heated - riser spacing: 70.66-cm
2. Outlet plenum floor height: 40.64-cm
3. Heater profile and heat flux: Variable burst, linear 40 zones, 56 & 82 kW_e
4. Chimney: Open vertical stacks, closed XC and fan lofts

The operating window for active test operations (powered heaters) during Run011 began at 10h20 on January 28th 2015 and spanned a period of 52 hours and 46 minutes. Two steady state periods were maintained, the first at 56 kW_e for 6 hours and the second at 82 kW_e for 16 hours. With completion of post-test data verification procedures and review of generated data sets, the test was found to be fully within the defined scope and set of procedures and thus is classified as successful and will be submitted for qualification for Type-A data.

All instruments were verified and checked for working operation prior to initiating active heating and test operations. Of the instruments included in the test documentation, none were found to be inoperable or out of conformance. A zero-flow condition was created by closing off all five chimney valves along with sealing the inlet plenum. All signals from flow devices were within expected ranges, and temperature gradients across the test structural were non-significant, Table 29. During the full test duration, the weather remained fair and

typical for a Midwestern winter day. An overview of the weather conditions across the span of the testing period is given below in Table 30.

Table 29: Pre-test zero flow system parameters for Run011

Zero flow values	Surface temperatures	Gas temperatures
Flow meter: 1.06 kg/min	Heated plate - 18.84 °C	Riser inlet - 18.39 °C
Humidity: 23.76 %	Riser duct wall - 19.81 °C	Riser outlet - 18.86 °C
Riser $\Delta P_1 - 12$: +0.93Pa	Adia. west wall - 19.48 °C	Chimney inlet - 20.72 °C
Chimney $\Delta P_{N,S}$: +0.03Pa	Ceramic heaters - 18.45 °C	Chimney outlet - 20.27 °C

Table 30: Summary of weather conditions during full test window of Run011

	Average	Span	
Rain (total)	0.0	0.0 - 0.25	mm
Rate fall rate	0	0.0 - 0.0	mm/hr
Barometric pressure	765.53	754.8 - 776.7	mm
Indoor temperature	23.14	21.9 - 24.7	°C
Outdoor temperature	-0.12	- 6 - 2.8	°C
Indoor humidity	21.14	16.0 - 26.0	%
Outdoor humidity	68.87	46.0 - 86.0	%
Wind run	0.24	0 - 0.59	km
Wind direction	244.17	22.5 - 337.5	°
Wind direction	NW	NNE - NNW	direction
Wind speed	4.02	0 - 9.8	m/s

7.1.1 General System Behavior at Baseline Conditions

The power-on ramp of the electric heaters spanned duration of 120 minutes, and as described earlier, was employed to allow gradual heat up of the facility components. Due to the massive thermal inertia of the structural supports and insulation materials, a response in the thermal powers was not observed until 1.6 hours into heating. Furthermore, nearly 15 hours were required to reach complete thermal equilibrium. A plot of the electric and thermal powers from one baseline case, Run011, is shown in Figure 76.

At steady-state conditions, the heated cavity reaches a thermal equilibrium with power supplied by the radiant heaters and power removed by natural convection within the gas space of the riser ducts. Contributions in the heat removal are also imposed by parasitic losses across the insulating panels, and are described in greater detail in previous works [22]. On average, between 60 and 70% of the source electric heat is removed by the RCCS, a value that is dependent on the specific test conditions and ambient temperatures. Figure 77 provides a representation of the steady-state temperatures of the primary surfaces within the heated cavity at baseline conditions. While the heated surface averages 390 °C, the convection heat flow within the risers maintains the remaining structures at significantly cooler temperatures. It is clear that radiation dominates the heat transfer modes, as the temperature dependence can be linearly scaled to the view factors and distance from the heated plate. As expected, the front face of the risers experience the highest temperature, the cold wall nominally lower, and the coldest temperatures are observed on the opposing faces - the cold face of the risers.

Though heat flux sensors were not available on all surfaces within the heated cavity, installation was made on each of the four faces for Riser #7 at the axial mid-plane. Figure 78 details the split in heat removal by a single duct across each of the four faces. While radiation from the heated plate dominates the faces in line-of-sight, contributions from convection supplement and aid in the deposition on remaining surfaces. The heat flux contributions highlight the major contribution to heat removal by the narrow front face, which accounts for nearly 40% of the total heat removal by a single duct. The wide faces remove approximately half of the power, while the remaining narrow rear (cold) face contributes a mere 10%.

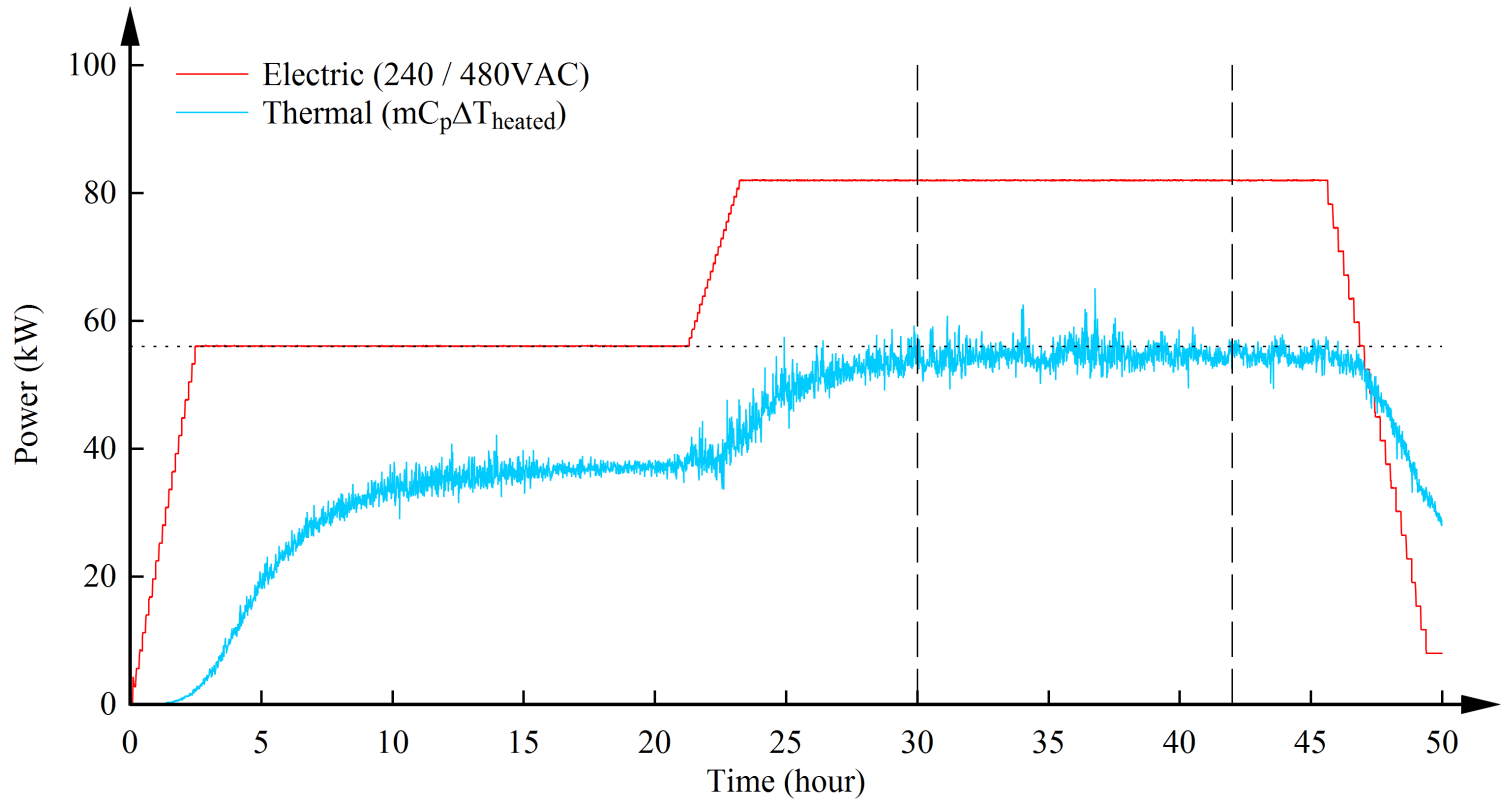


Figure 76: Electric and thermal powers from baseline test case, Run011. Long dashed lines indicate steady-state period, and dotted line indicates target power

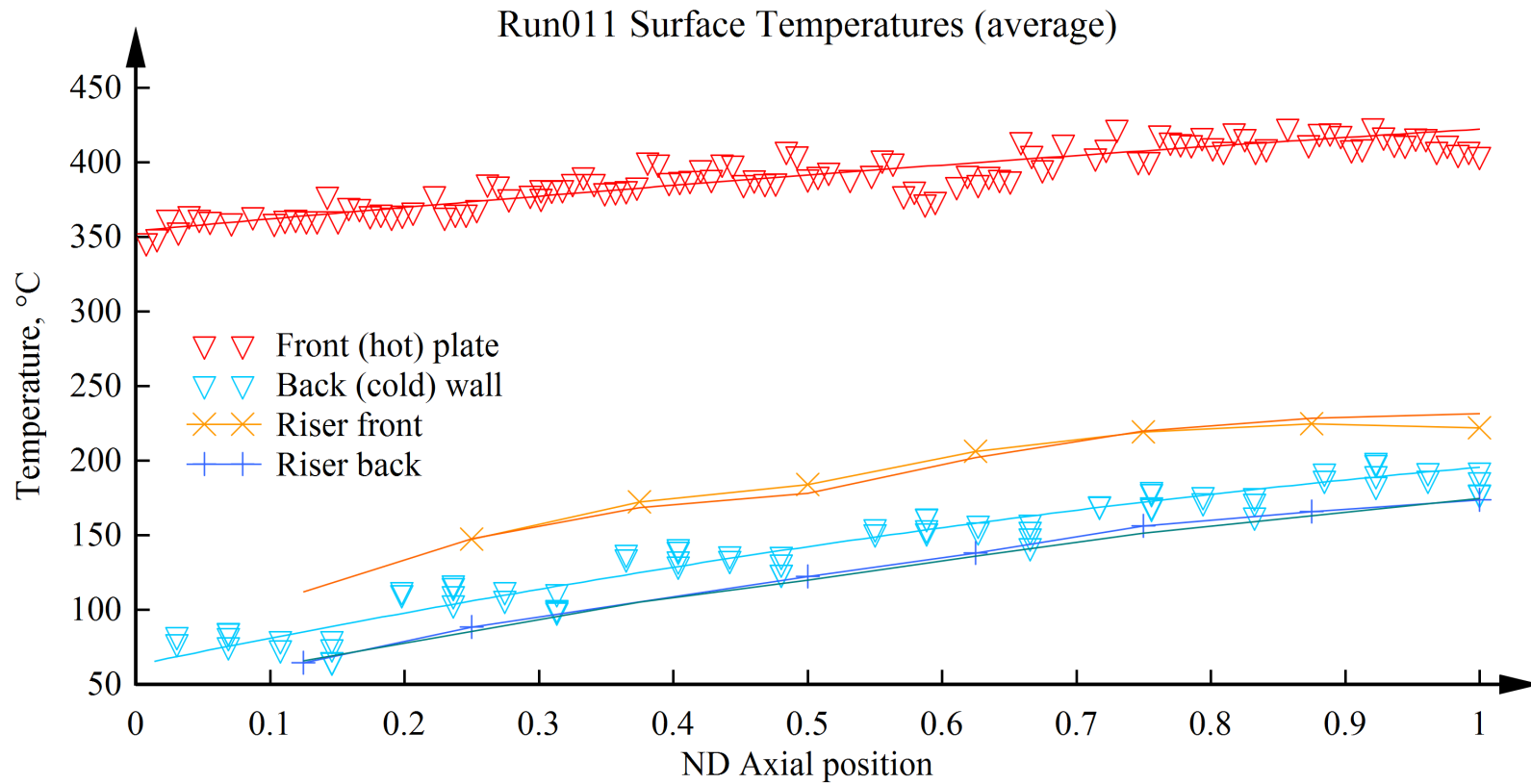


Figure 77: Axial temperatures for surfaces within the heated cavity, averaged over steady-state period at baseline conditions

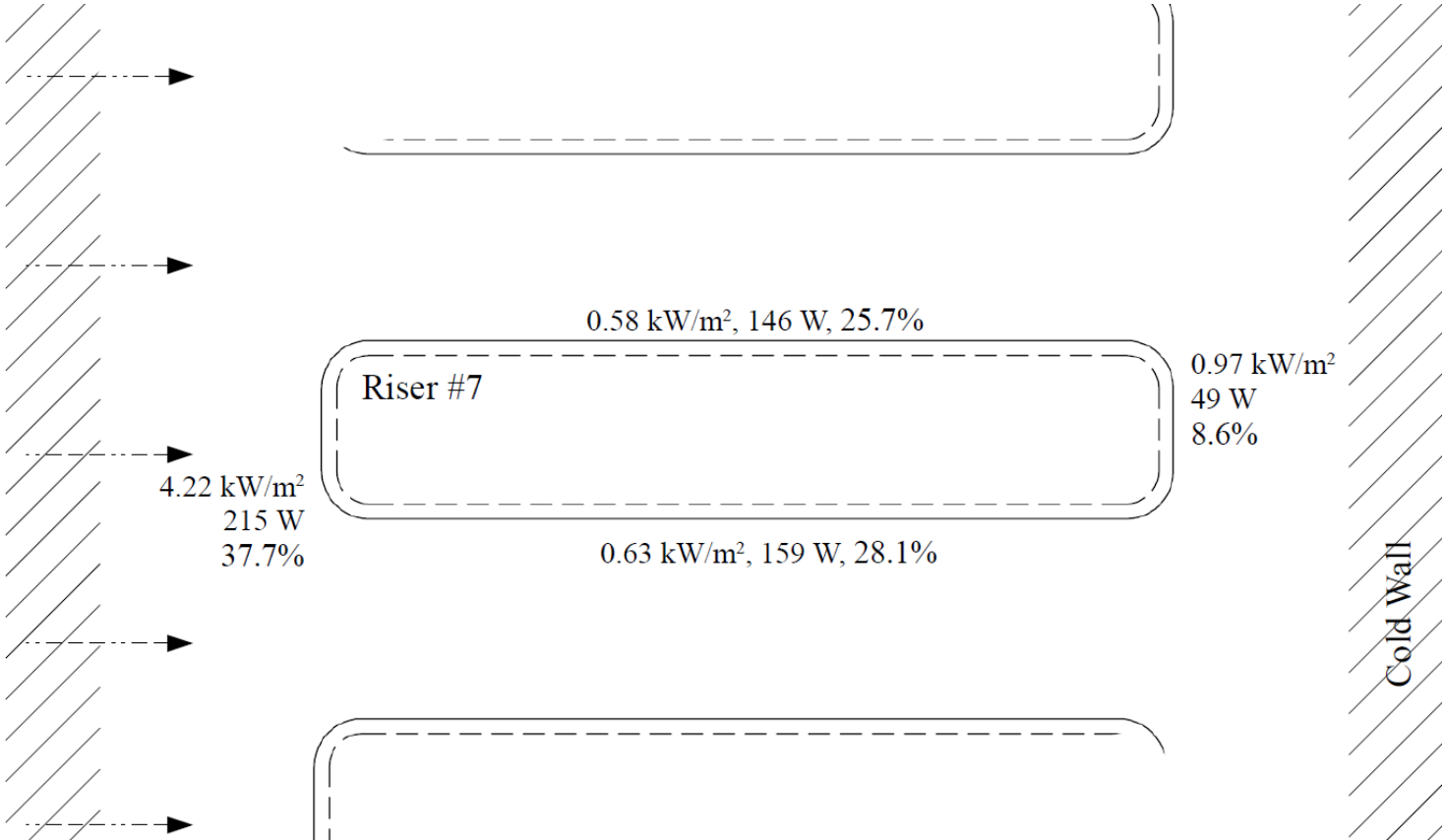


Figure 78: Heat flux contributions to four faces of Riser 7, steady-state baseline conditions

7.1.2 Baseline Repeatability

With an established procedure for baseline testing, repeat runs were performed on a regular basis to verify system repeatability and monitor long-term changes in the thermal hydraulic performance. Given that the the NSTF is exposed to the ambient conditions, regular testing across the 33-month cycle identified strong influences on the performance of the facility. Each test was performed in an identical facility configuration (uniform power profile, full elevation discharge via vertical chimney stacks) and in such a manner that maintained an equal time-power history across the test procedures.

Across the operational testing window, a total of eight baseline runs were conducted, with dates and outdoor temperature conditions summarized below in Table 31. Across the eight runs, the observed outdoor temperature spanned $-18.1\text{ }^{\circ}\text{C}$ to $23.7\text{ }^{\circ}\text{C}$, or a total range of $41.8\text{ }^{\circ}\text{C}$.

Table 31: Testing conditions for repeat baseline cases performed

Test No.	Test Quality	Dates Performed	Outdoor Temperature, $^{\circ}\text{C}$		
			Average	Minimum	Maximum
Run003	Trending	03/10-12/2014	n/a	n/a	n/a
Run004	Accepted	04/09-11/2014	13.9	10.2	17.1
Run011	Accepted	01/28-30/2015	2.09	1.4	2.8
Run020	Accepted	09/05-07/2015	23.3	22.5	23.7
SPEF003	Separate Effects	10/12-19/2015	11.5	11.1	12.2
Run022	Accepted	01/17-22/2016	-17.6	-18.1	-16.8
Run024	Accepted	04/08-14/2016	5.3	-4.9	17.3
Run026	Accepted	05/16-20/2016	13.6	5.8	21.6

Examinations were made on the multiple baseline test cases in an attempt to quantify and ascertain facility repeatability. A number of metrics were used for comparison, e.g. thermal power within the test section determined by $\dot{m}C_p\Delta T$, where \dot{m} is the total system flow rate, C_p is the specific heat determined at the average gas temperature, and ΔT is the difference between the gas at the outlet and inlet of the heated test section. Other metrics include as-

measured temperatures, pressure drop, etc. At first glance of the measured thermal powers, Figure 79, all test cases exhibit similar behavior and measured values fall within an acceptable variance from the sample mean. However, further examination of other parameters, such as the heated section temperature rise, Figure 80 and system mass flow rate, Figure 82, indicate large differences across the different runs.

Isothermal forced flow testing was performed on a regular basis and indicated that frictional losses, e.g. due to geometric changes, had not changed within the bounds of experimental uncertainty. The ambient conditions (outside temperature and wind) and the building interior temperature are likely the dominant factors.

The underlying cause of these differences can be attributed to differences in ambient weather conditions. The coldest baseline case, Run022, was performed during a typical Midwestern United States winter week and thus experienced significantly colder ambient temperatures ($-18.1\text{ }^{\circ}\text{C} \leq T_{outdoor} \leq -16.8\text{ }^{\circ}\text{C}$) than Run020 that was performed in summer months ($+23.7\text{ }^{\circ}\text{C} \leq T_{outdoor} \leq +22.5\text{ }^{\circ}\text{C}$). This effect propagates itself onto the system behavior two-fold: the first is by absolute temperature, and the 2nd from the buildings thermal footprint. With colder ambient temperatures there is an increase in the natural driving force that stems from differences in fluid densities, which in turn drives a higher system mass flow rate. Additionally, we believe there is a minor influence from the building thermal mapping, which during winter months with personnel heaters, creates a positive net pressure in the building that induces a forced flow out of the NSTF even at zero power states. However we believe the ambient temperatures to dominate over this minor influence, and have been confirmed by separate effects testing.

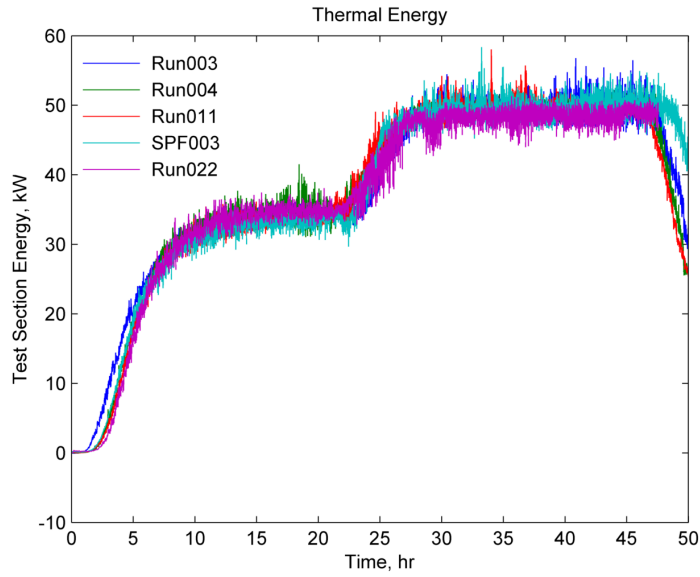


Figure 79: Thermal power, baseline repeats

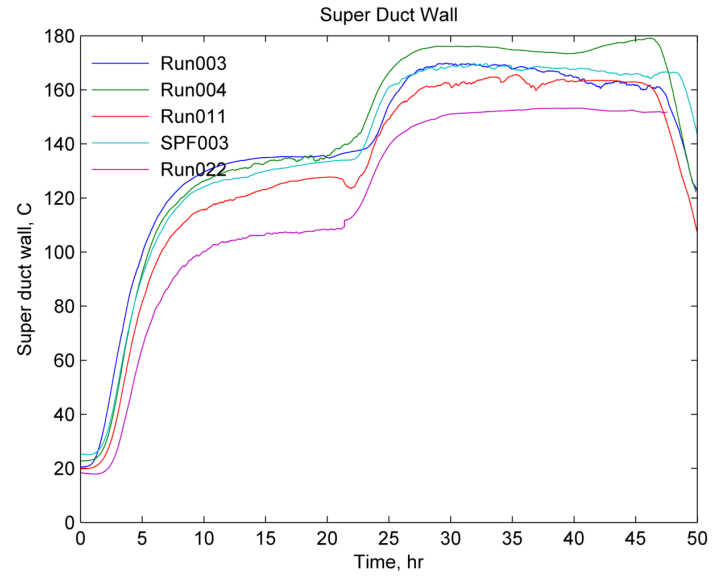


Figure 81: Riser wall temperature, baseline repeats

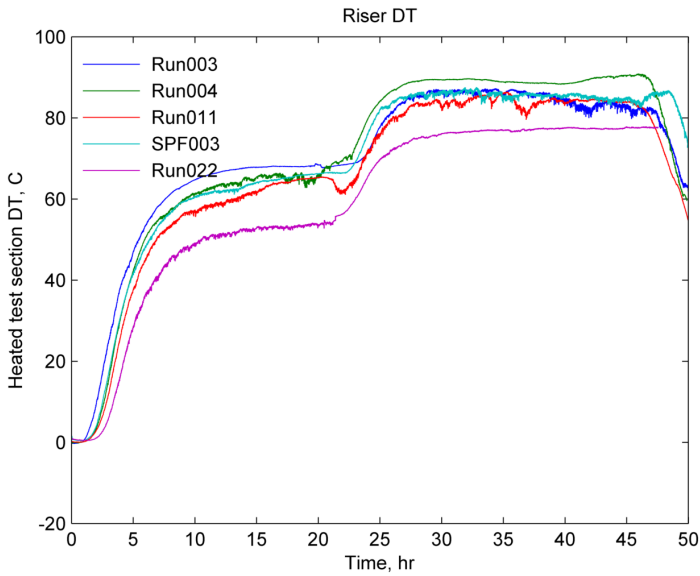


Figure 80: Riser ΔT , baseline repeats

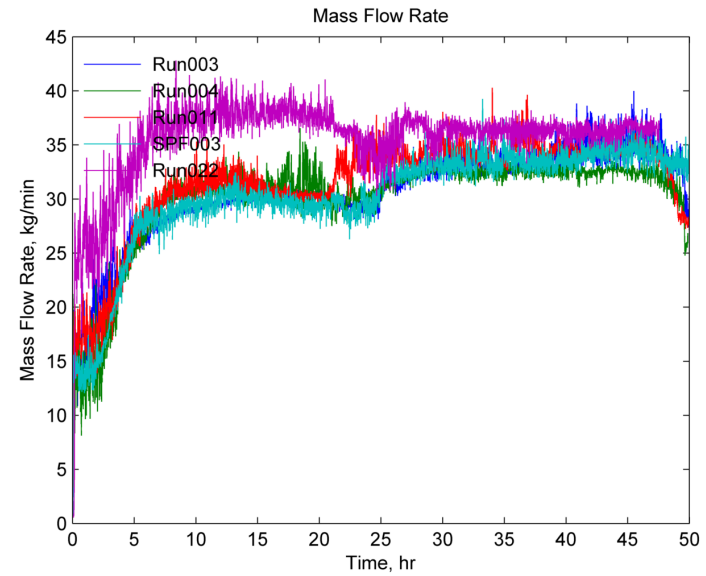


Figure 82: System flow rate, baseline repeats

With higher system mass flow rates from lower temperatures, but equal thermal powers, all other system parameters are affected: the heated section temperature rise decreases, frictional pressure drop increases, etc. Table 32 provides a comparison of system parameters collected during eight separate baseline test cases.

Plotting the heated section temperature rise versus ambient (outdoor) temperature, a clear relation is visible, Figure 83. With decreasing ambient temperatures, the driving chimney head is more effective thus the system mass flow rates are higher. For constant thermal powers, this requires the temperature rise to decrease. Though this behavior does not significantly change the integral performance, it is an important finding that must be considered when characterizing and studying the test facility.

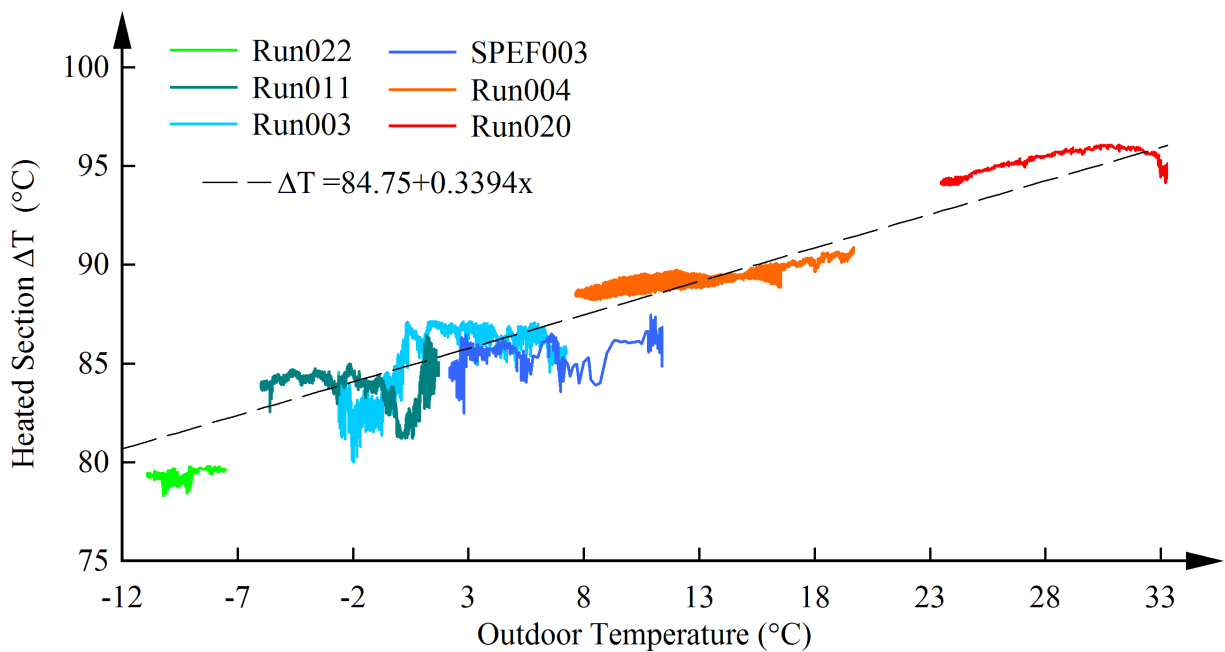


Figure 83: Relation between ΔT and ambient temperature across baseline test cases. Wind speeds were significantly higher during Run003, Run011, and SPEF003 resulting in fluctuations of the trend line

Table 32: Measured values across steady-state periods for all performed baseline test cases

Test No.		Run003	Run004	Run011	Run020	SP003	Run022	Run024	Run026				
Averaged period	hr	28-36	30-45	29-45	42-48	28-47	54-66	32-44	20-32	Max	Min	Mean	σ^2
Heater power	kW _e	78.40	78.94	81.99	81.88	81.98	79.96	79.98	79.98	78.4	82.0	80.4	2.0
Thermal power	kW _t	52.45	53.02	56.12	48.63	52.72	49.80	49.97	50.70	48.6	56.1	51.7	5.7
Heated plate, front	°C	392.36	395.57	390.66	397.51	392.03	382.45	385.39	387.90	382.5	397.5	390.5	25.5
Ceramic heaters	°C	576.53	578.77	568.41	568.32	564.32	554.52	557.00	558.33	554.5	578.8	565.8	79.9
Riser duct wall	°C	168.99	175.26	163.11	183.31	167.55	152.49	161.64	167.90	152.5	183.3	167.5	84.5
Cold (west) wall	°C	146.38	150.26	138.89	156.15	143.56	131.85	140.09	145.00	131.8	156.1	144.0	54.7
Outlet plenum wall	°C	98.32	103.62	75.12	98.68	85.09	78.88	85.06	89.90	75.1	103.6	89.3	102.9
Riser inlet gas	°C	20.79	23.55	19.74	29.98	23.80	19.86	23.54	26.85	19.7	30.0	23.5	12.6
Riser outlet gas	°C	107.19	112.74	103.85	124.20	109.27	96.89	105.09	111.35	96.9	124.2	108.8	63.2
Outlet plenum gas	°C	110.97	117.03	101.18	128.61	113.42	103.03	109.41	115.59	101.2	128.6	112.4	74.3
Chimney inlet gas	°C	108.16	113.72	98.96	125.95	111.11	100.43	107.43	113.08	99.0	125.9	109.9	71.7
Chimney outlet gas	°C	88.22	94.02	86.75	109.98	96.45	94.51	100.64	105.31	86.8	110.0	97.0	64.0
Mass flow rate	kg/min	33.21	32.55	34.46	28.08	33.75	36.27	33.60	32.75	28.1	36.3	33.1	5.5
Riser pressure drop	Pa	18.15	16.69	21.40	15.89	20.73	24.58	21.68	20.36	15.9	24.6	19.9	8.3
Inlet plenum humidity	%	28.47	21.05	22.69	52.18	31.91	12.66	19.20	24.42	12.7	52.2	26.6	140.8
High bay ambient	°C	26.21	29.31	23.86	33.29	26.63	31.50	29.71	33.99	23.9	34.0	29.3	12.7

7.2 Heated Source Variations

7.2.1 Cosine Shaping - Run013 & Run022

The heat flux profile off a typical RPV wall does not follow the idealized flat and linear profile commonly implemented in scaled test assemblies. To examine the influence of power shaping in the axial direction, two tests were performed on the NSTF that examined cosine shaped power skews. The first test case, Run013, defined a mid-plane peaked cosine and is representative of a full scale HTR RPV, while a second test case, Run022, defined a bottom peaked cosine that reflects early life of a generic nuclear RPV.

Each test case was first allowed to reach steady-state operation with a linear and flat power profile for a minimum period of 6 hours, after which the cosine power profile was gradually applied over a 2 hour period. The new operating state was subsequently allowed to stabilize and upon re-establishing steady-state operation, average values were pulled from a 6-hour period.

The influence of the cosine profiles had negligible impacts on the integral performance and primary system parameters did not change outside of normal fluctuations caused by meteorological variations. The only statistically significant change observed was the temperature profile within the gas space and along the walls of the riser ducts. The gas temperature profile exiting the risers, as measured by the LUNA fibers in Figure 84, show a smoother gradient during the bottom peaked cosine profiles when compared to the reference linear case. This result is intuitive - a higher portion of the total power is removed at lower elevations, providing a longer path for thermal hydraulic development. The measured difference, while perhaps visually distinct, is relatively minor. The ratio of peak to average temperatures for the linear and cosine cases change from 1.26 to 1.32%, respectively.

Differences can also be observed when examining the temperature profile of the riser duct wall surface. As shown in Figures 85 - 88, a clear hump is shown at the axial locations corresponding to the position of cosine peak in the power profile.

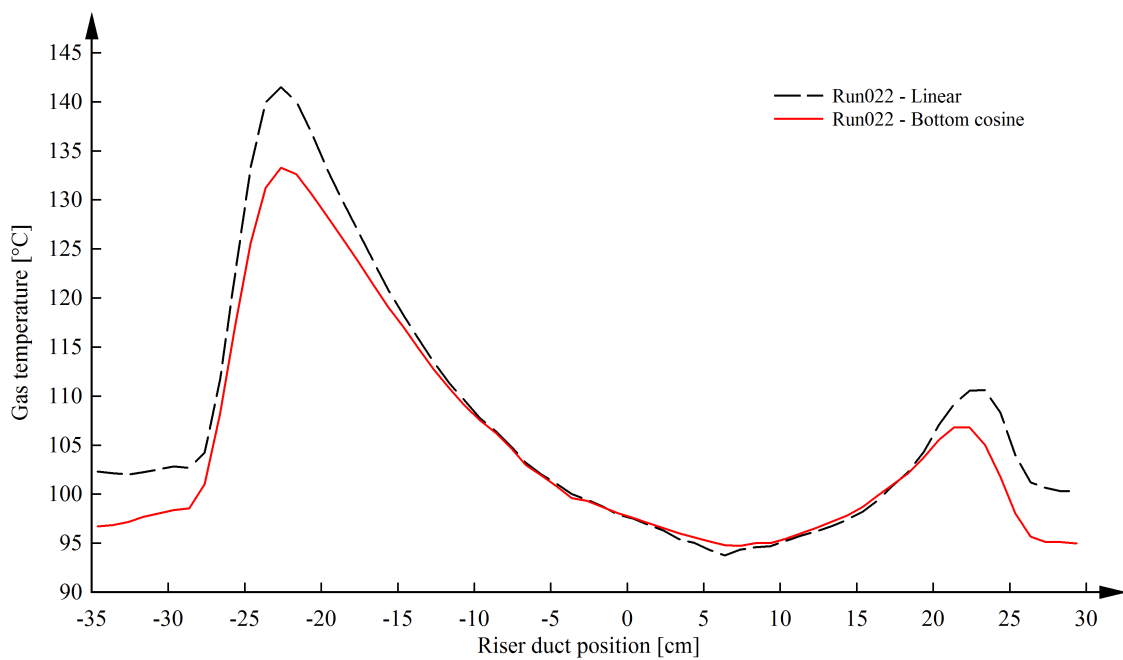


Figure 84: Temperature profile across 10-inch exit face of riser ducts during linear and bottom peaked cosine power profiles, Run022

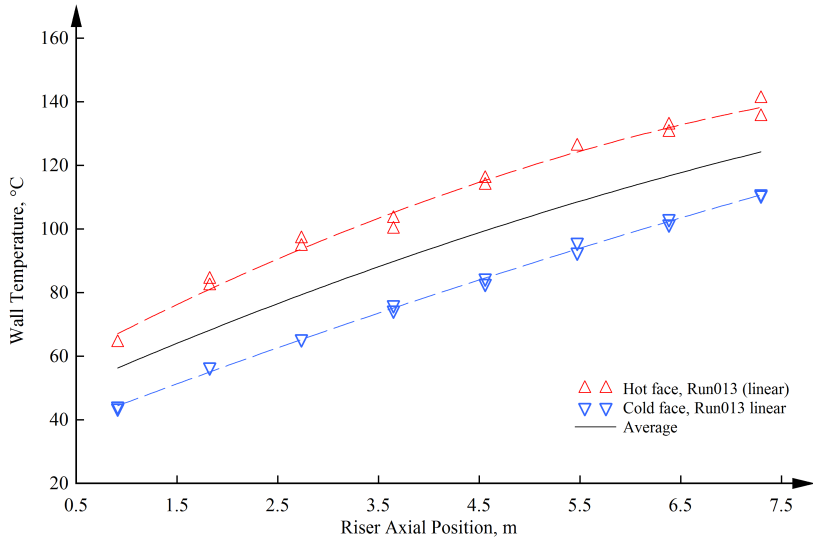


Figure 85: Run013 riser wall temperature, linear

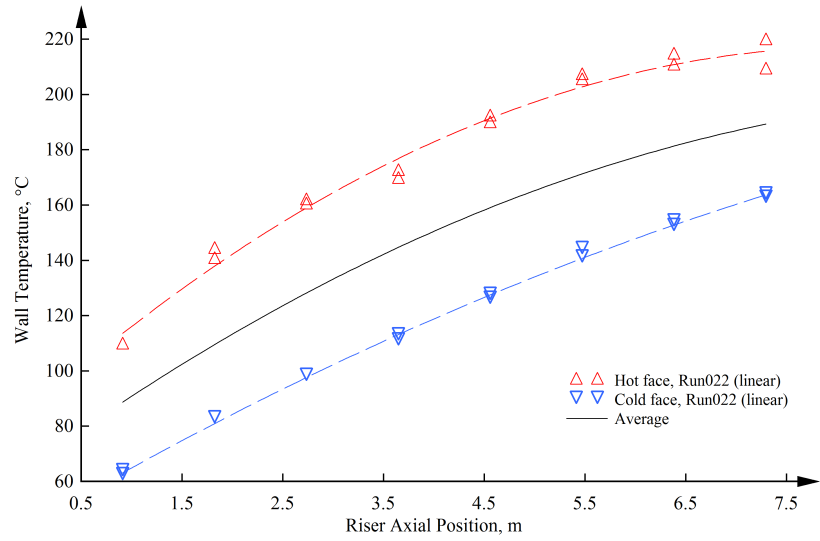


Figure 87: Run022 riser wall temperature, linear

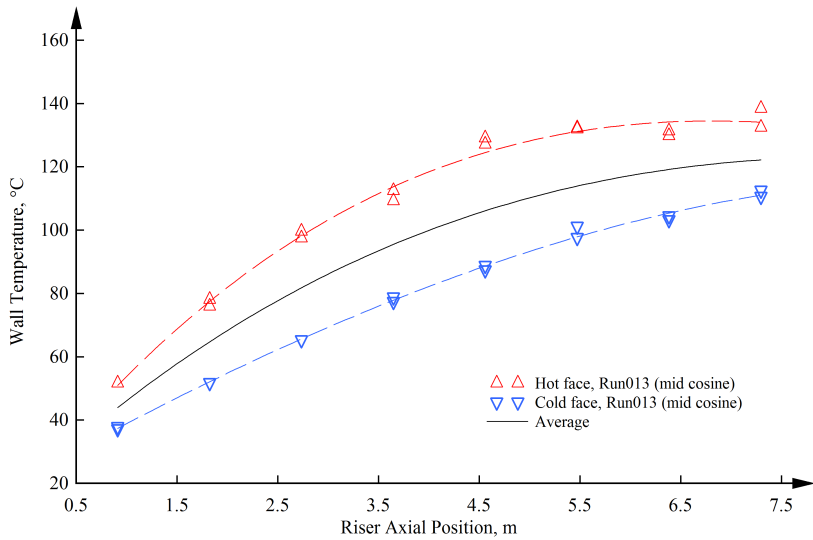


Figure 86: Run013 riser wall temperature, mid cosine

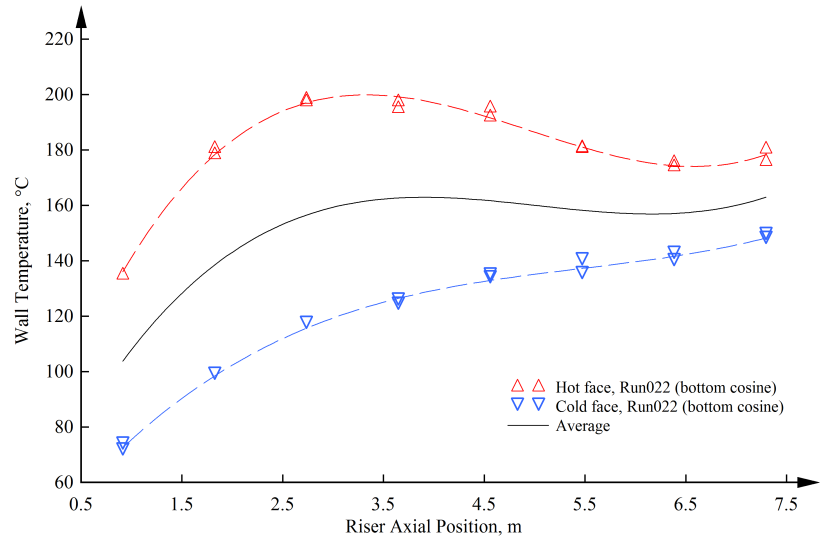


Figure 88: Run022 riser wall temperature, bottom cosine

7.2.2 Azimuthal Shaping - Run026

Variations onto the power profile in the radial, or azimuthal direction, were performed during DataQuality026. Three steady-state periods were studied: the first at 50/50%, the second at 60/40%, and the third and final at 65/35%, power split among the north and south heater banks, respectively. All stages supplied an integral power at the baseline conditions, with a target thermal power of 56 kW_t . Outside of variations due to meteorological influences, no statistically significant differences were observed when compared to the linear profiles. The only measurable difference was within the riser outlet gas temperatures, shown in Figure 89.

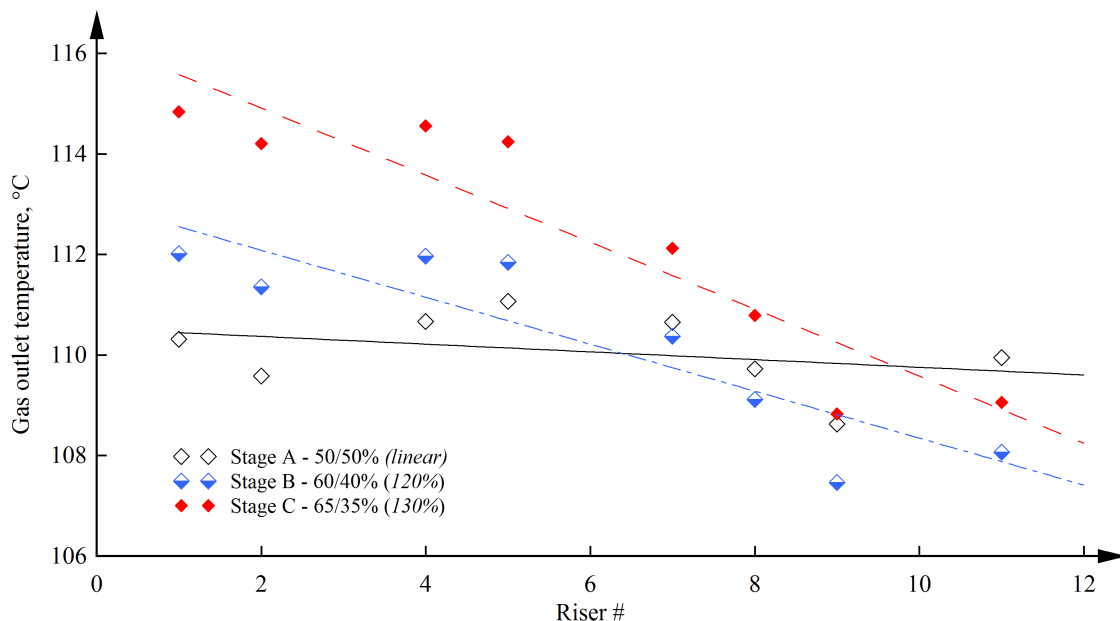


Figure 89: Riser outlet gas temperatures for varying levels of azimuthal skews, Run026

The objective of this test series was to study the behavior of a prototypic RCCS while exposed to the natural imperfections that would likely exist in a full scale installation. It is foreseeable to consider that with sufficiently high power skews, either due to blocked radiation view factors, local peaking by proximity, or other physical constraints, instabilities could be observed and cause performance degrading behavior in the RCCS channels. Thus, this study was an attempt at forcing such conditions however the testing window achieved was not able to observe any instabilities. Further testing would be necessary to reach the

physical limit on anticipated operating conditions and objectively assess the performance limitations.

The azimuthal power skew employed in the testing series was defined at the heated source (e.g. ceramic heaters) and experienced some smoothing due to radial conduction across the width of the heated plate. Given that heat flux sensors were unavailable at the surface of the heated plate, a 1-dimensional thermal analysis was performed using a simple conduction model for heat transfer. For the 120/80% split at the ceramic heaters, computational analysis indicate that the resulting power profile obtained at the heat sink resulted in only 107/93% split, Table 33 and Figure 90.

Obtaining a true power (sink) profile of 125 / 75% split, as suggested in previous analysis, would require a supplied power (source) profile of 160 / 40%. This level of skew would risk structural damage to the test facility (warping of heated plate due to extreme temperature gradients) and thus was not performed experimentally.

Table 33: Power skews at source and sink, 1-D steady-state thermal

Heater (source)			Riser (sink)		
North	South	N/S	North	South	N/S
120%	80%	1.50	107.0%	93.0%	1.15
125%	75%	1.67	109.9%	90.0%	1.22
130%	70%	1.86	111.4%	88.6%	1.26
150%	50%	3.00	112.0%	80.2%	1.40
160%	40%	4.00	123.8%	76.2%	1.62

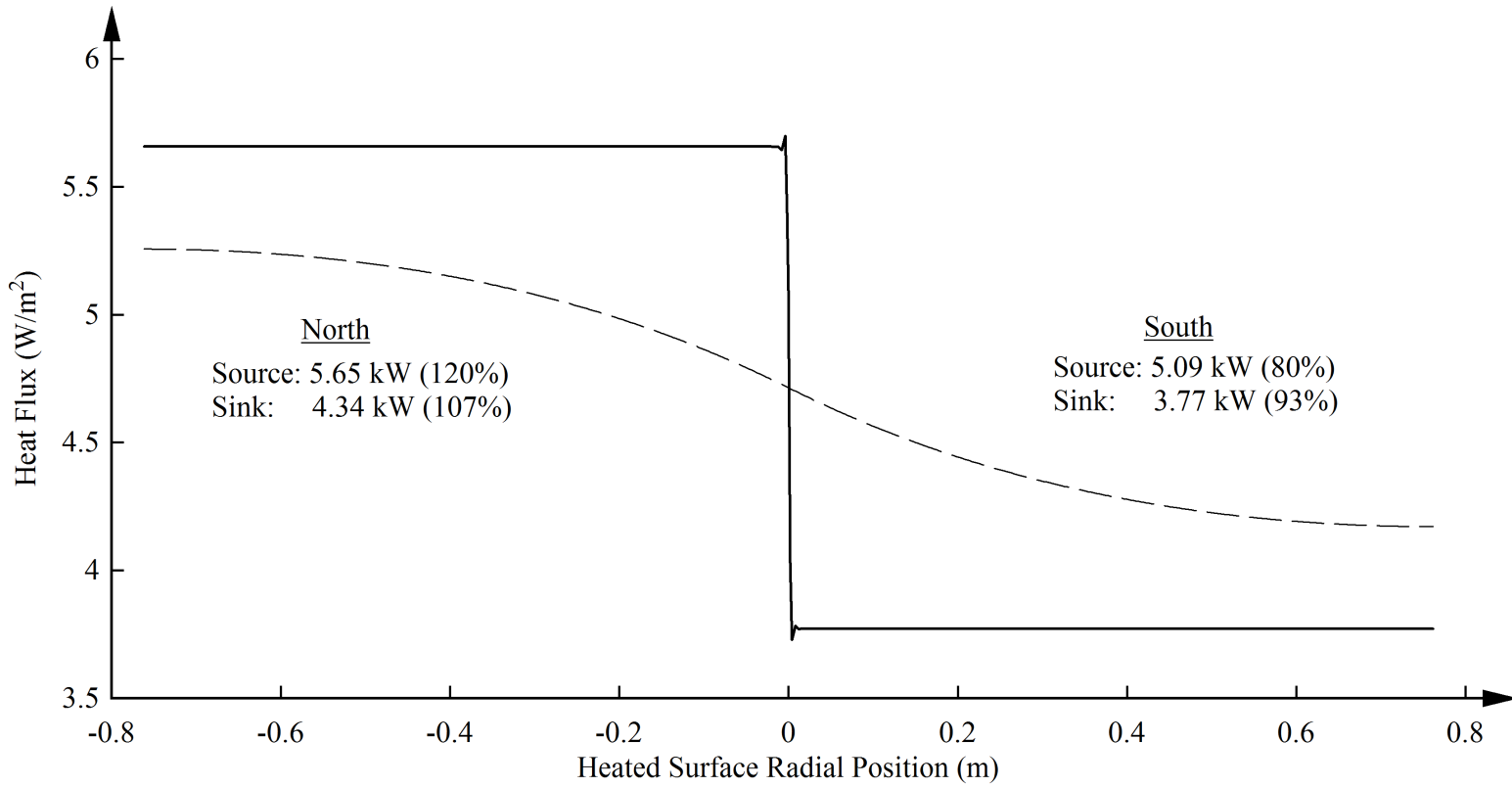


Figure 90: 1-D steady-state thermal analysis of azimuthal power skew at source and sink

7.3 Prototypic Studies

7.3.1 Accident Scenario Testing - Run014

The following provides a summary of the operating parameters including results of NSTF's Run014. The test objective was to simulate an accident scenario for the full scale GA-MHTGR. The test began by establishing steady-state at the normal operating heat load, which defines a full scale power of 700 kW_t, or 26.16 kW_t in the 1/2 scale NSTF.

Upon reaching stable operation and meeting the acceptance criteria, the accident sequence was initiated and the power followed a varying time history representative of the GA-MHTGR decay heat curve. The test was concluded after reaching the peak power, which occurred after 120 hours at 1.5 MW_t in the full scale, or 84.85 hours at 56.07 kW_t in the NSTF. A dated log of the primary procedural test events is provided below in Table 34. No unusual or unplanned events that occurred throughout the duration of the test.

Table 34: Test log for Run014 - GA-MHTGR summer

Date	Time	Action
4/6/2015	12h10	Zero flow verification, saved LabVIEW acquisition
4/6/2015	12h23	LUNA baseline calibration, saved LabVIEW acquisition
4/6/2015	12h29	Began data logging on LabVIEW, start of test operations
4/6/2015	12h31 - 14h26	Power ramp from 0 to 42.00 kW _e
4/7/2015	05h28 - 9h28	First steady-state period, 25.06 kW _t measured in test section
4/7/2015	09h57	Accident sequence initiation, reset clock to t _{accident} = 0
4/11/2015	00h28	Peak power condition reached, t _{accident} = 91.9hr, P = 54.45 kW _t
4/11/2015	18h40	Accident conclusion, t _{accident} = 110.1hr, t _{total} = 127.1 hr
4/11/2015	18h40 - 22h46	Power ramp from 89.15 to 0 kW _e
4/11/2015	22h51	Test conclusion. t _{accident} of 114.27hr, t _{total} = 130.37hr

Acceptance criteria were established both pre-accident steady-state and mid-accident peak power. Both were met upon review of immediately recent data, which showed a stable thermal energy balance within the heated test section for a period that did not change more than ±5%. A summary is provided in Table 35.

Overall, the facility was able to follow the full decay heat curve while successfully main-

Table 35: Summary of steady parameters for GA-MHTGR Run014

	Steady-State	Peak Accident
Span	17 - 23 hr	100 - 116 hr
Electric power, kW _e	42.08	90.07
Test sect. power, kW _t	25.06	54.49
System flow rate, kg/s	0.499	0.585
Riser ΔT , °C	49.44	90.32
Front heated plate, °C	275.32	408.72
Ceramic heaters, °C	404.13	591.26

taining the vessel wall at safe temperatures (408 °C at peak decay heat removal as measured in the NSTF). Due to the long time scales of the power profile, heat removal by the RCCS followed closely the decay power from the heated source. Perturbations in the system flow were observed due to meteorological fluctuations, which were most pronounced in the system flow rate and heated temperature rise. Furthermore, the test window saw dominating winds in the NE direction during the first half, which then shifted to westward in the second half. The impact on the test facility was an asymmetric flow among the parallel chimney ducts, which required the operators to use engineering controls (i.e. dampers along the chimney stacks) to maintain stable air flow out of the dual exhaust chimneys. Wind gusts, measured at speeds up to 21.9 m/s, or 49 mph, created strong perturbations near the outlet chimneys. If manual intervention was not made, experience from operating the NSTF suggests with high confidence that flow reversals would have occurred and resulted in degraded heat removal performance. All modifications via the duct dampers were logged and included in the formal data suite.

With completion of post-test data verification procedures and review of generated data sets, the test was found to be fully within the defined scope and set of procedures and thus is classified as successful and will be submitted for qualification for Type-A data.

7.3.2 Accident Weather Influences - Run018

The GA-MHTGR accident scenario was first performed during Run014 during winter conditions, which saw temperatures averaging near 10 °C (span of 2.9 - 22.5 °C). To examine the influences from weather, this test was repeated in Run018 during hot summer weather which saw temperatures averaging 25 °C (span of 19.1 - 32.1 °C). A detailed summary of the operating meteorological conditions over the course of both testing windows is provided in Table 36. Examining the system thermal hydraulic behavior, they performed and exhibited very similar trends. However, while the electric and thermal powers were nearly identical, the elevated ambient temperatures had a strong impact on absolute values of the system flow rates and gas temperatures. A summary is provided in Table 37.

Table 36: Summary of weather conditions for two GA-MHTGR tests, winter and summer

		Run014 - Winter		Run018 - Summer	
		<i>Average</i>	<i>Span</i>	<i>Average</i>	<i>Span</i>
Rain fall	mm	0.00	0-1.02	0.00	0-0.76
Rain fall rate	mm/hr	0.25	0-63	0.17	0-41.4
Barometric pressure	mm	760.06	748-769.5	762.32	754.8-765.2
Outdoor humidity	%	81.48	29-98	79.05	46-96
Indoor temperature	°C	22.58	20.4-28.2	29.23	25.2-33.9
Outdoor temperature	°C	9.99	2.9-22.5	24.85	19.1-32.1
Wind run	km	0.22	0-0.94	0.10	0-0.67
Wind direction	degrees	165.29	22.5-337.5	210.44	22.5-337.5
High wind speed	m/s	5.41	0-21.9	2.52	0-16.5

Table 37: Summary of GA-MHTGR accident scenario averaged thermal hydraulic parameters

		Normal Operation			Peak Accident		
		<i>Winter</i>	<i>Summer</i>	<i>% Diff.</i>	<i>Winter</i>	<i>Summer</i>	<i>% Diff.</i>
Electric power	kW_e	42.08	41.99	0.2%	90.08	90.07	0.0%
Thermal power	kW_t	25.06	23.04	8.4%	54.49	51.71	5.2%
Heated plate	$^{\circ}C$	275.33	281.56	2.2%	408.72	414.71	1.5%
Riser wall	$^{\circ}C$	98.71	113.99	14.4%	175.94	192.70	9.1%
Cold wall	$^{\circ}C$	90.29	102.88	13.0%	146.93	162.96	10.3%
Riser hot wall	kW/m^2	1.96	1.86	5.2%	3.81	3.59	6.0%
Riser cold wall	kW/m^2	0.53	0.48	10.0%	0.89	0.84	5.3%
Riser inlet gas	$^{\circ}C$	17.77	26.60	39.8%	20.10	28.04	33.0%
Riser outlet gas	$^{\circ}C$	67.52	82.03	19.4%	112.43	128.50	13.3%
Mass flow rate	kg/s	30.00	24.73	19.2%	35.11	30.59	13.8%
Riser ΔP	Pa	13.42	9.90	30.2%	19.71	16.56	17.3%
Inlet humidity	$\%$	43.98	59.09	29.3%	34.54	63.16	58.6%
High bay ambient	$^{\circ}C$	17.84	28.44	45.8%	20.56	31.40	41.7%

7.3.3 Adjacent Chimney Roles - Run017

The following provides a summary of the operating parameters and test conditions of NSTF's Run017. The primary test objective was to examine the system behavior while in an altered, adjacent chimney role configuration. In this state, the south chimney was connected to the inlet downcomer via a 24" flexible duct and served as the sole intake of fresh air. The north chimney maintained its regular function of serving as the exhaust. One steady-state period were established at 78 kW_e for a period of 6 hours.

The steady-state period was designated once the system reached stable flow conditions for a minimum period of 6 hours. Time averaged values over these 6 hours were then used to meet established acceptance criteria, which defined system parameters that did not vary more than 5% over the 6 hour period. The total test duration spanned 58.6 hours. With completion of post-test data verification procedures and review of generated data sets, the test was found to be fully within the defined scope and set of procedures and thus is classified as successful and will be submitted for qualification for Type-A data.

Acceptance criteria were established for the goal steady-state period, and were met upon review of immediately recent data, which showed a stable thermal energy balance within the heated test section for a period that did not change more than ±5% over a 6 hour window. A summary is given in Table 38.

Table 38: Summary of steady-state period during Run017 (prior to break area)

	6 hour average	Percent change
Electric power	77.98 kW _e	0.01%
Test section power	38.84 kW _t	0.70%
System mass flow rate	0.355 kg/s	1.63%
Riser ΔT	108.37 °C	0.93%
Front heated plate	394.94 °C	0.11%
Ceramic heaters	559.0 °C	0.03%

The impact of the new chimney configuration significantly altered the behavior of the test facility, as the inlet downcomer was no longer shielded by the laboratory building.

Thus the most apparent observation is a heightened sensitivity to ambient wind patterns, where the fully exposed inlet and outlet ducts readily propagated meteorological fluctuations through the entire test facility. In the baseline configuration, strong wind gusts would typically only alter the outlet conditions while the inlet patterns remained unaffected. In this configuration, strong wind gusts influences both the inlet and outlet, with observable spikes in inlet temperatures as system flow rates experienced brief periods of stagnation or minor oscillations. Furthermore, the added resistance of the inlet flow path reduced the efficiency of the stack effect and resulted in reduced system flow rates. With baseline configurations averaging flow rates of 0.5 kg/s, equal thermal powers in the adjacent configuration saw flow rates near 0.36 kg/s. To maintain the energy balance, system temperatures subsequently rose.

Short Circuit Scenario

The initial stages of Run017 were designed to ensure a normal flow path by drawing fresh air in and down the south chimney stack, heating across the riser ducts, and then exhausting out of the north chimney stack. Then, three series of chimney “short-circuits” were created, where a damper was opened in varying amounts. During this portion of the test, the breakages were simulated by actuating the cross-connect damper valve, LF-CX, allowing a portion of the inlet air supply to “short-circuit” the heated section and discharge directly to the outlet, Figure 91. Each of the three short-circuits series lasted 30 minutes each, and was allowed 60 minutes between to re-establish normal steady-state operation. A summary of the break areas and impact on the system behavior is provided below in Table 39.

Table 39: System behavior with varying amounts of chimney short-circuit break areas

	Stage #1	Stage #2	Stage #3
Break flow area, %	33.30%	50%	100%
Span, run time hr	0.5	0.5	0.5
Electric power, kW _e	77.96	77.97	77.97
Test sect. power, kW _t	29.65	27.51	23.28
System flow rate, kg/s	0.273	0.263	0.254
Riser ΔT , °C	107.16	103.29	90.64
Front heated plate, °C	397.43	399.41	400.18
Ceramic heaters, °C	560.22	561.55	562.22

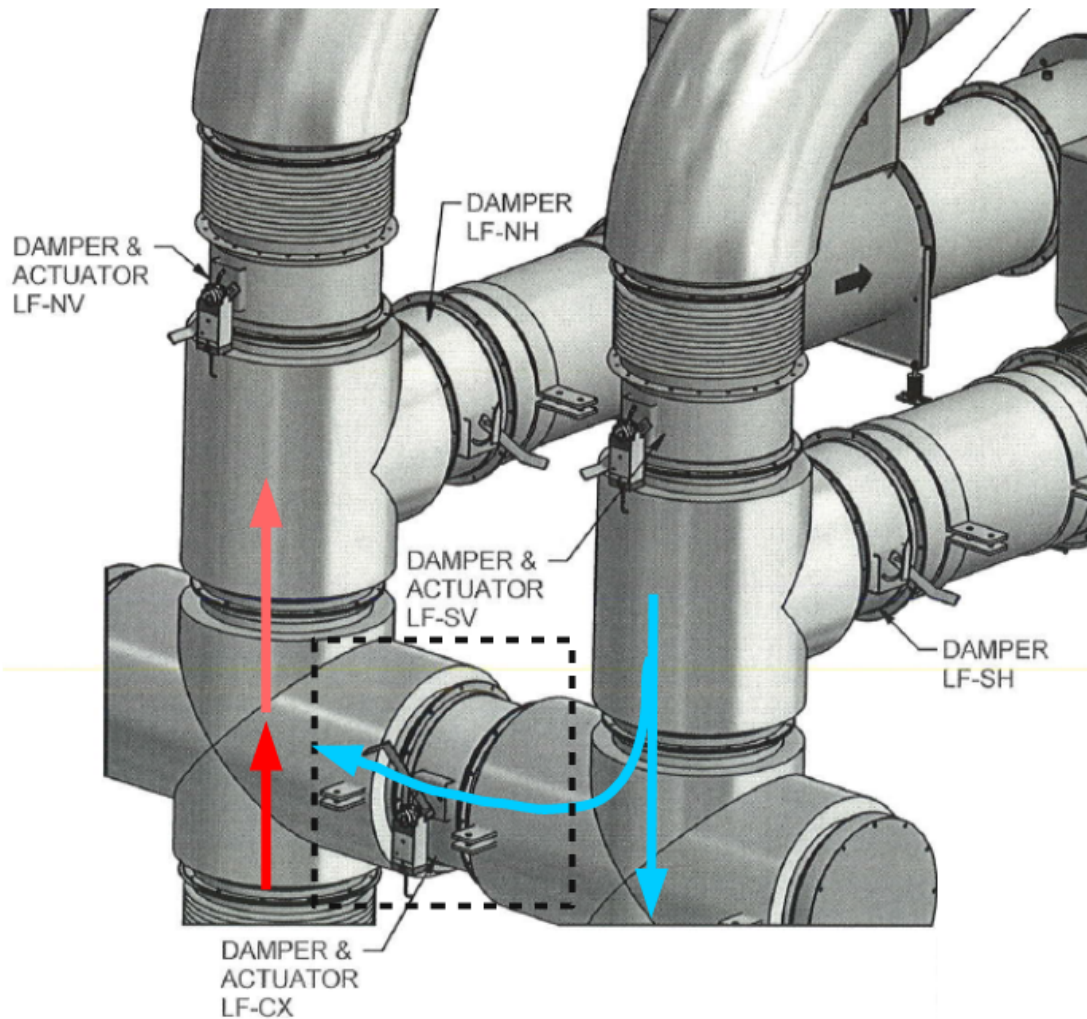


Figure 91: Short-circuit region and flow paths. Blue arrows indicate fresh inlet air supply, dark red indicates originating heated exhaust from test section. Mixing occurs across the dashed boxed region by opening the damper and actuator LF-CX

While examining the post-test results and discussing the observations with the modeling team, a heightened interest was expressed to further quantify and understand the behavior during these short-circuit breaks. Thus, an additional separate effects test was performed, SPEF001, that focused on additional instrumentation near the chimney break region. The test was performed similar to Run017, except that the 30 minute break period was extended to over 4 hours. With concerns for reaching the 300 °C temperature limit on the heat flux sensors (Run017 with 50% and 100% breakages saw these approach 292 °C), only a single break stage was created at a 33.3% open flow area between the north and south chimneys.

The new instrumentation centered on hot-wire measurements of the air velocity above the break area, a location that was selected to provide information on the total air draw by the NSTF. Combined with existing air flow measurements below the break region, the amount of air short-circuiting the heated region could be measured. Measurements were made on two instances prior to the break to verify mass balance and check that the measurement technique was valid. Then, this mass balance measurements were repeated during the chimney break with 33% open flow area after reaching steady-state conditions and summarized in Table 40. Based on these measurements, it is apparent that a significant portion of fresh air is being diverted into the break area and returning directly out the exhaust. Of the 0.566 kg/s total supply of air into the NSTF, only 0.3 kg/s of air entered the heated region while the remaining, nearly an equal amount of 0.258 kg/s, was diverted directly into the discharge exhaust. The breaks degraded the heat removal performance, and have profound impacts on all system temperatures, Figures 92 and 93.

Table 40: System segment flow rates during 33% break area between inlet & outlet chimneys

Break size	Run Time <i>hour</i>	Total Inlet <i>kg/s</i>	Heated Region <i>kg/s</i>	Break Region <i>kg/s</i>
0%	28.7	0.365	0.365	≤0.001
0%	57.5	0.384	0.382	0.002
33%	57.85	0.566	0.308	0.258

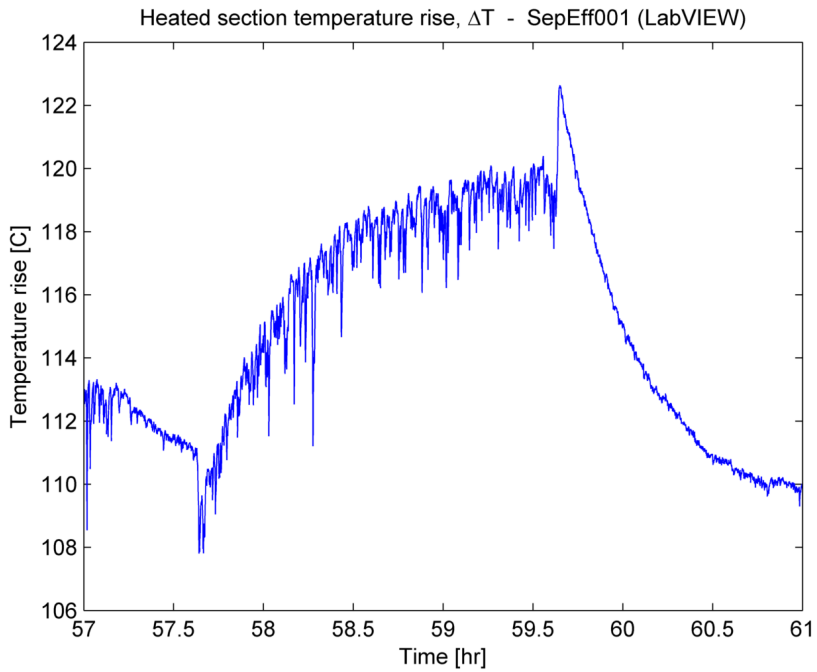


Figure 92: Impact of 33% break initiated at $t=57.6$ min. Average riser ΔT saw a 7.4°C rise

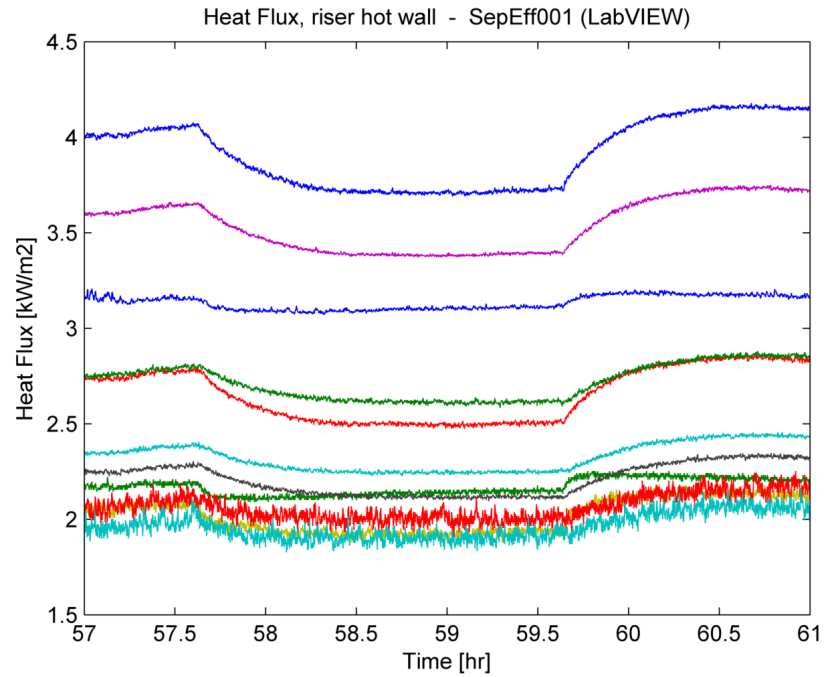


Figure 93: Impact of 33% break initiated at $t=57.6$ min. Average riser heat flux saw a -9.33% reduction

7.3.4 INERI Test Case - Run023

As part of a formal collaboration initiative with Korea Atomic Energy Institute (KAERI), a test series was drafted to examine differences in scaling philosophy. The testing was designed to be performed on three experimental test facilities: 1) Argonne 1/2 scale, 2) UW 1/4 scale, and 3) KAERI 1/4 scale. A high-level summary detailing the major differences provided in Table 41. All test facilities were based on the air-cooled RCCS design for the GA-MHTGR, however the KAERI facility used a PMR200 as their full scale RPV reference and thus used a different basis for determining their normal testing conditions [43].

Table 41: Summary of scale test facilities at collaborating institutions

		Argonne	KAERI	UW
Facility Name	-	NSTF	NACEF	-
Scale	-	1/2	1/4	1/4
Design Basis	-	GA-MHTGR	PMR200	GA-MHTGR
Heated surface type	-	Heaters + Plate	Heaters + Plate	Heaters only
Total riser height	m	7.2	4.5	3.76
Heated length of riser	m	6.82	4.05	3.51
Number ducts	#	12	6	6
Heated area	m ²	8.820	2.600	3.030

Earlier numerical work performed by KAERI suggested that the Planck number, a dimensionless group describing the ratio of radiation to conduction, dominates heat transfer in the reactor cavity, while the Richardson number dominates the modes of heat transfer within the risers. Preservation of the Richardson number was the basis for integral scaling of the NSTF, a scaling decision that favored heat transfer within the risers. Given that scaling distortions are unavoidable, e.g. the Richardson approach does not consider radiation within the cavity, it is of significant interest to perform experimental studies of the alternative philosophies. To compare and examine the differences in these two approaches, a test series was drafted in collaboration between KAERI, Argonne, and UW. The series was split into two parts, the first, ‘Case I’, preserves the Richardson number ($Ri_R = 1.0$), while

the second, ‘Case II’, preserves the heat flux ($q''_R = 1.0$). A table summarizing the target steady-state operating conditions is provided below in Table 42.

Table 42: Target testing conditions, INERI testing series Case I and Case II

		Reference	Case 1, $Ri_R = 1$			Case 2, $q''_1 = 1$		
Facility	-	PMR200	ANL	KAERI	UW	ANL	KAERI	UW
Scale	-	1	1/2	1/4	1/4	1/2	1/4	1/4
No. Risers	#	220	12	6	6	12	6	6
Flow rate, system	kg/s	10.39	0.359	0.138	0.129	0.227	0.067	0.058
Heated ΔT	$^{\circ}C$	98.0	98.0	98.0	98.0	98.0	98.0	98.0
Q, system	kW_t	1,027	35.47	16.67	12.72	22.47	6.67	5.78

The test cases, as performed on the NSTF, were completed as part of DataQuality023. The operating window for active test operations (powered heaters) began at 14h04 on February 15th 2016 and spanned a period of 191 hours and 19 minutes. The facility was configured for a forced flow configuration, which utilized exhaust flow out of the horizontal lofts and use of the forced fan blowers. Natural flow would have exceeded the target values for system flow rate, thus additional resistance was required along the system ductwork. This was accomplished by dampening the valves after the outlet plenum and immediately prior to the fan lofts. Two steady-state periods were maintained for the I-NERI objectives, the first at Case I conditions, and the second at Case II conditions. A summary of measured parameters during the steady-state, along with their difference from the target values, is provided in Table 43. With completion of post-test data verification procedures and review of generated data sets, the test was successfully able to meet acceptance criteria for both I-NERI cases.

The testing procedure specified an initial guess at the necessary electric power to obtain the desired thermal power. Based on characteristic NSTF performance from earlier testing, it was assumed that approximately 65% efficiency could be expected. For Case I, this prescribed initial estimates of 34.17 kW_e to obtain 22.2 kW_t , and for Case II initial estimates of 52.49 kW_e to obtain 34.1 kW_t . However, difficulties were encountered while attempting to meet the dual requirements for system flow rate and heated section temperature rise. Ultimately, only

Table 43: Acceptance criteria and results for INERI test cases, Run023

		Case 1, $Ri_R = 1.0$			Case 2, $q''_R = 1.0$		
		Planned	Actual	% diff.	Planned	Actual	% diff.
Run Time	hr	-	83 - 89	-	-	58 - 64	-
Electric Power	kW_e	-	65.99	-	-	51.99	-
Riser Inlet	$^{\circ}\text{C}$	-	22.32	-	-	17.61	-
Riser Outlet	$^{\circ}\text{C}$	-	114.55	-	-	93.34	-
Chimney Inlet	$^{\circ}\text{C}$	-	116.68	-	-	114.82	-
Flow Rate	kg/min	21.52	21.50	0.09%	13.63	13.60	0.25%
Thermal Power	kW_t	35.47	34.12	3.79%	22.47	22.21	0.82%
ΔT	$^{\circ}\text{C}$	98.0	94.36	3.90%	98.0	97.2	1.28%

42.7% efficiency was achieved during Case II, while 52% was archived during Case I. This low thermal efficiency stem from the significantly reduced system flow rates and elevated system temperatures and subsequent increased heat loss, but also due to degraded heat transfer within the riser ducts. LUNA fibers installed at the outlet face of the risers provide insight into the temperature profile, Figure 94. Visible is the flattened temperature gradient along the core of the risers, along with sharp rises near the wall of Case II. The references cases, including Case I and baseline cases, exhibit a more gradual gradient that follows a relatively smooth transition from the core to the walls.

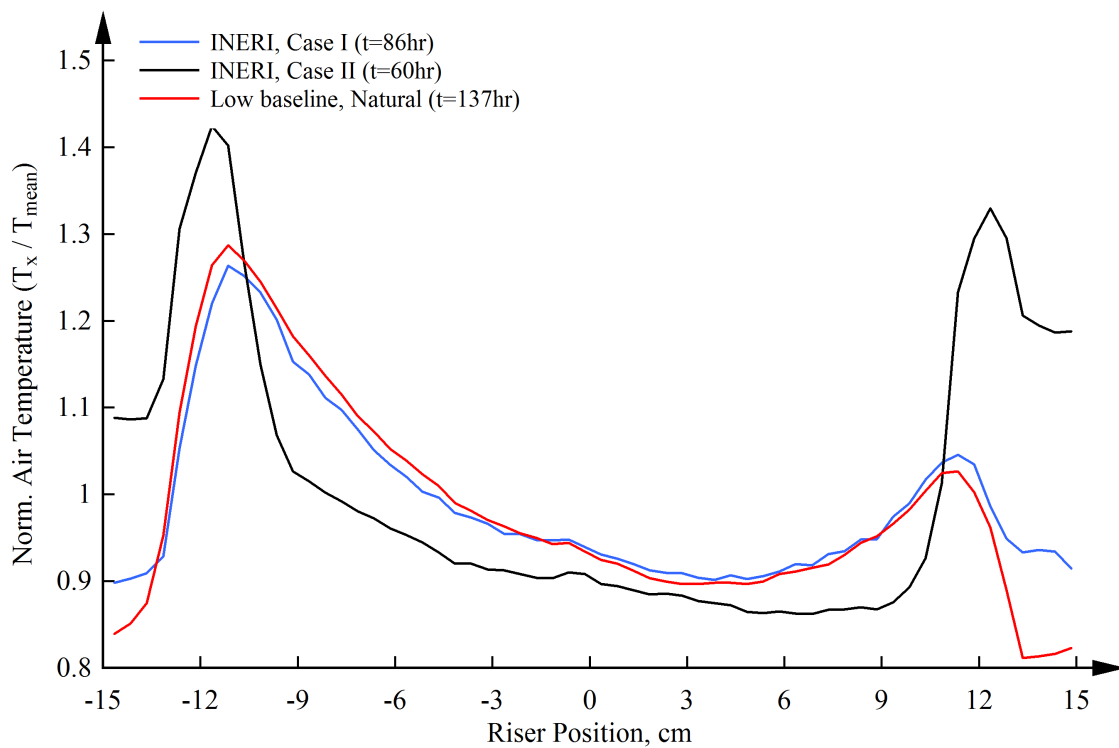


Figure 94: Temperature profile across outlet face of riser ducts, LUNA fibers

7.4 Off-normal Scenarios

7.4.1 Blocked Riser Channels - Run015

The following provides a summary of the operating parameters and test conditions of NSTF's Run015. The test objective was to examine system response and heat removal performance with blocked riser channels. The test began by establishing steady-state at the normal operating heat load, which defines a full scale power of 700 kW_t , or 26.16 kW_t in the $1/2$ scale NSTF. Then, three stages of degraded operation were initiated at 16.6%, 33.3%, and 50% blockage, which were accomplished by physically closing 2, 4, and 6 riser channels, respectively. The closures were done via mechanical flaps positioned at the inlet of each riser. The four stages are visually depicted in Figure 95, and the physical means for achieving the blockages is shown in Figure 96.

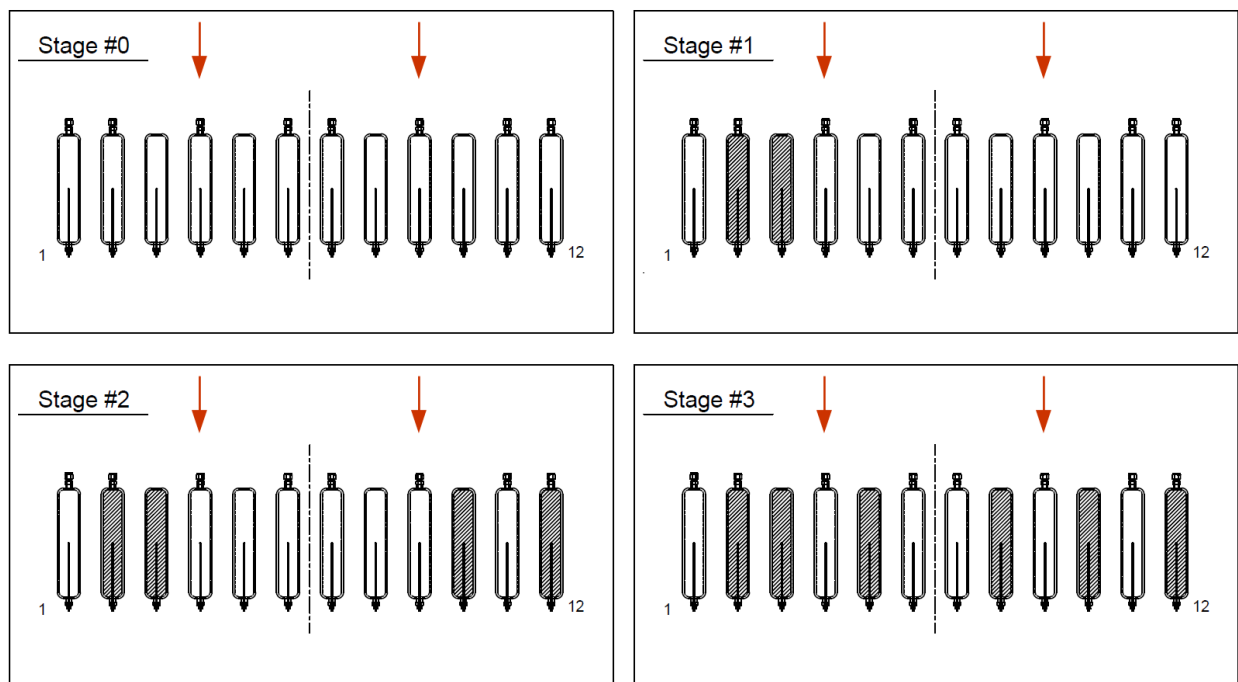


Figure 95: Four stages of riser blockages during Run015, red arrows indicate heated surface



Figure 96: Closure flaps used to remotely actuate a riser blockage

Each stage was allowed to reach stable, steady-state flow conditions for a minimum period of 6 hours. Time averaged values over these 6 hours were then used to meet established acceptance criteria, which defined system parameters that did not vary more than 5% over the 6 hour period. A dated log of the primary procedural test events is provided below in Table 44. No unusual or unplanned events occurred throughout the duration of the test. Acceptance criteria were established for each of the four steady state periods: full open, 2 risers blocked, 4 risers blocked, and 6 riser blocked. These criteria were verified with observations of live test data by the test operator (later confirmed by raw data processing), which showed a stable thermal energy balance within the heated test section for a period that did not change more than $\pm 5\%$ over a 6 hour window. A summary is provided in Table 45. The results are also shown as trends for the response of the system flow rate, both absolute as a function in time, Figure 97, and per step change, or percent change from one stage to the next, Figure 98. With completion of post-test data verification procedures and review of generated data sets, the test was found to be fully within the defined scope and set of procedures and thus is classified as successful.

While the total system flow rate was dramatically reduced at each stage, the facility's performance remained robust and continued to perform its heat removal function well. The heated plate temperature, simulating the walls of a RPV, averaged 279 °C for the normal, fully open operation, and only increased to 282, 288, and 292 °C at each respective stage. These minor rises in RPV temperature suggest high confidence in the system's ability to maintain high heat removal performance even in the event of blocked riser channels.

Table 44: Test log for Run015 - Performance testing with block riser tubes

Date	Time	Action
5/19/2015	10h32	Zero flow verification, saved LabVIEW acquisition
5/19/2015	10h48	LUNA baseline calibration, saved LabVIEW acquisition
5/19/2015	10h55	Began data logging on LabVIEW, start of test operations
5/19/2015	11h00 - 13h00	Power ramp from 0 to 42.00 kW _e
5/20/2015	13h43	Closure of Risers #2 & #3
5/21/2015	09h46	Closure of Risers #10 & #12
5/22/2015	09h02	Closure of Risers #5 & #8
5/22/2015	18h55 - 21h25	Power ramp from 42.00 to 0 kW _e
5/22/2015	21h48	Test conclusion, $t_{total} = 82.88$ hr

Table 45: Acceptance criteria and system parameter summary over four stages in Run015

	Stage #0	Stage #1	Stage #2	Stage #3
Riser Blockage, %	0%	16.60%	33.30%	50%
Risers Blocked	-	2,3	(2,3) + 10,12	(2,3,10,12) + 5,8
Span, run time hr	20 - 26	32 - 46	52 - 65	74 - 80
Electric power, kW _e	42	42	41.99	42
Test sect. power, kW _t	24.78	26.68	26.16	25.17
Sys. flow rate, kg/s	0.459	0.42	0.342	0.287
Riser ΔT , °C	53.6	54.92	59.41	63.49
Front heated plate, °C	278.93	282.32	288.17	291.96
Ceramic heaters, °C	405.96	408.27	412.34	414.88

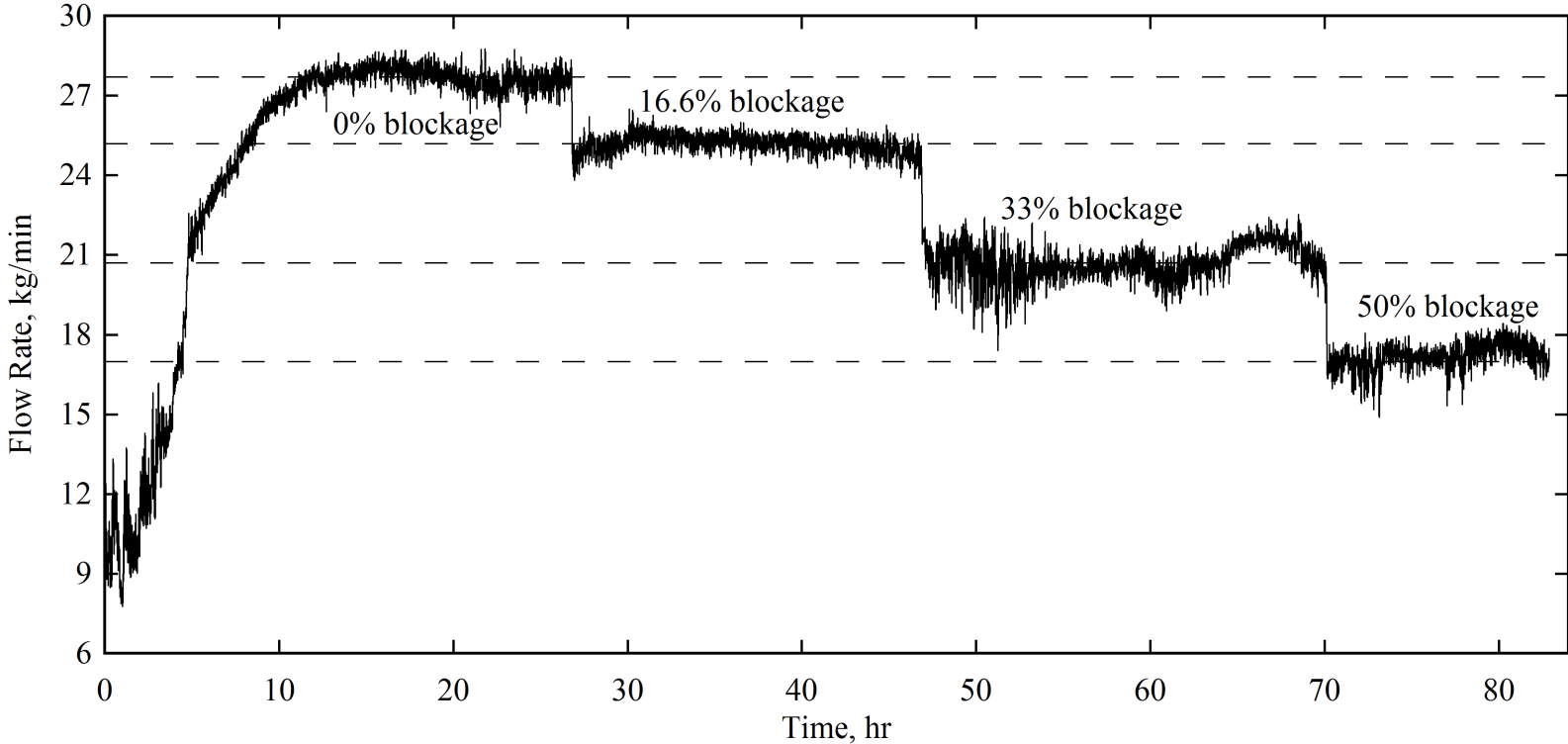


Figure 97: Time history of system flow rate with various blockage stages indicated

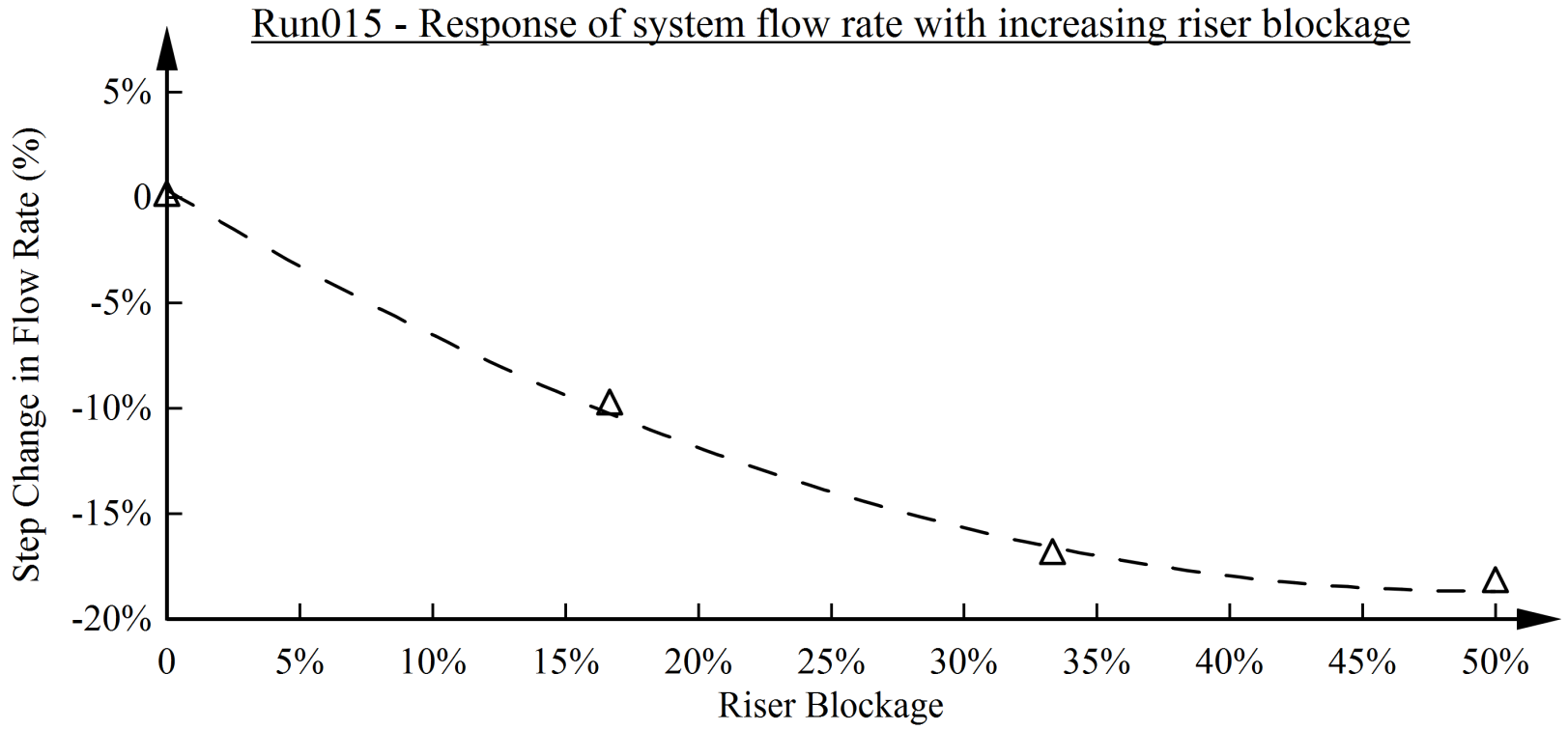


Figure 98: Step change in flow rate as a function of riser blockage

7.4.2 Heavy-gas Ingress - Run027

One hypothetical accident scenario is the ingress of a non-air gas into an operating RCCS. Such an event must be considered given the proximity of planned HTGR installations to chemical processing plants. To examine the performance of an RCCS under such a scenario, a test was devised and performed with the NSTF at Argonne. The objective of this test was to first establish steady-state, normal operating conditions in the NSTF with air and then introduce a transition of the inlet gas from air to a non-air gas, while observing the impact on the system behavior.

Carbon dioxide (CO₂) was initially proposed as a candidate for the non-air gas, however dangers of hypercapnia posed an unnecessary risk to involved personnel and ultimately argon was selected for use during the test. The risk of asphyxiation was still present however, and required laboratory specific attention to safety and oxygen monitoring, which were addressed by a revision to the projects WPC for testing operations.

The acceptance criteria defined by the testing team, established prior to testing execution, defined a minimum available gas volume of 1,000 cu-ft, at an average bulk concentration of less than 1% oxygen (95+% argon). A comparison of physical properties between ultra-high purity argon (the gas used for the NSTF testing) and dry air, at both STP (0 °C and 101.325 kPa) and elevated temperatures (100 °C, 101.325 kPa) is provided below in Tables 46 and 47, respectively.

Table 46: Physical Properties of Dry Air and Argon at STP (0 °C, 101.325 kPa)

			Air (dry)	Argon	% <i>diff.</i>
Ar	Molecular weight	g/mol	28.970	39.948	31.9%
ρ	Density	kg/m ³	1.292	1.784	31.9%
C_p	Heat capacity	kJ/kg-K	1.005	0.522	63.3%
k	Thermal conductivity	W/m-K	0.024	0.016	38.6%
Pr	Prandtl	-	0.711	0.665	6.7%
μ	Dynamic viscosity	10 ⁶ Ns/m ²	17.220	21.020	19.9%

Table 47: Physical Properties of Elevated Temperature Dry Air and Argon

			Air (dry)			Argon		
			0 °C	100 °C	<i>change</i>	0 °C	100 °C	<i>% change</i>
Ar	Molecular weight	g/mol	28.970	28.970	0.0%	39.948	39.948	0.0%
ρ	Density	kg/m ³	1.292	0.946	-26.8%	1.784	1.305	-26.8%
Cp	Heat capacity	kJ/kg-K	1.005	1.012	0.7%	0.522	0.521	-0.2%
k	Thermal conduct.	W/m-K	0.024	0.032	29.8%	0.016	0.021	29.3%
Pr	Prandtl	-	0.711	0.701	-1.5%	0.665	0.664	-0.2%
μ	Dynamic viscosity	10 ⁶ Ns/m ²	17.220	21.900	27.2%	21.020	27.170	29.3%

Gas Enclosure Design

A successful execution of the proposed testing plan required unique considerations to ensure the introduction of only a single variable: gas composition. Due to the sensitivity of natural circulation systems, changes in parameters such as pressure, temperature, geometry, among others, would introduce unwanted influences that would reduce the clarity of the observed behavior and confidence in the results. Thus, significant attention was given to the design of the apparatus and procedure of the transition sequence. An enclosure was constructed on the Bldg. 308 floor, directly above the downcomer inlet of the NSTF, that had the following features:

1. Contained a non-air gas volume of approximately 1,000 cu-ft
2. Ability to operate in ‘air by-pass’ and ‘argon ingress’ modes
3. Identical inlet flow areas for both modes
4. Transition between modes would not, even in a transient, cut-off air or gas flow

The enclosure itself measured 7x10x15 feet, and was constructed from a uni-strut frame and wrapped in two-layers of 6-mil (0.006-inch), moisture-resistance low-density polyethylene (LDPE) film. A normal-operation air duct (24-inch diameter) was positioned within the center of the enclosure, while four by-pass valves (12-inch diameter each) were positioned at each of the four top corners. The 24-inch air-duct featured a mating seal at the base of the enclosure, and under normal-operation allowed the NSTF to draw in fresh ambient air without introducing argon into the facility. During the transition sequence, the four

by-pass valves were first fully opened, then the 24-inch mating seal was broken by lifting the internal ductwork, allowing the quiescent argon to be entrained into the inlet downcomer of the NSTF. The transition sequence was actuated remotely and required approximately 30 seconds for the valves to fully open and seal to be broken.

Additional instrumentation included five oxygen sensors, two mounted within the enclosure, and three within the inlet plenum of the NSTF. The 20.3-mm sensors operate through an electrochemical, galvanic cell and exhibit low consumption, high sensitivity performance for detecting concentrations of oxygen in air. The sensors generate a current (μA) that is linearly proportional to the ambient oxygen concentration. This current can be measured by placing a load resistor between the cathode and the anode and measuring the resultant voltage drop. A description of each is provided below by Table 48, installation locations provided by Table 49. Oxygen sensors within the enclosure featured co-located thermocouples, 1/16-inch diameter of type-K.

Table 48: Oxygen Sensor Specifications

	Output μA , 20.9%O ₂	Response time t_{90} (s), 20.9-0% O ₂	Zero current μA in N ₂	Linearity % O ₂ deviation
O2-A1	200-240	< 15	< 2.5	< 0.6
O2-A2	80-120	< 15	< 2.5	0.6
ME2-O2	250	< 30	< 2	< 2

Table 49: Installed Oxygen Sensors

Sensor Type	ID	Location
AS O2-A1	1	Argon enclosure, 24-inch above base
AS O2-A1	2	Argon enclosure, 24-inch below top
W ME2-O2	3	Inlet plenum, base of 24-inch inlet duct
AS O2-A2	4	Inlet plenum, top of 24-inch inlet duct
AS O2-A2	5	Riser face plane, between risers #6 and #7

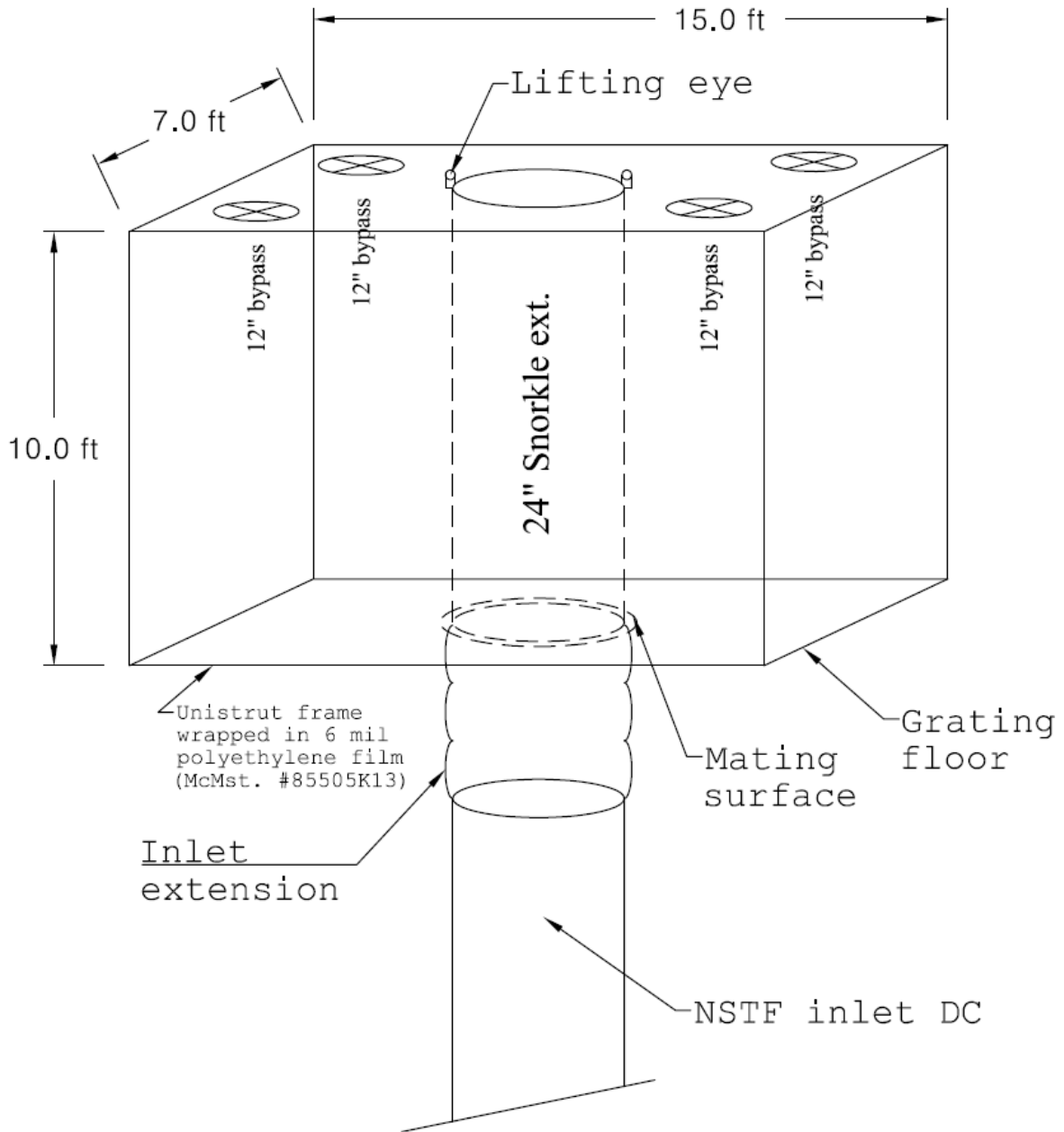


Figure 99: Diagram of argon-enclosure, positioned on Bldg. 308 floor above inlet

Gas Ingress Procedure

The NSTF was configured in a single-chimney flow path for the testing procedure, containing an internal volume for gas flow of approximately 587 cu-feet. Based on the gas enclosure dimensions, nearly two full volume cycles would be required to fully deplete the argon gas from the enclosure and reject it to the outside atmosphere. With an anticipated steady-state flow rate of 0.375 kg/s, 135 seconds would be required to clear the NSTF flow path of argon before returning to draw ambient air.

Filling the enclosure with argon was performed in a two-step process. The first consisted of collapsing the enclosure walls to reduce the overall internal volume, venting the four by-pass valves, then performing a low flow rate fill (30 CFH or 0.3 m/hr argon rise rate) over the course of 48 hours. This low-flow purge process, termed an ‘argon piston purge’ [36] minimized mixing of gases by maintaining a laminar boundary layer between the ambient air and newly introduced argon. The second step in the fill process then closed the four by-pass valves, and filled the enclosure at a higher rate of argon (200+CFH) while allowing the enclosure walls to bow out to accommodate the introduction of the additional argon. Ultra-high purity grade argon from a 160-L dewar was used, with the final gas composition of the 1,200 cu-foot enclosure immediately prior to the transition sequence recorded at <0.4% oxygen and >98% argon.

Upon meeting acceptance criteria for both oxygen concentration within the enclosure and steady-state operation of the test facility, see Table 50, the ingress sequence was initiated. This sequence, shown in Figure 100, was performed in two stages: the first was to fully open the four by-pass vent valves, visually verifying their position, then the second was to use the overhead crane to lift the 24-inch snorkel extension. Upon lifting the extension duct, the NSTF was allowed to respond without additional operation influence for a minimum period of 90 minutes.

Table 50: Measurement values used for acceptance criteria during Run027 prior to injection

		mean	% change
Electric Power	kW_e	41.99	0.02%
Heated Plate	$^{\circ}\text{C}$	407.25	0.87%
Riser Wall	$^{\circ}\text{C}$	118.98	3.01%
Chimney Inlet	$^{\circ}\text{C}$	87.29	2.90%
Flow Rate	kg/min	23.86	3.25%
Heated ΔT	$^{\circ}\text{C}$	57.44	3.57%
Thermal Power	kW_t	23.04	1.97%

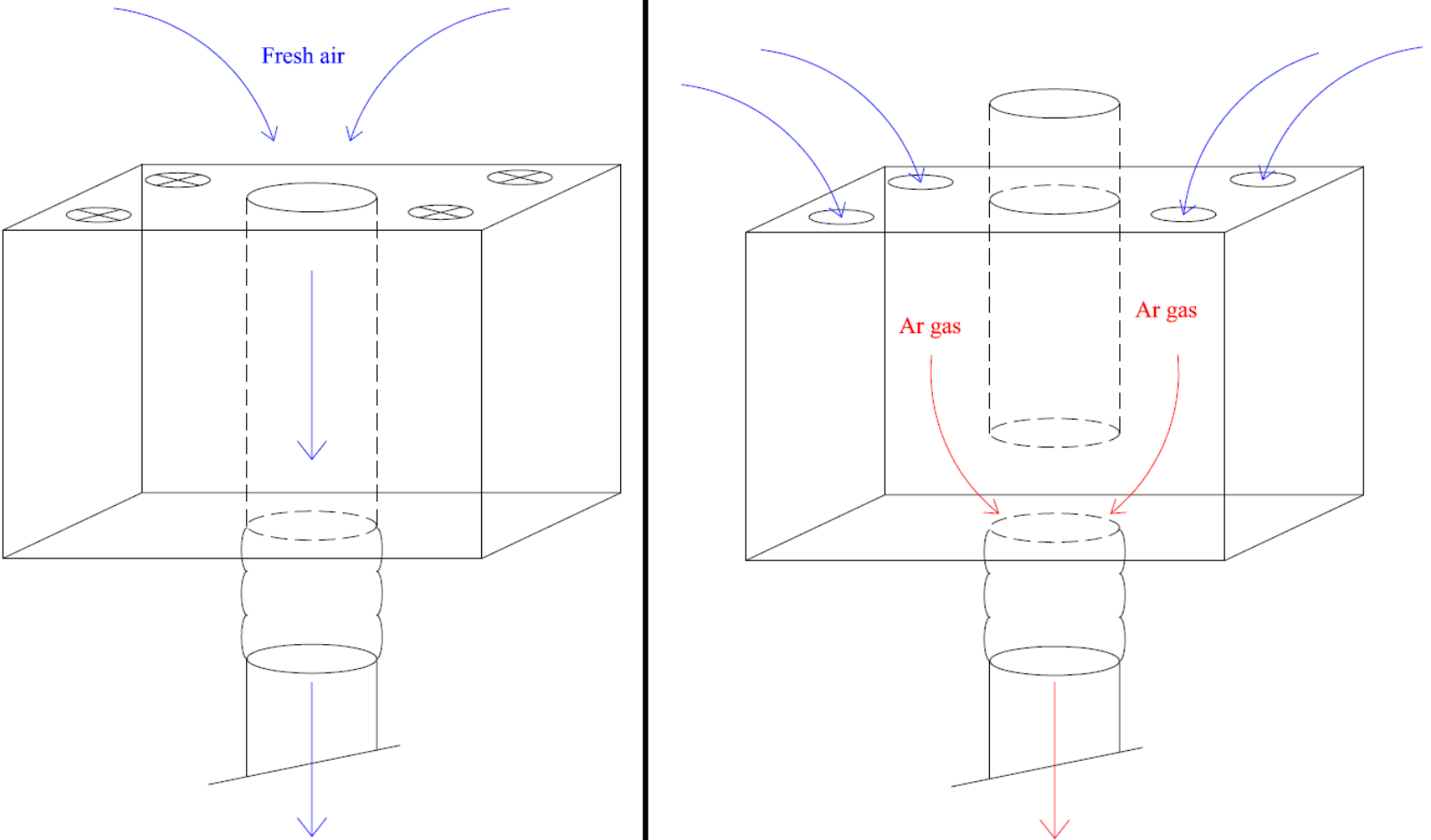


Figure 100: Operation of heavy-gas enclosure: normal air draw, argon by-pass



Figure 101: Argon enclosure constructed above downcomer inlet



Figure 103: Top view of argon enclosure



Figure 102: Extension from argon enclosure to inlet

Ingress Test Results

The ingress sequence of opening the valves spanned a period of approximately 45 seconds, after which point gas sensors within the inlet plenum began to measure reduced oxygen levels. Within a period of 2 seconds, oxygen concentrations within the inlet plenum fell to 11%, and after 6 seconds down to 1.8%, Figure 104. The response of the NSTF was immediately observed by a sharp reduction in the system flow rate, eventually leading to total flow stagnation after a period of only 90 seconds. Other system parameters saw immediate responses as well, including the riser outlet gas temperatures which sharply increased from the previous steady-state value of 91.3 °C to 126.2 °C. After approximately 7 minutes, a unique flow pattern developed within the riser ducts which resulted the first ever observed flow re-circulation within the riser tubes. A downward flow along the northern bank of risers was observed based on trends of the inlet and outlet gas temperatures within the risers, Figure 105.

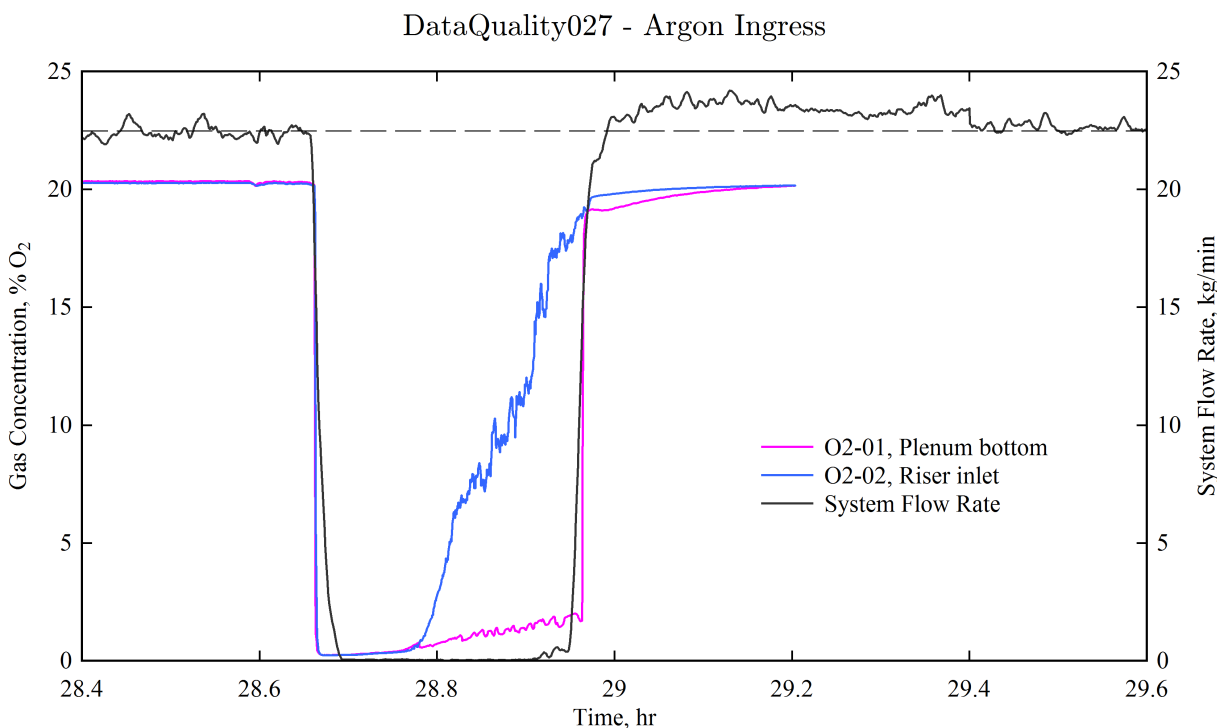


Figure 104: Gas sensor oxygen value and system flow rate, DataQuality027

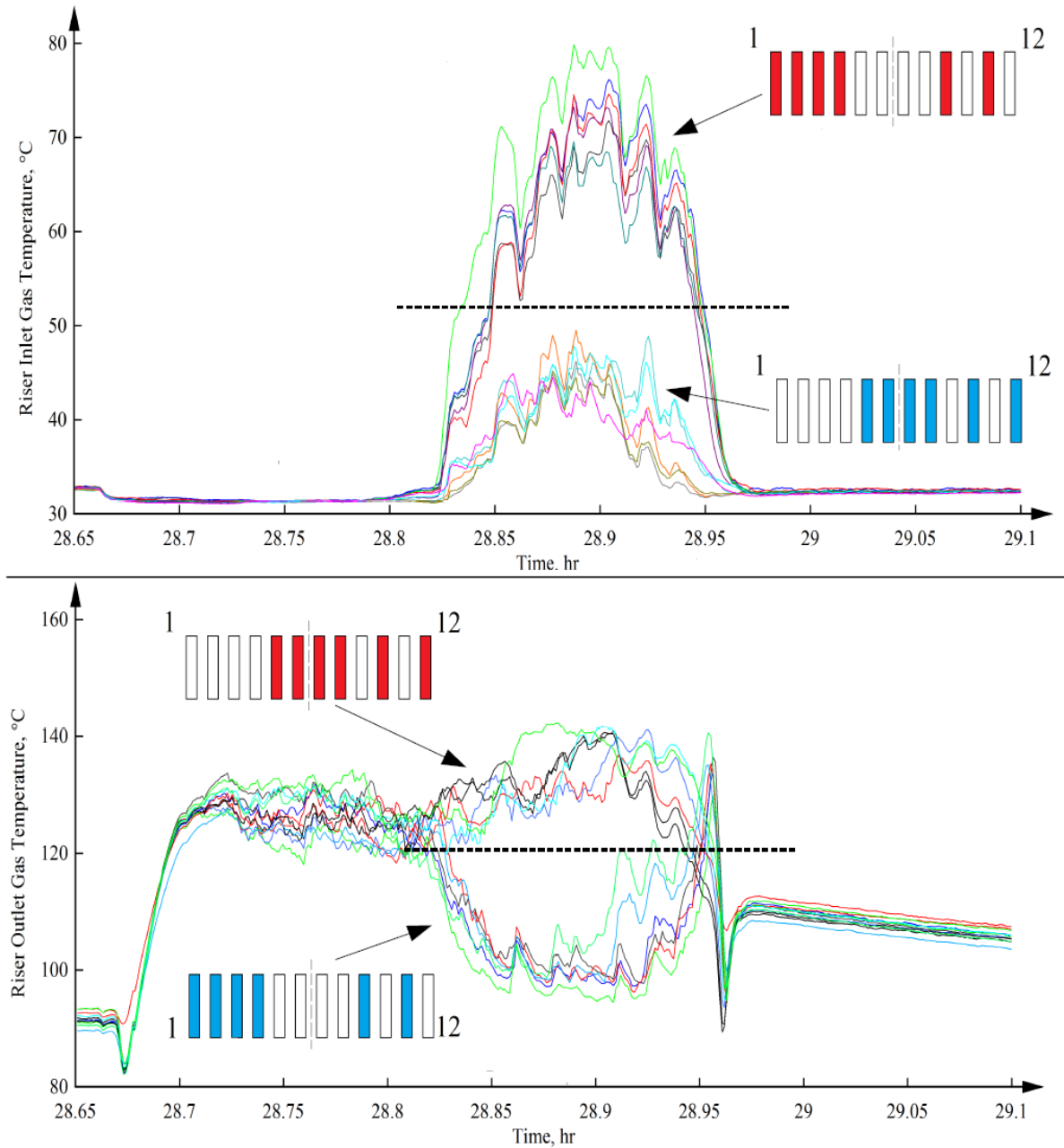


Figure 105: Riser inlet (top) and outlet (bottom) temperatures after argon ingress, DataQuality027. Riser plan view shading corresponds to thermocouple grouping

The unique flow re-circulation patterns, which occurred approximately 7 minutes after the starting sequence, provided a first indication of system recovery based on the measured oxygen levels at the inlet of the risers. While the overall system flow rate remained stagnant, the oxygen levels measured at this location showed a gradual rise from a concentration of 0.42% O₂ at 7 minutes to 18.5% O₂ at 16.5 minutes. It was at this time that the first change in flow rates was observed, which followed a sharp rise from the previous stagnant levels to previous non-argon ingress values, and was followed shortly by a rise in overall inlet plenum oxygen levels. A summary of the quasi-steady state measured values at 30 minutes prior to, during, and 30 minutes post injection sequence, is provided in Table 51.

Table 51: Before, During, and After Injection quasi-steady-state values, Run027

		30 min Prior 28-28.5hr	Injection 28.7-28.9hr	30 min Post 29-29.5hr
Electric Power	kW _e	41.99	41.98	41.98
Heated Plate	°C	284.95	285.70	288.85
Riser Wall	°C	123.31	129.91	129.95
Chimney Inlet	°C	91.19	90.57	96.40
Flow Rate	kg/min	22.51	0.04	22.94
Heated ΔT	°C	58.95	59.23	63.14
Thermal Power	kW _t	22.31	0.05	24.36

Ingress Discussion

Upon initiation of the ingress sequence, the pocket of argon traveled down and settled in the inlet plenum while the risers and chimney remained filled with normal air. The density difference between the heated air in the chimney and cool argon at the inlet was insufficient to maintain a natural circulation flow pattern and disrupted the system flow. As the existing, stagnant air within the heated region of the test section began to reach elevated temperatures, the driving head was increased and began to pull part of the quiescent argon from within the inlet plenum up into the risers. This newly introduced argon was gradually heated by the high temperature riser walls, but at a degraded rate due to the lower specific heat capacity and

thermal conductivity of the argon (compared to dry air). Eventually, the argon was heated to a point where the density was reduced sufficiently such that the natural circulation flow was re-established and the performance of the NSTF was recovered.

A direct correlation was observed between the measured oxygen concentration and the degraded performance of the NSTF, the latter of which was best represented by a reduced system flow rate. Furthermore, the reduction in system flow rate behaved in a binary fashion, by either full stagnation with near-zero flow rates, or normal operation with regular steady-state levels of system flow. Thus it can be deduced that the volume of argon gas was drawn through the NSTF without significant mixing and traveled as a homogeneous pocket of gas. This behavior was intended during the design of the testing procedure and represents a worst-case scenario of ingress of a high purity non-air gas into the facility. However, it did not allow for the study of a mixed concentration gas, which remains an area of significant interest and suggested future work.

The recovery by the NSTF directly coincided with the depletion of the argon gas within enclosure, thus the test was unable to create conditions with measured system flow and ductwork filled with argon. Thus, the question of if recovery was only achieved after depleting argon, or if recovery would have occurred regardless, remains unanswered.

Ingress Repeatability

The facility was allowed a 24-hour recovery period, at which time the transition procedure was repeated with air. The purpose of this test was to verify that the mechanical actions and testing procedure did not influence the behavior observed during the argon ingress test, ensuring confidence that the influence was solely due to gas composition. As with the argon fill, the enclosure was reset and filled with standard compressed air. The results, shown below in Figure 106, confirm that the NSTF remained unaffected by any mechanical or procedural influences due to the gas enclosure, and the previously observed response was solely due to gas composition.

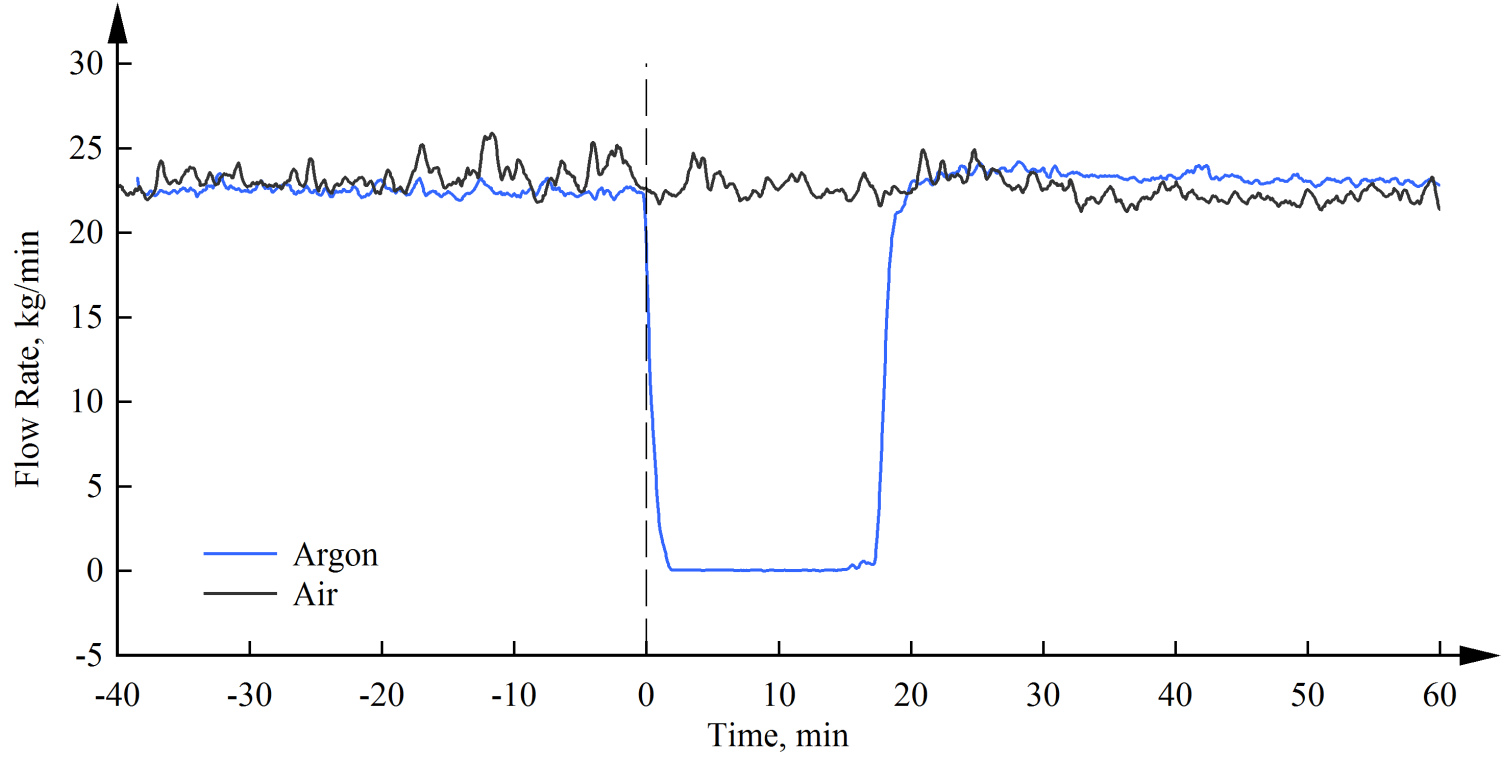


Figure 106: Comparison of identical transition sequence procedure, argon and air gas compositions

7.5 Meteorological Influences

The influence of weather played a major factor in defining behavior during active testing and, in extreme cases, critically impaired the heat removal performance. A number of runs experienced total disruption and inability to meet target objectives, either during steady-state periods or while attempting start-up of natural circulation flow. Other, milder influences, included perturbing the symmetry of the exhaust flow, difficulty in achieving ideal repeatability, and localized fluctuations in system behavior.

The natural draft of air was continuously observed before power was turned on in NSTF experiments. The natural ventilation by air inflow and outflow depends on the size and location of all air leakage sites on the building envelope and the indoor-outdoor pressure difference across each of these sites. These pressure differences are the result of a non-linear interaction between wind pressures on the exterior of the building and stack effect pressures caused by the density difference between indoor and outdoor air. The independent wind and stack effects would naturally interact to set the building indoor pressure that maintains a balance between the overall inflow and outflow mass flow rates across the building envelope.

The wind would also affect the air infiltration dependent on leakage distribution, pressure coefficients, and inflow and outflow balance. In general, wind flowing over the top of a chimney can increase draft by producing a driving pressure that assists in pulling air from the chimney. However, under different geometric configurations and wind directions, the wind can be adverse to the chimney upward flow by creating positive pressure at the top of the chimney. The wind blowing around a building produces a positive pressure zone on the windward side and a negative pressure zone on the downwind side. These pressures act on the leaks in the building envelope, causing airflow through them and changing the pressures within the building. Assuming the largest leakage path of the Building 308 is through the NSTF chimney outlet, the wind would always enhance the flow in NSTF tests.

Variations in system performance can also be partially attributed to changes in the build-

ing temperature. This effect can be described as follows: the driving pressure head of a natural circulation system is highly dependent on the density difference between the cold and hot segments. Given the non-linear relationship between density and temperature for an ideal air gas, Figure 107, the absolute inlet temperature plays a role, even for two systems with identical temperature differences. With higher absolute inlet temperatures, the $\Delta\rho / \Delta T$ is reduced, which lowered the driving pressure head and reduced the overall efficiency of the stack effect.

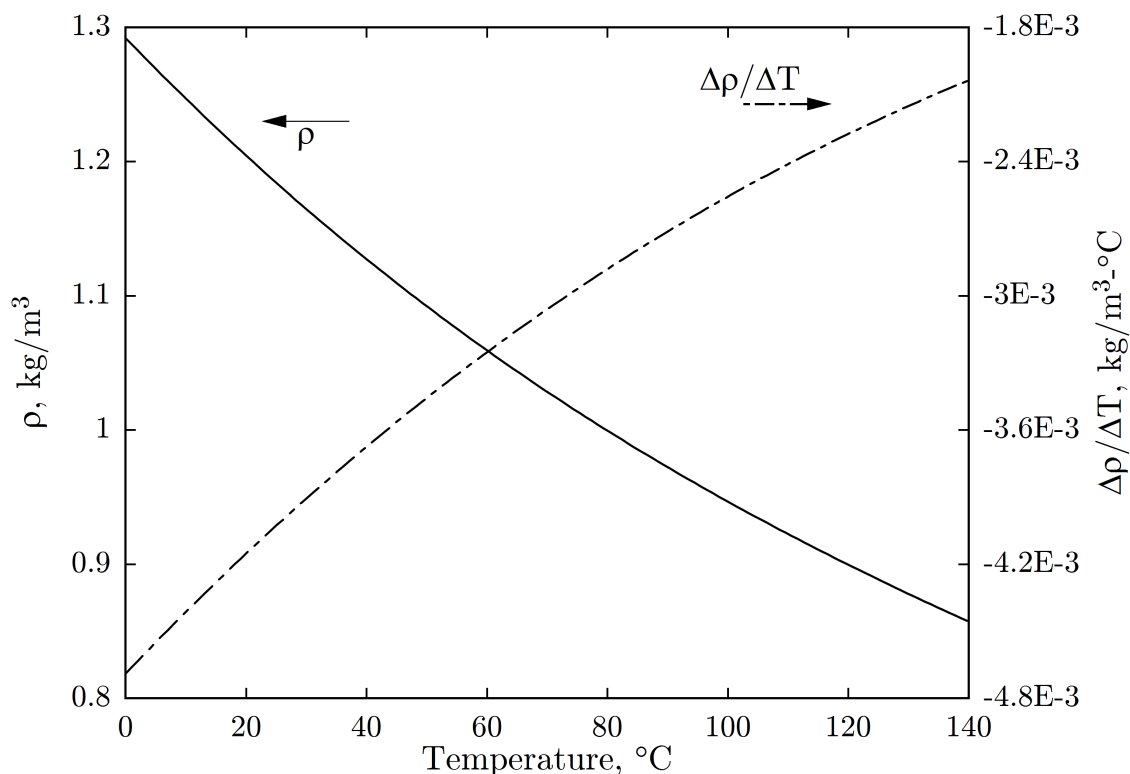


Figure 107: Density and temperature relationship for elevated air temperatures

Thus, with elevated downcomer inlet temperatures causing a reduction in the driving head, the mass flow rate is reduced, and to maintain equal thermal powers, all of system parameters shift. Specifically, the air temperature rise increases, absolute gas temperature increases, frictional pressure drop decreases, etc. The inlet temperature effect can be easily captured by applying realistic air property models in the computational models.

7.5.1 Start-up Sensitivity - Run016

While testing the facility in the adjacent chimney configuration, two attempts were required to successfully complete the test objectives and meet acceptance criteria. This facility configuration, unlike the baseline, featured an inlet that was not shielded by the building and instead fully exposed to the outdoor weather. This created a heightened sensitivity to meteorological conditions, and furthermore, challenged efforts to start the facility and establish as-intended natural circulation flow.

Beginning at 12h00 on July 22nd, an attempt was made to perform a data-quality test in the adjacent chimney configuration. While the winds were relatively calm early in the afternoon, they gradually increased throughout the day and eventually reached a 6 m/s average that extended through the early evening. Combined with periodic gusts, the NSTF was challenged in establishing the as-intended flow path. These occasional perturbations induced system wide oscillations with reverse flow transients that discharged heated air from the inlet of the heated test section. By 17h00, these oscillations sent high temperature air (58 °C observed) into the inlet plenum, Figure 108, and emergency procedures were enacted to protect the sensitive instrumentation. The impact of these wind related perturbations has profound effects on the heat removal performance. When compared against the subsequent attempt that was successful, Run017, elevated component temperatures of the riser duct walls and mock RPV surface were observed. A figure of the duct wall temperature with comparison to a successful repeat highlights the degraded performance, Figure 109. Emergency procedures were enacted by enabling the forced loft blowers near the 6-hour testing mark.

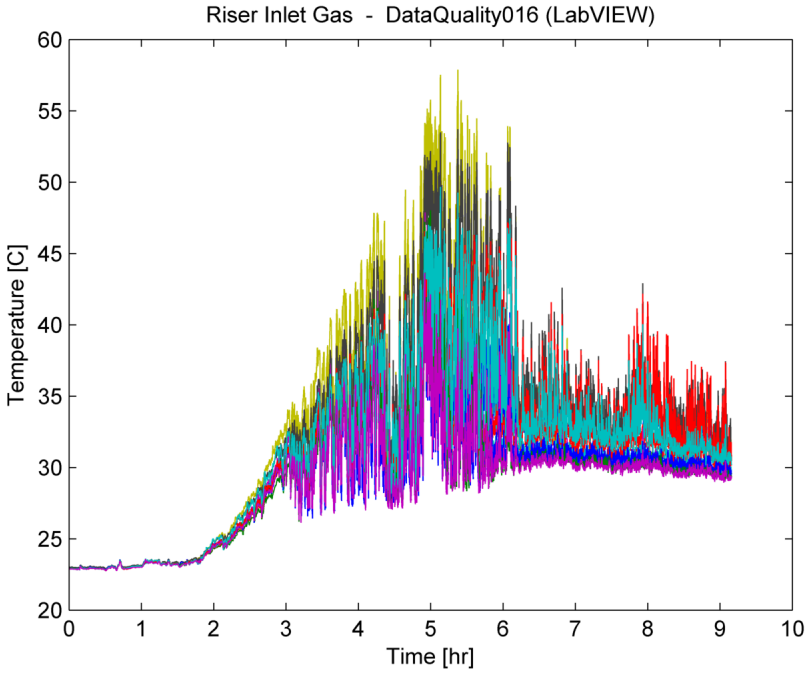


Figure 108: System wide reverse flow observed during failed Run016 created dangerous temperatures at inlet

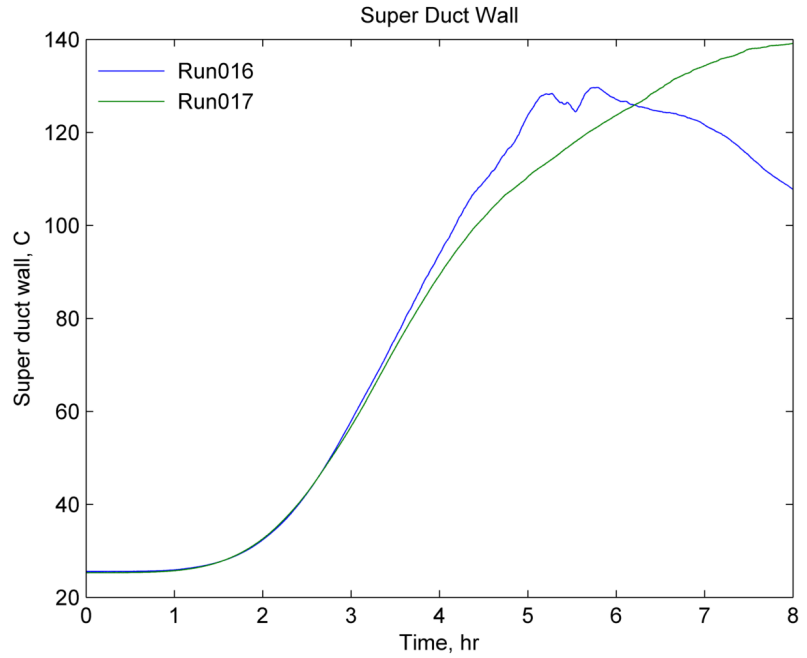


Figure 109: Impact extended into overall system and caused degraded heat removal and elevated temperatures

7.5.2 Wind Gusts

A unique event occurred during the cool-down period of DataQuality018, the summer investigations of the GA-MHTGR accident scenario. During the power down process, an approaching storm created an extreme change in ambient conditions. From a calm 3 m/s average wind speed, an approach of the storm gave way to sudden gusts exceeding 21 m/s. The transient impact onto the NSTF was profound, and saw dramatic perturbations onto all system parameters, Figure 110. Furthermore, the coming storm could be first observed by a drop in ambient temperatures, which were reflected along the chimney stack wall thermocouples, as shown shortly after hour 129 in Figures 111 and 112. The wind speed then hit the building near hour 128.4, which perturbed the system flow rate first and then the system temperatures. The storm quickly passed and the system returned to its normal operating state.

It is important to note that the gusts observed in this instance originated from the western direction (i.e. the wind blew from the west to the east). Thus, the winds impacted both chimneys uniformly and did not preferentially influence a single chimney. Had the wind gusts originated from a northern or southern direction, the result would have likely created flow asymmetries in the test facility.

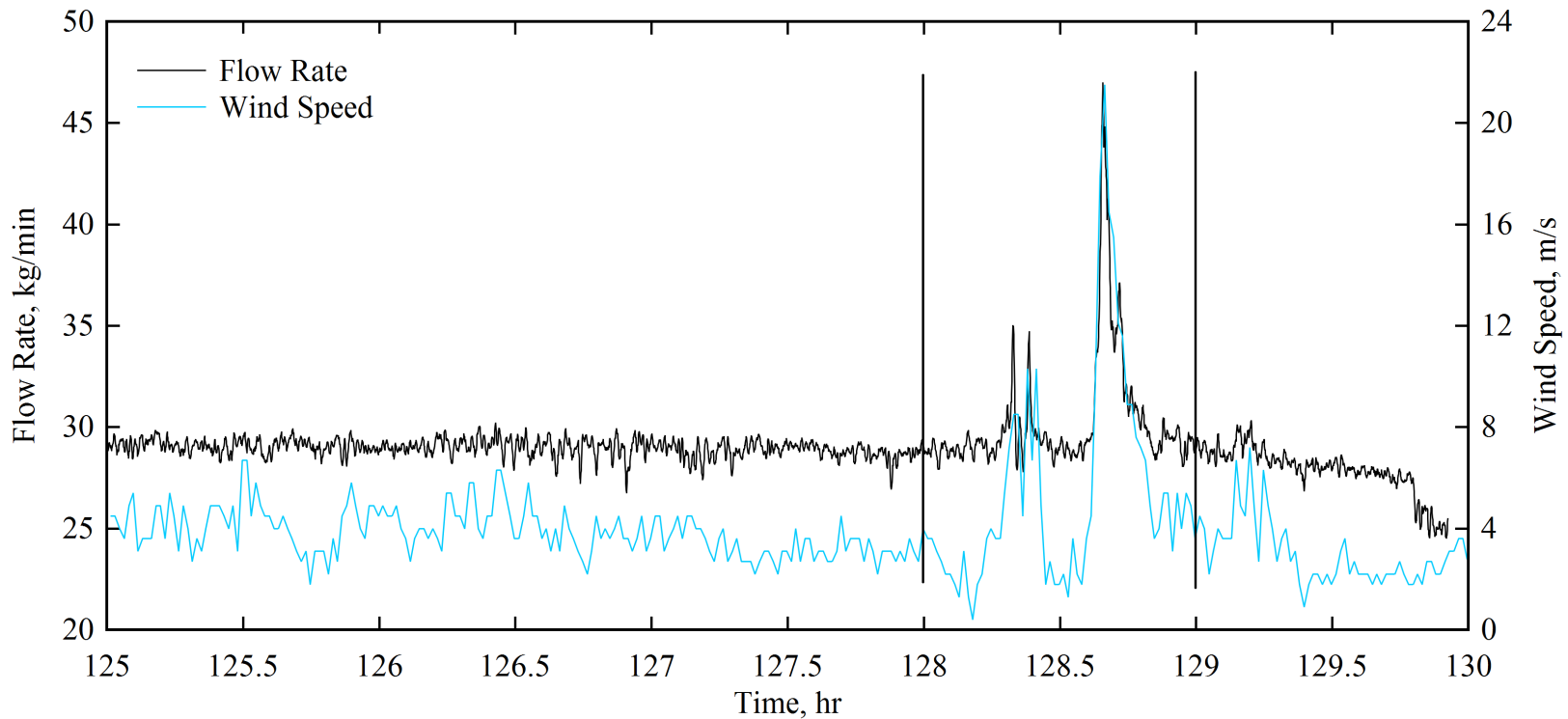


Figure 110: Impact on otherwise calm cool-down period after Run018 from a sudden wind gust

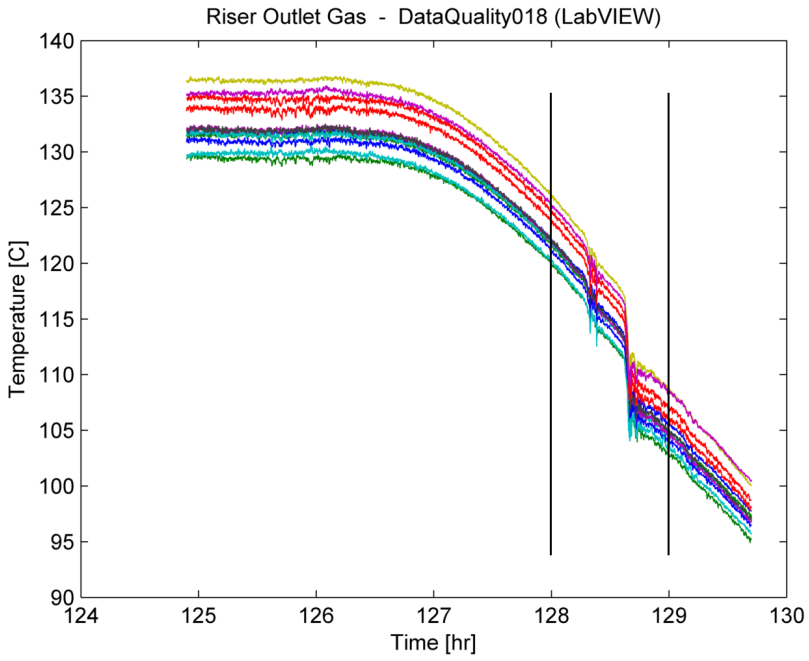


Figure 111: Drop in riser outlet gas temperatures from wind gust

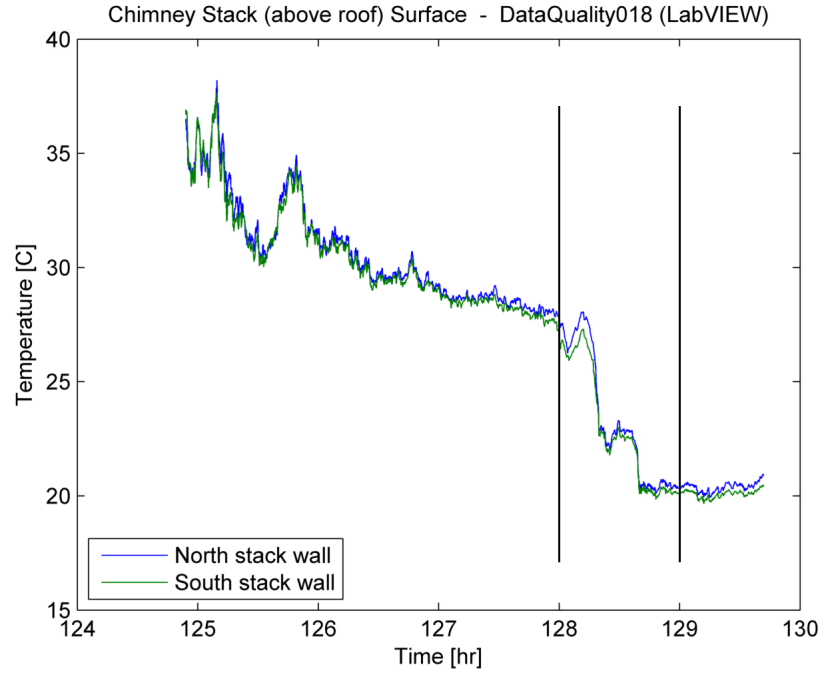


Figure 112: Early warning signs via wall temperatures

This page was intentionally left blank.

Chapter 8

Discussion

8.0.1 Analytical and Computational Support

The tasks completed in the early stages of the NSTF program, prior to experimental testing or even facility construction, were performed for the purposes of identifying anticipated facility behavior and operating conditions. Activities such as scaling studies, system modeling in RELAP5, bench scale separate effects testing, etc. were conducted with best available information and ultimately proved valuable in areas of sizing sensors and identifying high-impact locations for installation. When making comparisons to now-available data, values provided in earlier reports [11] show RELAP5-3D models significantly over predicted actual measured values; mass flow rates were over-predicted by 160%, heated surface temperatures by 150%, etc.. However, the overall trends are correct and the presented parametric studies follow similar patterns to experimental data. These differences are not alarming given the nature of first-stage predictive efforts, which often include assumptions due to unavailability of as-built geometry and dimensions. Thus, had there been no unknowns in design and constructed, the predicted values would have likely matched up very well to experimental data.

These early preparation tasks assumed not only idealized conditions, but also considered only those boundary conditions that were expected based on developer experience and intuition. Thus, real world influences such as fabrication tolerances, mass-transfer heat loss (e.g. leaks between heater panel seams), and meteorological variations were not included (their omission of these is acceptable during early modeling efforts given their difficulty in quantification). Changes to form losses, geometry, boundary conditions, etc. are known to

influence the system behavior, and with known ranges in a single-variable parametric study, can be included with relatively high confidence. However, it is the large number of permutations of known influencing factors, that when coupled with the introduction of unknown influencing factors, does the limitations of early stage preparation tasks become apparent. Under these conditions, a physical test facility stands as a necessary tool in identifying real world behavior and system responses.

8.1 Lessons Learned

Given the complexity of test assemblies such as the NSTF, it is improbable to assume consummate success in the first iterations of design, construction, and operation. Furthermore, the physical size introduces unique requirements for design and record keeping. As a test facility scales in size, the effort to maintain high confidence in exact dimensions and spatial positions becomes increasingly difficult. Compounded by the sensitive nature of natural circulation systems, stringent documentation becomes critical for establishing high data pedigree. This requirement can be brought into light during analysis efforts by 3rd parties, where incomplete documentation and drawings quickly hamper their efforts and questions ensue.

The NSTF project team was able to experience such scenarios while the program was still active, and proved to be a strong reinforcement of these important considerations for larger facility intended for model comparisons. First revisions of the nearly 425 unique drawings were given significant attention to ensure completeness and adequacy for machining and fabrication purposes. However, a comprehensive inclusion of all dimensions of interested to modeling tasks could not be anticipated. Creation of new drawings, or revision to existing drawings, detailing previously undocumented dimensions, along with documenting aspects of the facility by picture camera, could be completed in short time and provided to the interested 3rd party.

The lessons learned from the above experiences place a high priority on not only thorough and detailed design documentation, but application-specific usage by a 3rd party to vet and

validate the adequacy of documentation records. The core project team tends to develop a deep understanding of the physical intricacies of their test facility and may overlook certain areas they consider common knowledge. Thus, only when an outside perspective is given can the rigor and thoroughness of facility documentation truly be assessed.

Throughout the course of the NSTF program, a number of improvement opportunities were identified that either replaced deficient, optimized existing, or introduced new features within the test assembly. Several of these were the result of observations made by the analytical team during review of previous data, and ultimately proved valuable in strengthening the overall impact of the experimental program. A summary of these improvements is provided below in Table 52.

Table 52: Summary of major improvements to test facility

Improvement	Driving Observation	Description	Date
Matte stripes painted along outside of insulation panels	Characterization of the facility heat losses would benefit from exterior wall temperatures, however the shiny aluminum provided false IR readings	A high temperature paint was used to mark areas of the insulation panels to allow accurate thermal imaging	04/25/2014
New mounting of LUNA fibers within riser gas	The early iteration of SuperDuct, containing five fibers within the gas space, utilized positioning studs that unintentionally conducted heat causing temperature spikes	The 2nd iteration of SuperDuct featured spring-loaded mounting studs that only support the fiber at the inlet and exit of the riser	09/15/2014
Thermocouples installed along chimney above roofline	An interest was made to measure the heat loss along the chimney network installed outside of the laboratory building	New thermocouples were added along within the duct centerline and wall of the chimney above the roof	02/27/2015
Additional outlet plenum insulation	A selected number of wall TCs within the outlet plenum were reading abnormally cool temperatures. These were determined to reside near the joint of the outlet plenum cavity and false wall partition	Gas-sealing insulation strips were added to the outlet plenum wall joints to reduce hot-air exchange between false wall partition and outlet cavity	07/21/2015
Differential pressure impulse tubing temperature measurement	To obtain a common reference for modeling comparisons, experimental measurements should include the gravitational head of the impulse plumbing	Thermocouples were added along the differential pressure impulse tubing to accurately measure the added gravitational head	10/07/2015
Bldg. 308 ambient temperature measurement	Need for improved accuracy in calculating parasitic heat loss to environment	Additional thermocouples were added at multiple elevations within the Bldg. 308 high bay to measure ambient temperatures	10/07/2015
Anti-down draft chimney caps	Prevent performance degrading, wind-induced, flow reversals during heated operation	New chimney caps were installed to mitigate weather induced down-drafts	11/24/2015
Sealed loft damper valves	Comparisons against RELAP5 suggested temperature loss in measurements abnormal	Fan loft ductwork was fully sealed to prevent air by-pass	01/11/2016
Split of LUNA riser outlet	Measurement points near end points of fiber were excessively noisy due to long fiber length	LUNA fiber was split into two separate sensors to improve data clarity	04/05/2016

8.1.1 Sealed Fan Loft Damper Valve

Of these improvements, the sealed loft damper valves, which caused leakage of air past the fan loft damper valves, was a significant finding and addressed within the Quality Assurance Plan (QAP), ANL-NSTF-000000-DAR-005-R0. The chimney damper (butterfly) valves used to close the flow paths along the horizontal loft segments allow a portion of fresh air ingress due to a 0.125-in gap between the valve disk and inside duct walls, Figure 113. Across the 23.75-in diameter of the duct, this gap areas sums to 9.275-in² per chimney, or an area equivalent to a circle 3.437-in in diameter.



Figure 113: Gap between butterfly valve and inner ductwork. Average gap across entire circumference of 0.125-in

Temperature losses along the length of the chimney stack were questioned during comparisons to CFD and RELAP5 models. Experimental losses averaged 10-15 °C from the upper plenum outlet to the chimney exit, while modeling results, which were confirmed by analytical calculations, suggested a temperature loss closer to 5 °C. During a separate effects study, the horizontal fan lofts were physically sealed from the outside and a baseline test was performed, resulting in a chimney temperature loss that fell within the 5 °C.

Another study was performed to quantify the amount of leakage/ingress, and consisted of returning the duct loft to the original configuration and performed volumetric flow measurements of the leakages. This was supplemented by RELAP5, and analytical parametric, which allow higher confidence quantification of the impact of the leak in previous data.

The effect of air ingress to system flow rate can be determined by RELAP5 simulations of the NSTF. This model allows varying amount of fresh air ingress at the chimney ducts and is an accurate representation of the physical leakage observed. The influences on the system flow rate at varying leakage rates are shown below in Table 53.

Table 53: Influence on system flow rate due to varying levels of air ingress past damper valve

Normalized Air-Ingress Flow	System Flow (kg/s)	Deviation
0%	0.627	0.00%
5%	0.621	0.96%
10%	0.615	1.91%
15%	0.610	2.71%

Based on these two simple analyses above, along with the modeled system flow rate influence, the air ingress flow rate can be calculated and to correct measured values from the data sets with influence of the chimney leakage. A sample calculation is provided below in Table 54 and is representative of a typical cold weather baseline test case ($Q_{full} = 1.5 MW_t$, $Q_{NSTF} = 56 kW_t$).

Table 54: Measured (original) and corrected values, sample baseline case

System Parameter	As-measured	Corrected
System flow rate, kg/s	0.574	0.583
Chimney ΔT , °C	-12.21	-5.70
Chimney leakage flow rate, kg/s	0.042	0.0

8.1.2 Weather Mitigation Efforts

The observation of wind induced flow reversals were unknowingly observed during early scoping runs, when familiarity with the facility was relatively unknown and available sensors were limited. The addition of the weather station, mounted on the roof the laboratory building, provided valuable information and new insight into the initiating mechanism of these instabilities. To avoid repeat of these debilitating (from a testing objective point of view) conditions, early testing was performed with the aid of time-dependent loafer valves along the chimney ductwork. A gradual opening over an extended period allowed the system to remain shielded from wind perturbations while the components underwent initial heat-up and the system was allowed to establish the as-intended flow path. However, this user action directly conflicts with the overarching RCCS safety philosophy and would not be a feasible solution for a full scale installation. Thus, it was found of high interest to examine various anti-draft or draft-reducing weather caps for the NSTF chimneys stacks to replace the actuator valves. Varying solutions for passive control were investigated and focused on a study for improving the design of the outlet chimney cap. With unique requirements for a nuclear and safety-grade installation, a solution would be required to meet the following criteria:

1. Fully passive (no human input or active power)
2. Prevent chimney reversals during start-up transients and low power conditions
3. Maintain the low frictional drop and not restrict airflow
4. Contain no moving parts

The observed flow reversals and need for improved cap designs is not unique to the NSTF program. This problem is shared with the chimney or gas flue industry; common household fireplaces will often see downdraft during cold weather attempts to start a fire indoors, sending smoking down and into the living areas. Household solutions commonly entail the act of lighting a stack of newspapers on fire within the flue, creating an initial updraft, priming the chimney, and establishing the correct flow path for exhaust smoke.

More permanent solutions take the form of chimney-top appurtenances, commonly known as a chimney cap. The variations in design, complexity, and aesthetic appeal span an enormous range, however the NSTF project team was unable to find an off-the-shelf solution that could meet the four criteria listed previously. Most claim to prevent downdraft, but the majority either rely on mechanical movement of a wind shield, such as a rotating vane that shields the wind, or severely restrict the outflow exhaust and impede the natural circulation flow.

Work began by constructing a separate effects test assembly, which would provide the ability to examine varying chimney cap designs and their ability to prevent downdraft during conditions representative of typical NSTF testing. The test facility was designed and constructed from 4" galvanized steel ductwork, Figure 114, whose size was chosen in order to create a 1/6 scale model of the NSTF experiment, or 1/12 full scale. Heated air (approximately 40 °C) was simulated by a forced heated blower fan, while wind was modeled through the use of a fan attached to a 4" flexible duct mounted to the ceiling and directed at either one or both of the riser chimneys depending on the experiment. A characterization of the heated inlet and simulated wind was performed to establish a normal or baseline behavior. Then, varying chimney caps were examined for their effectiveness in preventing reversal flow. Testing was first performed on the "as-built" design installed on the NSTF to verify testing procedures and ability to create downdrafts under representative flow conditions. Then, alternative designs that were either purchased off the shelf or custom designed were tested and compared against their ability to prevent downdraft of cold air.

The final chimney cap, as designed by the NSTF project team, resulted in a hybrid design that was successful in its ability to meet the four listed criteria on the scaled test facility. The design was then fabricated on a full scale, and installed on the NSTF in Bldg. 308. A comparison to the old chimney cap style is provided in Figure 115, with installation pictures shown in Figures 116 and 117. Lastly, the design was submitted by the project team to the US Patent Office¹.

¹U.S. Patent Application "PASSIVE AND NO-LOSS WEATHER CAP FOR PROTECTION OF WIND INDUCED DOWNDRAFT IN SENSITIVE EXHAUST SYSTEMS", filed on July 13, 2016



Figure 114: Picture of 1/12, chimney duct-work only, forced flow mini-NSTF

(Figure 118 has been deleted)

Figure 115: New (left) and existing (right) NSTF outlet chimney caps



Figure 117: New caps installed, Bldg. 308



Figure 116: Installation of new caps

(this figure has been deleted)

(this figure has been deleted)

8.2 Collaborative Efforts

The overall motivation to study the performance of RCCS concepts extends to collaborating institutions both domestically and abroad. As part of an International Nuclear Energy Research Initiative (I-NERI), Argonne has partnered² with the Korea Atomic Energy Institute (KAERI) and the University of Wisconsin - Madison (UW). Furthermore, domestic relationships were formed through Nuclear Energy University Program (NEUP) projects. Across the involved institutions, experiment test facilities were built upon similar scaling philosophies and concept designs. A summary of the related test facilities is provided below in Table 55. Since the start of the collaborative initiatives, the breadth of study towards a full scale implementation has grown dramatically. A radar plot of the completed test parameters across the collaborating facilities is shown in Figure 119.

Table 55: Summary of scale test facilities at collaborating institutions

	Argonne	UW - Madison		TAMU		KAERI
Scale	1/2	1/4	1/4	1/4	Sep. effects	1/4
Working Fluid	Air	Air	Water	Water	Air	Air
Full Scale Ref.	MHTGR	MHTGR		MHTGR		PMR200
Location	IL, USA	WI, USA		TX, USA		Daejeon, SK

As part of the I-NERI workscope, similar testing was performed across the involved institutions and test facilities. The testing objectives, described previously in Section 7.3.4, resulted in data sets that may be used to verify scaling laws and assess the validity of predicting performance at alternative physical scales. However, acceptance criteria for steady-state conditions were not well established across all institutions. Given the large thermal mass of these testing facilities, the ability to achieve true steady-state required operating for an extended duration and imposed difficulties on some administrative staff. Furthermore, differences in the heated surface (see previous Table 41) introduced significant changes in the

²2014-006-K, "Comparative Study on Scaling Analysis between Two Reduced Scale Tests for RCCS"

measured temperature profiles regardless of integral power levels. Thus, cross-facility comparisons using the available data sets may only be appropriate for a quantitative transient analysis with considerations for differences in time scales, as steady-state, integral comparisons are likely not appropriate.

Regardless, some qualitative comparisons are appropriate and allow some general conclusions to be drawn. Foremost, a clear similarity among the facilities was observed in regards to their sensitivity to wind induced instabilities; a phenomenon directly measured in both $1/4$ scale facilities at KAERI and UW - Madison. Furthermore, integral system behavior such as ratios of system flow rate to heated temperature rise, electric to thermal efficiencies, and riser wall temperature profiles (Figure 118) were found to follow similar trends.

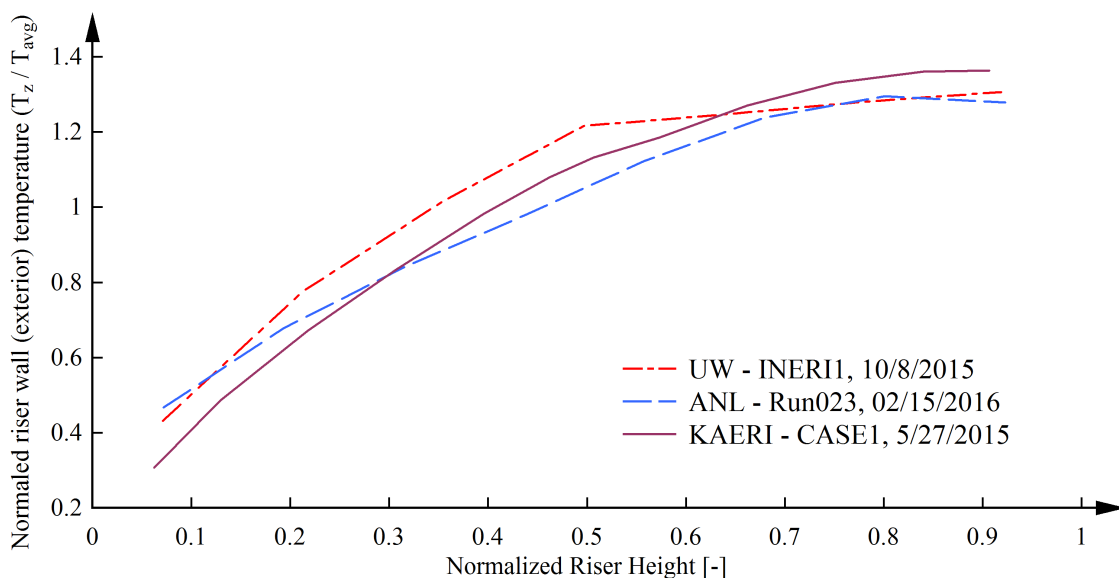


Figure 118: Temperature profiles (normalized dimensions) across KAERI, UW, and ANL facilities for 'I-NERI Test Case 1'

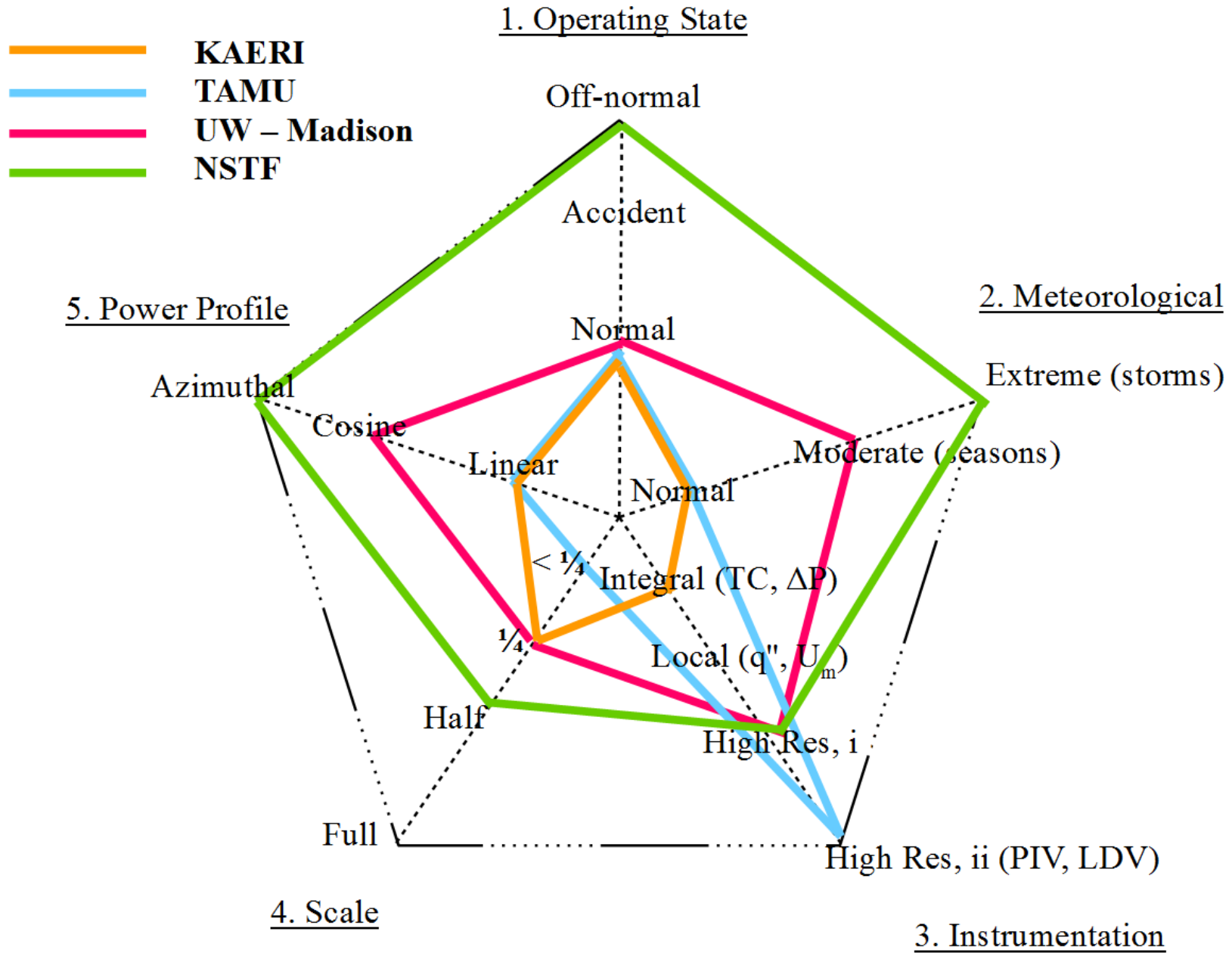


Figure 119: Radar map of the current testing envelope by ANL and collaborators for RCCS concept

8.3 Design Viability

8.3.1 System Longevity

The ability of an RCCS installation to maintain intended function throughout the 40-year life of a commercial reactor would be primarily contingent on the corrosion and structural integrity of material components. Given an omission of moving parts, maintenance efforts would be substantially reduced and limited to a) adequate material preparation, and b) regular inspection. Aside from seismic events which would affect the reactor building as a whole, dynamic loading would be negligible due the guaranteed single-phase state of air. However, the choice of carbon steel by GA RCCS [10] presents non-trivial challenges in maintenance efforts.

The riser ducts installed within the test facility at Argonne were selected to match GA specifications³, and purchased new from local distributors. All riser ducts were fabricated from welded structural rectangular steel tubing, ASTM A 500 Gr. B. Newly installed, the tubes featured a dark grey color, smooth surfaces, and average emissivity of 0.62 [14]. Throughout the 2,250 hours of active testing, average heat fluxes of 5.92 kW/m² caused significant corrosion and the creation of loose rust particles, Figure 120. The induced aging on the surface emissivity occurred on a relatively short time scale, increasing to an average 0.78 after only 450 hours of test operations, and have since remained relatively constant. The surface corrosion takes the form of iron oxide (commonly known as rust), and is a perpetual mechanism that if left unmitigated could impose severe complications to the structural integrity of the riser ducts. Furthermore, the introduction of water, a consideration that GA has expected based on references to drain connections located at the four corners of the lower cold plenum [10], would further augment the process.

³HTR-86-023, Vol. 1, Section 5.5.4.1 System Configuration

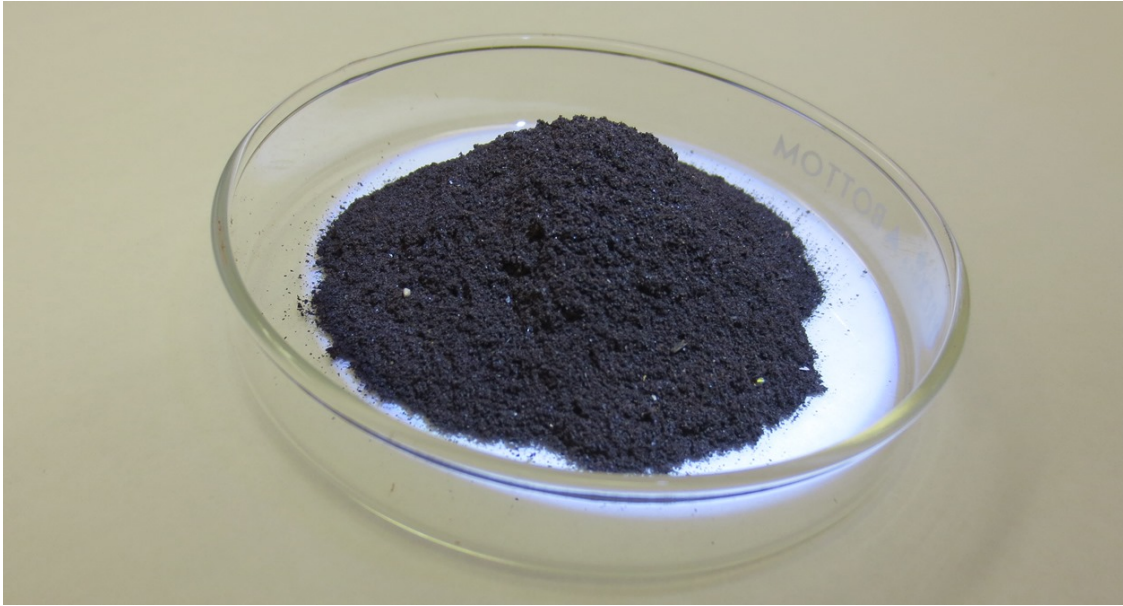


Figure 120: Rust from riser ducts collected in inlet plenum. 13.86 g over 100 day period

8.3.2 Full Scale Application

Best attempts were made to accurately capture the primary features of the GA RCCS installation, however a select number of differences remain between the scaled NSTF and a conceptual full size installation. Thermal hydraulic distortions have been reduced by scaling studies and similarity relationships, e.g. $\Delta T_R = 1$, however these were focused to the heated length and areas near the RPV. The geometry and mechanics of isothermal segments remain unique to a full scale installation, however several of the tests performed in the NSTF provide valuable insight into their influences and most probable system response.

Readily apparent is the difference between the NSTF and full GA RCCS inlet or downcomer ductwork. The GA downcomers run the full length of the heated cavity and are positioned between the concrete containment and the heated riser ducts. This installation introduces two considerations: 1) concrete containment (NSTF cold wall) surface temperatures, and 2) riser gas inlet temperatures. The first would not influence the overall heat removal performance of the RCCS, however the concrete temperature is one area of interest for reactor designers and would require further work to accurately predict. The second would

have strong influences on the RCCS performance; co-located downcomers would create elevated riser inlet temperatures to near 40 °C, analogous to the studied hot-weather testing performed on the NSTF, e.g. Run020. Based on the observations and results of this test, elevated inlet temperatures reduced the overall efficiency of the stack effect and induced deteriorated system performance due to the lower values of $\Delta\rho/\Delta T$. Thus, the NSTF represented a best case scenario and it can be expected that performance would be reduced with a containment housed downcomer ductwork.

The second difference, stemming from the relative elevations and flow lengths of the inlet and outlet ductwork, are significant contributors to the performance and worthy of discussion. Beginning with the former, the inlet to the NSTF is located within the laboratory space and 2.72 feet below the thermal center of the heated cavity. The outlet is positioned above the roof line, 64.45-feet above the thermal center, and results in a total elevation delta between inlet and outlet faces of 56.47-feet. The total elevation delta for the full scale GA RCCS, as described in literature [10], reflects a dimension of only 24.67-feet. A summary of the physical elevations for relevant configurations is provided below in Table 56.

Table 56: Elevations of inlet and exhaust ports, all dimensions in meters

	Inlet Port [m]		Outlet Port [m]		Δ [m]
	Rel. Grade	Rel. Core	Rel. Grade	Rel. Core	
NSTF (baseline)	-1.64	-0.83	18.84	19.64	20.47
GA RCCS	36.88	20.80	44.40	28.31	7.52
NSTF (adj. config.)	18.84	19.64	18.84	19.64	0.00

Moreover, the presence of above-grade inlet ductwork inherently requires additional ductwork to plumb the working fluid from the inlet port to the heated risers. These piping runs add frictional losses and increase the overall flow restriction from the outside environment to the heated region. It has been shown by previous works [37] that the introduction of a constricted entry region to a natural circulation system can restrict the laminar upward flow through the heated region, altering the pattern of natural convective flow. The boundary

layer nearest the heated wall demands more fluid than the cooler center can provide, resulting in a near zero centerline velocity. The authors defined a key parameter l_i/l , where l_i is the length of the unheated and l is the length of the heated ducts. The length is analogous to a restriction based on frictional losses and can be used to generalize any system with bends, constrictions, added lengths, etc.. A summary of these parameters, as applied to the NSTF and full scale RCCS designs, is provided by Table 57.

Table 57: Geometric ratios of loop segments. l_i refers to all inlet ductwork, l the heated length, and l_{exit} the exit chimney length

	Lengths l_i/l	Flow Area $l_i/(l+l_{exit})$	Wetted Perimeter $l_i/(l+l_{exit})$
NSTF (baseline)	0.62	0.10	0.07
GA RCCS	6.06	2.01	1.20
NSTF (adj. config.)	4.64	1.39	0.70

As shown by Run017, a baseline test case performed with the NSTF in the ‘adjacent chimney’ configuration, the NSTF saw a reduction in both heat removal performance and stability. The observations made were based on a over-representation of the full scale design, however raises important points on the stability of safety grade natural circulation systems. A stable system should, in an ideal case, reflect a single vertical pipe with a heated length near the base and a tall adiabatic chimney length. As the requirements of physical installations are often unable to cater to ideal geometry, the closer an installation trends towards a U-loop, and away from a vertical pipe, the less confidence can be had on predictability and system stability. This uncertainty manifests itself through a reduced level of confidence in the flow direction within the network. As shown by the NSTF program, along with similar research efforts, a U-shaped network experiencing natural circulation flow can readily shift flow directions in either chaotic (e.g. toroidal thermosiphon [38]) or unstable modes (e.g. minor perturbations as observed in the NSTF).

The third and final difference between the scaled and full size RCCS designs is the

number of parallel channels within the overall piping network. As discussed earlier, the dual chimney configuration presented challenges in maintaining as-intended flow direction. With four parallel chimney paths in the full size design, it is improbable to expect the system will maintain symmetric and equal flow across all legs. A minor increase in air flow rate within a single chimney lowers the pressure in that region of the chimney, thus increasing the driving buoyancy force and induced draft. With increased draft the chimney would draw more air from the plenum region, escalating a self-perpetuating cycle and exacerbate the flow asymmetry. While counter-intuitive, the reduction in total available parallel paths, along with introduction of channel asymmetries, would increase system stability (working against this philosophy is the consideration for redundancy, a balance that is difficult to define).

This page was intentionally left blank.

Chapter 9

Conclusion

The NSTF program at Argonne successfully completed over 2,250 hours of active test operations across a 33-month period to evaluate the feasibility of the air-based RCCS concept for decay heat removal of advanced reactor technologies. The efforts by the project team have established confidence in the program's ability to conduct high quality tests across a wide range of conditions with sufficient instrumentation to adequately capture pertinent thermal hydraulic phenomena. The rigorous NQA-1 procedures that directed operations have ensured high quality test data that was supported by a strong administrative program.

The test facility was observed to be most stable when operating at high powers in a single chimney configuration. During early start-up periods with multiple chimney exhausts, the natural convection phenomena was unable to maintain symmetric flow out of the chimneys which was observed to lead to degraded heat removal performance. Perturbations at the outlet boundaries (e.g. wind fluctuations) caused instabilities to form, leading to reverse flow situations where cool air was drawn down one chimney while hot air was exhausted out of the other.

Engineering controls (e.g. damper valves) were used in order to reach the desired stable flow conditions, however to maintain a passive philosophy of any decay heat removal system, these would be undesirable in a full scale implementation. Tests performed in the adjacent inlet / outlet configuration, a state that mimicked the full scale design basis, showed a destabilizing effect on the overall behavior. The introduction of high frictional losses at the inlet, compounded with a transition from a 'heated vertical pipe' to a 'heated U-loop' geometry facilitated system system-wide reversals that were otherwise not observed in baseline testing. Finally, under conditions of a heavy (non-air) gas ingress, the facility exhibited complete

stagnation of system flow and subsequent failure of heat removal function.

Based on the observations from the overall testing program, a number of unresolved issues remain. The coupling of low flow velocities, small differences in density when using air as the working fluid, and multiple parallel paths create a system that is vulnerable to instabilities with even minor flow disruptions.

9.1 Program Impact

One of the key passive safety features of many advanced nuclear reactor designs, including the GA-MHTGR, is the RCCS, designed to remove decay heat by natural circulation. The air-cooled RCCS concept is particularly similar to the RVACS concept that was developed for the GE PRISM sodium-cooled fast reactor. The DOE-NE ART Severe Accident Heat Removal Testing research program is part of the ART Methods Development work package dedicated to Validation and Verification (V&V). This DOE sponsored program, also known as the NSTF program, has been carried out at Argonne since 2005 and has successfully provided a robust, traceable, and valuable set of validation data suitable for guiding design decisions of future reactor concepts. This DOE experimental testing program has been carried out in collaboration with international partners through an I-NERI program (Japan Atomic Energy Agency (JAEA) and KAERI), reactor vendors such as AREVA and General Atomics, and a number of domestic university partners including TAMU, UW - Madison, and U-Idaho with input from the US-NRC. The centerpiece of this so-called RCCS alliance has been the NSTF program since the scale of the facility resembles that of the full-scale reactor system. While the NSTF air-based experiment was half-scale the bounds of the scaling distortions were well understood and minimized through a parallel scaling and analytical effort. Additionally, the data generated by the NSTF experiment was accomplished through a controlled, traceable, and NQA-1 compliant program that can be used to develop predictive capability for RCCS concept computational models. The data archived by the program has been made available to reactor vendors and the regulator for guiding design decisions for advanced reactor RCCS

concepts for passive decay heat removal.

9.2 Relevance and Contributions to DOE Vision

The mission of the Office of ART within DOE-NE is to sponsor research, development and deployment (RD&D) to “promote safety, technical, economical, and environmental advancements of innovative Generation IV nuclear energy technologies”. The NSTF program supports all four of these tenets, particularly through the generation of a significant quantity of pedigreed technical data that can be used to assist in selection and design of advanced passive decay heat removal systems for advanced reactors. The primary contribution to improving economic advancements has been through reduction of licensing uncertainties of passive advanced reactor technologies. The NSTF data set removes licensing risk, and thus cost, to both the reactor vendor and regulator by providing a traceable set of NQA-1 quality information on the passive decay heat removal of air-based RCCS concepts. The technical maturity of advanced reactor designs was improved by the NSTF program through the demonstration of the performance of the air-based RCCS concept and the design and testing of an innovative low-pressure loss chimney cap component. Combined with the follow-on water-based NSTF program starting in 2016 at Argonne, this program will substantially contribute to the technological development and reduction of technical risks necessary for the significant deployment of advanced reactors by DOE’s 2050 goal.

9.3 Path Forward

With conclusion of the air-based testing program on July 1st of 2016, efforts have shifted to a controlled, archival-style disassembly of air components. With the exception of the heated cavity, each component will be removed, inspected, labeled (south chimney segment shown in Figure 121), and placed into long term dry storage. Sign-off sheets will be filled out for each removed piece, documenting the date of removal, observations or abnormal discoveries, specific storage locations, and involved personnel. These sign-off sheets will be compiled and reviewed by the program manager before being achieved in the program's control records. Lastly, any changes in materials, structure, or significant corrosion (e.g. risers in Figure 122) will be photographed and documented.

Instrumentation and sensors expiring within 2 months of the testing conclusion date will receive project-end calibrations. All hardware, including sensors, thermocouples, transmitters, DAS, etc. will be placed into locked indoor storage units. Electronic copies of testing records, mirrored across three hard drives (two external, one internal) will be disconnected from service and placed within locked storage cabinets across two separate buildings at Argonne. Since no cutting or permanent alterations will be made during the disassembly process, the air-based NSTF will be capable of re-assembly at a future date should interest in an air-based RCCS concept be revitalized.

The disassembly process is scheduled to be completed by the end of calendar year 2016, at which point installation of water-based components will commence. Procurement of water-specific instrumentation and materials have been on-going since the start of FY16 and will continue in parallel with air disassembly efforts. The design and review of major water components was completed in FY15 [39] and fabrication is in-progress for the eight riser channel test section and 1,000 gallon water storage tank. As the program transitions to water-based studies, it will continue to undergo regular assessments to maintain compliance and secure the project's ultimate objective of generating high-quality data for licensing purposes.



Figure 121: Removed south chimney section of air-based NSTF



Figure 122: Exposed riser ducts (outlet) after removal of upper plenum, August 2016

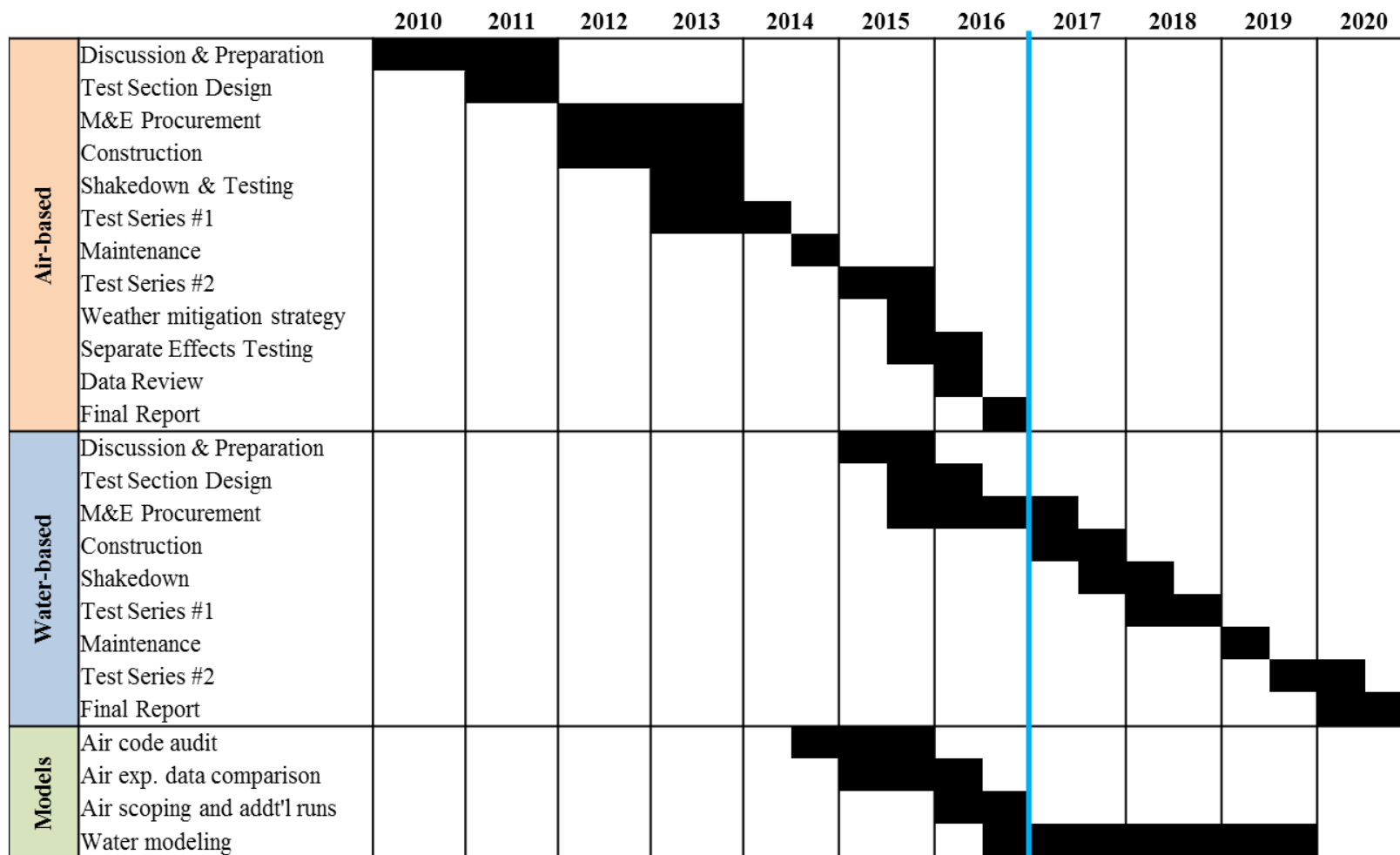


Figure 123: Timeline for air- and water-based NSTF program

Acknowledgments

This work was supported by the U.S. Department of Energy Office of Nuclear Energy's Advanced Reactor Technology (ART) program under contract number DE-AC02-06CH11357. The program team wishes to extend our gratitude for the funding, support, and guidance from our program sponsor and associated laboratories:

Federal Point of Contact - Steve Reeves (DOE-NE)

Technical Area Lead - Diane Croson (INL)

Guidance - Jim Kinsey (INL), Hans Gougar (INL)

Additionally, we wish to acknowledge the work of all involved since the programs inception:

Program Manager: Mitch Farmer, Tom Wei

Principal Investigator: Darius Lisowski

Facility Manager: Craig Gerardi

Design: Dennis Kilsdonk, Nathan Bremer, Art Vik

Instrumentation: Steve Lomperski

Quality Assurance: John Woodford, Roberta Riel

Analytical: Rui Hu, Taeseung Lee

Computational (System): Matt Bucknor, Qiuping Lv

Computational (CFD): Elia Merzari, Adam Kraus, Dave Pointer

Technical: Bruce Herdt, Dave Engel, Tony Tafoya, Dick Koehl, Bob Aeschlimann

Summer Students: Skyler Perot, Jordan Cox, James Schneider, Molly McCulloch

This page was intentionally left blank.

References

- [1] Wei, T. Y. C., Argonne National Laboratory, unpublished information, 2012
- [2] ASME NQA-1-2008 (with 1a 2009 addenda) “Quality Assurance Requirements for Nuclear Facility Applications”, 2008
- [3] ANL Quality Assurance Plan, current revision
- [4] ANL Laboratory-Wide Argonne Procedure LMS-PROC-50, “Control and Calibration of Measuring and Test Equipment”, Rev. 4, 2014
- [5] ANL Laboratory-Wide Argonne Procedure LMS-PROC-3, “Control of Nonconforming Products and Services”, Rev. 4, 2015
- [6] ANL Nuclear Engineering Division Local Work Planning and Control NE-WPC-01, 2012
- [7] INL Document PLN-2690, Rev. 10, “Quality Assurance Program Plan VHTR Technology Development Office,” effective 2013
- [8] Code of Federal Regulations, Title 10, Part 50 (10CFR50), Appendix B, “Quality Assurance Criteria for Nuclear Power Plants and Fuel Processing Plants,” 2006
- [9] Steward, R. R., Argonne National Laboratory, unpublished information, 1987
- [10] “Preliminary Safety Information Document for the Standard MHTGR,” HTGR-86-024, Vol. 1, Amendment 13, U.S. Department of Energy, 1992
- [11] Lomperski, S., Pointer, W. D., Tzanos, C. P., et al., “Generation IV Nuclear Energy System Initiative: Air-Cooled Option RCCS Studies and NSTF Preparation”, ANL-GenIV-179, Argonne National Laboratory, 2011
- [12] Turner, J. S., “Jets and Plumes with Negative or Reversing Buoyancy”, J. Fluid, Mech. 26, 779-792, 1966

- [13] INL Document MCP-2691, Rev. 2, "Data Qualification" effective July 20th 2012.
- [14] Lisowski, D., Argonne National Laboratory, unpublished information, 2014
- [15] Lienhard, J.H., Helland, K.N. "An experimental analysis of fluctuating temperature measurements using hot-wires at different overheats", *Exp. in Fluids*, **7**, 1989
- [16] Jorgensen, F.E, "How to measure turbulence with hot-wire anemometers - a basic guide", Dantec Dynamics A/S, 2004
- [17] Lomperski, S., Gerardi, C., Pointer, D. W., "Distributed fiber optic temperature sensing for CFD code validation", 15th Int Top Mtg Nuc Reactor Thermal Hydraulics, NURETH-15, Pisa, Italy May 12-17, 2013
- [18] Yuksel, K., Megret, P., and Wuilpart, M., "A quasi-distributed temperature sensor interrogated by optical frequency-domain reflectometer", *Meas. Sci. Technol.*, **22**, 2011
- [19] Lisowski, D., Gerardi, C., Lomperski, S., "Thermal Cycling Testing of Distributed Fiber Optic Temp. Sensors for High-Temp", *App., Proc. of NURETH-16*, Chicago, IL, Aug. 30 - Sept. 4th, 2015
- [20] Lomperski, S., Gerardi, G., Lisowski, D., "High-Resolution Temperature Mapping of a Jet Flow Field using Fiber Optic Distributed Sensors", *J. Vis. Exp., final review, awaiting production* 2016
- [21] Arkal Shenoy, personal communication, 2016
- [22] Hu, R., Kraus, Argonne National Laboratory, unpublished information, 2015
- [23] Incropera, F. P., and DeWitt, D. P., "Fundamentals of heat and mass transfer". New York: J. Wiley, 2002
- [24] Metais, B., and Eckert, E. R. B., *J. Heat Transfer, Trans. ASME*, **86**:295, 1964
- [25] Bar-Cohen, A., and W. M. Rohsenow, *J. Heat Transfer*, **106**, 116, 1984
- [26] Winterton, R. H. S., *Int. J. Heat Mass Transfer*, **41**, 809, 1998

- [27] Churchill, S. W., and Chu., H. H. S., *Int. J. Heat Mass Transfer*, **18**, 1049, 1975
- [28] Elenbaas, W., *Physica*, **9**, 1, 1942
- [29] Goldstein, R. J., E. M. Sparrow, and D. C. Jones, *Int. J. Heat Mass Transfer*, **16**, 1025, 1973
- [30] Hu, R., and Pointer, W. D., “CFD Analyses of Natural Circulation in the Air-Cooled Reactor Cavity Cooling System,” Proceedings of MC 2013, Sun Valley, ID, May 5-9, 2013
- [31] The RELAP5-3D Code Development Team, “RELAP5-3D Code Manual,” Idaho National Laboratory, Idaho Falls, ID, INEEL-EXT-98-00834, Rev. 4, 2012
- [32] CD-Adapco, “STAR-CCM+ 9.04 Manual,” Melville, NY 2014
- [33] Hu, R., Argonne National Laboratory, unpublished information 2016
- [34] Simoneau, J. P., Champigny, J., Mays, B., Lommers, L., “Three-dimensional simulation of the coupled convective, conductive, and radiative heat transfer during decay heat removal in an HTR”, *Nuc. Eng. Des.*, **237**, 15-17, pp1923-1937, 2007
- [35] Haque, H., Feltes, W., Brinkmann, G., “Thermal response of a modular high temperature reactor during passive cooldown under pressurized and depressurized conditions”, *Nuclear Engineering and Design*, Volume 236, 5 - 6, pp 475-484, 2006
- [36] Montanari, D., et. al., “Performance and Results of the LBNE 35 Ton Membrane Cryostat Prototype”, *Physics Procedia*, **67**, pp. 308-313, 2014
- [37] Dyer, J. R., “Natural-convective flow through a vertical duct with a restricted entry” *Int. J. Heat Mass Transfer*, **21**, pp. 1341-1354, 1978
- [38] Merzari, E., Fischer, P, and Ninokata, H., “Numerical simulation of the flow in a toroidal thermosiphon”, *Proc. of ASME Joint Fluids Engineering Conference*, Hamamatsu, Japan, Jul. 24 - 29, 2011
- [39] Lisowski, D., Argonne National Laboratory, unpublished information, 2015 (a)

- [40] Lisowski, D., Argonne National Laboratory, unpublished information, 2015 (b)
- [41] Lisowski, D., Farmer, M. T., et al., “Design Report for the 1/2 Scale Air-Cooled RCCS Tests in the Natural convection Shutdown heat removal Test Facility (NSTF)”, ANL-SMR-8 Argonne National Laboratory, 2014
- [42] Hecht, M., “MHTGR - nuclear engine or world development,” EIR, Vol. 16, 49, pp. 22 - 28, 1989
- [43] Bae, Y.Y., Cho B.H., Kim, J.H., Kim, M.H., Kim, Y.W., “Design of 1/4 Scale Performance Test Facility for the PMR200 RCCS”, Proc. of ICONE22, Prague, Czech Republic, July 7 - 11, 2014

Appendix A: Project Organization

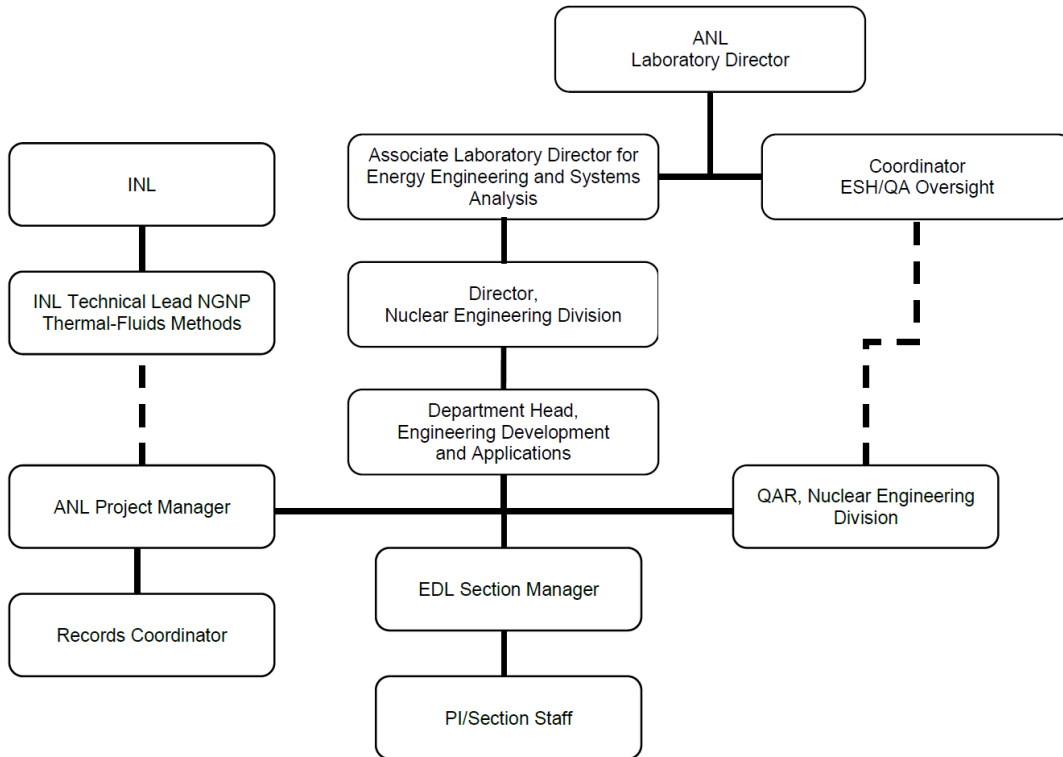


Figure 124: NE Division, Engineering Development Labs Organization Chart

Table: Identification and Role of Key Program Personnel

Role	Assignee	Responsibilities
ANL Project Manager	M. T. Farmer	Approval of ADMIN documents; interface with DOE
Facility Manager	C. D. Gerardi	Approval of all other documents, facility oversight and training
Principal Investigator	D. D. Lisowski	Oversight of facility experiment operations
Quality Assurance Representative	J. B. Woodford	Preparation of QA plan, oversee quality related activities and procurement
Configuration Manager	D. D. Lisowski	Maintenance of the CMS
Records Coordinator	D. D. Lisowski	Maintenance of facility records
Lead Experimenter	D. D. Lisowski	Develop test procedures, conduct tests, document results
DAS / Instrumentation Engineer	S. Lomperski	Support DAQ programming, instrumentation procurement and calibration
Facility Designer	D. J. Kilsdonk	Facility design and shops interface
Test Engineer – Electrical & Mechanical	N. Bremer	Facility mechanical and electrical systems
Project Personnel	R. Aeschlimann D. Engel B. Herdt E. Koehl A. Vik	Project specialists contributing to design, fabrication, operation, and maintenance of the test facility

Appendix B: QAPP Control Records

(this section has been deleted)

This page was intentionally left blank.

Appendix C: Project Publications

(this section has been deleted)

This page was intentionally left blank.

Appendix D: Data Review Minutes

Air-Based NSTF — Test Series & Data Review

Meeting Minutes

January 26, 2016

Argonne National Laboratory

Nuclear Engineering Division, Building 208

Contents

1. Attendance.....	3
2. Meeting Time and Location	3
3. Meeting Agenda.....	4
4. Final Action Items.....	5
5. Comments and Discussion (in order of presentations)	6
6. External Comments and Questions	14

1. Attendance

Name	Organization
Darius Lisowski	Argonne
Matt Richards	Ultra-Safe Nuclear (prev. General Atomics)
Arkal Shenoy	Self (prev. General Atomics)
Adam Kraus	Argonne
Casey Tompkins	University of Wisconsin
Craig Gerardi	Argonne
Rui Hu	Argonne
Jim Kinsey	Idaho National Laboratory
Brian Woods	Oregon State University
Robert Hill	Argonne
Chris Grandy	Argonne
Jim Wolf	Idaho National Laboratory
Diane Croson	Idaho National Laboratory
Steve Reeves	Department of Energy
Lewis Lommers	AREVA (prev. General Atomics)
Matthew Bucknor	Argonne
Dennis Kilsdonk	Argonne
Steve Lomperski	Argonne
Nathan Bremer	Argonne
Sud Basu (remote)	Nuclear Regulatory Commission (NRC)
Yassin Hassan (remote)	Texas A&M University
Olu Omotowa (remote)	North Carolina State University

2. Meeting Time and Location

Meeting start: 9:00

Location: Nuclear Engineering Division, Building 208, Room A138

Scribe: Katie Elyce Jones, Argonne

Meeting end: 16:30

3. Meeting Agenda

09:00 Welcome and Introduction

09:15 RCCS Background and NSTF Programmatic Introduction

10:00 Past Efforts and Development of R&D Towards Licensing

10:30 Air NSTF Testing Objectives and Accomplishments (Part 1)

11:30 Water NSTF Conversion Progress and Recent Updates

12:00 Lunch

13:00 MHTGR Safety Design and Role of RCCS

13:30 Air NSTF Testing Objectives and Accomplishments (Part 2)

14:00 Review and Discussion of NSTF Air Testing Series

15:30 Adjourn

15:30 Facility Tour of NSTF in Building 308 (Optional)

4. Final Action Items

- a) **Azimuthal Power Skew:** Discussed skew for projecting full-scale temperature effects in cavity, specifically corner areas. Discussed on what basis NSTF team should set their experimental skew levels that would meet industry needs.
 - **Action Item 1:** Look at legacy reports to find view factors for corner ducts in GA-MHTGR containment cavity. Perform an analysis of the view factors in both MHTGR and NSTF cavities, and evaluate the desired azimuthal power skewness in the experiment. If within a physically feasible range to test experimentally, do so.

- b) **Preservation of Knowledge:** Discussed need to document interesting experimental observations that might otherwise not make it into formal testing.
 - **Action Item 2:** We will complete this in our final report. Argonne has built in two to three months dedicated to writing a report in this fiscal year. The analysts will develop their report first so data is available in early stages. Argonne will also hold a group meeting to discuss separate effects and lessons learned so they can be collected and documented.

- c) **Analysis of data sets from similar facilities:** Discussed how to use data from collaborators at different facilities when delivering results of NSTF experiments.
 - **Action Item 3:** Will review current data from other facility and provide NSTF perspective on how other data may be interpreted if not drawing a direct comparison.

- d) **External gas ingestion:** Participants noted that an air-based RCCS could potentially be exposed to gases other than air. Discussed how NSTF modeling and experiments could investigate the introduction of light to heavy gases, such as helium and carbon dioxide.
 - **Action Item 4:** Will investigate the behavior of natural circulation system in the presence of gases such as carbon dioxide and helium in RELAP simulations. Lisowski will discuss possible experimental set-ups with safety officer(s). If simulations suggest there could be phenomena of interest and safety officers allow testing, these will be completed.

- e) **Role of RCCS:** A question regarding the overall role of the RCCS was made after the meeting (see Section 6, External Comments, Item V)
 - Action Item 5:** A study will be performed to understand the fundamental difference between experimental and actual RPV boundary conditions, and used to support a documented response within the final project report addressing the overall role of the RCCS. Considerations will be made to address the relationship between heat load, performance, and thermal response of both the RCCS and reactor core.

5. Comments and Discussion (in order of presentations)

A. Welcome and Introduction, Lisowski

Lisowski stated purpose of meeting: to share progress of the air-based Natural Convection Shutdown Heat Removal Test Facility (NSTF) and review results.

Lisowski reviewed agenda and invited participants on facility tour following the meeting.

B. RCCS Background and NSTF Programmatic Introduction, Gerardi

Gerardi said he hoped the meeting would achieve consensus and agreement that the air-based testing process is near completion.

Following presentation, Lisowski invited perspective on whether the data they would present in the following presentations would be ready for a stringent review.

Kinsey noted that related tests at other facilities are going on concurrently, and he was interested to see how those results would compare to NSTF results.

Lommers asked if they were going to present complementary data.

Lisowski said they did have slides from other facilities and participants representing those facilities at the meeting.

Basu asked if Tompkins [University of Wisconsin] and Richards [Ultra Safe Nuclear, prev. General Atomics] were going to present.

Lisowski said Richards was going to present.

C. Past Efforts and Development of R&D Towards Licensing, Kinsey

Kinsey presented on what will need to be demonstrated for licensing in the future.

Shenoy asked if they were going to address seven points raised by NRC during assessment of GA's MHTGR in the 1989 assessment of RCCS cooling system. Shenoy referred to number two in particular: the effects of high winds and regenerative heat transfer on inlet/outlet ducts.

Lisowski said he and Tompkins could discuss that point.

Basu said that, looking at the design criterion given in the presentation, he recognized changes in the language that removed shield design limits from the core radionuclide release. He said he thinks the NRC will want the fuel design limits addressed.

Kinsey said the NRC would be putting out a draft for public comment on a proposal submitted in Dec. 2014, so they would see the agency's criteria next month.

Lisowski said they were confident of the accuracy of the temperature of the outside vessel of the reactor pressure vessel, and that provided the temperature of the outside wall, they would look to do heat transfer conduction from actual fuel.

Kinsey said the scope of the work at the NSTF was different than that being discussed.

Lommers suggested the paragraph [referring to the core radionuclide release] may not be applicable for some designs because it is conceivable that you could have a design with a small core that doesn't need an RCCS, such as a 100 or 50 MW design for remote sites.

Kinsey said the criterion was written to be flexible and doesn't require an RCCS.

Lisowski, Kinsey, and Lommers discussed whether any current vendors are looking at RCCS options. No one knew conclusively.

Lommers said there are so many possible configurations that it is best to capture the basic characteristics in the criterion.

Shenoy said this is why verification and validation of predictive tools is important. He said he looked forward to seeing how close 1D and 2D modeling results compared to experimental data.

Lisowski said there wouldn't be any direct information on this but suggested modeling consortium in the room could provide insight and upcoming publications in review would provide that kind of analysis and comparison.

Dismissed for break at 10:15.

Reconvened at 10:20.

D. Air NSTF Testing Objectives and Accomplishments (Part 1), Lisowski

Following slide on baseline testing procedure, Lommers asked if, because the boundary conditions for their baseline testing procedure was a fixed heat flux on the vessel, if they were seeing a drop in the vessel wall effective temperature. Lisowski said yes but only a few degrees.

Lommers asked how those experimental results compared to predictive modeling. Lisowski said they began to look at force-flow testing because the ambient temperature is so important to the overall system.

Bucknor noted he did vary emissivity in models but the change would be on the order of a few degrees, and with all other factors involved, it does not show sensitivity to that.

Lommers agreed the nature of the system is such it shouldn't be very sensitive but it would be helpful to put that observation in the report.

Woods asked if they measured emissivity at all different temperatures. Lisowski said no because their instrumentation for measuring emissivity is limited to room temperature. Woods reinforced suggestion from Lommers to include a note on the change of temperature, despite its low impact.

Lisowski described the corrosion on the inside of the ducts after one year of testing, including rust.

Lommers asked if they had assessed the impact of conductive radiation on the optic fiber cables [instrumentation]. Lisowski said that no this had not been addressed, but believes the temperature gradients along the duct are gradual enough that conduction would not artificially smooth out any natural gradients. Thus, Darius believes even with the stainless steel capillary the temperature measured by the fiber is well representative of the actual duct gas temperatures. Additionally, Darius mentioned that due to the rust particles within the duct, and since the hot wire probes are delicate, he began pulling them out so they wouldn't get damaged from rust particles.

Basu asked for the maximum variation in reactor pressure vessel temperature across experimentation for constant power and all other variations. Lisowski said less than 20 degrees assuming constant power and that he had upcoming slides to address that question.

Following slide on testing procedure after 2014-2015 maintenance period, Woods asked Lisowski if they check all the loops during shakedown calibration. Lisowski said, yes, part of their instrumentation verification procedure was to check each thermocouple response on the data acquisition system.

Following slide on PTAR Test conditions and pre-checks, weather monitoring, and 16-hour steady-state test, Shenoy asked if inlet/outlets were located in the same place. Lisowski said the inlet is located inside the pit in the building and there is a pressure difference because it is

protected from winds. Therefore, the inlet and outlet conditions are different, so they looked at adjacent chimney roles and have data on that as well.

After Lisowski presented on local geometry #1, inlet down, and local geometry #2, riser outlet, Lommers asked if they had calculated K-loss for the whole system since they have done so for the risers. Lisowski said yes, but it is not included in the presentation; K-loss is enormously low and a challenge to measure in the chimney ducts and they see most of the loss in the risers.

After discussing the dimensions of optic fibers and their position in outlet plenum, Lommers noted figures provided were cavity dimensions not fiber distances.

Lisowski said they are still working on the best way to analyze with this kind of data. The LUNA fibers in the facility are the first installed in a large-scale thermal hydraulics test facility. It's a mutual trial and NSTF is trying out the LUNA fibers to see how they work in these conditions.

Lommers said the fibers might be relevant to Quality Assurance and asked what software program was translating the uncertainty introduced by a limited number of real data points. Lisowski said they don't publish this type of data because all the data they present from the NSTF is real data, un-manipulated, and they cannot yet quantify the uncertainty because the technology is so new. Lommers said that down the road they could address the higher uncertainty in the outlet plenum through post-processing. Lisowski agreed and said the figure on the slide [Local Geometry #3] is not part of the archived QA dataset and has been post-processed as discussed.

Basu referred to the Baseline Behavior plot. Lisowski said this is a steady-state snapshot in time looking at various surfaces. Basu remarked that there is a variation in temperature of about 50 degrees or so in the reactor pressure vessel. Lisowski confirmed and said that it is looking at the full axial extent of those plates about eight meters tall. Basu asked if there is a 50-degree variation in baseline behavior with all other parameters fixed, within reason, what variation in temperature did they expect to see with changing parameters. Lisowski said he would show a graphic in the afternoon presentation.

Lommers noted that for the purposes of testing, a constant heat flux boundary condition must be picked, but in the real system, there is not a constant heat flux boundary condition and, from an overall safety perspective, must keep that in mind. Lisowski said that for experimental practices, they have to settle on boundary conditions but they document and keep constant across tests.

On discussion of thermal efficiency, Lommers asked if thermal efficiency is measured at riser inlet and outlet. Lisowski said that now it is measured at riser inlet and chimney inlet with duct center and average measurements because they found a lot of mixing. Lommers asked if they take into account velocity profiles. Lisowski said no, it's something they've asked the analysts to help with. Lommers said since it's a mixed convection regime, the velocity profile would be interesting.

In presentation, Lisowski said they saw a difference in ΔT behavior in summer and winter months, and they believed they would see this in a full-scale facility.

Lommers asked if humidity played a role. Lisowski said none. Lommers suggested it varies with absolute humidity but not relative humidity.

Shenoy suggested that after verifying reactor design parameters in RELAP, to go back and predict what would happen in reactor conditions and test at those conditions so the results of those tests provide published information such as NRC would want.

Woods also suggested if there is something in the code that reflects some of these results, to explain why it was included in the code.

Lisowski said they are working on the final report with these considerations.

E. Water NSTF Conversion Progress and Recent Updates, Lisowski

On instrumentation slide, Lommers asked where vapor-carry over is taken. Lisowski said steam quality is taken at the outlet of the water tank, from which they could get other liquid parameters.

Lommers asked how the chiller would be connected. Lisowski said a steam line connects the tank to the chiller. Lommers asked about the condenser. Lisowski said that flat plate HXG also works as a condenser too and care will be taken to prevent plugging and creation of slugs of liquid.

Woods noted the chimney line discharge is below the normal water level of the tank and in the design it is sized so that it's submerged. Kinsey said he assumed it became uncovered at some point. Lisowski said they did a test at University of Wisconsin facility and found that even if the water level was four or five inches below the inlet, it was still cooling because of swelling in the chimney region. Lommers said there is an unusable volume at the bottom of the tank to take into account. Lisowski said that void fraction measurements will be in a number of places in the risers, likely in the riser exit and chimney region. Woods asked if that is how they are getting

steam quality data. Lisowski said there will be a flow meter installed for each riser, so there are multiple flow meters per riser in order to measure parallel channel interactions, which they've seen at the University of Wisconsin facility.

Lisowski said they are looking at two vendors for stainless steel water-membrane fabrication: the Argonne internal shop and CTI Power, which uses helium laser arc welding. Lisowski noted it is difficult to find vendors and they would like to use a company if possible to establish a relationship but it is more expensive.

Lommers said with stainless steel they will have more difficult getting desired emissivity.

Lisowski said they would have much high contributions to side panels because radiation would bounce around, and they decided on stainless steel from a pragmatic standpoint because they want to retain the water chemistry in mild steel tubes and there are too many modifications when you add coating, etc. with materials like carbon steel.

Lommers suggested carbon steel because of the thermal gradient in the wall. Lisowski and Lommers discussed whether stainless steel would remain an option for industry. Lommers said stainless steel might need to be conditioned.

Lommers said the simulated vessel temperature that will be measured with stainless steel will not be representative of what would be seen in a given heat system because they are sensitive to emissivity. He said the conductivity in the panel and the single loop operation would be different.

Lisowski said they have analyzed those and are satisfied and are going with stainless steel because of water chemistry; in this case, it would be difficult to work with water in untreated carbon steel.

Lommers and Lisowski discussed the inlet design for water storage tank. Lisowski noted that TAMU [Hassan] has experienced vapor bubbles getting trapped in a downward facing spout, influencing system behavior, so NSTF will have flexible discharge port.

Lommers and Lisowski discussed header diameter. Lommers suggested larger header diameter. Lisowski asked if increasing diameter of header pipe would be enough or if they would need to change the diameter of the entire loop. Lommers said it would mostly be useful for the header. Lisowski said they could look into that.

Shenoy asked how long it would take for NSTF to modify from a water-cooling system to an air-cooling system. Lisowski said two to three months to disassemble and two to three to

reassemble for a total six-month conversion period; they are going to put all the current equipment in storage.

Dismissed for lunch at 12:45.

Reconvened at 1:45.

F. MHTGR Safety Design and Role of RCCS, Richards

During presentation on role of multiple barriers during MHTGR LOCA, Lommers asked if the log scale on the I-131 release was fast or slow depressurization.

Richards said it was either a small or moderate leak. The VLPC attenuates for about 10 times, not a factor of 100 or 1,000 as in light-water reactors. If you develop new models based on new fuel, you may not need this factor of 10.

Lisowski asked Richards if GA had estimates for the lifetime of the RCCS system, considering water drainage, in the potential event for mild steel corrosion. Richards said they did not reach that stage. Shenoy suggested that if stainless steel was used to prevent rusting and it didn't have a high emissivity to start with, the surfaces could be roughened to increase emissivity. Lisowski said it would depend on the length-scale of the grooves.

G. Air NSTF Testing Objectives and Accomplishments (Part 2), Lisowski

Lisowski noted that in this presentation he would not go into details of test parameters as the purpose of this presentation is to assess the breadth of testing completed.

During discussion of test blocking riser channels, Shenoy asked if they looked at different configurations of outlet chimneys and, if so, which is most insensitive to weather conditions. Lisowski said they looked at two: one standard and one inverted conical design, but they have optimized their own chimney design for weather conditions. Lisowski said they generated data on their design but he would be conservative in extrapolating what that meant at full-scale.

Woods asked the frequency of data collection. Lisowski said once every four seconds. Reeves noted that at hour-50 in the more than 80 hours of testing there was a lot of perturbation [shown on graph]. Lisowski said that perturbation occurred at night. To correlate to weather conditions, Lisowski said they installed a weather station for comparison; and every perturbation can be contributed to wind, which influences the outlet boundary condition.

Lisowski suggested that by configuring the inlet and outlet to see the same wind boundary condition would cause them to cancel out. Shenoy mentioned data from [NSTF predecessor]. Lisowski pointed out that [the predecessor test reactor] only had one chimney. Lommers said fluctuations would have no effect in terms of long-term heat removal.

In discussing axial and radial variation of average temperature on heated plates, Lisowski returned to Basu's earlier question [see page 6] of the total distribution: it is 350-450°C.

Lisowski, Shenoy, and Lommers discussed how they could look at edges or other regions of the plate for average temperature. Lisowski said when they run a test, they aim to achieve uniform temperature across the plate, so they boost power at the edge. Lisowski said it is a technical challenge to maintain constant temperature across reactor pressure vessel and would not be representative of full-scale.

In discussing U-loop geometry of riser outlet and inlet, Lisowski noted that they had some instabilities during start-up when flow would go down one chimney and mix with air but, once running, flow was robust.

Discussing the effect of wind, Hassan noted that their indoor facility also experienced reverse flow, so even in the absence of wind, there is some reverse flow. Lisowski said the reason is likely multiple, parallel paths in any natural flow system is going to create asymmetry and the wind exacerbates this phenomenon. Lisowski noted they need to further understand why Hassan is seeing those effects as well and the driving force that switches it from symmetrical to asymmetrical flow.

H. Air NSTF Testing Objectives and Accomplishments (Part 2): Test Series Data presentation, Lisowski

During discussion of early comparisons of data sets presented from NSTF, KAERI, and University of Wisconsin, Lisowski said he would revisit figure of temperature of riser wall across facilities.

I. Review and Discussion of NSTF Air Testing Series

These notes are included on page 3 as Final Action Items.

6. External Comments and Questions

- i. “Since this data is being used for V&V, I recommend that you look at whatever V&V standard (like ASME V&V 20) you are using and run through it to make sure that you have all of the information that you need before you change to the water cooled RCCS configuration. Obviously, once you make the change much of the information you might need would be irretrievable.”
 - a. ANL Response: *We appreciate the feedback and will be sure the comment is addressed in our final report.*

- ii. “This may have been discussed as I was leaving yesterday, but in relation to the instability seen in all of the test facilities—including the A&M’s indoor facility—you might want to look at the scaling of the three facilities to see if that explains why A&M sees the instability indoors. I would start by looking at the Richardson number to see how it compares between your tests and the tests for which A&M saw the instability. That might explain why they see it even without the wind on the exhaust. It might also be worthwhile to compare the scaled conditions at which each of the facilities operates. If they have been operated at different non-dimensional conditions, you might want to run one set of tests matching the dominant characteristic ratios, like Richardson Number, and compare them.”
 - a. ANL Response: *We appreciate the feedback and will be sure the suggestions are included and addressed in our final report.*

- iii. “I gave some thought to the experimentally observed and analytically calculated RCCS flow instabilities with the configuration as a “u-tube” with the downcomer inlet near the elevation of the riser outlet, fairly consistent with the MHTGR and NGNP designs. I have questions on when this instability is observed: Is it observed only during startup? Is the heat up the only mechanism used to imitate flow? Or has this bifurcation been observed during steady-state? If this is only a startup/transient issue, then a potential design solution is to incorporate an “RCCS Startup System.” Before reactor system startup, a small forced flow would be activated through the RCCS flow paths. “Small” could be 5%, 10%, etc. (parametrically evaluated) of normal operation (parasitic RCCS heat loss) flow. As the reactor/vessel system (slowly) heats up, natural convection forces should take over in the right direction and the startup blower/pump can be shut down. I think this may be worth investigating both experimentally and analytically.’
 - a. ANL Response: *The instability is most often observed during start-up, when the chimney ducts are still cold. However, we also see the instability during low power test cases. Both conditions create a relatively cold exhaust system with low flow velocities, and allow the system to be sensitive to wind induced perturbations. To address the start-up difficulties, a subset of tests utilized a time-varying chimney damper valve to allow a gradual heat-up of the ductwork while shielding the system from wind. This has proven*

successful in achieving test acceptance criteria at steady-state, however does not maintain an ‘inherently safe and fully passive’ design philosophy. The mere introduction of a mechanical device may present a safety risk and would require extensive consideration prior to a full scale implementation.

- iv. “I like to emphasize one comment in particular and that is the need to translate R&D results into products that can be used directly for the licensing purpose. This connection was not apparent from the presentation and discussion. I will recommend that this point be articulated in the report in a manner that is easily understandable.”
 - a. ANL Response: *We appreciate the feedback and will be sure the comment is addressed in our final report.*

- v. “I have conceptual difficulty with the test findings that the RCCS design parameters have virtually no influence on the vessel wall temperature and, by implication, on residual core heat removal. What does it say about the role of RCCS in removing heat? I may need some coaching from the ANL staff on this matter.”
 - a. ANL Response: *We believe this comment is alluding to the specific scenario where we ran a low-power test with incremental riser blockages (and similarly when we created the fault scenario with a short-circuit in the inlet/outlet ducts). While the observed change in “RPV” temperature was minimal, all other system parameters saw large responses that would have significant impacts on a hypothetical full scale plant. During our blocked riser test, normal operation (0% blockage) saw average RPV temperatures of 279°C, and at 50% riser blockage, this increased to 291°C. Perhaps a +4.5% (12°C) change is minor; but due to the T^4 relation of radiative heat transfer, all other components saw very large changes. Our average riser duct wall temperature increased by +21%, gas temperatures by +22%, and upper plenum wall temperatures +25%. Conservation of energy requires the heat to go somewhere, and given that our measured thermal powers changed by only 1.5% (within the bounds of our measurement uncertainty) the heat was indeed still successfully being removed by the RCCS. A more rigorous follow-up to this question has been added as an action item in the meeting minutes.*

- vi. “Referring to Jim Kinsey’s presentation (one slide in particular where he identifies three needs the NSTF program is presumably addressing – core heat removal, code validation, and accident simulation), can one conceivably make the argument that you don’t need sophisticated CFD code(s) to study natural convection in finer details if the predominant mode of core heat removal is radiation? You probably need that level of sophistication if the focus is on predicting the RCCS performance with sufficient precision with regard to natural convection heat removal. So, which is your focus – core heat removal (safety) or RCCS performance and integrity (investment protection)? You may want to give some thought.”

- a. ANL Response: *With regards to the role of CFD simulations for this project, they are supplemental to the system code simulations to support the NSTF experimental program. CFD simulations can give us insights and fine details of local phenomena while system code simulations only focus on the integral behavior. For example, we model the radiation heat transfer and natural convection inside the cavity in the CFD simulations, which would improve our understanding of the temperature distributions among all the walls. Also, in the modeling of the air flow in the duct networks, the convective heat transfer in the riser ducts and thermal mixing in the upper plenum are of particular interests in the CFD simulations*

- vii. “I was thinking about the scaled comparison plot you showed during the meeting and it's possible that the surface temperature difference is so large because we were attempting to get the same temperature rise in our systems. Therefore the 1/4 scale UW system would require higher temperatures than the 1/2 scale NSTF, so if we divide the temperatures by the heat flux scaling parameter we might end up with much closer results. I think the term is $1/\sqrt{L_R}$, where L_r is the scaled ratio.”
 - a. ANL Response: *We appreciate the feedback and will be sure to consider this comment in our final report.*

This page was intentionally left blank.

Appendix E: Testing Procedure

Argonne National Laboratory
9700 S. Cass Avenue
Argonne, IL 60439

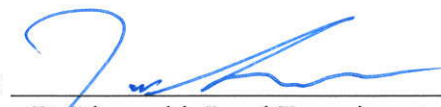
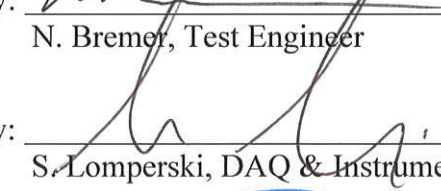
DQ022

Nuclear Engineering Division

**NSTF Test Procedure for
Data Collection (NQA-1, Type A)**

ANL-NSTF-000000-TEST-004-R2

January 14th 2016

Prepared by:		<u>01/17/2016</u>
	D. Lisowski, Lead Experimenter	Date
Reviewed by:		<u>03 FEB 2016</u>
	N. Bremer, Test Engineer	Date
Reviewed by:		<u>02/02/16</u>
	S. Lomperski, DAQ & Instrumentation Engineer	Date
Approved by:		<u>02/03/16</u>
	C. D. Gerardi, NSTF Facility Manager	Date

Notice: Printed and electronic copies of this document are not controlled. The current approved release of this document is maintained by the Configuration Manager.

Note: This document is fully representative of the identifier only when the revision number on the pages correspond with that in the index below

REVISION HISTORY

Rev	Date	Purpose	Authorization
0	01/26/2015	ANL-NSTF-000000-TEST-004 Initial Release	D. D. Lisowski
1	08/25/2015	Added training and calibration requirements, added pre-test visual verification of chimney operation	D. D. Lisowski
2	01/14/2016	Added additional test objectives: cosine, axial	D. D. Lisowski

NSTF TEST PROCEDURE FOR DATA COLLECTION (NQA-1, TYPE A)	Identifier:	ANL-NSTF-000000-TEST-004	Page 3 of 23
	Revision:	02	
	Effective Date:	January 14 th 2016	

Test Series & No: Data Quality 022 Test Dates: Jan. 17th - 2016
 Test Objective: Analyst drives testing Baseline w/ extended low power period, bottom peaked cosine, azimuthal steering
 Involved Personnel (IP): Darius Lisowski

0.0 **Scope** – This procedure governs activities related to conduct of an NSTF test for data collection for purposes of qualification at Type A data metrics under NQA-1 standards. The following steps are to be directed by the Lead Experimenter, with approval from the Project Manager. Only Involved Personnel identified above may participate in test operations. Outlined tasks are to be conducted in the prescribed, sequential order, according to the written procedure.

1.0 **Prerequisites**

- 1.1 Training - All Involved Personnel must: i) undergo NSTF indoctrination training, and ii) undergo training for this test procedure (training documented in Appendix A), and be up-to-date on the active WPC training through their TMS profile.
- 1.2 Access control – Non-involved personnel shall not modify or otherwise access critical data acquisition or chimney ducting including cDAQ units or loafer valves for a period beginning 2 days prior to test commencement until a period of 4 days post-test conclusion. These control areas are to be marked and posted with visible signage. Any of these activities performed by Involved Personnel must be carried out under the lead experimenter's guidance and control. Related computer systems shall be limited to test specific activities only.
- 1.3 Delegation of roles and monitoring shifts - Given the multiday duration of the test, the lead experimenter will designate responsibilities and operating shifts for the full duration of heater-on power testing. Active monitoring is not required during overnight periods, but efforts should be made to: minimize unattended operation to periods no greater than 8 hours and only after at least 10 hours of initial heating, or at the lead experimenters' discretion.
- 1.4 The following attachments must be printed and included in the final test report folder
 - 1.4.1 A tabulated list of all relevant engineering drawings, their number (including revision), and a summary description
 - 1.4.2 A complete set of instrumentation-related engineering drawings printed in full (8.5"x11") that provide details of sensor types, locations, and names
 - 1.4.3 A tabulated data acquisition list detailing connected devices, cDAQ channels, that cross-reference instrumentation-related engineering drawings
 - 1.4.4 Tabulated list of calibration dates for applicable instruments

Date: 1/17 Initial: DL

NSTF TEST PROCEDURE FOR DATA COLLECTION (NQA-1, TYPE A)	Identifier:	ANL-NSTF-000000-TEST-004	Page 4 of 23
	Revision:	02	
	Effective Date:	January 14 th 2016	

2.0 Documentation of System Setup and Configuration

2.1 Document chimney loafer / valve position (per ANL-NSTF-DUCT01-DWG-0028)

LF-NV	Open
LF-SV	Open
LF-NH	Closed & Sealed
LF-SH	Closed & Sealed
LF-XC	Closed

2.1.1 Riser tube – heated wall setback distance (per ANL-NSTF-RCCS01-DWG-0008)

27.82"

2.1.2 Outlet plenum floor spacing (per ANL-NSTF-RCCS01-DWG-0008)

16.00"

Date: 1/17 Initial: DL

2.2 Global summary of data acquisition channel and devices:

2.2.1 Obtain a hard copy of thermocouple and instrumentation summary. Initial, date, and note test name. The print out will include: Instrument identification name, signal output, range, accuracy, manufacturer, calibration (if applicable, and if so ensure calibration date is valid for test duration), DAQ channel, and engineering drawing reference numbers.

Date: 1/17 Initial: DL

2.3 Engineering drawings of included instrumentation position

2.3.1 Obtain hard copies of engineering drawings which detail above devices and correspond to the above reference numbers. Initial, date, and note test name.

Date: 1/17 Initial: DL

2.4 Specifications of analogue flow and pressure devices. Include original output signal, resistor value (if applicable for I->V), full scale range, and any user-configurable settings

	Model	Full Scale	Output	Resis. Ω	Other
Flow meter	Sierra 640S	0 – 1 kg/s	4 – 20 mA	250	K = 1.25
Humidity	Dwyer RHP	0 – 100% RH	4 – 20 mA	250	n/a
Riser ΔP	Dwyer 668	± 0.25 "WC	4 – 20 mA	250	n/a
Chimney ΔP	Dwyer 607	± 0.10 "WC	4 – 20 mA	250	n/a

Date: 1/17 Initial: DL

2.5 Differential pressure impulse plumbing (per ANL-NSTF-DUCT01-DWG-042-R1)

Configuration: D. Pitot tube

Transmitter	Pressure Tap	Impulse Connection
North, 607-OB (53)	Low	North pitot
	High	
South, 607-OB (51)	Low	South pitot
	High	

Date: 1/17 Initial: DL

2.6 LUNA fiber serial and position in duct (per ANL-NSTF-RCCS01-DWG-031 & 032)

Fiber	FOS Channel	Fiber Serial	Duct Position
Fiber #01	1	872	GF-E
Fiber #02	2	553	GF-EC
Fiber #03	3	550	GF-C
Fiber #04	4	544	GF-WC
Fiber #05	5	387	GF-W
Fiber #06	13	001	PL-N
Fiber #07	15	002	PL-S
Fiber #08	16	009	PL-R
Fiber #09			
Fiber #10			
Fiber #11			
Fiber #12			
Fiber #13			

Date: 1/17 Initial: DL

2.7 Document any abnormalities, deviations, findings discovered, or comments on tasks performed in task 2.0 Documentation of System Setup and Configuration

- New chimney caps installed and in-use
- Bldg 308 VDP monitor installed, Dwyer RSM-2-A
Outdoor connected to "4", indoor to "1" or "reference" Not calibrated!!

- Out-of-calibration devices below however considered valid for service based on engineering judgment, experience, nature of strain based pressure devices, and that pre-2 calibrations had not drifted over 2 years
 - x8 riser ΔP , Dwyer 668-11
 - x2 chimney ΔP , Dwyer 607-008
 - x1 humidity, Dwyer RH1-2011
 - x1 Bldg 308 ΔP , Dwyer RSM-2-A

Date: 1/17 Initial: DL

NSTF TEST PROCEDURE FOR DATA COLLECTION (NQA-1, TYPE A)	Identifier:	ANL-NSTF-000000-TEST-004
	Revision:	02
	Effective Date:	January 14 th 2016

Page 8 of 23

3.4 Confirm working communication with WSN (signal, %) and battery (V)

	Serial	Battery (V)	Signal (%)
Stack	663	1.325V	96%
Loft	508	1.225V	92%
Roof	05E	1.275V	89%
T-Junc	806	1.325V	93%

Date: 1/17 Initial: DL

3.5 Confirm working communication with Davis weather station and local console

Date: 1/17 Initial: DL

3.6 Confirm working UPS operation and communication with computer

Date: 1/17 Initial: DL

3.7 Confirm working remote desktop operation via laptop

Date: 1/17 Initial: DL

3.8 Enable remote watchdog in LabVIEW. Verify operation and triggered communication

Date: 1/17 Initial: DL

0.1 Verify movement of chimney loafer valves NV, SV, and XC. Cycle full open and full closed in LabVIEW, and visually verify that the valves move as intended.

Date: 1/17 Initial: DL

0.2 Document any abnormalities, deviations, other findings discovered, or comments on tasks performed in task 3.0 Pre-test setup and hardware verifications

All okay

Date: 1/17 Initial: DL

NSTF TEST PROCEDURE FOR DATA COLLECTION (NQA-1, TYPE A)	Identifier: ANL-NSTF-000000-TEST-004	Page 7 of 23
	Revision: 02	
	Effective Date: January 14 th 2016	

3.0 Pre-test setup and hardware verifications

3.1 Data acquisition computer preparation

3.1.1 Reboot primary control computer

3.1.1.1 Update system clock to 'time.nist.org'

3.1.1.2 Create test folder,

'C:\NSTF_DataStorage\dataQuality%N%_%DATE%'

3.1.2 Open communication lines with Eurotherm & Mini controllers

3.1.2.1 Launch iTools OPC Server

3.1.2.1.1 Network -> Start One-Shot Scan

3.1.2.2 Launch iTools Engineering Studio

3.1.2.2.1 Device – Enable Background Scans

3.1.2.2.2 Scan from '201 – 220'

3.1.2.3 Launch iTools Scope

3.1.3 Launch NI-MAX

3.1.3.1 Reset and reserve x4 chassis (listed in §3.3)

3.1.3.2 Export NI-MAX configuration 'NSTF_%DATE%.html'

3.1.4 Launch LabVIEW 2010 'NSTF_Main.proj'

3.1.4.1 Backup full VI library within test folder 'viDataQuality_%DATE%'

3.1.5 Attached latest release of ANL-NSTF-000000-SC (software config.)

3.1.6 Attached latest release of ANL-NSTF-000000-SB (calibration records)

3.1.7 Record specific LabVIEW vi filename and revision number

3.1.7.1 .vi name, revision

NSTFMain 2016.vi, rev 791 (DSC)

Date: 1/17 Initial: DL

3.2 Confirm working communication with iTools

Main1_2 OK
 Main3_4 OK
 Main5_6 OK
 Main7_8 OK
 Main9_10 OK
 Mini1 OK
 Mini3 OK

Guard1_2 OK
 Guard3_4 OK
 Guard5_6 OK
 Guard7_8 OK
 Guard9_10 OK
 Mini2 OK

Date: 1/17 Initial: DL

3.3 Confirm working communication with cDAQ

LowerNorth OK
 UpperNorth OK

LowerSouth OK
 UpperSouth OK

Date: 1/17 Initial: DL

1.0 Test Day, cold-start and zero-flow baseline

1.1 On day test day, but before commencing test operations, perform cold-start, zero-flow verifications

1.1.1 Verify that heater power has not been enabled for at least 4 days prior (ensuring no elevated temperatures)

1.1.2 Establish zero-flow condition by closing all dampers and covering the inlet down comer cap

1.1.3 Monitor thermocouples within LabVIEW. Verify that all read values nominally near ambient (variations will exist due to natural temperature gradients). Document any abnormalities, and if open TC detected, document the location and channel

1.1.4 Record cold-start, zero-flow values for 5 – 10 minutes in LabVIEW

1.1.4.1 Data file name: Data Quality 022 - zero Flow.

1.1.5 Monitor flow meter and differential pressure. Verify that readings are within nominal ranges, and then record actual value.

1.1.5.1 Mass flow meter 0.55 kg/min (< 1.5 kg/min)

1.1.5.2 Riser diff. pressure 1.4 Pa (< 10 Pa)

1.1.5.3 Chimney diff. pressure 0.0 Pa (< 4 Pa)

Date: 1/17 Initial: DL

1.2 Document any abnormalities, deviations, other findings discovered, or comments on tasks performed in task 4.0 Test Day, cold-start and zero-flow baseline

• Open TC:

- /UW/Mod 1/ai0 - 6N-TC75 • Δ prior #12 = 2Pa
- /UW/Mod 2/ai5 - 10N-TC117 • Δ prior #1-11 = 12Pa
- /UW/Mod 2/ai7 - 10N-TC121
- /US/Mod 2/ai10 - 45-TC53 • Humidity - 107.
- /LS/Mod 3/ai2 - 55-TC70 •
- /US/Mod 1/ai7 - 75-TC87
- /US/Mod 2/ai5 - 105-TC116

• Noisy HFm:

- 938 - 0 ± 8mV
- 941 - 4.5 ± 2mV
- 936 - 2.2 ± 0mV
- 939 - 0 ± 2mV

Date: 1/17 Initial: DL

NSTF TEST PROCEDURE FOR DATA COLLECTION (NQA-1, TYPE A)	Identifier: ANL-NSTF-000000-TEST-004
	Revision: 02
	Effective Date: January 14 th 2016

Page 10 of 23

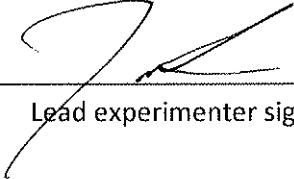
– Hold Point –

Do not proceed unless the following tasks have been completed:

- 1.0 Prerequisites
- 2.0 Documentation of System Setup and Configuration
- 3.0 Pre-test setup and hardware verification
- 4.0 Test Day, cold-start and zero-flow baseline

Confirm that the loft fan blowers have been shut off. Confirm that the valves are oriented in the prescribed positions (North Vertical, South Vertical, and Cross Connect). Confirm that horizontal valves are closed (North Horizontal, South Horizontal)

I verify that the tasks above have been completed according to the written procedure, and that they were done so in a manner that is consistent with the scope of the test objective. I also verify that unless otherwise stated, these were performed while the facility was in a cold state (surrounding metal and insulation is, within reasonable judgment, near ambient temperatures). Any deviations from the written test procedure have been approved by the lead experimenter and documented.



Lead experimenter signature

Jan 17th, 2016, 12:30

Date/Time

This area intentional left blank

2.0 Test day starting procedures**2.1 Building & administrative tasks**

- 2.1.1 Notify building occupants, directory, and manager of 308
- 2.1.2 Inspect test area to ensure no combustibles are present.
- 2.1.3 Post 'DANGER – HOT SURFACE' warning signs around test and heater area.
- 2.1.4 Post "ACCESS CONTROL - TEST IN PROGRESS" over DAQ and heater panel.
- 2.1.5 Post "NO UNAUTHORIZED PERSONNEL" signs over 308 pit staircase
- 2.1.6 Verify railings are in place to prevent access to 240 / 480 VAC power leads
- 2.1.7 Verify that garage doors to Bldg. 308 are closed and ventilation fans are off

Date: 1/17 Initial: DL**2.2 LUNA tasks**

- 2.2.1 Via LUNA laptop in pit, log on using 'NSTF' username
- 2.2.2 Update system clock to 'time.nist.org'
- 2.2.3 Create test folder, 'C:\data\NSTF\dataQuality%N%_%DATE%'
- 2.2.4 Beginning logging in LabVIEW, and append '_baseline' to file name.
- 2.2.5 On LUNA system, perform baseline measurement
- 2.2.6 Stop logging on LabVIEW, and begin automated acquisition sequences across all fibers on LUNA system, specifying a measurement interval of '20 minutes', with '2 seconds' between fibers in a given interval
- 2.2.7 Verify written data files, and preview results to ensure as expected
- 2.2.8 Verify working remote access and communication from control room by launching "Remote Connection" and entering '192.168.0.106'

Date: 1/17 Initial: DL**2.3 LabVIEW logging tasks**

- 2.3.1 Update system clock to 'time.nist.org'
- 2.3.2 Verify '0' power signal to all 40 Eurotherm modules (within iTools)
- 2.3.3 Signal to personnel to enable 20 main and 20 guard contactors
 - 2.3.3.1 Verify 240V line voltage (within iTools) across guards
 - 2.3.3.2 Verify 480V line voltage (within iTools) across mains
- 2.3.4 Define trip override temperature for heater banks, '650°C'
- 2.3.5 Initialize data logging on LabVIEW
 - 2.3.5.1 Enter test name, 'dataQuality%N%_%date%'
 - 2.3.5.2 Specify recording interval of '4 seconds', enable logging
 - 2.3.5.3 Verify data file was created and is being appended

Date: 1/17 Initial: DL**2.4 Power-on initialization**

- 2.4.1 Initialize power ramp in LabVIEW
 - 2.4.1.1 Enter desired power on 'Heaters' tab, 56 kW_e
 - 2.4.1.2 Enable 'Ramping', specify desired ramp up time period, 2 hour
 - 2.4.1.3 Enable 'Power On' button

NSTF TEST PROCEDURE FOR DATA COLLECTION (NQA-I, TYPE A)	Identifier: ANL-NSTF-000000-TEST-004	Page 12 of 23
	Revision: 02	
	Effective Date: January 14 th 2016	

2.4.2 Monitor & observe power ramp operation

2.4.2.1 Ensure power ramp executes and completes as intended

Date: 1/17 Initial: DL

2.5 Document any abnormalities, deviations, other findings discovered, or comments on tasks performed in task 5.0 Test day starting procedures

Report completed Jan

Date: 1/17 Initial: DL

3.0 Monitoring procedures during test

3.1 Safe operating limits

3.1.1 Heat flux sensors. Monitor TC near heat flux meters to ensure that their maximum rated operating temperature of 300°C are not met throughout the duration of the test. If these are approached, it will be up to the lead experimenter and project manager to use their discretion if testing shall resume as planned, conditions adjusted, or all-together conclusion of test.

3.1.2 Heater surface temperature. Monitor heater surface temperatures and ensure that the safety trip point of 650°C is not met. If these are approached, it will be up to the lead experimenter and project manager to use their discretion if testing shall resume as planned, conditions adjusted, or all-together cancellation of heater-power and conclusion of test. Enabling of forced blowers may be initiated if deemed necessary to protect safety of structural components.

Date: 1/22 Initial: DL

3.2 Logging of data

3.2.1 Ensure, at intervals of no more than 6 hours apart, that data logging file is being written. This can be verified by the "last modified" date in Windows Explorer or by checking that the file size is increasing with time. If any abnormalities are discovered, best efforts must be made to mitigate the situations without interrupting the quality of the test data. Document these, if any, discovered during testing.

Date: 1/22 Initial: DL

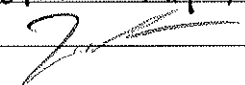
NSTF TEST PROCEDURE FOR DATA COLLECTION (NQA-1, TYPE A)	Identifier:	ANL-NSTF-000000-TEST-004	Page 13 of 23
	Revision:	02	
	Effective Date:	January 14 th 2016	

3.3 Acceptance criteria #1 – 26 kW_t steady-state

3.3.1 Monitor energy balance within heated test section as provided by LabVIEW, and perform secondary verifications by hand calculations. $Q = \dot{m}C_p \Delta T$, where the temperature rise is as measured across the riser inlet to upper plenum outlet. For acceptance of steady-state conditions this value is to be within 5% of the target goal for the given test.

3.3.2 Monitor long-term time history of flow rate, temperatures, and energy balance. For acceptance of steady-state conditions, these values are to not change by more than 5% over the course of 6 hours. Given the variations in atmospheric conditions, natural effects will induce fluctuations in these measurements and ultimately it is up to the lead experimenter’s discretion to determine when acceptable steady-state conditions have been met.

Steady-state acceptance criteria Stable \dot{m} , ΔT , thermal energy
35.80 kg/min, $\Delta T = 58.45^\circ C$, $\dot{Q}_t = 35.14 kW_t$

Time and date met run = 43.5 hr, 1/19/16 @ 7:15am
 Lead experimenter signature 

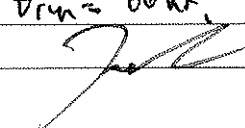
3.4 Acceptance criteria #2 – 56 kW_t steady-state

3.4.1 Upon successfully meeting Acceptance Criteria #1 – 26 kW_t steady-state, apply 90-minute ramp to 78 kW_e (adjusted based on operator discretion) to yield target goal 56 kW_t

3.4.2 Monitor energy balance within heated test section as provided by LabVIEW, and perform secondary verifications by hand calculations. $Q = \dot{m}C_p \Delta T$, where the temperature rise is as measured across the riser inlet to upper plenum outlet. For acceptance of steady-state conditions this value is to be within 5% of the target goal for the given test.

3.4.3 Monitor long-term time history of flow rate, temperatures, and energy balance. For acceptance of steady-state conditions, these values are to not change by more than 5% over the course of 6 hours. Given the variations in atmospheric conditions, natural effects will induce fluctuations in these measurements and ultimately it is up to the lead experimenter’s discretion to determine when acceptable steady-state conditions have been met.

Steady-state acceptance criteria Stable \dot{m} , ΔT , Heat energy
36.27 kg/min, $32.57^\circ C$, 49.12 kW_t

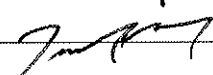
Time and date met run = 66 hr, 1/20/16 @ 06:00am
 Lead experimenter signature 

NSTF TEST PROCEDURE FOR DATA COLLECTION (NQA-1, TYPE A)	Identifier: ANL-NSTF-000000-TEST-004	Page 14 of 23
	Revision: 02	
	Effective Date: January 14 th 2016	

- 3.5 Acceptance criteria #3 – Cosine power shape, 56 kW_t steady-state
 - 3.5.1 Upon successfully meeting Acceptance Criteria #2 – 56 kW_t steady-state, apply bottom peaked cosine power profile over a 2 hour period. Ensure total power to heater banks remain constant. Document power peaking factors, P=f(z).
 - 3.5.1.1 P(Z) = N*Ppeak -> P(0) = 0.225, P(1) = 0.45,
P(2) = 0.65, P(3) = 0.9, P(4) = 1.15, P(5) = 1.275,
P(6) = 1.375, P(7) = 1.425, P(8) = 1.325, P(9) = 1.225
 - 3.5.2 Monitor energy balance within heated test section as provided by LabVIEW, and perform secondary verifications by hand calculations. $Q = \dot{m}C_p \Delta T$, where the temperature rise is as measured across the riser inlet to upper plenum outlet. For acceptance of steady-state conditions this value is to be within 5% of the target goal for the given test.
 - 3.5.3 Monitor long-term time history of flow rate, temperatures, and energy balance. For acceptance of steady-state conditions, these values are to not change by more than 5% over the course of 6 hours. Given the variations in atmospheric conditions, natural effects will induce fluctuations in these measurements and ultimately it is up to the lead experimenter’s discretion to determine when acceptable steady-state conditions have been met.

Steady-state acceptance criteria sketch in ΔT , hand energy
 $\dot{m} = 35.17 \text{ kg/hr}$ $\Delta T = 79.60^\circ\text{C}$ $Q_t = 48,43 \text{ kW}$

Time and date met 6 hrs = 9/hr, 1/21/16 @ 06:45am

Lead experimenter signature 

- 3.6 Acceptance criteria #4 – Azimuthal power shape, 56 kW_t steady-state
 - 3.6.1 Upon successfully meeting Acceptance Criteria #3 – Cosine 56 kW_t steady-state, return to linear power over a 2 hour period.
 - 3.6.2 Allow additional 4 hours at uniform (linear) power for system to settle
 - 3.6.3 Apply azimuthal power profile, beginning with P(N) = 1.2 P(S). Ensure total power to heater banks remains constant. Closely monitor plate TC’s at all times, verifying that no abnormal levels of breakage occurs. Using discretion, ensure that heated plate maintains allowable levels of thermal stress. If conditions suggest unsafe operation, lead operator may return to linear power. If conditions suggest minimal change onto either system behavior and/or thermal gradients, operator may choose to increase power skew, up to P(N) = 1.5 P(S).
 - 3.6.4 Monitor energy balance within heated test section as provided by LabVIEW, and perform secondary verifications by hand calculations. $Q = \dot{m}C_p \Delta T$, where the temperature rise is as measured across the riser inlet to upper plenum outlet.

For acceptance of steady-state conditions this value is to be within 5% of the target goal for the given test.

- 3.6.5 Monitor long-term time history of flow rate, temperatures, and energy balance. For acceptance of steady-state conditions, these values are to not change by more than 5% over the course of 6 hours. Given the variations in atmospheric conditions, natural effects will induce fluctuations in these measurements and ultimately it is up to the lead experimenter's discretion to determine when acceptable steady-state conditions have been met.

Steady-state acceptance criteria Stable in, ΔT , \dot{Q}_{Heater}
0.35.98 kg/min, 22.77°C, \dot{Q}_{Heater} : 46.03 kW

Time and date met 6hr: 113hr, 1/22/16, @ 04:45am

Lead experimenter signature



3.7 Unexpected event response

- 3.7.1 In the event of non-emergency, unexpected events, document these in writing and take best-approach actions to mitigate the situations. Inform lead operator and test manager.
- 3.7.2 If thermal conditions on heated plate, heated plate thermocouples, or ceramic heaters are seemed unsafe during either axial cosine or radial azimuthal power shaping, lead operator may use discretion and return to linear power profile

3.8 Emergency event response

- 3.8.1 In the event of site-wide emergency (e.g. tornado or snow warning), proceed as expected and no human intervention is required
- 3.8.2 In the event of local, building 308 emergencies make best efforts to ensure safety of all personnel, and if deemed necessary, power down heaters for safety.
- 3.8.3 In the event of loss of 120VAC power, resume test operations if local UPS backups are successfully able to maintain active power to ALL test related systems for the period of power outage. If 120VAC power is lost for a period greater than the capacity of UPS systems, active in-site monitoring may take place for a period of no more than 60 minutes. After this point, manual power down of heaters must be performed to prevent unmonitored damage to heater system.
- 3.8.4 In the event of 240/480 VAC power loss, test will be concluded and documented as unsuccessful.

- 3.9 Document any abnormalities, deviations, other findings discovered, or comments on tasks in 6.0 Monitoring procedures during test (if additional lines requirement, document continuation and location)

• ~~A~~ Partial load failure on Manin 4-N observed
by impedance (Z) change from 26 Ω to 52 Ω
occurred at $t_{run} = 83.98$ hr, 23h 44min on 01/20/2016

• Azimuthal skew limit at 45% / 55%, then
finally steady state at South: 60%, North: 40%

Date: 1/22 Initial: RL

NSTF TEST PROCEDURE FOR DATA COLLECTION (NQA-1, TYPE A)	Identifier:	ANL-NSTF-000000-TEST-004	Page 18 of 23
	Revision:	02	
	Effective Date:	January 14 th 2016	

5.0 Post-test data achieve (to be performed 4 hours after power down)

5.1 LabVIEW logging closure

5.1.1 Conclude logging on LabVIEW

5.1.2 Verify that all expected data files have been written (1 excel file per day)

Date: 1/22 Initial: DL

5.2 LUNA logging closure

5.2.1 Conclude data acquisition and logging on LUNA

5.2.2 Verify that all expected data files have been written (1 .orb2 file per fiber per 20 minute period logged, 1 .csv file per fiber for full logging period)

5.2.3 Copy data files to external hard drive, and copy onto primary control computer into folder designated for test

Date: 1/22 Initial: DL

5.3 Davis Weather data download

5.3.1 Launch "WeatherStation.exe"

5.3.2 Connect to station '308-NSTF'

5.3.3 Download full data set, verify period spans test duration

5.3.4 Move file, 'C:\WeatherLink\308NSTF\download.txt' to designated test folder

Date: 1/22 Initial: DL

5.4 Backup and archive

5.4.1 Launch CiscoVPN service and authenticate

5.4.2 Launch SyncToy and perform data sync. Verify that all appropriate test files have been copied onto remote system

Date: 1/22 Initial: DL

5.5 Document any abnormalities, deviations, other findings discovered, or comments on tasks in task 8.0 Post-test data archive

All okay

Date: 1/22 Initial: DL

6.0 **Post-test, cold and zero-flow verification and survey** (to be performed at cold conditions)

6.1 Physical configuration verification

- 6.1.1 Visually inspect the inlet, exit plenum, insulation panels, and chimney duct work for evidence of damage
- 6.1.2 Verify that all differential pressure taps, flow meter connections, and other visually viewable wiring or components remained in position
- 6.1.3 Confirm position of fan loafers, and verify they did not shift during test
- 6.1.4 Perform general inspection for other abnormalities

Date: 1/27 Initial: DL

6.2 Verify that instrumentation did not exceed designed operating limits

- 6.2.1 Type-K thermocouples: 1,350°C
- 6.2.2 Heat flux sensors: 300°C
- 6.2.3 Series 668 pressure transmitters: 68 kPa
- 6.2.4 Series 607 pressure transmitters: 68 kPa
- 6.2.5 Sierra 640S flow meter: 50°C (ambient), 177°C (process)

Date: 1/27 Initial: DL

6.3 Continuity and general instrument check

- 6.3.1 Using LabVIEW, check for continuity on all 40 heater banks
- 6.3.2 Document any thermocouples or devices with saturated or '0' voltage signals

Date: 1/27 Initial: DL

6.4 LUNA measurement verification

- 6.4.1 Perform measurement across all fibers with LUNA system
- 6.4.2 Verify that readings are still physical and within expected ranges for cold, room temperatures
- 6.4.3 Document any non-physical or erroneous readings

Date: 1/27 Initial: DL

6.5 Zero-flow post-check

- 6.5.1 Establish zero-flow condition by closing all dampers and covering inlet down comer cap
- 6.5.2 Monitor thermocouples within LabVIEW. Verify that all read values nominally near ambient (variations will exist due to natural temperature gradients). Document any abnormalities, and if open TC detected, document the location and channel
- 6.5.3 Monitor flow meter and differential pressure. Verify that readings are within 2% of pre-test ranges

Date: 1/27 Initial: DL

- 6.6 Document any abnormalities, deviations, other findings discovered, or comments on tasks in task 9.0 Post-test, cold and zero-flow verification and survey

• New Open TC: /UN/ Mod 2 / a4 - 9N-R115

• #Fim 939 $\rightarrow 0 \pm 2.2mV$

941 $\rightarrow 2.2 \pm 0.5mV$

936 $\rightarrow 1.8 \pm 1mV$

938 $\rightarrow 0 \pm 10mV$

• DP #12 $\rightarrow 1.8Pa$

#1-11 $\rightarrow 1.1Pa$

• Eurotherm Mach 4-N₁ PLP!!

Date: 1/27 Initial: DL

NSTF TEST PROCEDURE FOR DATA COLLECTION (NQA-1, TYPE A)	Identifier:	ANL-NSTF-000000-TEST-004	Page 21 of 23
	Revision:	02	
	Effective Date:	January 14 th 2016	

7.0 Test Conclusion

Test Series & No Data Quality 022

Test Dates Jan. 17th - 22nd 2016

- Fully within scope and procedures (submit for Type A evaluation)
- Suggested Classification Areas outside scope or procedures (submit for trend evaluation)
- Failed (data not suitable for evaluation or use)

Date: 1/27 Initial: DL

Work Performed by:  Date: 01/29/2016

_____ Date: _____

_____ Date: _____

_____ Date: _____

_____ Date: _____

_____ Date: _____

_____ Date: _____

Work Approved by:  Date: 02/03/2016

Facility Manager

NSTF TEST PROCEDURE FOR DATA COLLECTION (NQA-1, TYPE A)	Identifier:	ANL-NSTF-000000-TEST-004	Page 22 of 23
	Revision:	02	
	Effective Date:	January 14 th 2016	

Attachment documents (record description and page count below, then attached)

Electronic test by attached

Other comments or notes

MA

Appendix F: DAQ Channel Listing

cDAQ	Slot	Pin	TC #	Name	Type	Description	Range	Accuracy	PO #
S. Up	1	0	74	TS-hot-wall-SC-3556	K	Twall upper heated section south of centerline at 3556 mm	0-1250°C	±2.2°C / 0.75%	2A-36163
S. Up	1	1	76	TS-hot-wall-SE-3632	K	Twall upper heated section south edge at 3632 mm	0-1250°C	±2.2°C / 0.75%	2A-36163
S. Up	1	2	78	TS-hot-wall-SM-3708	K	Twall upper heated section mid-south side at 3708 mm	0-1250°C	±2.2°C / 0.75%	2A-36163
S. Up	1	3	79	TS-hot-wall-SC-3708	K	Twall upper heated section south of centerline at 3708 mm	0-1250°C	±2.2°C / 0.75%	2A-36163
S. Up	1	4	80	TS-hot-wall-SC-3708-o	K	Twall upper heated section south of centerline outer surface at 3708 mm	0-1250°C	±2.2°C / 0.75%	2A-36163
S. Up	1	5	83	TS-hot-wall-SE-3937	K	Twall upper heated section south edge at 3937 mm	0-1250°C	±2.2°C / 0.75%	2A-36163
S. Up	1	6	85	TS-hot-wall-SC-4013	K	Twall upper heated section south of centerline at 4013 mm	0-1250°C	±2.2°C / 0.75%	2A-36163
S. Up	1	7	87	TS-hot-wall-SE-4293	K	Twall upper heated section south edge at 4293 mm	0-1250°C	±2.2°C / 0.75%	2A-36163
S. Up	1	8	89	TS-hot-wall-SC-4369	K	Twall upper heated section south of centerline at 4369 mm	0-1250°C	±2.2°C / 0.75%	2A-36163
S. Up	1	9	92	TS-hot-wall-SE-4597	K	Twall upper heated section south edge at 4597 mm	0-1250°C	±2.2°C / 0.75%	2A-36163
S. Up	1	10	94	TS-hot-wall-SC-4674	K	Twall upper heated section south of centerline at 4674 mm	0-1250°C	±2.2°C / 0.75%	2A-36163
S. Up	1	11	96	TS-hot-wall-SE-4953	K	Twall upper heated section south edge at 4953 mm	0-1250°C	±2.2°C / 0.75%	2A-36163
S. Up	1	12	98	TS-hot-wall-SM-5029	K	Twall upper heated section mid-south side at 5029 mm	0-1250°C	±2.2°C / 0.75%	2A-36163
S. Up	1	13	99	TS-hot-wall-SC-5029	K	Twall upper heated section south of centerline at 5029 mm	0-1250°C	±2.2°C / 0.75%	2A-36163
S. Up	1	14	100	TS-hot-wall-SC-5029-o	K	Twall upper heated section south of centerline outer surface at 5029 mm	0-1250°C	±2.2°C / 0.75%	2A-36163
S. Up	1	15	103	TS-hot-wall-SE-5258	K	Twall upper heated section south edge at 5258 mm	0-1250°C	±2.2°C / 0.75%	2A-36163
S. Up	2	0	105	TS-hot-wall-SC-5334	K	Twall upper heated section south of centerline at 5334 mm	0-1250°C	±2.2°C / 0.75%	2A-36163
S. Up	2	1	107	TS-hot-wall-SE-5613	K	Twall upper heated section south edge at 5613 mm	0-1250°C	±2.2°C / 0.75%	2A-36163
S. Up	2	2	109	TS-hot-wall-SC-5690	K	Twall upper heated section south of centerline at 5690 mm	0-1250°C	±2.2°C / 0.75%	2A-36163
S. Up	2	3	112	TS-hot-wall-SE-5918	K	Twall upper heated section south edge at 5918 mm	0-1250°C	±2.2°C / 0.75%	2A-36163
S. Up	2	4	114	TS-hot-wall-SC-5994	K	Twall upper heated section south of centerline at 5994 mm	0-1250°C	±2.2°C / 0.75%	2A-36163
S. Up	2	5	116	TS-hot-wall-SE-6274	K	Twall upper heated section south edge at 6274 mm	0-1250°C	±2.2°C / 0.75%	2A-36163
S. Up	2	6	118	TS-hot-wall-SC-6350	K	Twall upper heated section south of centerline at 6350 mm	0-1250°C	±2.2°C / 0.75%	2A-36163
S. Up	2	7	120	TS-hot-wall-SE-6579	K	Twall upper heated section south edge at 6579 mm	0-1250°C	±2.2°C / 0.75%	2A-36163
S. Up	2	8	122	TS-hot-wall-SM-6655	K	Twall upper heated section mid-south side at 6655 mm	0-1250°C	±2.2°C / 0.75%	2A-36163
S. Up	2	9	123	TS-hot-wall-SC-6655	K	Twall upper heated section south of centerline at 6655 mm	0-1250°C	±2.2°C / 0.75%	2A-36163
S. Up	2	10	124	TS-hot-wall-SC-6655-o	K	Twall upper heated section south of centerline outer surface at 6655 mm	0-1250°C	±2.2°C / 0.75%	2A-36163
S. Up	2	11				<i>empty</i>			
S. Up	1	11				<i>empty</i>			
S. Up	2	12				<i>empty</i>			
S. Up	2	13				<i>empty</i>			

S. Up	2	14	<i>empty</i>						
S. Up	2	15	<i>empty</i>						
S. Up	3	0	223	SW 4676	K	South west I-beam, z=184.1" (4676)	0-1250°C	±2.2°C / 0.75%	3A-31214
S. Up	3	1	224	SW 6556	K	Wall temperatures along I-beams on adiabatic side walls	0-1250°C	±2.2°C / 0.75%	3A-31214
S. Up	3	2	229	SC 3736	K	Wall temperatures along I-beams on adiabatic side walls	0-1250°C	±2.2°C / 0.75%	3A-31214
S. Up	3	3	230	SC 4676	K	Wall temperatures along I-beams on adiabatic side walls	0-1250°C	±2.2°C / 0.75%	3A-31214
S. Up	3	4	231	SC 5616	K	Wall temperatures along I-beams on adiabatic side walls	0-1250°C	±2.2°C / 0.75%	3A-31214
S. Up	3	5	232	SC 6556	K	Wall temperatures along I-beams on adiabatic side walls	0-1250°C	±2.2°C / 0.75%	3A-31214
S. Up	3	6	237	SE 3736	K	Wall temperatures along I-beams on adiabatic side walls	0-1250°C	±2.2°C / 0.75%	3A-31214
S. Up	3	7	238	SE 4676	K	Wall temperatures along I-beams on adiabatic side walls	0-1250°C	±2.2°C / 0.75%	3A-31214
S. Up	3	8	239	SE 5616	K	Wall temperatures along I-beams on adiabatic side walls	0-1250°C	±2.2°C / 0.75%	3A-31214
S. Up	3	9	240	SE 6556	K	Wall temperatures along I-beams on adiabatic side walls	0-1250°C	±2.2°C / 0.75%	3A-31214
S. Up	3	10	<i>empty</i>						
S. Up	3	11	<i>empty</i>						
S. Up	3	12	<i>empty</i>						
S. Up	3	13	<i>empty</i>						
S. Up	3	14	<i>empty</i>						
S. Up	3	15	<i>empty</i>						
S. Up	4	0	301	TG-UP-W-1	K	Upper plenum gas temperature west side 1449 mm below lid	0-1250°C	±2.2°C / 0.75%	3A-35734
S. Up	4	1	302	TG-UP-W-2	K	Upper plenum gas temperature west side 1195 mm below lid	0-1250°C	±2.2°C / 0.75%	3A-35734
S. Up	4	2	303	TG-UP-W-3	K	Upper plenum gas temperature west side 941 mm below lid	0-1250°C	±2.2°C / 0.75%	3A-35734
S. Up	4	3	304	TG-UP-W-4	K	Upper plenum gas temperature west side 687 mm below lid	0-1250°C	±2.2°C / 0.75%	3A-35734
S. Up	4	4	305	TG-UP-W-5	K	Upper plenum gas temperature west side 433 mm below lid	0-1250°C	±2.2°C / 0.75%	3A-35734
S. Up	4	5	306	TG-UP-W-6	K	Upper plenum gas temperature west side 179 mm below lid	0-1250°C	±2.2°C / 0.75%	3A-35734
S. Up	4	6	307	TG-UP-CS-1	K	Upper plenum gas temperature center-south 1449 mm below lid	0-1250°C	±2.2°C / 0.75%	3A-35734
S. Up	4	7	308	TG-UP-CS-2	K	Upper plenum gas temperature center-south 1195 mm below lid	0-1250°C	±2.2°C / 0.75%	3A-35734
S. Up	4	8	309	TG-UP-CS-3	K	Upper plenum gas temperature center-south 941 mm below lid	0-1250°C	±2.2°C / 0.75%	3A-35734
S. Up	4	9	310	TG-UP-CS-4	K	Upper plenum gas temperature center-south 687 mm below lid	0-1250°C	±2.2°C / 0.75%	3A-35734
S. Up	4	10	311	TG-UP-CS-5	K	Upper plenum gas temperature center-south 433 mm below lid	0-1250°C	±2.2°C / 0.75%	3A-35734
S. Up	4	11	312	TG-UP-CS-6	K	Upper plenum gas temperature center-south 179 mm below lid	0-1250°C	±2.2°C / 0.75%	3A-35734
S. Up	4	12	313	TG-UP-ES-1	K	Upper plenum gas temperature east-center 1449 mm below lid	0-1250°C	±2.2°C / 0.75%	3A-35734
S. Up	4	13	314	TG-UP-ES-2	K	Upper plenum gas temperature east-center 1195 mm below lid	0-1250°C	±2.2°C / 0.75%	3A-35734
S. Up	4	14	315	TG-UP-ES-3	K	Upper plenum gas temperature east-center 941 mm below lid	0-1250°C	±2.2°C / 0.75%	3A-35734
S. Up	4	15	316	TG-UP-ES-4	K	Upper plenum gas temperature east-center 687 mm below lid	0-1250°C	±2.2°C / 0.75%	3A-35734
S. Up	5	0	317	TG-UP-ES-5	K	Upper plenum gas temperature east-center 433 mm below lid	0-1250°C	±2.2°C / 0.75%	3A-35734
S. Up	5	1	318	TG-UP-ES-6	K	Upper plenum gas temperature east-center 179 mm below lid	0-1250°C	±2.2°C / 0.75%	3A-35734
S. Up	5	2	319	TS-UP-LNW-1	K	Upper plenum lid wall inner surface temperature, north west side	0-1250°C	±2.2°C / 0.75%	3A-35734
S. Up	5	3	320	TS-UP-LCW-2	K	Upper plenum lid wall inner surface temperature, center west side	0-1250°C	±2.2°C / 0.75%	3A-35734

S. Up	5	4	321	TS-UP-LSW-3	K	Upper plenum lid wall inner surface temperature, south west side	0-1250°C	±2.2°C / 0.75%	3A-35734
S. Up	5	5	322	TS-UP-LNE-1	K	Upper plenum lid wall inner surface temperature, north east side	0-1250°C	±2.2°C / 0.75%	3A-35734
S. Up	5	6	323	TS-UP-LCE-2	K	Upper plenum lid wall inner surface temperature, center east center	0-1250°C	±2.2°C / 0.75%	3A-35734
S. Up	5	7	324	TS-UP-LSE-3	K	Upper plenum lid wall inner surface temperature, south east side	0-1250°C	±2.2°C / 0.75%	3A-35734
S. Up	5	8				<i>empty</i>			
S. Up	5	9				<i>empty</i>			
S. Up	5	10				<i>empty</i>			
S. Up	5	11				<i>empty</i>			
S. Up	5	12				<i>empty</i>			
S. Up	5	13				<i>empty</i>			
S. Up	5	14				<i>empty</i>			
S. Up	5	15				<i>empty</i>			
S. Up	6	0	376	RCCSD-EX-9	K	Gas temperature in duct 9 outlet at 6900 mm	0-1250°C	±2.2°C / 0.75%	3A-35734
S. Up	6	1	377	RCCSD-EX-10	K	Gas temperature in duct 10 outlet at 6900 mm	0-1250°C	±2.2°C / 0.75%	3A-35734
S. Up	6	2	378	RCCSD-EX-11	K	Gas temperature in duct 11 outlet at 6900 mm	0-1250°C	±2.2°C / 0.75%	3A-35734
S. Up	6	3	379	RCCSD-EX-12	K	Gas temperature in duct 12 outlet at 6900 mm	0-1250°C	±2.2°C / 0.75%	3A-35734
S. Up	6	4	380	TS-UP-STW-1	K	Upper plenum South wall inner surface temperature, top west side	0-1250°C	±2.2°C / 0.75%	3A-35734
S. Up	6	5	381	TS-UP-SCW-2	K	Upper plenum South wall inner surface temperature, top east side	0-1250°C	±2.2°C / 0.75%	3A-35734
S. Up	6	6	382	TS-UP-SBW-3	K	Upper plenum South wall inner surface temperature, center west side	0-1250°C	±2.2°C / 0.75%	3A-35734
S. Up	6	7	383	TS-UP-STE-4	K	Upper plenum South wall inner surface temperature, center east side	0-1250°C	±2.2°C / 0.75%	3A-35734
S. Up	6	8	384	TS-UP-SCE-5	K	Upper plenum South wall inner surface temperature, bottom west side	0-1250°C	±2.2°C / 0.75%	3A-35734
S. Up	6	9	385	TS-UP-SBE-6	K	Upper plenum South wall inner surface temperature, bottom east side	0-1250°C	±2.2°C / 0.75%	3A-35734
S. Up	6	10				<i>empty</i>			
S. Up	6	11				<i>empty</i>			
S. Up	6	12				<i>empty</i>			
S. Up	6	13				<i>empty</i>			
S. Up	6	14				<i>empty</i>			
S. Up	6	15				<i>empty</i>			
S. Up	7	0	368	RCCSD-EX-1	K	Gas temperature in duct 1 outlet at 6900 mm	0-1250°C	±2.2°C / 0.75%	3A-35734
S. Up	7	1	369	RCCSD-EX-2	K	Gas temperature in duct 2 outlet at 6900 mm	0-1250°C	±2.2°C / 0.75%	3A-35734
S. Up	7	2	370	RCCSD-EX-3	K	Gas temperature in duct 3 outlet at 6900 mm	0-1250°C	±2.2°C / 0.75%	3A-35734
S. Up	7	3	371	RCCSD-EX-4	K	Gas temperature in duct 4 outlet at 6900 mm	0-1250°C	±2.2°C / 0.75%	3A-35734
S. Up	7	4	372	RCCSD-EX-5	K	Gas temperature in duct 5 outlet at 6900 mm	0-1250°C	±2.2°C / 0.75%	3A-35734
S. Up	7	5	373	RCCSD-EX-6	K	Gas temperature in duct 6 outlet at 6900 mm	0-1250°C	±2.2°C / 0.75%	3A-35734
S. Up	7	6	374	RCCSD-EX-7	K	Gas temperature in duct 7 outlet at 6900 mm	0-1250°C	±2.2°C / 0.75%	3A-35734
S. Up	7	7	375	RCCSD-EX-8	K	Gas temperature in duct 8 outlet at 6900 mm	0-1250°C	±2.2°C / 0.75%	3A-35734
S. Up	7	8	401	TG-D-plen ex-S	K	Plenum exit gas temperature south duct	0-1250°C	±2.2°C / 0.75%	F3-113043
S. Up	7	9				<i>empty</i>			

S. Up	7	10					empty			
S. Up	7	11					empty			
S. Up	7	12					empty			
S. Up	7	13					empty			
S. Up	7	14					empty			
S. Up	7	15					empty			
S. Up	8	0					empty			
S. Up	8	1					empty			
S. Up	8	2					empty			
S. Up	8	3					empty			
S. Up	8	4					empty			
S. Up	8	5					empty			
S. Up	8	6					empty			
S. Up	8	7					empty			
S. Low	1	0	1	TS-hot-wall-SC-127	K	Twall lower heated section south of centerline at 127 mm	0-1250°C	±2.2°C / 0.75%	1A-40882	
S. Low	1	1	3	TS-hot-wall-SE-203	K	Twall lower heated section south edge at 203 mm	0-1250°C	±2.2°C / 0.75%	1A-40882	
S. Low	1	2	5	TS-hot-wall-SC-279	K	Twall lower heated section south of centerline at 279 mm	0-1250°C	±2.2°C / 0.75%	1A-40882	
S. Low	1	3	6	TS-hot-wall-SM-279	K	Twall lower heated section mid-south side at 279 mm	0-1250°C	±2.2°C / 0.75%	1A-40882	
S. Low	1	4	10	TS-hot-wall-SC-432	K	Twall lower heated section south of centerline at 432 mm	0-1250°C	±2.2°C / 0.75%	1A-40882	
S. Low	1	5	12	TS-hot-wall-SE-508	K	Twall lower heated section south edge at 508 mm	0-1250°C	±2.2°C / 0.75%	1A-40882	
S. Low	1	6	14	TS-hot-wall-SC-584	K	Twall lower heated section south of centerline at 584 mm	0-1250°C	±2.2°C / 0.75%	1A-40882	
S. Low	1	7	16	TS-hot-wall-SC-787	K	Twall lower heated section south of centerline at 787 mm	0-1250°C	±2.2°C / 0.75%	1A-40882	
S. Low	1	8	18	TS-hot-wall-SE-864	K	Twall lower heated section south edge at 864 mm	0-1250°C	±2.2°C / 0.75%	1A-40882	
S. Low	1	9	21	TS-hot-wall-SC-940	K	Twall lower heated section south of centerline at 940 mm	0-1250°C	±2.2°C / 0.75%	1A-40882	
S. Low	1	10	20	TS-hot-wall-SM-940	K	Twall lower heated section mid-south side at 940 mm	0-1250°C	±2.2°C / 0.75%	1A-40882	
S. Low	1	11	22	TS-hot-wall-SC-940-o	K	Twall lower heated section south of centerline outer surface at 940 mm	0-1250°C	±2.2°C / 0.75%	1A-40882	
S. Low	1	12	25	TS-hot-wall-SC-1092	K	Twall lower heated section south of centerline at 1092 mm	0-1250°C	±2.2°C / 0.75%	1A-40882	
S. Low	1	13	27	TS-hot-wall-SE-1168	K	Twall lower heated section south edge at 1168 mm	0-1250°C	±2.2°C / 0.75%	1A-40882	
S. Low	1	14	29	TS-hot-wall-SC-1245	K	Twall lower heated section south of centerline at 1245 mm	0-1250°C	±2.2°C / 0.75%	1A-40882	
S. Low	1	15	31	TS-hot-wall-SC-1448	K	Twall lower heated section south of centerline at 1448 mm	0-1250°C	±2.2°C / 0.75%	1A-40882	
S. Low	2	0	33	TS-hot-wall-SE-1524	K	Twall lower heated section south edge at 1524 mm	0-1250°C	±2.2°C / 0.75%	1A-40882	
S. Low	2	1	35	TS-hot-wall-SC-1600	K	Twall lower heated section south of centerline at 1600 mm	0-1250°C	±2.2°C / 0.75%	1A-40882	
S. Low	2	2	38	TS-hot-wall-SC-1753	K	Twall lower heated section south of centerline at 1753 mm	0-1250°C	±2.2°C / 0.75%	1A-40882	
S. Low	2	3	37	TS-hot-wall-SM-1753	K	Twall lower heated section mid-south side at 1753 mm	0-1250°C	±2.2°C / 0.75%	1A-40882	
S. Low	2	4	42	TS-hot-wall-SE-1829	K	Twall lower heated section south edge at 1829 mm	0-1250°C	±2.2°C / 0.75%	1A-40882	
S. Low	2	5	44	TS-hot-wall-SC-1905	K	Twall lower heated section south of centerline at 1905 mm	0-1250°C	±2.2°C / 0.75%	1A-40882	
S. Low	2	6	46	TS-hot-wall-SC-2108	K	Twall lower heated section south of centerline at 2108 mm	0-1250°C	±2.2°C / 0.75%	1A-40882	
S. Low	2	7	48	TS-hot-wall-SE-2184	K	Twall lower heated section south edge at 2184 mm	0-1250°C	±2.2°C / 0.75%	1A-40882	

S. Low	2	8	50	TS-hot-wall-SC-2261	K	Twall lower heated section south of centerline at 2261 mm	0-1250°C	±2.2°C / 0.75%	1A-40882
S. Low	2	9	52	TS-hot-wall-SC-2413	K	Twall lower heated section south of centerline at 2413 mm	0-1250°C	±2.2°C / 0.75%	1A-40882
S. Low	2	10	53	TS-hot-wall-SC-2413	K	Twall lower heated section south of centerline outer surface at 2413 mm	0-1250°C	±2.2°C / 0.75%	1A-40882
S. Low	2	11	55	TS-hot-wall-SE-2489	K	Twall lower heated section south edge at 2489 mm	0-1250°C	±2.2°C / 0.75%	1A-40882
S. Low	2	12	57	TS-hot-wall-SC-2565	K	Twall lower heated section south of centerline at 2565 mm	0-1250°C	±2.2°C / 0.75%	1A-40882
S. Low	2	13	59	TS-hot-wall-SC-2769	K	Twall lower heated section south of centerline at 2769 mm	0-1250°C	±2.2°C / 0.75%	1A-40882
S. Low	2	14	61	TS-hot-wall-SE-2845	K	Twall lower heated section south edge at 2845 mm	0-1250°C	±2.2°C / 0.75%	1A-40882
S. Low	2	15	63	TS-hot-wall-SC-2921	K	Twall lower heated section south of centerline at 2921 mm	0-1250°C	±2.2°C / 0.75%	1A-40882
S. Low	3	0	66	TS-hot-wall-SC-3073	K	Twall lower heated section south of centerline at 3073 mm	0-1250°C	±2.2°C / 0.75%	1A-40882
S. Low	3	1	65	TS-hot-wall-SM-3073	K	Twall lower heated section mid-south side at 3073 mm	0-1250°C	±2.2°C / 0.75%	1A-40882
S. Low	3	2	70	TS-hot-wall-SE-3150	K	Twall lower heated section south edge at 3150 mm	0-1250°C	±2.2°C / 0.75%	1A-40882
S. Low	3	3	72	TS-hot-wall-SC-3226	K	Twall lower heated section south of centerline at 3226 mm	0-1250°C	±2.2°C / 0.75%	1A-40882
S. Low	3	4	221	SW 1245	K	Wall temperatures along I-beams on adiabatic side walls	0-1250°C	±2.2°C / 0.75%	3A-31214
S. Low	3	5	222	SW 3124	K	Wall temperatures along I-beams on adiabatic side walls	0-1250°C	±2.2°C / 0.75%	3A-31214
S. Low	3	6	225	SC 305	K	Wall temperatures along I-beams on adiabatic side walls	0-1250°C	±2.2°C / 0.75%	3A-31214
S. Low	3	7	226	SC 1245	K	Wall temperatures along I-beams on adiabatic side walls	0-1250°C	±2.2°C / 0.75%	3A-31214
S. Low	3	8	227	SC 2184	K	Wall temperatures along I-beams on adiabatic side walls	0-1250°C	±2.2°C / 0.75%	3A-31214
S. Low	3	9	228	SC 3124	K	Wall temperatures along I-beams on adiabatic side walls	0-1250°C	±2.2°C / 0.75%	3A-31214
S. Low	3	10	233	SE 305	K	Wall temperatures along I-beams on adiabatic side walls	0-1250°C	±2.2°C / 0.75%	3A-31214
S. Low	3	11	234	SE 1245	K	Wall temperatures along I-beams on adiabatic side walls	0-1250°C	±2.2°C / 0.75%	3A-31214
S. Low	3	12	235	SE 2184	K	Wall temperatures along I-beams on adiabatic side walls	0-1250°C	±2.2°C / 0.75%	3A-31214
S. Low	3	13	236	SE 3124	K	Wall temperatures along I-beams on adiabatic side walls	0-1250°C	±2.2°C / 0.75%	3A-31214
S. Low	3	14	<i>empty</i>						
S. Low	3	15	<i>empty</i>						
S. Low	4	0	261	HF-duct1-hot-100	TP	Heat flux on hot side of duct 1 at 100 mm height, shiny	0-300 kW/m2	±5%	2A-40996
S. Low	4	1	262	HF-duct1-hot-100	TP	Heat flux on hot side of duct 1 at 100 mm height	0-300 kW/m2	±5%	2A-40996
S. Low	4	2	263	HF-duct1-hot-3500	TP	Heat flux on hot side of duct 1 at 3500 mm height	0-300 kW/m2	±5%	2A-40996
S. Low	4	3	264	HF-duct1-hot-7000	TP	Heat flux on hot side of duct 1 at 7000 mm height	0-300 kW/m2	±5%	2A-40996
S. Low	4	4	265	HF-duct1-cold-7000	TP	Heat flux on cold side of duct 1 at 7000 mm height, shiny	0-300 kW/m2	±5%	2A-40996
S. Low	4	5	266	HF-duct1-cold-7000	TP	Heat flux on cold side of duct 1 at 7000 mm height	0-300 kW/m2	±5%	2A-40996
S. Low	4	6	267	HF-duct7-hot-3500	TP	Heat flux on hot side of duct 7 at 3500 mm height, shiny	0-300 kW/m2	±5%	2A-40996
S. Low	4	7	268	HF-duct7-hot-3500	TP	Heat flux on hot side of duct 7 at 3500 mm height	0-300 kW/m2	±5%	2A-40996
S. Low	4	16	269	HF-duct7-hot-7000	TP	Heat flux on hot side of duct 7 at 7000 mm height	0-300 kW/m2	±5%	2A-40996
S. Low	4	17	270	HF-duct7-cold-3500	TP	Heat flux on cold side of duct 7 at 3500 mm height, shiny	0-300 kW/m2	±5%	2A-40996
S. Low	4	18	271	HF-duct7-cold-3500	TP	Heat flux on cold side of duct 7 at 3500 mm height	0-300 kW/m2	±5%	2A-40996
S. Low	4	19	272	HF-duct11-hot-3500	TP	Heat flux on hot side of duct 11 at 3500 mm height	0-300 kW/m2	±5%	2A-40996
S. Low	4	20	273	HF-duct11-hot-7000	TP	Heat flux on hot side of duct 11 at 7000 mm height, shiny	0-300 kW/m2	±5%	2A-40996
S. Low	4	21	274	HF-duct11-hot-7000	TP	Heat flux on hot side of duct 11 at 7000 mm height	0-300 kW/m2	±5%	2A-40996

S. Low	4	22	275	HF-duct11-cold-3500	TP	Heat flux on cold side of duct 11 at 350 mm height	0-300 kW/m ²	±5%	2A-40996
S. Low	4	23	276	HF-duct11-cold-7000	TP	Heat flux on cold side of duct 11 at 700 mm height	0-300 kW/m ²	±5%	2A-40996
S. Low	5	0	277	TS-duct1-hot-100	K	Temperature channel on heat flux meter	0-300 kW/m ²	±5%	2A-40996
S. Low	5	1	278	TS-duct1-hot-100	K	Temperature channel on heat flux meter	0-300°C	±2.2°C / 0.75%	2A-40996
S. Low	5	2	279	TS-duct1-hot-3500	K	Temperature channel on heat flux meter	0-300°C	±2.2°C / 0.75%	2A-40996
S. Low	5	3	280	TS-duct1-hot-7000	K	Temperature channel on heat flux meter	0-300°C	±2.2°C / 0.75%	2A-40996
S. Low	5	4	281	TS-duct1-cold-7000	K	Temperature channel on heat flux meter	0-300°C	±2.2°C / 0.75%	2A-40996
S. Low	5	5	282	TS-duct1-cold-7000	K	Temperature channel on heat flux meter	0-300°C	±2.2°C / 0.75%	2A-40996
S. Low	5	6	283	TS-duct7-hot-3500	K	Temperature channel on heat flux meter	0-300°C	±2.2°C / 0.75%	2A-40996
S. Low	5	7	284	TS-duct7-hot-3500	K	Temperature channel on heat flux meter	0-300°C	±2.2°C / 0.75%	2A-40996
S. Low	5	8	285	TS-duct7-hot-7000	K	Temperature channel on heat flux meter	0-300°C	±2.2°C / 0.75%	2A-40996
S. Low	5	9	286	TS-duct7-cold-3500	K	Temperature channel on heat flux meter	0-300°C	±2.2°C / 0.75%	2A-40996
S. Low	5	10	287	TS-duct7-cold-3500	K	Temperature channel on heat flux meter	0-300°C	±2.2°C / 0.75%	2A-40996
S. Low	5	11	288	TS-duct11-hot-3500	K	Temperature channel on heat flux meter	0-300°C	±2.2°C / 0.75%	2A-40996
S. Low	5	12	289	TS-duct11-hot-7000	K	Temperature channel on heat flux meter	0-300°C	±2.2°C / 0.75%	2A-40996
S. Low	5	13	290	TS-duct11-hot-7000	K	Temperature channel on heat flux meter	0-300°C	±2.2°C / 0.75%	2A-40996
S. Low	5	14	291	TS-duct11-cold-3500	K	Temperature channel on heat flux meter	0-300°C	±2.2°C / 0.75%	2A-40996
S. Low	5	15	292	TS-duct11-cold-7000	K	Temperature channel on heat flux meter	0-300°C	±2.2°C / 0.75%	2A-40996
S. Low	6	0	1	FlowInlet	RTD	Inlet mass flow rate, Sierra 640s (0 - 1 kg/s)	0-1 kg/s	±1%	F1-272004
S. Low	6	1	2	Humidity	RH	Humidity bulk space of inlet plenum, Dwyer RHP (0-100%RH)	0-100% RH	±2%	4A-31704
S. Low	6	2	3	dP Riser 1	dP	Differential pressure riser ducts, Dwyer 668 (+/- 0.25 inWC)	± 0.25 in WC	±1%	4A-31410
S. Low	6	3	4	dP Riser 2	dP	Differential pressure riser ducts, Dwyer 668 (+/- 0.25 inWC)	± 0.25 in WC	±1%	4A-31410
S. Low	6	4	5	dP Riser 4	dP	Differential pressure riser ducts, Dwyer 668 (+/- 0.25 inWC)	± 0.25 in WC	±1%	4A-31410
S. Low	6	5	6	dP Riser 6	dP	Differential pressure riser ducts, Dwyer 668 (+/- 0.25 inWC)	± 0.25 in WC	±1%	4A-31410
S. Low	6	6	7	dP Riser 7	dP	Differential pressure riser ducts, Dwyer 668 (+/- 0.25 inWC)	± 0.25 in WC	±1%	4A-31410
S. Low	6	7	8	dP Riser 9	dP	Differential pressure riser ducts, Dwyer 668 (+/- 0.25 inWC)	± 0.25 in WC	±1%	4A-31410
S. Low	6	16	9	dP Riser 11	dP	Differential pressure riser ducts, Dwyer 668 (+/- 0.25 inWC)	± 0.25 in WC	±1%	4A-31410
S. Low	6	17	10	dP Riser 12	dP	Differential pressure riser ducts, Dwyer 668 (+/- 0.25 inWC)	± 0.25 in WC	±1%	4A-31410
S. Low	6	18	11	dP North Chim	dP	Differential pressure chimney, Dwyer 607 (+/- 0.1 inWC)	± 0.1 in WC	± 0.5%	4A-31410
S. Low	6	19	12	dP South Chim	dP	Differential pressure chimney, Dwyer 607 (+/- 0.1 inWC)	± 0.1 in WC	± 0.5%	4A-31410
S. Low	6	20				<i>empty</i>			
S. Low	6	21				<i>empty</i>			
S. Low	6	22				<i>empty</i>			
S. Low	6	23				<i>empty</i>			
S. Low	7	0				<i>empty</i>			
S. Low	7	1				<i>empty</i>			
S. Low	7	2				<i>empty</i>			
S. Low	7	3				<i>empty</i>			

N. Up	1	10	95	TS-hot-wall-NC-4674	K	Twall upper heated section north of centerline at 4674 mm	0-1250°C	±2.2°C / 0.75%	2A-36163
N. Up	1	11	97	TS-hot-wall-NE-4953	K	Twall upper heated section north edge at 4953 mm	0-1250°C	±2.2°C / 0.75%	2A-36163
N. Up	1	12	102	TS-hot-wall-NM-5029	K	Twall upper heated section mid-north side at 5029 mm	0-1250°C	±2.2°C / 0.75%	2A-36163
N. Up	1	13	101	TS-hot-wall-NC-5029	K	Twall upper heated section north of centerline at 5029 mm	0-1250°C	±2.2°C / 0.75%	2A-36163
N. Up	1	14	104	TS-hot-wall-NE-5258	K	Twall upper heated section north edge at 5258 mm	0-1250°C	±2.2°C / 0.75%	2A-36163
N. Up	1	15	106	TS-hot-wall-NC-5334	K	Twall upper heated section north of centerline at 5334 mm	0-1250°C	±2.2°C / 0.75%	2A-36163
N. Up	2	0	108	TS-hot-wall-NE-5613	K	Twall upper heated section north edge at 5613 mm	0-1250°C	±2.2°C / 0.75%	2A-36163
N. Up	2	1	110	TS-hot-wall-NC-5690	K	Twall upper heated section north of centerline at 5690 mm	0-1250°C	±2.2°C / 0.75%	2A-36163
N. Up	2	2	111	TS-hot-wall-SC-5690-o	K	Twall upper heated section north of centerline outer surface at 5690 mm	0-1250°C	±2.2°C / 0.75%	2A-36163
N. Up	2	3	113	TS-hot-wall-NE-5918	K	Twall upper heated section north edge at 5918 mm	0-1250°C	±2.2°C / 0.75%	2A-36163
N. Up	2	4	115	TS-hot-wall-NC-5994	K	Twall upper heated section north of centerline at 5994 mm	0-1250°C	±2.2°C / 0.75%	2A-36163
N. Up	2	5	117	TS-hot-wall-NE-6274	K	Twall upper heated section north edge at 6274 mm	0-1250°C	±2.2°C / 0.75%	2A-36163
N. Up	2	6	119	TS-hot-wall-NC-6350	K	Twall upper heated section north of centerline at 6350 mm	0-1250°C	±2.2°C / 0.75%	2A-36163
N. Up	2	7	121	TS-hot-wall-NE-6579	K	Twall upper heated section north edge at 6579 mm	0-1250°C	±2.2°C / 0.75%	2A-36163
N. Up	2	8	126	TS-hot-wall-NM-6655	K	Twall upper heated section mid-north side at 6655 mm	0-1250°C	±2.2°C / 0.75%	2A-36163
N. Up	2	9	125	TS-hot-wall-NC-6655	K	Twall upper heated section north of centerline at 6655 mm	0-1250°C	±2.2°C / 0.75%	2A-36163
N. Up	2	10	<i>empty</i>						
N. Up	2	11	<i>empty</i>						
N. Up	2	12	<i>empty</i>						
N. Up	2	13	<i>empty</i>						
N. Up	2	14	<i>empty</i>						
N. Up	2	15	<i>empty</i>						
N. Up	3	0	203	NW-3736	K	Wall temperatures along I-beams on adiabatic side walls	0-1250°C	±2.2°C / 0.75%	3A-31214
N. Up	3	1	204	NW-5616	K	Wall temperatures along I-beams on adiabatic side walls	0-1250°C	±2.2°C / 0.75%	3A-31214
N. Up	3	2	209	NC-3736	K	Wall temperatures along I-beams on adiabatic side walls	0-1250°C	±2.2°C / 0.75%	3A-31214
N. Up	3	3	210	NC-4676	K	Wall temperatures along I-beams on adiabatic side walls	0-1250°C	±2.2°C / 0.75%	3A-31214
N. Up	3	4	211	NC-5616	K	Wall temperatures along I-beams on adiabatic side walls	0-1250°C	±2.2°C / 0.75%	3A-31214
N. Up	3	5	212	NC-6556	K	Wall temperatures along I-beams on adiabatic side walls	0-1250°C	±2.2°C / 0.75%	3A-31214
N. Up	3	6	217	NE-3736	K	Wall temperatures along I-beams on adiabatic side walls	0-1250°C	±2.2°C / 0.75%	3A-31214
N. Up	3	7	218	NE-4676	K	Wall temperatures along I-beams on adiabatic side walls	0-1250°C	±2.2°C / 0.75%	3A-31214
N. Up	3	8	219	NE-5616	K	Wall temperatures along I-beams on adiabatic side walls	0-1250°C	±2.2°C / 0.75%	3A-31214
N. Up	3	9	220	NE-6556	K	Wall temperatures along I-beams on adiabatic side walls	0-1250°C	±2.2°C / 0.75%	3A-31214
N. Up	3	10	402	TG-D-plen ex-N	K	Plenum exit gas temperature north duct	0-1250°C	±2.2°C / 0.75%	3A-35734
N. Up	3	11	<i>empty</i>						
N. Up	3	12	<i>empty</i>						
N. Up	3	13	<i>empty</i>						
N. Up	3	14	<i>empty</i>						
N. Up	3	15	<i>empty</i>						

N. Up	4	0	325	TG-UP-CN-1	K	Upper plenum gas temperature center-north 1449 mm below lid	0-1250°C	±2.2°C / 0.75%	3A-35734
N. Up	4	1	326	TG-UP-CN-2	K	Upper plenum gas temperature center-north 1195 mm below lid	0-1250°C	±2.2°C / 0.75%	3A-35734
N. Up	4	2	327	TG-UP-CN-3	K	Upper plenum gas temperature center-north 941 mm below lid	0-1250°C	±2.2°C / 0.75%	3A-35734
N. Up	4	3	328	TG-UP-CN-4	K	Upper plenum gas temperature center-north 687 mm below lid	0-1250°C	±2.2°C / 0.75%	3A-35734
N. Up	4	4	329	TG-UP-CN-5	K	Upper plenum gas temperature center-north 433 mm below lid	0-1250°C	±2.2°C / 0.75%	3A-35734
N. Up	4	5	330	TG-UP-CN-6	K	Upper plenum gas temperature center-north 179 mm below lid	0-1250°C	±2.2°C / 0.75%	3A-35734
N. Up	4	6	331	TG-UP-CC-1	K	Upper plenum gas temperature center-center 1449 mm below lid	0-1250°C	±2.2°C / 0.75%	3A-35734
N. Up	4	7	332	TG-UP-CC-2	K	Upper plenum gas temperature center-center 1195 mm below lid	0-1250°C	±2.2°C / 0.75%	3A-35734
N. Up	4	8	333	TG-UP-CC-3	K	Upper plenum gas temperature center-center 941 mm below lid	0-1250°C	±2.2°C / 0.75%	3A-35734
N. Up	4	9	334	TG-UP-CC-4	K	Upper plenum gas temperature center-center 687 mm below lid	0-1250°C	±2.2°C / 0.75%	3A-35734
N. Up	4	10	335	TG-UP-CC-5	K	Upper plenum gas temperature center-center 433 mm below lid	0-1250°C	±2.2°C / 0.75%	3A-35734
N. Up	4	11	336	TG-UP-CC-6	K	Upper plenum gas temperature center-center 179 mm below lid	0-1250°C	±2.2°C / 0.75%	3A-35734
N. Up	4	12	337	TG-UP-EN-1	K	Upper plenum gas temperature east-north 1449 mm below lid	0-1250°C	±2.2°C / 0.75%	3A-35734
N. Up	4	13	338	TG-UP-EN-2	K	Upper plenum gas temperature east-north 1195 mm below lid	0-1250°C	±2.2°C / 0.75%	3A-35734
N. Up	4	14	339	TG-UP-EN-3	K	Upper plenum gas temperature east-north 941 mm below lid	0-1250°C	±2.2°C / 0.75%	3A-35734
N. Up	4	15	340	TG-UP-EN-4	K	Upper plenum gas temperature east-north 687 mm below lid	0-1250°C	±2.2°C / 0.75%	3A-35734
N. Up	5	0	341	TG-UP-EN-5	K	Upper plenum gas temperature east-north 433 mm below lid	0-1250°C	±2.2°C / 0.75%	3A-35734
N. Up	5	1	342	TG-UP-EN-6	K	Upper plenum gas temperature east-north 179 mm below lid	0-1250°C	±2.2°C / 0.75%	3A-35734
N. Up	5	2	343	TG-UP-EC-1	K	Upper plenum gas temperature east-center 1449 mm below lid	0-1250°C	±2.2°C / 0.75%	3A-35734
N. Up	5	3	344	TG-UP-EC-2	K	Upper plenum gas temperature east-center 1195 mm below lid	0-1250°C	±2.2°C / 0.75%	3A-35734
N. Up	5	4	345	TG-UP-EC-3	K	Upper plenum gas temperature east-center 941 mm below lid	0-1250°C	±2.2°C / 0.75%	3A-35734
N. Up	5	5	346	TG-UP-EC-4	K	Upper plenum gas temperature east-center 687 mm below lid	0-1250°C	±2.2°C / 0.75%	3A-35734
N. Up	5	6	347	TG-UP-EC-5	K	Upper plenum gas temperature east-center 433 mm below lid	0-1250°C	±2.2°C / 0.75%	3A-35734
N. Up	5	7	348	TG-UP-EC-6	K	Upper plenum gas temperature east-center 179 mm below lid	0-1250°C	±2.2°C / 0.75%	3A-35734
N. Up	5	8	386	TS-UP-WTN-1	K	Upper plenum West wall inner surface temperature, top north side	0-1250°C	±2.2°C / 0.75%	3A-35734
N. Up	5	9	387	TS-UP-WTS-2	K	Upper plenum West wall inner surface temperature, top south side	0-1250°C	±2.2°C / 0.75%	3A-35734
N. Up	5	10	388	TS-UP-WCN-3	K	Upper plenum West wall inner surface temperature, center north side	0-1250°C	±2.2°C / 0.75%	3A-35734
N. Up	5	11	389	TS-UP-WCS-4	K	Upper plenum West wall inner surface temperature, center south side	0-1250°C	±2.2°C / 0.75%	3A-35734
N. Up	5	12	390	TS-UP-WBN-5	K	Upper plenum West wall inner surface temperature, bottom north center	0-1250°C	±2.2°C / 0.75%	3A-35734
N. Up	5	13	391	TS-UP-WBS-6	K	Upper plenum West wall inner surface temperature, bottom south side	0-1250°C	±2.2°C / 0.75%	3A-35734
N. Up	5	14				<i>empty</i>			
N. Up	5	15				<i>empty</i>			
N. Up	6	0	394	TS-UP-NCE-3	K	Upper plenum North wall inner surface temperature, center east side	0-1250°C	±2.2°C / 0.75%	3A-35734
N. Up	6	1	395	TS-UP-NCW-4	K	Upper plenum North wall inner surface temperature, center west side	0-1250°C	±2.2°C / 0.75%	3A-35734
N. Up	6	2	396	TS-UP-NBE-5	K	Upper plenum North wall inner surface temperature, bottom east side	0-1250°C	±2.2°C / 0.75%	3A-35734
N. Up	6	3	397	TS-UP-NBW-6	K	Upper plenum North wall inner surface temperature, bottom west side	0-1250°C	±2.2°C / 0.75%	3A-35734
N. Up	6	4	410	TS-UP-ETS-1	K	Upper plenum East wall inner surface temperature, top south side	0-1250°C	±2.2°C / 0.75%	3A-35734
N. Up	6	5	411	TS-UP-ETN-2	K	Upper plenum East wall inner surface temperature, top north side	0-1250°C	±2.2°C / 0.75%	3A-35734

N. Up	6	6	412	TS-UP-ECS-3	K	Upper plenum East wall inner surface temperature center south side	0-1250°C	±2.2°C / 0.75%	3A-35734
N. Up	6	7	413	TS-UP-ECN-4	K	Upper plenum East wall inner surface temperature, center north side	0-1250°C	±2.2°C / 0.75%	3A-35734
N. Up	6	8	414	TS-UP-EBS-5	K	Upper plenum East wall inner surface temperature, bottom south side	0-1250°C	±2.2°C / 0.75%	3A-35734
N. Up	6	9	415	TS-UP-EBN-6	K	Upper plenum East wall inner surface temperature, bottom north side	0-1250°C	±2.2°C / 0.75%	3A-35734
N. Up	6	10	392	TS-UP-NTE-1	K	Upper plenum North wall inner surface temperature, top east side	0-1250°C	±2.2°C / 0.75%	3A-35734
N. Up	6	11	393	TS-UP-NTW-2	K	Upper plenum North wall inner surface temperature, top west side	0-1250°C	±2.2°C / 0.75%	3A-35734
N. Up	6	12	537	TS-CW-SC-3635	K	Lower section west (cold) wall south of centerline at 3635 mm	0-1250°C	±2.2°C / 0.75%	2A-38118
N. Up	6	13	538	TS-CW-NC-3635	K	Lower section west (cold) wall north of centerline at 3635 mm	0-1250°C	±2.2°C / 0.75%	2A-38118
N. Up	6	14	539	TS-CW-SM-3889	K	Lower section west (cold) wall mid-south side at 3889 mm	0-1250°C	±2.2°C / 0.75%	2A-38118
N. Up	6	15	540	TS-CW-SC-3889	K	Lower section west (cold) wall south of centerline at 3889 mm	0-1250°C	±2.2°C / 0.75%	2A-38118
N. Up	7	0	541	TS-CW-NC-3889	K	Lower section west (cold) wall north of centerline at 3889 mm	0-1250°C	±2.2°C / 0.75%	2A-38118
N. Up	7	1	542	TS-CW-NM-3889	K	Lower section west (cold) wall mid-north side at 3889 mm	0-1250°C	±2.2°C / 0.75%	2A-38118
N. Up	7	2	543	TS-CW-SC-4143	K	Lower section west (cold) wall south of centerline at 4143 mm	0-1250°C	±2.2°C / 0.75%	2A-38118
N. Up	7	3	544	TS-CW-NC-4143	K	Lower section west (cold) wall north of centerline at 4143 mm	0-1250°C	±2.2°C / 0.75%	2A-38118
N. Up	7	4	545	TS-CW-SM-4397	K	Lower section west (cold) wall mid-south side at 4397 mm	0-1250°C	±2.2°C / 0.75%	2A-38118
N. Up	7	5	546	TS-CW-SC-4397	K	Lower section west (cold) wall south of centerline at 4397 mm	0-1250°C	±2.2°C / 0.75%	2A-38118
N. Up	7	6	547	TS-CW-NC-4397	K	Lower section west (cold) wall north of centerline at 4397 mm	0-1250°C	±2.2°C / 0.75%	2A-38118
N. Up	7	7	548	TS-CW-NM-4397	K	Lower section west (cold) wall mid-north side at 4397 mm	0-1250°C	±2.2°C / 0.75%	2A-38118
N. Up	7	8	549	TS-CW-SC-4740	K	Lower section west (cold) wall south of centerline at 4740 mm	0-1250°C	±2.2°C / 0.75%	2A-38118
N. Up	7	9	550	TS-CW-NC-4740	K	Lower section west (cold) wall north of centerline at 4740 mm	0-1250°C	±2.2°C / 0.75%	2A-38118
N. Up	7	10	551	TS-CW-SM-4994	K	Lower section west (cold) wall mid-south side at 4994 mm	0-1250°C	±2.2°C / 0.75%	2A-38118
N. Up	7	11	552	TS-CW-SC-4994	K	Lower section west (cold) wall south of centerline at 4994 mm	0-1250°C	±2.2°C / 0.75%	2A-38118
N. Up	7	12	553	TS-CW-NC-4994	K	Lower section west (cold) wall north of centerline at 4994 mm	0-1250°C	±2.2°C / 0.75%	2A-38118
N. Up	7	13	554	TS-CW-NM-4994	K	Lower section west (cold) wall mid-north side at 4994 mm	0-1250°C	±2.2°C / 0.75%	2A-38118
N. Up	7	14	555	TS-CW-SC-5248	K	Lower section west (cold) wall south of centerline at 5248 mm	0-1250°C	±2.2°C / 0.75%	2A-38118
N. Up	7	15	556	TS-CW-NC-5248	K	Lower section west (cold) wall north of centerline at 5248 mm	0-1250°C	±2.2°C / 0.75%	2A-38118
N. Up	8	0	557	TS-CW-SM-5502	K	Lower section west (cold) wall mid-south side at 5502 mm	0-1250°C	±2.2°C / 0.75%	2A-38118
N. Up	8	1	558	TS-CW-SC-5502	K	Lower section west (cold) wall south of centerline at 5502 mm	0-1250°C	±2.2°C / 0.75%	2A-38118
N. Up	8	2	559	TS-CW-NC-5502	K	Lower section west (cold) wall north of centerline at 5502 mm	0-1250°C	±2.2°C / 0.75%	2A-38118
N. Up	8	3	560	TS-CW-NM-5502	K	Lower section west (cold) wall mid-north side at 5502 mm	0-1250°C	±2.2°C / 0.75%	2A-38118
N. Up	8	4	561	TS-CW-SC-5845	K	Lower section west (cold) wall south of centerline at 5845 mm	0-1250°C	±2.2°C / 0.75%	2A-38118
N. Up	8	5	562	TS-CW-NC-5845	K	Lower section west (cold) wall north of centerline at 5845 mm	0-1250°C	±2.2°C / 0.75%	2A-38118
N. Up	8	6	563	TS-CW-SM-6099	K	Lower section west (cold) wall mid-south side at 6099 mm	0-1250°C	±2.2°C / 0.75%	2A-38118
N. Up	8	7	564	TS-CW-SC-6099	K	Lower section west (cold) wall south of centerline at 6099 mm	0-1250°C	±2.2°C / 0.75%	2A-38118
N. Up	8	8	565	TS-CW-NC-6099	K	Lower section west (cold) wall north of centerline at 6099 mm	0-1250°C	±2.2°C / 0.75%	2A-38118
N. Up	8	9	566	TS-CW-NM-6099	K	Lower section west (cold) wall mid-north side at 6099 mm	0-1250°C	±2.2°C / 0.75%	2A-38118
N. Up	8	10	567	TS-CW-SC-6353	K	Lower section west (cold) wall south of centerline at 6353 mm	0-1250°C	±2.2°C / 0.75%	2A-38118
N. Up	8	11	568	TS-CW-NC-6353	K	Lower section west (cold) wall north of centerline at 6353 mm	0-1250°C	±2.2°C / 0.75%	2A-38118

N. Up	8	12	569	TS-CW-SM-6607	K	Lower section west (cold) wall mid-south side at 6607 mm	0-1250°C	±2.2°C / 0.75%	2A-38118
N. Up	8	13	570	TS-CW-SC-6607	K	Lower section west (cold) wall south of centerline at 6607 mm	0-1250°C	±2.2°C / 0.75%	2A-38118
N. Up	8	14	571	TS-CW-NC-6607	K	Lower section west (cold) wall north of centerline at 6607 mm	0-1250°C	±2.2°C / 0.75%	2A-38118
N. Up	8	15	572	TS-CW-NM-6607	K	Lower section west (cold) wall mid-north side at 6607 mm	0-1250°C	±2.2°C / 0.75%	2A-38118
N. Low	1	0	2	TS-hot-wall-NC-127	K	Twall lower heated section north of centerline at 127 mm	0-1250°C	±2.2°C / 0.75%	1A-40882
N. Low	1	1	4	TS-hot-wall-NE-203	K	Twall lower heated section north edge at 203 mm	0-1250°C	±2.2°C / 0.75%	1A-40882
N. Low	1	2	7	TS-hot-wall-NM-279	K	Twall lower heated section mid-north side at 279 mm	0-1250°C	±2.2°C / 0.75%	1A-40882
N. Low	1	3	9	TS-hot-wall-NC-279	K	Twall lower heated section north of centerline at 279 mm	0-1250°C	±2.2°C / 0.75%	1A-40882
N. Low	1	4	8	TS-hot-wall-NM-279-o	K	Twall lower heated section mid-north, outer surface at 279 mm	0-1250°C	±2.2°C / 0.75%	1A-40882
N. Low	1	5	11	TS-hot-wall-NC-432	K	Twall lower heated section north of centerline at 432 mm	0-1250°C	±2.2°C / 0.75%	1A-40882
N. Low	1	6	13	TS-hot-wall-NE-508	K	Twall lower heated section north edge at 508 mm	0-1250°C	±2.2°C / 0.75%	1A-40882
N. Low	1	7	15	TS-hot-wall-NC-584	K	Twall lower heated section north of centerline at 584 mm	0-1250°C	±2.2°C / 0.75%	1A-40882
N. Low	1	8	17	TS-hot-wall-NC-787	K	Twall lower heated section north of centerline at 787 mm	0-1250°C	±2.2°C / 0.75%	1A-40882
N. Low	1	9	19	TS-hot-wall-NE-864	K	Twall lower heated section north edge at 864 mm	0-1250°C	±2.2°C / 0.75%	1A-40882
N. Low	1	10	24	TS-hot-wall-SM-940	K	Twall lower heated section mid-north side at 940 mm	0-1250°C	±2.2°C / 0.75%	1A-40882
N. Low	1	11	23	TS-hot-wall-NC-940	K	Twall lower heated section north of centerline at 940 mm	0-1250°C	±2.2°C / 0.75%	1A-40882
N. Low	1	12	26	TS-hot-wall-NC-1092	K	Twall lower heated section north of centerline at 1092 mm	0-1250°C	±2.2°C / 0.75%	1A-40882
N. Low	1	13	28	TS-hot-wall-NE-1168	K	Twall lower heated section north edge at 1168 mm	0-1250°C	±2.2°C / 0.75%	1A-40882
N. Low	1	14	30	TS-hot-wall-NC-1245	K	Twall lower heated section north of centerline at 1245 mm	0-1250°C	±2.2°C / 0.75%	1A-40882
N. Low	1	15	32	TS-hot-wall-NC-1448	K	Twall lower heated section north of centerline at 1448 mm	0-1250°C	±2.2°C / 0.75%	1A-40882
N. Low	2	0	34	TS-hot-wall-NE-1524	K	Twall lower heated section north edge at 1524 mm	0-1250°C	±2.2°C / 0.75%	1A-40882
N. Low	2	1	38	TS-hot-wall-NC-1600	K	Twall lower heated section north of centerline at 1600 mm	0-1250°C	±2.2°C / 0.75%	1A-40882
N. Low	2	2	39	TS-hot-wall-NC-1753	K	Twall lower heated section north of centerline at 1753 mm	0-1250°C	±2.2°C / 0.75%	1A-40882
N. Low	2	3	41	TS-hot-wall-NM-1753	K	Twall lower heated section mid-north side at 1753 mm	0-1250°C	±2.2°C / 0.75%	1A-40882
N. Low	2	4	40	TS-hot-wall-NC-1753-o	K	Twall lower heated section north of centerline outer at 1753 mm	0-1250°C	±2.2°C / 0.75%	1A-40882
N. Low	2	5	43	TS-hot-wall-NE-1829	K	Twall lower heated section north edge at 1829 mm	0-1250°C	±2.2°C / 0.75%	1A-40882
N. Low	2	6	45	TS-hot-wall-NC-1905	K	Twall lower heated section north of centerline at 1905 mm	0-1250°C	±2.2°C / 0.75%	1A-40882
N. Low	2	7	47	TS-hot-wall-NC-2108	K	Twall lower heated section north of centerline at 2108 mm	0-1250°C	±2.2°C / 0.75%	1A-40882
N. Low	2	8	49	TS-hot-wall-NE-2184	K	Twall lower heated section north edge at 2184 mm	0-1250°C	±2.2°C / 0.75%	1A-40882
N. Low	2	9	51	TS-hot-wall-NC-2261	K	Twall lower heated section north of centerline at 2261 mm	0-1250°C	±2.2°C / 0.75%	1A-40882
N. Low	2	10	54	TS-hot-wall-NC-2413	K	Twall lower heated section north of centerline at 2413 mm	0-1250°C	±2.2°C / 0.75%	1A-40882
N. Low	2	11	56	TS-hot-wall-NE-2489	K	Twall lower heated section north edge at 2489 mm	0-1250°C	±2.2°C / 0.75%	1A-40882
N. Low	2	12	58	TS-hot-wall-NC-2565	K	Twall lower heated section north of centerline at 2565 mm	0-1250°C	±2.2°C / 0.75%	1A-40882
N. Low	2	13	60	TS-hot-wall-NC-2769	K	Twall lower heated section north of centerline at 2769 mm	0-1250°C	±2.2°C / 0.75%	1A-40882
N. Low	2	14	62	TS-hot-wall-NE-2845	K	Twall lower heated section north edge at 2845 mm	0-1250°C	±2.2°C / 0.75%	1A-40882
N. Low	2	15	64	TS-hot-wall-NC-2921	K	Twall lower heated section north of centerline at 2921 mm	0-1250°C	±2.2°C / 0.75%	1A-40882
N. Low	3	0	67	TS-hot-wall-NC-3073	K	Twall lower heated section north of centerline at 3073 mm	0-1250°C	±2.2°C / 0.75%	1A-40882
N. Low	3	1	69	TS-hot-wall-NM-3073	K	Twall lower heated section mid-north side at 3073 mm	0-1250°C	±2.2°C / 0.75%	1A-40882

N. Low	3	2	71	TS-hot-wall-NE-3150	K	Twall lower heated section north edge at 3150 mm	0-1250°C	±2.2°C / 0.75%	1A-40882
N. Low	3	3	73	TS-hot-wall-NC-3226	K	Twall lower heated section north of centerline at 3226 mm	0-1250°C	±2.2°C / 0.75%	1A-40882
N. Low	3	4	201	NW-305	K	Wall temperatures along I-beams on adiabatic side walls	0-1250°C	±2.2°C / 0.75%	3A-31214
N. Low	3	5	202	NW-2184	K	Wall temperatures along I-beams on adiabatic side walls	0-1250°C	±2.2°C / 0.75%	3A-31214
N. Low	3	6	205	NC-305	K	Wall temperatures along I-beams on adiabatic side walls	0-1250°C	±2.2°C / 0.75%	3A-31214
N. Low	3	7	206	NC-1245	K	Wall temperatures along I-beams on adiabatic side walls	0-1250°C	±2.2°C / 0.75%	3A-31214
N. Low	3	8	207	NC-2184	K	Wall temperatures along I-beams on adiabatic side walls	0-1250°C	±2.2°C / 0.75%	3A-31214
N. Low	3	9	208	NC-3124	K	Wall temperatures along I-beams on adiabatic side walls	0-1250°C	±2.2°C / 0.75%	3A-31214
N. Low	3	10	213	NE-305	K	Wall temperatures along I-beams on adiabatic side walls	0-1250°C	±2.2°C / 0.75%	3A-31214
N. Low	3	11	214	NE-1245	K	Wall temperatures along I-beams on adiabatic side walls	0-1250°C	±2.2°C / 0.75%	3A-31214
N. Low	3	12	215	NE-2184	K	Wall temperatures along I-beams on adiabatic side walls	0-1250°C	±2.2°C / 0.75%	3A-31214
N. Low	3	13	216	NE-3124	K	Wall temperatures along I-beams on adiabatic side walls	0-1250°C	±2.2°C / 0.75%	3A-31214
N. Low	3	14	<i>empty</i>						
N. Low	3	15	<i>empty</i>						
N. Low	4	0	241	TS-duct6-hot-912	K	Surface temperature on front of duct 6 at 912 mm from inlet	0-1250°C	±2.2°C / 0.75%	3A-31214
N. Low	4	1	242	TS-duct6-hot-1824	K	Surface temperature on front of duct 6 at 1824 mm from inlet	0-1250°C	±2.2°C / 0.75%	3A-31214
N. Low	4	2	243	TS-duct6-hot-2736	K	Surface temperature on front of duct 6 at 2736 mm from inlet	0-1250°C	±2.2°C / 0.75%	3A-31214
N. Low	4	3	244	TS-duct6-hot-3648	K	Surface temperature on front of duct 6 at 3648 mm from inlet	0-1250°C	±2.2°C / 0.75%	3A-31214
N. Low	4	4	245	TS-duct6-hot-4560	K	Surface temperature on front of duct 6 at 4560 mm from inlet	0-1250°C	±2.2°C / 0.75%	3A-31214
N. Low	4	5	246	TS-duct6-hot-5472	K	Surface temperature on front of duct 6 at 5472 mm from inlet	0-1250°C	±2.2°C / 0.75%	3A-31214
N. Low	4	6	247	TS-duct6-hot-6384	K	Surface temperature on front of duct 6 at 6384 mm from inlet	0-1250°C	±2.2°C / 0.75%	3A-31214
N. Low	4	7	248	TS-duct6-hot-7296	K	Surface temperature on front of duct 6 at 7296 mm from inlet	0-1250°C	±2.2°C / 0.75%	3A-31214
N. Low	4	8	249	TS-duct6-cold-912	K	Surface temperature on back of duct 6 at 912 mm from inlet	0-1250°C	±2.2°C / 0.75%	3A-31214
N. Low	4	9	250	TS-duct6-cold-1824	K	Surface temperature on back of duct 6 at 1824 mm from inlet	0-1250°C	±2.2°C / 0.75%	3A-31214
N. Low	4	10	251	TS-duct6-cold-2736	K	Surface temperature on back of duct 6 at 2738 mm from inlet	0-1250°C	±2.2°C / 0.75%	3A-31214
N. Low	4	11	252	TS-duct6-cold-3648	K	Surface temperature on back of duct 6 at 3648 mm from inlet	0-1250°C	±2.2°C / 0.75%	3A-31214
N. Low	4	12	253	TS-duct6-cold-4560	K	Surface temperature on back of duct 6 at 4560 mm from inlet	0-1250°C	±2.2°C / 0.75%	3A-31214
N. Low	4	13	254	TS-duct6-cold-5472	K	Surface temperature on back of duct 6 at 5472 mm from inlet	0-1250°C	±2.2°C / 0.75%	3A-31214
N. Low	4	14	255	TS-duct6-cold-6384	K	Surface temperature on back of duct 6 at 6384 mm from inlet	0-1250°C	±2.2°C / 0.75%	3A-31214
N. Low	4	15	256	TS-duct6-cold-7296	K	Surface temperature on back of duct 6 at 7296 mm from inlet	0-1250°C	±2.2°C / 0.75%	3A-31214
N. Low	5	0	350	TG-duct1-inlet-n150	K	Gas temperature in duct 1 inlet at -150 mm	0-1250°C	±2.2°C / 0.75%	3A-35734
N. Low	5	1	351	TG-duct2-inlet-n150	K	Gas temperature in duct 2 inlet at -150 mm	0-1250°C	±2.2°C / 0.75%	3A-35734
N. Low	5	2	352	TG-duct3-inlet-n150	K	Gas temperature in duct 3 inlet at -150 mm	0-1250°C	±2.2°C / 0.75%	3A-35734
N. Low	5	3	353	TG-duct4-inlet-n150	K	Gas temperature in duct 4 inlet at -150 mm	0-1250°C	±2.2°C / 0.75%	3A-35734
N. Low	5	4	354	TG-duct5-inlet-n150	K	Gas temperature in duct 5 inlet at -150 mm	0-1250°C	±2.2°C / 0.75%	3A-35734
N. Low	5	5	355	TG-duct6-inlet-n150	K	Gas temperature in duct 6 inlet at -150 mm	0-1250°C	±2.2°C / 0.75%	3A-35734
N. Low	5	6	356	TG-duct7-inlet-n150	K	Gas temperature in duct 7 inlet at -150 mm	0-1250°C	±2.2°C / 0.75%	3A-35734
N. Low	5	7	357	TG-duct8-inlet-n150	K	Gas temperature in duct 8 inlet at -150 mm	0-1250°C	±2.2°C / 0.75%	3A-35734

N. Low	5	8	358	TG-duct9-inlet-n150	K	Gas temperature in duct 9 inlet at -150 mm	0-1250°C	±2.2°C / 0.75%	3A-35734
N. Low	5	9	359	TG-duct10-inlet-n150	K	Gas temperature in duct 10 inlet at -150 mm	0-1250°C	±2.2°C / 0.75%	3A-35734
N. Low	5	10	360	TG-duct11-inlet-n150	K	Gas temperature in duct 11 inlet at -150 mm	0-1250°C	±2.2°C / 0.75%	3A-35734
N. Low	5	11	361	TG-duct12-inlet-n150	K	Gas temperature in duct 12 inlet at -150 mm	0-1250°C	±2.2°C / 0.75%	3A-35734
N. Low	5	12	501	TS-CW-NC-204	K	Lower section west (cold) wall south of centerline at 204 mm	0-1250°C	±2.2°C / 0.75%	2A-38118
N. Low	5	13	502	TS-CW-SC-204	K	Lower section west (cold) wall north of centerline at 204 mm	0-1250°C	±2.2°C / 0.75%	2A-38118
N. Low	5	14	503	TS-CW-NC-457	K	Lower section west (cold) wall mid-south side at 457 mm	0-1250°C	±2.2°C / 0.75%	2A-38118
N. Low	5	15	504	TS-CW-SC-457	K	Lower section west (cold) wall south of centerline at 457 mm	0-1250°C	±2.2°C / 0.75%	2A-38118
N. Low	6	0	505	TS-CW-NM-457	K	Lower section west (cold) wall north of centerline at 457 mm	0-1250°C	±2.2°C / 0.75%	2A-38118
N. Low	6	1	506	TS-CW-SM-457	K	Lower section west (cold) wall mid-north side at 457 mm	0-1250°C	±2.2°C / 0.75%	2A-38118
N. Low	6	2	507	TS-CW-NC-711	K	Lower section west (cold) wall south of centerline at 711 mm	0-1250°C	±2.2°C / 0.75%	2A-38118
N. Low	6	3	508	TS-CW-SC-711	K	Lower section west (cold) wall north of centerline at 711 mm	0-1250°C	±2.2°C / 0.75%	2A-38118
N. Low	6	4	509	TS-CW-NC-965	K	Lower section west (cold) wall mid-south side at 965 mm	0-1250°C	±2.2°C / 0.75%	2A-38118
N. Low	6	5	510	TS-CW-SC-965	K	Lower section west (cold) wall south of centerline at 965 mm	0-1250°C	±2.2°C / 0.75%	2A-38118
N. Low	6	6	511	TS-CW-NM-965	K	Lower section west (cold) wall north of centerline at 965 mm	0-1250°C	±2.2°C / 0.75%	2A-38118
N. Low	6	7	512	TS-CW-SM-965	K	Lower section west (cold) wall mid-north side at 965 mm	0-1250°C	±2.2°C / 0.75%	2A-38118
N. Low	6	8	513	TS-CW-NC-1308	K	Lower section west (cold) wall south of centerline at 1308 mm	0-1250°C	±2.2°C / 0.75%	2A-38118
N. Low	6	9	514	TS-CW-SC-1308	K	Lower section west (cold) wall north of centerline at 1308 mm	0-1250°C	±2.2°C / 0.75%	2A-38118
N. Low	6	10	515	TS-CW-NC-1562	K	Lower section west (cold) wall mid-south side at 1562 mm	0-1250°C	±2.2°C / 0.75%	2A-38118
N. Low	6	11	516	TS-CW-SC-1562	K	Lower section west (cold) wall south of centerline at 1562 mm	0-1250°C	±2.2°C / 0.75%	2A-38118
N. Low	6	12	517	TS-CW-NM-1562	K	Lower section west (cold) wall north of centerline at 1562 mm	0-1250°C	±2.2°C / 0.75%	2A-38118
N. Low	6	13	518	TS-CW-SM-1562	K	Lower section west (cold) wall mid-north side at 1562 mm	0-1250°C	±2.2°C / 0.75%	2A-38118
N. Low	6	14	519	TS-CW-NC-1816	K	Lower section west (cold) wall south of centerline at 1816 mm	0-1250°C	±2.2°C / 0.75%	2A-38118
N. Low	6	15	520	TS-CW-SC-1816	K	Lower section west (cold) wall north of centerline at 1816 mm	0-1250°C	±2.2°C / 0.75%	2A-38118
N. Low	7	0	521	TS-CW-NC-2070	K	Lower section west (cold) wall mid-south side at 2070 mm	0-1250°C	±2.2°C / 0.75%	2A-38118
N. Low	7	1	522	TS-CW-SC-2070	K	Lower section west (cold) wall south of centerline at 2070 mm	0-1250°C	±2.2°C / 0.75%	2A-38118
N. Low	7	2	523	TS-CW-NM-2070	K	Lower section west (cold) wall north of centerline at 2070 mm	0-1250°C	±2.2°C / 0.75%	2A-38118
N. Low	7	3	524	TS-CW-SM-2070	K	Lower section west (cold) wall mid-north side at 2070 mm	0-1250°C	±2.2°C / 0.75%	2A-38118
N. Low	7	4	525	TS-CW-NC-2413	K	Lower section west (cold) wall south of centerline at 2413 mm	0-1250°C	±2.2°C / 0.75%	2A-38118
N. Low	7	5	526	TS-CW-SC-2413	K	Lower section west (cold) wall north of centerline at 2413 mm	0-1250°C	±2.2°C / 0.75%	2A-38118
N. Low	7	6	527	TS-CW-NC-2667	K	Lower section west (cold) wall mid-south side at 2667 mm	0-1250°C	±2.2°C / 0.75%	2A-38118
N. Low	7	7	528	TS-CW-SC-2667	K	Lower section west (cold) wall south of centerline at 2667 mm	0-1250°C	±2.2°C / 0.75%	2A-38118
N. Low	7	8	529	TS-CW-NM-2667	K	Lower section west (cold) wall north of centerline at 2667 mm	0-1250°C	±2.2°C / 0.75%	2A-38118
N. Low	7	9	530	TS-CW-SM-2667	K	Lower section west (cold) wall mid-north side at 2667 mm	0-1250°C	±2.2°C / 0.75%	2A-38118
N. Low	7	10	531	TS-CW-NC-2921	K	Lower section west (cold) wall south of centerline at 2921 mm	0-1250°C	±2.2°C / 0.75%	2A-38118
N. Low	7	11	532	TS-CW-SC-2921	K	Lower section west (cold) wall north of centerline at 2921 mm	0-1250°C	±2.2°C / 0.75%	2A-38118
N. Low	7	12	533	TS-CW-NC-3175	K	Lower section west (cold) wall mid-south side at 3175 mm	0-1250°C	±2.2°C / 0.75%	2A-38118
N. Low	7	13	534	TS-CW-SC-3175	K	Lower section west (cold) wall south of centerline at 3175 mm	0-1250°C	±2.2°C / 0.75%	2A-38118

N. Low	7	14	535	TS-CW-NM-3175	K	Lower section west (cold) wall north of centerline at 3175 mm	0-1250°C	±2.2°C / 0.75%	2A-38118
N. Low	7	15	536	TS-CW-SM-3175	K	Lower section west (cold) wall mid-north side at 3175 mm	0-1250°C	±2.2°C / 0.75%	2A-38118
N. Low	8	0				<i>empty</i>			
N. Low	8	1				<i>empty</i>			
N. Low	8	2				<i>empty</i>			
N. Low	8	3				<i>empty</i>			
N. Low	8	4				<i>empty</i>			
N. Low	8	5				<i>empty</i>			
N. Low	8	6				<i>empty</i>			
N. Low	8	7				<i>empty</i>			
N. Low	8	8				<i>empty</i>			
N. Low	8	9				<i>empty</i>			
N. Low	8	10				<i>empty</i>			
N. Low	8	11				<i>empty</i>			
N. Low	8	12				<i>empty</i>			
N. Low	8	13				<i>empty</i>			
N. Low	8	14				<i>empty</i>			
N. Low	8	15				<i>empty</i>			



Nuclear Engineering Division

Argonne National Laboratory
9700 South Cass Avenue, Bldg. 206
Argonne, IL 60439-4854

www.anl.gov



Argonne National Laboratory is a U.S. Department of Energy
laboratory managed by UChicago Argonne, LLC